



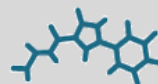
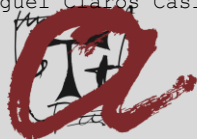
DEVELOPMENT OF VISIBLE LIGHT PHOTOREDOX METHODOLOGIES TOWARDS THE ACTIVATION OF CARBON-HALOGEN BONDS

Miguel Claros Casielles

ADVERTIMENT. L'accés als continguts d'aquesta tesi doctoral i la seva utilització ha de respectar els drets de la persona autora. Pot ser utilitzada per a consulta o estudi personal, així com en activitats o materials d'investigació i docència en els termes establerts a l'art. 32 del Text Refós de la Llei de Propietat Intel·lectual (RDL 1/1996). Per altres utilitzacions es requereix l'autorització prèvia i expressa de la persona autora. En qualsevol cas, en la utilització dels seus continguts caldrà indicar de forma clara el nom i cognoms de la persona autora i el títol de la tesi doctoral. No s'autoritza la seva reproducció o altres formes d'explotació efectuades amb finalitats de lucre ni la seva comunicació pública des d'un lloc aliè al servei TDX. Tampoc s'autoritza la presentació del seu contingut en una finestra o marc aliè a TDX (framing). Aquesta reserva de drets afecta tant als continguts de la tesi com als seus resums i índexs.

ADVERTENCIA. El acceso a los contenidos de esta tesis doctoral y su utilización debe respetar los derechos de la persona autora. Puede ser utilizada para consulta o estudio personal, así como en actividades o materiales de investigación y docencia en los términos establecidos en el art. 32 del Texto Refundido de la Ley de Propiedad Intelectual (RDL 1/1996). Para otros usos se requiere la autorización previa y expresa de la persona autora. En cualquier caso, en la utilización de sus contenidos se deberá indicar de forma clara el nombre y apellidos de la persona autora y el título de la tesis doctoral. No se autoriza su reproducción u otras formas de explotación efectuadas con fines lucrativos ni su comunicación pública desde un sitio ajeno al servicio TDR. Tampoco se autoriza la presentación de su contenido en una ventana o marco ajeno a TDR (framing). Esta reserva de derechos afecta tanto al contenido de la tesis como a sus resúmenes e índices.

WARNING. Access to the contents of this doctoral thesis and its use must respect the rights of the author. It can be used for reference or private study, as well as research and learning activities or materials in the terms established by the 32nd article of the Spanish Consolidated Copyright Act (RDL 1/1996). Express and previous authorization of the author is required for any other uses. In any case, when using its content, full name of the author and title of the thesis must be clearly indicated. Reproduction or other forms of for profit use or public communication from outside TDX service is not allowed. Presentation of its content in a window or frame external to TDX (framing) is not authorized either. These rights affect both the content of the thesis and its abstracts and indexes.



Development of Visible Light Photoredox Methodologies towards the Activation of Carbon- Halogen Bonds

Miguel Claros Casielles



DOCTORAL THESIS
2020

UNIVERSITAT ROVIRA I VIRGILI
DEVELOPMENT OF VISIBLE LIGHT PHOTOREDOX METHODOLOGIES TOWARDS THE ACTIVATION
OF CARBON-HALOGEN BONDS
Miguel Claros Casielles

UNIVERSITAT ROVIRA I VIRGILI
DEVELOPMENT OF VISIBLE LIGHT PHOTOREDOX METHODOLOGIES TOWARDS THE ACTIVATION
OF CARBON-HALOGEN BONDS
Miguel Claros Casielles

UNIVERSITAT ROVIRA I VIRGILI
DEVELOPMENT OF VISIBLE LIGHT PHOTOREDOX METHODOLOGIES TOWARDS THE ACTIVATION
OF CARBON-HALOGEN BONDS
Miguel Claros Casielles

PhD Thesis

Development of Visible-Light Photoredox Methodologies
towards the Activation of Carbon-Halogen Bonds

Miguel Claros Casielles

Supervised by Prof. Julio Lloret-Fillol
and
Prof. Alicia Casitas Montero

Tarragona

May 2020



UNIVERSITAT ROVIRA I VIRGILI
DEVELOPMENT OF VISIBLE LIGHT PHOTOREDOX METHODOLOGIES TOWARDS THE ACTIVATION
OF CARBON-HALOGEN BONDS
Miguel Claros Casielles



Prof. Dr. Julio Lloret Fillol, Group Leader of the Institut Català d'Investigació Química (ICIQ) and Research Professor of Institució Catalana de Recerca i Estudis Avançants (ICREA), and Prof. Dr. Alicia Casitas Montero, assistant professor (W1) at Philipps-Universität Marburg (Germany).

CERTIFY that the present study entitled **“Development of Visible-Light Photoredox Methodologies towards the Activation of Carbon-Halogen Bonds”**, presented by Miguel Claros Casielles to receive the PhD degree in Chemistry, has been carried out under our supervision, in the Institut Català d'Investigació Química (ICIQ).

Tarragona, 8th April 2020

PhD Thesis supervisor

Prof. Dr. Julio Lloret Fillol

PhD Thesis supervisor

Prof. Dr. Alicia Casitas Montero

UNIVERSITAT ROVIRA I VIRGILI
DEVELOPMENT OF VISIBLE LIGHT PHOTOREDOX METHODOLOGIES TOWARDS THE ACTIVATION
OF CARBON-HALOGEN BONDS
Miguel Claros Casielles

Acknowledgments

Cuatro años dan pa muiitu, veintinueve pa un pocu más. Diz el refraneru español “*Ye de bon nacíu ser estimosu*” y con ello voi ocupar les siguientes páxines.

Como no, mis primeras líneas en este aspecto tienen que ser para ti, **Alicia**. Hace 4 años aceptaste el reto de supervisar y enseñar a este astur que poco sabía (y poco le gustaba) del mundo de la química orgánica. Pues bien, tras estos años conseguiste que aprendiera un poco (a pesar de que la segunda premisa sigue igual o peor...). Faltarán líneas en esta tesis para agradecerte todo lo que me enseñaste y toda la paciencia que tuviste conmigo. GRACIAS.

No menos importante es la que fue mi hermana mayor durante este tiempo. **Sara**. Seguí tus pasos desde ese entrañable laboratorio de la planta 3 de UniOvi hasta aquí. Recuerdo que te dije que no me iba a volver tan loco con la química como esta gente. Creo que no lo conseguí... Gracias por estar siempre ahí para darme ese consejo, corregirme un mail o pa tomar unas “aguas manchadas” de esas que te gustan a tí.

Por supuesto no estaría aquí de no ser por **Eire** y **Pilar**. Despertasteis la vena investigadora en mí. Gracias por ello. Por supuesto a todos y cada uno de los integrantes de *DesespeLab* (Cristian, Isaac, Irene, Luci, Marichu, Pedrito, Silvia, SuperJavi, María y a aquellos de quienes seguro me olvido). Muchas gracias. Como no, creo que el culpable de que hoy esté escribiendo esto eres tú, **Xerxis**. Recuerdo perfectamente tu cara cuando te dije que me había inscrito en el máster después de estar un mes intentando convencerme de que hiciera el master contigo y decirte yo que pasaba de estar 12 horas metido en la Uni. También recuerdo cuando intentaste convencerme de hacer la tesis que serían risas con **Enol**, **Dani**, **Berti** y **Mata** y te dije que no, que yo pasaba de tesis. Pues bien, me fui a la otra punta de la península a hacerla. Gracias por todo hermano. **Nuri**, **Moráis**, **Jorgito**, nunca vos di las gracias (y hoy no será excepción). Quiérovos. También a esa gente que conoces *sidra'n*

manu y que acaban siendo colegas pa tó la vida **Chusín, Pedri, Alba, Jaco, Nere**. Nun nos matamos a estudiar, pero pasámoslo bien que ye lo importante.

Poco tienen que ver con la química ni con la investigación, pero sin ellos no habría llegado a ningún lado. **Alberto, Vero, Jony, Rosa, Adri, Artime** y toda la familia del **Club Natación Las Anclas**. Me enseñasteis unos valores de constancia y sacrificio que sin duda recordaré el resto de mis días. **Jose, Iván, Pablín, Diego** (Galluuu), **Raquel, Sofi, Clau, Alba** y todos los que vinieron después que no enumeraré ya que me quedo sin páginas. Gracias de verdad.

Creo qu'a los míos colegas de tola vida nun fai falta estima-yos na (sabéis de sobra tolo que vos estimo tar ahí). **Pablín, Tuji, Sarita, Nus, M8, Loce, Chapi, Manolin, Pirulina** (nun sabía onde metete si aquí o cola familia) sigue intentando siempre superame aunque nun lu consigas, quiérote igual. **Adri, Ponga, Davicín** hay que dir a comer unes sardinuques a Candás.

Y bien, no podría haber sobrevivido estos 4 años sin esa gente que acabo siendo parte de mi familia. Empezando por la primera en llegar (a mí, claro): **Ester**. Cantidad de cosas te hice churri (el barro en Siurana, el hospital, el orujo en tu casa...) todas con todo mi cariño, pero aún así siempre con una sonrisa. Sapss que t'estim molt eskimo (¿¿viste que dominio??). **Nuri**, que decirte. Gracias por intentar poner un poco de orden en mi vida y servir de nexo lingüístico a mi llegada, algo mejoramos. Sé que de lo que más orgullosa estás es de que consiguiera organizar un año mi cumpleaños, el resto es secundario. Siempre serás mi *cazurra* favorita. Mi manchega favorita, **Alicia**, vaya percal entenderte al principio compañera. Siempre recordaré tu cara de fascinación al ver los acantilados por el *Camí de Ronda*. Pobrecita... espero poder enseñarte pronto los parajes astures y compartir siempre quesucos ricos. Por cierto, perdona por haberte quitao el novio... **Criollete**, no me olvido de ti con lo de manchega favorita. Desde tu llegada me dejaste "*con el culo ladeao*". Esa energía, ese estrés... No cambies nunca. **Cris**, la espía del PB2, siempre controlándome...que sería de esos paseos hacia los reactores sin saludarte 14 veces como si todas fueran la primera. Gracias por aportar madurez al grupo (de vez en

cuando claro...) y hacernos recordar que se puede llegar a vieyu siendo joven. **Victoria**, la mejor pinche de cocina de la historia, gracias por esos bailes y los champis. Algún día conseguiré quitarte el biberón, ¡¡¡que lo sepas!!! (aunque igual pa cuando puedas leer esto ya no usas de eso...). **Alicia**, vecina, mira que no te di la vara con los gatetes, las llaves de repuesto cuando me dejaba las mías en el ICIQ (un par de veces al día por lo menos...) o con otros asuntillos que no mencionaré aquí. Gracias por estar “siempre” enfrente. Siempre serás mi vecina favorita. **Raul**, brosito, siempre te odiaré por haberte llevado a mi vecina y dejarme solu en este edificio. Aun así, y a pesar de que siempre tamos insultándonos, siempre serás mi bro (a ver si te curras una invitación pa probar esa supuesta agua “maravillosa” que dices tener en Madrid... aunque casi prefiero un buen cocido...). Siguiendo por el piso de arriba (o el de abajo si haces el pino), **Andreu**, el mejor paellero que conocí nunca (aunque tu padre no lo hace mal tampoco...). Gràcies per aportar sempre una mica de seny, paciència i serenitat al grup i perdona per aqueixes partides de trivial que vas perdre per la meua culpa, ya saps que yo si no hay ovellines.... Y hablando de ovelles, José Enrique, J, Pepín, **Kike**, como quieras... gracias por aportar siempre ese estrés, esa agonía... esas noches en Manchester cambiaron mi vida. Te quiero tío... Ese **Chuchiii**, que mal lo pasé durante tu escritura macho... pero era una buena excusa para ir a tomar cerveza después del labo. Por más rutas de montaña y cerveza y whisky y lo que bien quieras, en Ávila, Milán o donde sea.

Siento dejarte pal final hermano. El primero con el que eché unas cerves cuando vine a la entrevista. Mucha culpa tienes de la locura que me entró con la química (nunca pensé que yo fuera a ir voluntariamente un domingo a currar). Gracias por esas charlas de química después de 14 cervezas (o veintisiete!!), por esos mensajes de “me va a dar un ictus, necesito cermeza”. Siempre tendrás aquí un compañero pa echar una, 3 o cuarentaicuatro.

I do not forget those with whom I shared the laboratory and from whom in a certain way I learned what I know. **Fede, Vlad, Noufal, Felix, Katia, Sergi**; thanks for all the knowledge you share with me and for helping me in the different projects

and techniques. I will always be grateful to you. **Bea**, siempre dispuesta a echar una mano, a explicarme 14 veces las cosas y recordarme esas cosas burocráticas que tanto me gustan... **Arnau**, *tarzanello*, gràcies per triar compartir taula amb mi, poc productives eren aquelles tardes (científicament parlant) però apreníem coses diverses. Por muchas más noches de intensa pesca (igual algún día algo sacamos). **Albe** un altro che non parliamo di chimica, ma di pizza, google maps o varie merde.... Grazie per avermi aiutato a sopportare il ragazzo polacco... **Dominika**, rapacina, what stress to endure you every day, but in the end, I got a little love from you (very little but...). Good luck for what is coming, you will need it. And the rest, just good luck. Por supuesto, no podría olvidarme de **León** y **Xavi**, sin los que no habría podido hacer ni la mitad del trabajo descrito en esta tesis. Dos fieras tanto dentro como fuera del taller. Queda pendiente una parrillada y unas sidras

Ya para acabar, mi familia, **Padre**, **Madre**, **Hermano**, siempre un apoyo, un ejemplo y una guía para mis pasos, gracias por todo. **Maye** y **Mark**, I will not be able to thank you all your effort in the correction of the English in the manuscript, I will compensate it with a mariscada or something when you come back to Asturias. Mi segunda familia, la vasca, gracias por estar ahí y servirme de repostaje cuando voy pa casa. Por supuesto, mis últimas palabras serán para quien no está, **Abuela**, siempre quisiste ver a un nieto doctor, creo que fue una de las razones por las que hoy estoy aquí. En algún sitio estarás y espero lo disfrutes.

Lo dicho, muchas gracias a todos los que aportáis algo a mi vida (bueno o malo, todo suma en la formación de una persona). Fuerza, Salud y Rock&Roll. Nos vemos en los bares. ¡¡Viva la Kilika!!

UNIVERSITAT ROVIRA I VIRGILI
DEVELOPMENT OF VISIBLE LIGHT PHOTOREDOX METHODOLOGIES TOWARDS THE ACTIVATION
OF CARBON-HALOGEN BONDS
Miguel Claros Casielles

UNIVERSITAT ROVIRA I VIRGILI
DEVELOPMENT OF VISIBLE LIGHT PHOTOREDOX METHODOLOGIES TOWARDS THE ACTIVATION
OF CARBON-HALOGEN BONDS
Miguel Claros Casielles

Financial Support

The present doctoral thesis has been made possible thanks to funding received from Fundació Privada Cellex and the Severo Ochoa predoctoral grant (SEV-2013-0319).

The thesis work has been developed within the following projects: AEI/MINECO (Severo Ochoa Excellence Accreditation 2014-2018 (SEV-2013-0319) and ERC (648304 — GREENLIGHT_REDCAT).

Fundació Privada
CELLEX


erc
European Research Council


EXCELENCIA
SEVERO
OCHOA




ICIQ
Institute of Chemical
Research of Catalonia

UNIVERSITAT ROVIRA I VIRGILI
DEVELOPMENT OF VISIBLE LIGHT PHOTOREDOX METHODOLOGIES TOWARDS THE ACTIVATION
OF CARBON-HALOGEN BONDS
Miguel Claros Casielles

Curriculum Vitae

Miguel Claros Casielles was born on February 28th, **1991** in Gijón (Asturias, Spain). He studied chemistry at the *University of Oviedo*, obtaining his BSc degree in June **2014**. In September of **2014**, he started his MSc degree in “*Chemistry and Sustainable Development*” at the *University of Oviedo*, under the supervision of Professor Pilar Gamasa Bandrés. During his MSc studies, his research was focused on the “*Development of New Enantiopure Ruthenium(II) Complexes for the Asymmetric Hydrogenation of Ketones*”. He obtained his MSc degree in July **2015**. After that, he spent a period of 4 months expanding this research within the same group. In March **2016** he moved to Tarragona for embarking on his PhD studies under the supervision of Professor Julio Lloret Fillol and Professor Alicia Casitas Montero at the *Institute of Chemical Research of Catalonia*. His research was financially supported with *Fundació Privada Cellex* and *Severo Ochoa* undergraduate fellowship (SEV-203-0319). The PhD results have been communicated at different national and international conferences, such as the Young Researchers Symposium of the RSEQ in Logroño (**2016**), the PhD Day of the ICIQ in Tarragona (**2017** and **2018**) the XXXVI Biennial of the RSEQ in Sitges (**2017**), the XI Edition of the International School of Organometallic Chemistry in San Benedetto del Tronto (Italy, **2017**), the Girona Seminar in Girona (**2018**), the 21st International Symposium on Homogeneous Catalysis in Amsterdam (Netherlands, **2018**), the Photo4Future meeting in Eindhoven (Netherlands, **2018**), the XXXVII Biennial of the RSEQ in San Sebastian (**2019**), the XII International School on Organometallic Chemistry in Castellón (**2019**), the 4th EuCheMS conference on Green and Sustainable Chemistry in Tarragona (**2019**) and the ICIQ RedINTECAT school in Tarragona (**2019**).

UNIVERSITAT ROVIRA I VIRGILI
DEVELOPMENT OF VISIBLE LIGHT PHOTOREDOX METHODOLOGIES TOWARDS THE ACTIVATION
OF CARBON-HALOGEN BONDS
Miguel Claros Casielles

List of Publications

- Miguel Claros, Felix Ungeheuer, Federico Franco, Vlad Martin-Diaconescu, Alicia Casitas and Julio Lloret-Fillol. “*Reductive Cyclization of Unactivated Alkyl Chlorides with Tethered Alkenes under Visible-Light Photoredox Catalysis*”. *Angew. Chem. Int. Ed.* **2019**, 58, 4869 - 4874. (10.1002/anie.201812702).
- Miguel Claros, Alicia Casitas, Julio Lloret-Fillol. “*Visible-Light Reductive Cyclization of Nonactivated Alkyl Chlorides*”. *Synlett* **2019**; 30(13), 1496 - 1507. (10.1055/s-0037-1611878).
- Noufal Kandoth, Miguel Claros, Nuria Rodríguez and Julio Lloret-Fillol. “*Photoinduced Electron-Transfer in Coordination Compounds with First-Row Transition Metals: Fundaments and Catalytic Applications*”. Springer Handbook of Inorganic Photochemistry, Springer.
- Miguel Claros, Felix Ungeheuer, Jordi Aragón Alicia Casitas, Julio Lloret-Fillol. “*Procedure for the Activation of Organic Chloride Compounds and a Catalytic Composition used in the Process*” *European Patent* **2018** (EP3404007A1).

Other publication related to other activities performed during this thesis which is not described in this doctoral dissertation.

- Ignacio Rosa-Pardo, Carla Casadevall, Luciana Schmidt, Miguel Claros, Raquel E. Galian, Julio Lloret-Fillol and Julia Pérez-Prieto. “*The Synergy between the CsPbBr₃ Nanoparticle Surface and the Organic Ligand Becomes Manifest in a Demanding Carbon–Carbon Coupling Reaction*”. *Chem. Commun.*, **2020**, Advance Article (10.1039/D0CC01339K).

UNIVERSITAT ROVIRA I VIRGILI
DEVELOPMENT OF VISIBLE LIGHT PHOTOREDOX METHODOLOGIES TOWARDS THE ACTIVATION
OF CARBON-HALOGEN BONDS
Miguel Claros Casielles

Table of Contents

Preface	25
Summary	27
List of Abbreviations	29
Chapter I: General Introduction	
I.1. Contents	41
I.2. The Starting Point of Photoredox Catalysis	45
I.2. 1 [Ru(bpy) ₃] ²⁺ : The Development of the First Photoredox Catalysts	47
I.2. 2 Early Examples from 70's to 00's	48
I.2. 3 Starting 21 st century	51
I.3. Fundamentals on Photophysical Features	53
I.3. 1 Types of electronic transitions	54
I.3. 2 Selection rules	56
I.3. 3 Deactivation pathways	57
I.3. 4 General Photoredox Catalytic Cycle	59
I.3. 5 Quantification of Excited-State Processes in Photocatalysis	61
I.4. First-Row Transition Metal Photocatalysts	62
I.5. B₁₂-Derivates in Reductive Organic Reactions	67
I.6. References of the Chapter	73
Chapter II: Objectives	83
Chapter III: Photocatalytic Activation of Carbon-Halogen Bonds	
III.1. Contents	91
III.2. State-of-the-art	95
III.2. 1 Early Examples of Activation of <i>Carbon-Halogen</i> Bonds	99
III.3. Results and Discussion	107
III.3. 1 Screening of the Conditions for the Activation of <i>C-Cl</i> Bonds	107

III.3. 2	Photoredox Activation of Halogenated Drugs and Derivatives	110
III.3. 3	Photoredox Activation of Organohalide Pesticides	113
III.3. 4	Photoredox Activation of Alkyl Fluorides	115
III.4.	Conclusions	125
III.5.	Experimental Section	127
III.5. 1	Material and Reagents	127
III.5. 2	Instrumentation	127
III.5. 3	Experimental Procedures	129
III.5. 4	Synthesis of Metal Complexes	130
III.5. 5	Synthesis and Characterization of Substrates	141
III.5. 6	Characterization of Products	142
III.6.	References of the Chapter	145
 Chapter IV: Visible-Light Reductive Cyclizations from non-Activated Alkyl Halides		
IV.1	Contents	153
IV.2	State-of-the-art	157
IV.2.1	Light-Driven Intramolecular Reductive Cyclizations of Alkyl Halides with Pendant Alkenes.	161
IV.3	Results and Discussion	165
IV.3.1	Visible-Light Photoredox Reductive Cyclization of non-Activated Alkyl Bromides with Tethered Alkenes	165
IV.3.2	Visible-Light Photoredox Reductive Cyclization of non-Activated Alkyl Chlorides with Tethered Alkenes	169
IV.3.3	Visible-Light Photoredox Reductive Cyclization of non-Activated Alkyl Chlorides with Tethered Alkynes	185
IV.3.4	Unsuccessful Substrates	188
IV.4	Conclusions	189
IV.5	Experimental Section	191
IV.5.1	Material and Reagents	191
IV.5.2	Instrumentation	191
IV.5.3	Experimental Procedures	194

IV.5.4	Synthesis and Characterization of Metal Complexes	197
IV.5.5	Synthesis and Characterization of Substrates	201
IV.5.6	Synthesis and Characterization of Products	244
IV.6	References of the Chapter	261
Chapter V: Mechanistic Understanding of Visible-Light Activation of Carbon-Chloride Bonds		
V.1	Contents	271
V.2	State-of-the-art	277
V.2.1	Two-Electron Redox Mechanism	278
V.2.2	Single-Electron Mechanism	281
V.2.3	Photoredox Coupled Mechanism	285
V.3	Results and Discussion	293
V.3.1	Detection of Carbon-Centered Radical Intermediates	293
V.3.2	Detection of the Ni-Active Species	298
V.3.3	Exploring the Reaction between Ni-Active Compound and Alkyl-Chlorides.	304
V.3.4	DPA-based System	310
V.3.5	Mechanism Proposal	317
V.4	Conclusions	319
V.5	Experimental Section	321
V.5.1	Material and Reagents	321
V.5.2	Instrumentation	321
V.5.3	Synthesis of Metal Complexes	323
V.5.4	Characterization of Products	324
V.6	References of the Chapter	329
Chapter VI:	General Conclusions	335

UNIVERSITAT ROVIRA I VIRGILI
DEVELOPMENT OF VISIBLE LIGHT PHOTOREDOX METHODOLOGIES TOWARDS THE ACTIVATION
OF CARBON-HALOGEN BONDS
Miguel Claros Casielles

Preface

The work presented in this dissertation has been performed at the Institute of Chemical Research of Catalonia (*ICIQ*), during the period from March 2016 until April 2020 under the supervision of Professor Julio Lloret Fillol and Professor Alicia Casitas Montero. This thesis is divided into six sections: a general introduction, the aims of the thesis, three research chapters and a chapter in which the overall conclusions of the work are presented. Each of the research chapters includes a brief introduction on the topic, followed by the collected results and their discussion, the main conclusions, and finally a detailed experimental section. References and their numbering are independently organized by chapters.

Summary

Visible-light photoredox catalysis has opened a venue of more sustainable $C-C$ and $C-Heteroatom$ bond-forming reactions. In this regard, organic halides are versatile and widely used electrophilic coupling partners in bond-forming events as they can be activated through *single electron transfer (SET)* reactions from photosensitizers. In this line, the moderate redox potential in the ground state of commonly employed photosensitizers, such as organic dyes (i.e. eosyn Y, rhodamine B) and Ru^{II} and Ir^{III} polypyridyl complexes, enables only the cleavage of activated or weak $C-Halogen$ bonds, mostly aryl and alkyl iodides or activated alkyl bromides. Continuous development of novel photoredox catalysts that provide higher reducing power has expanded the redox-potential window facilitating the cleavage of alkyl bromides via *SET* processes. König and co-workers have shown that the less reactive and more accessible aryl chlorides, which present extremely negative reduction potentials, can be functionalized by using the energy of two photons for each catalytic cycle, or the reducing power of lanthanides. Alternatively, the synergistic merger of a photosensitizer that reduces the oxidation state of a coordination metal complex has enabled, for instance, the employment of alkyl bromides in Csp^3-Csp^3 bond-forming reactions and more recently, also the carboxylation of aryl chlorides.

Chloroalkanes are superior to other electrophilic reagents (i.e. bromoalkanes and iodoalkanes) used in many organic transformations such as in bond-forming reactions because they are commercially available, economic and bench stable feedstocks. However, they are at the edge of our capability to activate strong chemical bonds with high selectivity and under mild reaction conditions. Indeed, owing to the chemical inertness of Csp^3-Cl bonds, the catalytic functionalization of alkyl chlorides mediated by transition-metal complexes remains so far underdeveloped.

The work presented in this doctoral dissertation shows an efficient and selective metallaphotoredox system based on earth-abundant metals (Cu, Co, Ni) that enables the activation of Csp^3-X bonds using visible-light as source of energy. The portfolio of metallaphotoredox catalytic systems aiming at the cleavage of strong σ -bonds can be broadened through rational ligand design. Earth-abundant transition-metal octahedral complexes with tetra- and pentadentate ligands based on aminopyridine scaffolds lead to highly active catalysts for functionalizing strong Csp^3-X bonds.

The combination of spectroscopical (UV-Vis, EPR, NMR) with electrochemical techniques (CV, SEC) allowed us to shine light into the mechanism. Upon light irradiation a photoexcitable copper catalyst quenched by reaction with an alkyl amine acting as sacrificial electron donor (*ED*), undergoes a *SET* to the aminopyridine-based catalyst (Co or Ni) forming a transient low-valent Co or Ni catalyst. The photogenerated low-valent species reacts with the halide substrate forming the carbon-centered radical which is quenched by reaction with the solvent. This novel reactivity has been applied towards the development of a sustainable methodology for hydro-dehalogenation reactions of alkyl chlorides and fluorides and the intramolecular reductive cyclizations of a wide range of alkyl chlorides. Our findings contribute in a broad sense to the field of catalysis and chemical reactivity since we have introduced a new paradigm in using neutral multidentate nitrogen-based ligands to enhance the reactivity of low-valent metal complexes. We envision that the new conceptual ligand design introduced herein will trigger the development of more sustainable catalytic transformations that aims at achieving novel chemical reactivity.

List of Abbreviations

In this doctoral thesis, the abbreviations and acronyms most commonly used in organic chemistry are based on the recommendations of the ACS “Guidelines for authors” which can be found at <https://pubs.acs.org/doi/10.1021/bk-2006-STYG.ch010>

General Abbreviations

[]	Concentration
Δ	Field Splitting
Å	Angstrom(s)
aq	Aqueous
atm	atmosphere(s)
°C	degrees Celsius
cal	Calorie
calcd	Calculated
Cat	Catalyst
Conv	Conversion
Deact	Deactivated
eq	Equation, equivalent
FT	Fourier Transform
FC	Frack-Condon
Hal	Halogen
Het	Heteroatom
HRP	Horseradish Peroxidase
(P)JT	(pseudo)Jahn Teller
LED	Light Emitting Diode
Ln	Lanthanide

max	Maximum
MCR	Methyl-Coenzyme Reductase
min	minute(s); minimum
mM	millimolar (millimoles per liter)
MW	molecular weight
N	normal (equivalents per liter)
PC	Photocatalyst
rt	Room Temperature
s	second(s), solvent
SM	Starting Material
SPS	Solvent Purification System
SV	Stern Volmer
t	time
T	temperature
Vol	Volume
wt	Weight

Characterization Techniques

Anal	Combustion Elemental Analysis
AIS	Automatic Identification System
Bp	Boiling Point
CI	Chemical Ionization
EI	Electron Impact
EPR	Electron Paramagnetic Resonance
ESR	Electron Spin Resonance
ESI	Electrospray Ionization
FAB	Fast Atom Bombardment
FID	Flame Ionization Detector
GC	Gas Chromatography

HPLC	High-Performance Liquid Chromatography
HRMS	High-Resolution Mass Spectrometry
IR	Infrared
MALDI	Matrix-Assisted Laser Desorption Ionization
MCD	Magnetic Circular Dichroism
mp	Melting Point
MS	Mass Spectrometry
m/z	mass-to-charge ratio
ORD	Optical Rotary Dispersion
TLC	Thin-Layer Chromatography

NMR

Nuclear Magnetic Resonance

δ	Chemical shift in parts per million downfield from tetramethylsilane
<i>J</i>	Coupling Constant (in NMR spectrometry)
ppm	part(s) per million
br	Broad
s	Singlet
d	Doublet
dd	Doublet of doublets
ddd	Double doublet of doublets
ddt	Double doublet of triplets
t	Triplet
td	Triplet of doublets
tdd	Triplet doublet of doublets
q	Quartet
m	Multiplet

UV-Vis

Ultraviolet-Visible spectroscopy

τ	Lifetime
Abs	Absorption
cm⁻¹	Wavenumber(s)
Fl	Fluorescence
NR	Non-radiative decay
Ph	Phosphorescence

CV

Cyclic Voltammetry

Fc	Ferrocene
NHE	Normal Hydrogen Electrode
OTTLE	Optically Transparent Thin-Layer Electrode
Redox	Reduction–Oxidation
SCE	Saturated Calomel Electrode
SEC	Spectroelectrochemistry

Theoretical Calculations

AO	Atomic Orbital
B3LYP	3-parameter hybrid Becke exchange/ Lee–Yang–Parr correlation functional
BDE	Bond Dissociation Energy
DFT	Density Functional Theory
HF	Hartree–Fock
HOMO	Highest Occupied Molecular Orbital
LUMO	Lowest Unoccupied Molecular Orbital
MO	Molecular Orbital
SOMO	Single-Occupied Molecular Orbital
TS	Transition State

Mechanistic Considerations

A	Acceptor
CHAA	Concerted Halogen-Atom Abstraction
CT	Charge Transfer
D	Donor
ED	Electron Donor
EDA	Electron Donor-Acceptor
ET	Electron Transfer
HAA	Halogen Atom Abstraction
HAT	Hydrogen Atom Transfer
HC	Homolytic Cleavage
IC	Internal Conversion
ISC	InterSystem Crossing
LC	Ligand Centered
LMCT	Ligand to Metal Charge Transfer
MC	Metal-centered Charge transfer
MLCT	Metal-to-Ligand Charge Transfer
Nu	Nucleophile
OA	Oxidative Addition
OSCT	Outer-Sphere Charge Transfer
PET	Photoinduced Electron Transfer
Q	Quencher
RE	Reductive Elimination
S₀	Single Ground State
S₁	Single Excited State
SET	Single Electron Transfer
S_N1	Unimolecular Nucleophilic Substitution
S_N2	Bimolecular Nucleophilic Substitution
T₁	Triplet Excited State

TOF Time-Of-Flight; turnover frequency
TON Turnover Number

Organic Chemistry Abbreviations

Ac Acetyl
AcOH Acetic Acid
AcrH₂ 10-methyl-9,10-dihydroacridine
AdoCbl 5'-deoxy-5'-adenosylcobalamin
AIBN 2,2'-azobisisobutyronitrile
Ar Aryl
BNAH 1-Benzyl-1,4-dihydronicotinamide
Boc tert-butoxycarbonyl
Bpin Bis(pinacolato)diboron
***n*-Bu** normal (primary) butyl
***t*-Bu** tert-butyl
CHD 1,4-Cyclohexadiene
DABCO 1,4-diazabicyclo[2.2.2]octanedansyl 5-(dimethylamino)- 1-
naphthalenesulfonyl
dba Dibenzylideneacetone
DCM Dichloromethane
DDE Dichlorodiphenyldichloroethylene
DDT bis(4-chlorophenyl)-2,2,2-trichloroethane
DIBAL-H Diisobutylaluminum Hydride
DIPEA Diisopropyl ethyl amine
DMAP 4-(N,N-dimethylamino)pyridine
DME 1,2-dimethoxyethane
DMF Dimethylformamide
DMM Dimethyl Methoxy
DMN 1,5-dimethoxynaphthalene

DMSO	Dimethyl Sulfoxide
DPA	Di-(2-pyridyl)amine
EDC	N-(3-Dimethylaminopropyl)-N'-ethylcarbodiimide
EDTA	ethylenediaminetetraacetic acid
Et	Ethyl
Et₂O	Diethylether
Et₃N	Triethylamine
EtOAc	Ethyl acetate
EtOH	Ethanol
HCB	Hexachlorobenzene
HMPA	Hexamethylphosphoric Triamide (hexamethylphosphoramide)
LDA	Lithium Diisopropylamide
MCP	dimethyl- bis(pyridinylmethyl)cyclohexane-1,2-diamine
Me	Methyl
MeCbl	Methylcobalamin
MeCN	Acetonitrile
MeOH	Methanol
MOM	Methoxymethyl
NBS	N-bromosuccinimide
NCS	N-chlorosuccinimide
NHC	N-heterocyclic Carbene
OTf	Triflate
Ph	Phenyl
Phen	1,10-fenantroline
iPr	Isopropyl
iPrOH	Isopropanol
PTFE	Polytetrafluoroethylene
PTH	N-phenylphenothiazine
Py	Pyridine
TBABr	Tetrabutylammonium Bromide

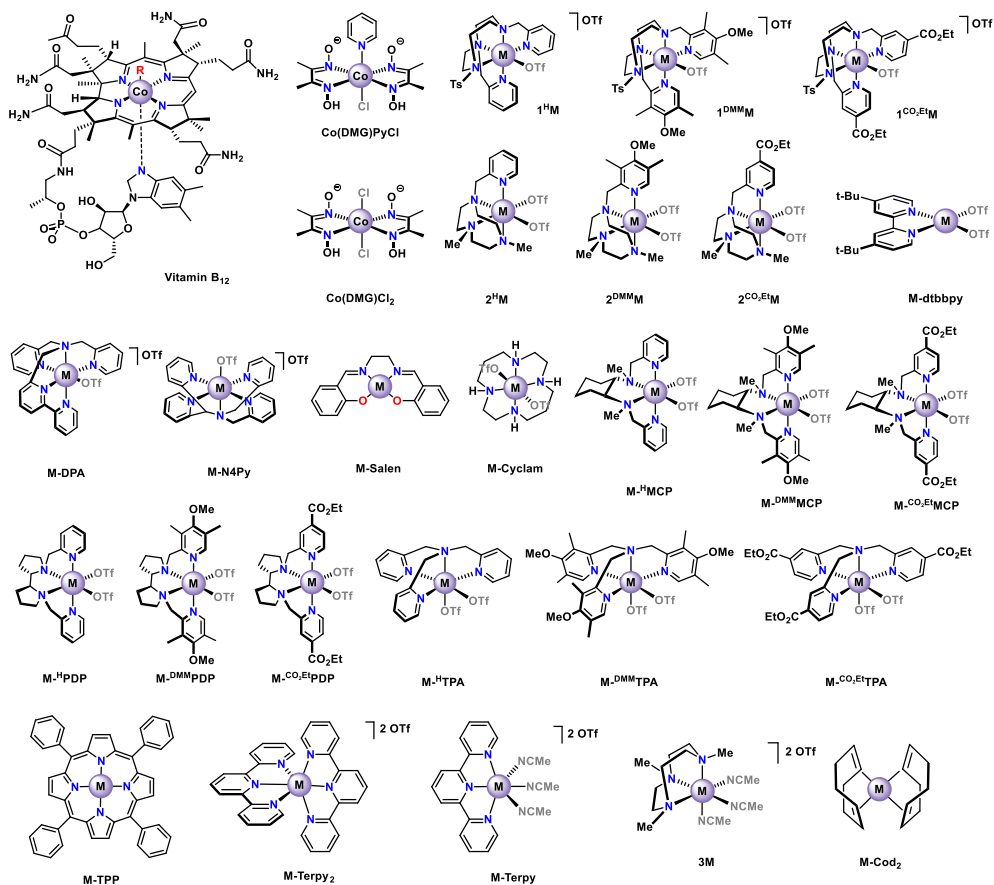
TBACl	Tetrabutylammonium Chloride
TBAF	Tetrabutylammonium Fluoride
TBS	Tert-Butyldimethylsilyl
TDAE	(tetrakis(dimethylamino)ethylene)
TEMPO	2,2,6,6-tetramethylpiperidin-1-oxyl
THF	Tetrahydrofuran
TMS	Trimethylsilyl; Tetramethylsilane
Ts	<i>p</i> -toluenesulfonyl (tosyl)
TTMSS	tris(trimethylsilyl)silane

Ligands

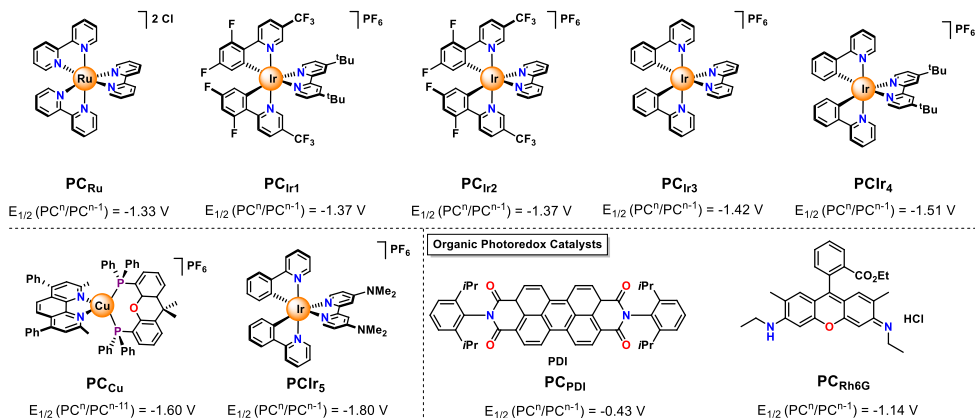
Acac	Acetylacetonate
bpy	2,2'-bipyridyl
Cod	1,5-Cyclooctadiene
DMG	Dimethylglyoxime
dppf	Bis(diphenylphosphino)ferrocene
dppm	Bis(diphenylphosphanyl)methane
dtbbpy	Ditertbutylbipyridine
Glyme	1,2-dimethoxyethane
N4Py	1,1-di(pyridin-2-yl)-N,N-bis(pyridin-2-ylmethyl)methanamine
PDP	dimethyl-bis(pyridin-2-ylmethyl)cyclohexane-1,2-diamine
Tacn	triazacyclononane
Terpy	Terpyridine
TPA	Tris(2-pyridylmethyl)amine
TPP	Tetraphenylporphyrin

Structures and Abbreviations of the Catalysts

Aminopyridine-Based Catalysts

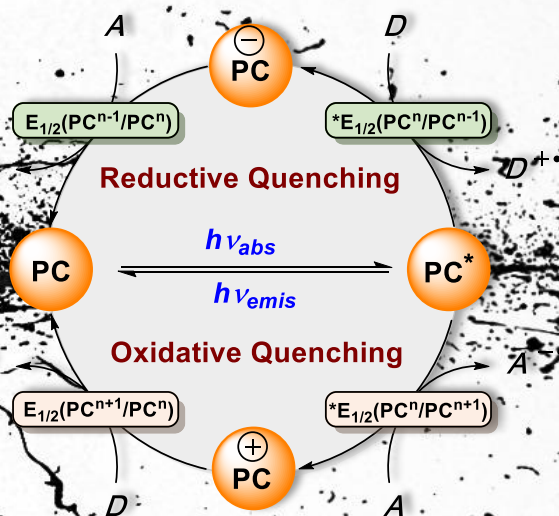


Photoredox Catalysts



UNIVERSITAT ROVIRA I VIRGILI
DEVELOPMENT OF VISIBLE LIGHT PHOTOREDOX METHODOLOGIES TOWARDS THE ACTIVATION
OF CARBON-HALOGEN BONDS
Miguel Claros Casielles

Chapter I



General Introduction

UNIVERSITAT ROVIRA I VIRGILI
DEVELOPMENT OF VISIBLE LIGHT PHOTOREDOX METHODOLOGIES TOWARDS THE ACTIVATION
OF CARBON-HALOGEN BONDS
Miguel Claros Casielles

I.1.	Contents	
I.2.	The Starting Point of Photoredox Catalysis	45
I.2. 1	[Ru(bpy) ₃] ²⁺ : The Development of the First Photoredox Catalysts	47
I.2. 2	Early Examples from 70's to 00's	48
I.2. 3	Starting 21 st century	51
I.3.	Fundamentals on Photophysical Features	53
I.3. 1	Types of electronic transitions	54
I.3. 2	Selection rules.....	56
I.3. 3	Deactivation pathways	57
I.3. 4	General Photoredox Catalytic Cycle.....	59
I.3. 5	Quantification of Excited-State Processes in Photocatalysis	61
I.4.	First-Row Transition Metal Photocatalysts	62
I.5.	B₁₂-Derivates in Reductive Organic Reactions	67
I.6.	References of the Chapter	73

Figure I.1 Ciamician's reaction for the photocoupling of ketones to form diols ..	45
Figure I.2 Ciamician's intramolecular [2+2] cycloaddition and photochemical disproportionation of 2-nitrobenzaldehyde	45
Figure I.3 Simplified representation of the electrons in the HOMO of an irradiated molecule going from the singlet ground state to the singlet and triplet excited state and then, the deactivation to the initial singlet ground state.....	46
Figure I.4 Simplified potential energy surface diagram for $[\text{Ru}(\text{bpy})_3]^{2+}$ excited states	47
Figure I.5 Kellogg's photoreduction strategy of phenacyl sulfonium salts.....	48
Figure I.6 Pac's photoreduction of activated olefins procedure with BNAH	49
Figure I.7 Pac's photosensitized reductions of carbonyl compounds (top), and Willner's reduction of activated ketones (bottom)	50
Figure I.8 Photooxidation of carbinols to aldehydes via visible-light photoredox catalysis with $[\text{Ru}(\text{bpy})_3]\text{Cl}_2$	50
Figure I.9 Proposed mechanism for copper based Sonogashira type coupling	51
Figure I.10 Light-promoted copper-free Sonogashira coupling reaction	52
Figure I.11 Papers published per year in the field of organic photoredox catalysis.	52
Figure I.12 Recent photoredox transformation for organic synthesis via reductive (green) or oxidative (orange) $[\text{Ru}(\text{bpy})_3]^{2+}$ quenching cycles	53
Figure I.13 Representation of molecular orbital diagram of an octahedral complex of a transition metal and its field splitting with ligands	55
Figure I.14 General Jablonski diagram ($h\nu_1$ = photon absorption, $h\nu_2$ = fluorescence, $h\nu_3$ = phosphorescence)	57

Figure I.15 General photocatalytic cycle including reductive and oxidative electron-transfer quenching processes from the photoexcited state (D and A stands for donor and acceptor molecules) 59

Figure I.16 Schematic representation of ground states and excited states redox potentials and its connection with E_{00} 61

Figure I.17 Simplified Jablonski diagram showing photoexcitation dynamics and associated structural changes occurring in Cu^{I} homoleptic complexes between the ground state and MLCT excited states (bottom) 64

Figure I.18 General caption for heteroleptic $[\text{Cu}(\text{N}^{\wedge}\text{N})(\text{P}^{\wedge}\text{P})]$ (left) and homoleptic $[\text{Cu}(\text{N}^{\wedge}\text{N})_2]$ photoredox catalysts (top). 65

Figure I.19 The use of PC_{Cu} in reductive and oxidative electron transfer pathway and its molecular structure together with H_2 evolving molecular catalysts, FeCat 66

Figure I.20 Structure (left) and proposed mechanism of B_{12} derivatives (center)⁹⁷ and Ni-corphin F_{430} (right)..... 68

Figure I.21 Reactivity of heterogeneous and hybrid B_{12} - TiO_2 catalysts for reductive transformations in alcoholic solvents under UV-light irradiation 69

Figure I.22 Light-driven decarboxyolefination of carboxylic acids catalyzed by a dual Ir/Co catalytic system 70

Figure I.23 Aminopyridine-cobalt complexes used in water reduction (left) and proposed mechanism for water reduction catalyzed by 2^{X}Co complexes (right)... 71

Figure I.24 Proposed mechanistic scenarios for the photoreduction of aromatic ketones and aldehydes 71

UNIVERSITAT ROVIRA I VIRGILI
DEVELOPMENT OF VISIBLE LIGHT PHOTOREDOX METHODOLOGIES TOWARDS THE ACTIVATION
OF CARBON-HALOGEN BONDS
Miguel Claros Casielles

I.2. The Starting Point of Photoredox Catalysis.

Visible-light has been used in synthetic chemistry since the early 20th century when the Italian photochemist Giacomo Ciamician and his collaborator Paul Silber, inspired by the photosynthesis in green plants, studied the exposition of chemicals to sunlight on a terrace of the University of Bologna.¹ Among the different findings, the so-called *Ciamician's reaction* consists in the reductive photocoupling of ketones to the formation of 1,2-diols (**Figure I.1**).² In the following years, they showed the versatility of the use of sunlight to drive reactions, reporting the intramolecular [2+2] cycloaddition of (-)-carvone and the photochemical disproportionation of 2-nitrobenzaldehyde (**Figure I.2**).³

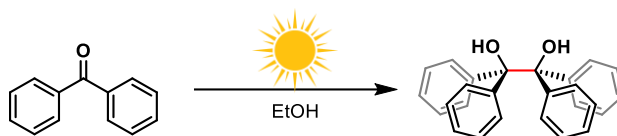


Figure I.1 Ciamician's reaction for the photocoupling of ketones to form diols.

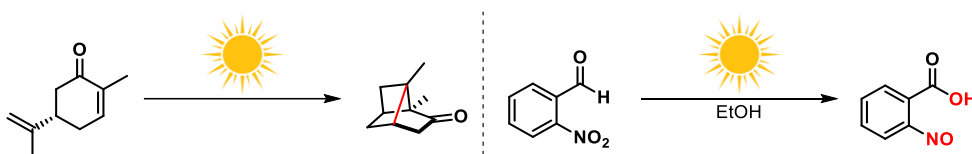


Figure I.2 Ciamician's intramolecular [2+2] cycloaddition and photochemical disproportionation of 2-nitrobenzaldehyde.

These initial studies reported by Ciamician, Silber and co-workers can be considered the starting point of the use of light as a driving force to produce synthetically useful organic transformations. Since then, photochemical *cis-trans* isomerizations,^{4,5} fragmentations,⁶⁻⁸ reductive additions,^{9,10} electrocyclic reactions,¹¹ sigmatropic reactions¹² and cycloaddition reactions¹³ were reported.

Photochemical transformations relies on the absorption of photons by a molecule that promotes a reorganization of the electrons. As a consequence, the molecule reaches an excited state, which is more reactive than the ground state. The

deactivation of these excited states could proceed by unimolecular processes corresponding to classical photochemical transformations such as isomerization or rearrangements or by interaction with other species (bimolecular processes) (**Figure I.3**). In this last case, the excited state can be deactivated mainly by an energy-transfer¹⁴ or by an electron-transfer processes, concepts that will be discussed throughout this chapter.

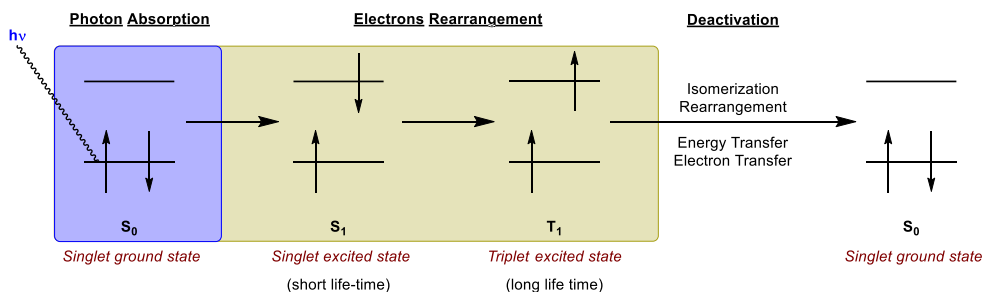


Figure I.3 Simplified representation of the electrons in the HOMO of an irradiated molecule going from the singlet ground state to the singlet and triplet excited state and then, the deactivation to the initial singlet ground state.

Although, the reactivity of excited states can be controlled to perform useful chemical transformations, it is limited to the intrinsic properties and direct reactivity of substrates with light. In this regard, a way to decouple the light absorption and direct reactivity of excited states with light is through the use of a photocatalysts (PC), which are molecules that can engage in catalytic cycles triggered by the absorption of photons. Followed by the transfer of the excited state's energy *via* energy transfer mechanisms or by engaging photoinduced electron-transfer processes in bimolecular processes. This versatility is most likely behind the success of photocatalysis strategies in the design of new light-induced chemical reactions.¹⁵⁻¹⁷ The operative cycle of photoredox catalysts involves the absorption of light by allowing electronic transitions of a PC which produces an excited state that is more reactive than the ground state. Fundamental concepts of photocatalysis will be covered in more detail throughout this introductory chapter.

I.2.1 $[\text{Ru}(\text{bpy})_3]^{2+}$: The Development of the First Photoredox Catalysts.

One of the photocatalysts most widely used since the beginning of photoredox catalysis has been the tris(bipyridine)ruthenium(II) complex ($[\text{Ru}(\text{bpy})_3]^{2+}$) due to its chemically robustness and remarkable configurational stability.¹⁸⁻²⁴ $[\text{Ru}(\text{bpy})_3]^{2+}$ is a d^6 system with bipyridine ligands possessing σ -donor orbitals localized on the nitrogen atoms and π -donor and π -acceptor orbitals delocalized on the aromatic rings. The absorption of a visible photon ($\lambda_{\text{max}} = 452$ nm) by $[\text{Ru}(\text{bpy})_3]^{2+}$ moves an electron from a metal centered (t_{2g} or π_M) to a ligand centered orbital (π^*), so called *metal-to-ligand charge transfer (MLCT)*. The formed single excited state ($^1\text{MLCT}$) undergoes intersystem crossing (*ISC*) yielding a long-lived luminescent triplet excited state $[\text{Ru}(\text{bpy})_3]^{2+*}$ ($^3\text{MLCT}$). This electronic structure is simultaneously both an oxidant and a reductant and consequently the $[\text{Ru}(\text{bpy})_3]^{2+}$ $^3\text{MLCT}$ can undergo both types of bimolecular electron transfer processes.¹⁶ In the absence of any second electron donating or accepting molecule the populated long-lived $^3\text{MLCT}$ excited state decays back to the ground state by luminescence or *via* other non-radiative process (**Figure I.4**).

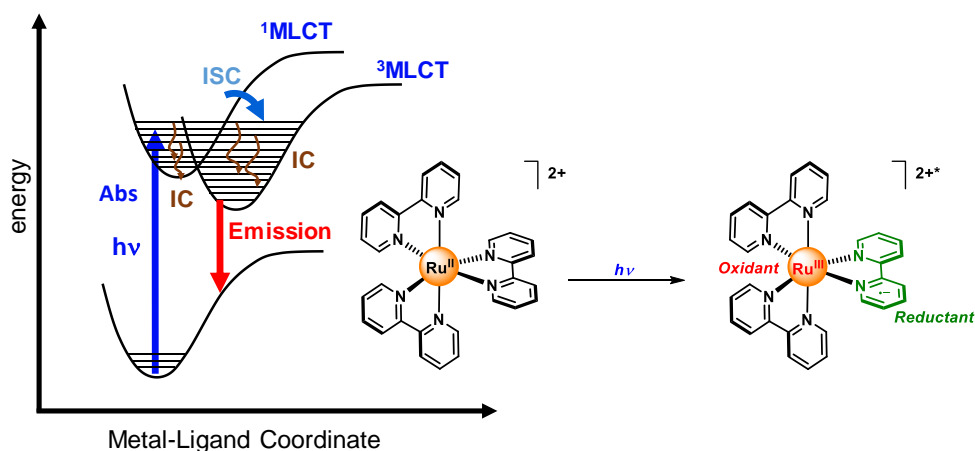


Figure I.4 Simplified potential energy surface diagram for $[\text{Ru}(\text{bpy})_3]^{2+}$ excited states.

1.2.2 Early Examples from 70's to 00's.

In 1978, Kellogg's group reported one of the first examples of photoinduced redox processes.²⁵ In this study, $[\text{Ru}(\text{bpy})_3]\text{Cl}_2$ was employed as photosensitizer to mediate the reduction of phenacylsulphonium salts by 1,4-dihydropyridine using visible-light as source of energy (**Figure I.5**). The reaction achieved complete conversion under room-light irradiation after 48 h in the presence of $[\text{Ru}(\text{bpy})_3]\text{Cl}_2$. The necessity of light and the photosensitizer was illustrated by performing control experiments performed. In the absence of light and photosensitizer, no conversion was observed after 72 h. The light-induced *single-electron transfer (SET)* from the excited dye was also effective in the reduction of related substrates such as ammonium or phosphonium salts, but not for the reduction of nitrobenzyl halides.²⁶

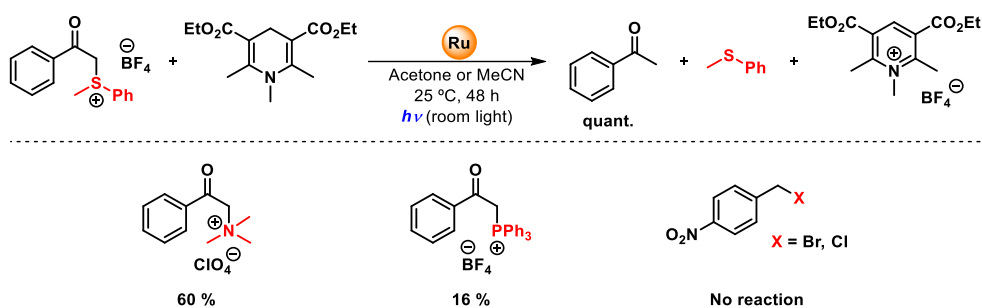


Figure I.5 Kellogg's photoreduction strategy of phenacyl sulphonium salts.

A few years later, Pac and co-workers extended the reactivity to the reduction of activated olefins.^{27,28} In the proposed mechanism, the $[\text{Ru}^{\text{II}}]^{2+}$ excited state is quenched by the sacrificial electron donor (1-benzyl-1,4-dihydronicotinamide, *BNAH*) producing a reduced $[\text{Ru}^{\text{I}}]$ intermediate. Then, the $[\text{Ru}^{\text{I}}]$ undergoes a *SET* reaction to the olefin forming a carbon centered radical intermediate that is further reduced and protonated to afford the final reduced product (**Figure I.6**).

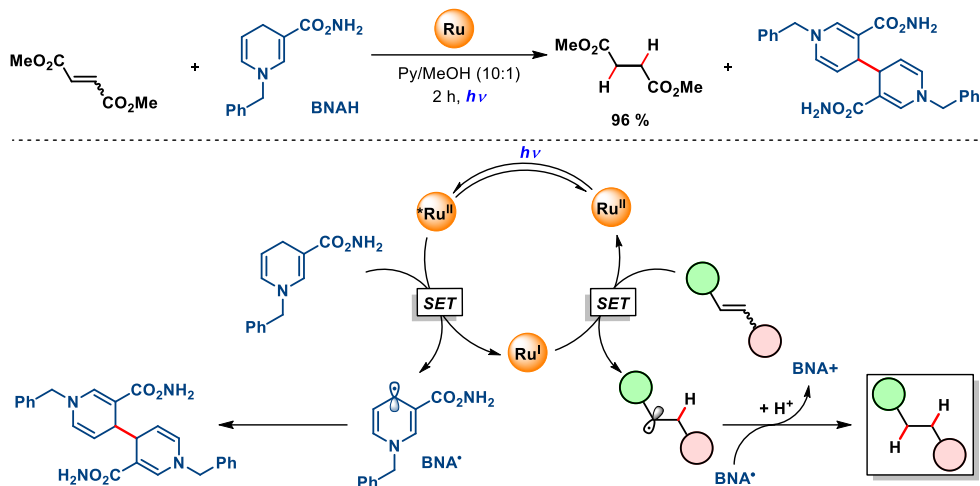


Figure I.6 Pac's photoreduction of activated olefins procedure with BNAH.

In a related work, the same group demonstrated the reactivity of aromatic carbonyls with *BNAH* under similar reaction conditions.²⁹ In the case of bis(2-pyridyl)ketone, the easiest ketone to reduce, the corresponding alcohol was formed; whereas using aromatic aldehydes, the secondary alcohol coupled with the hydronicotinamide was formed (Figure I.7, top).²⁹ In this case, the mechanism is similar to the one proposed for the reduction of olefins. First, the ketone is reduced by the excited $[\text{Ru}(\text{bpy})_3]\text{Cl}_2$ to form the ketyl radical which is then reduced or reacts with the *BNAH*. In 1990, Willner and co-workers reported an analogous approach for the reduction of ethyl benzoylformate and diphenylethanedione by the reductive quenching of the *in situ* photogenerated excited state $[\text{Ru}(\text{bpy})_3]^+$ with Et_3N (Figure I.7, bottom).³⁰

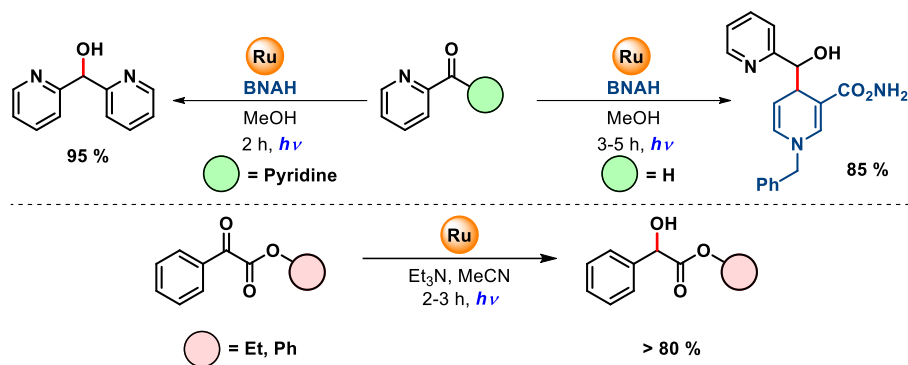


Figure I.7 Pac's photosensitized reductions of carbonyl compounds (top), and Willner's reduction of activated ketones (bottom).

Besides photoinduced reductions, the ruthenium $[\text{Ru}(\text{bpy})_3]\text{Cl}_2$ photocatalyst also promotes oxidative quenching as Deronzier and co-workers demonstrated in 1984 and 1987 for the photooxidation of aryldiazonium salts to phenanthrene derivatives³¹ and the oxidation of carbinols to aldehydes,³² respectively (**Figure I.8**).

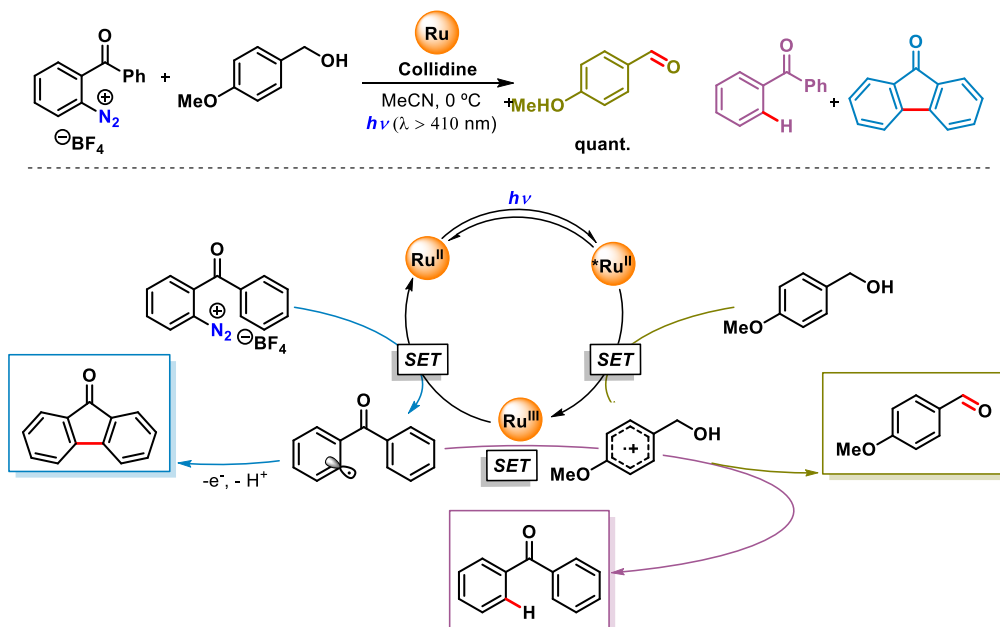


Figure I.8 Photooxidation of carbinols to aldehydes via visible-light photoredox catalysis with $[\text{Ru}(\text{bpy})_3]\text{Cl}_2$.

I.2.3 Beginning of the 21st century.

Despite the remarkable potential of photoredox catalysis, it was not until the middle of the first decade of the 21st century when the field started to flourish. Inspired by previous works from research groups like Balzani's and Creutz's on water dissociation,^{33,34} and Ziesel's and Willner's on CO₂ photoreduction,^{35,36} Osawa and co-workers reported a copper-free Sonogashira-type reaction under visible-light irradiation using [Ru(bpy)₃](PF₆)₂ as photocatalyst.³⁷ In that work, ruthenium photocatalyst has been suggested to take part in the formation of Pd⁰ species and during the oxidative addition step. Typical procedures for Pd-catalyzed *Sonogashira coupling* reactions involves the use of Cu^I salts as co-catalyst, amines as base and equimolar phosphine ligands for palladium catalyst (**Figure I.9**).

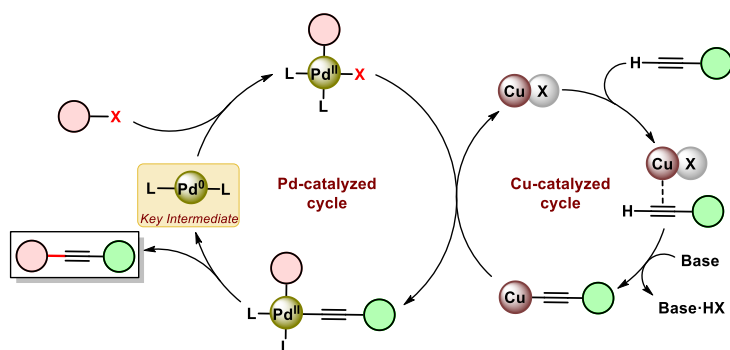


Figure I.9 Proposed mechanism for copper based *Sonogashira type coupling*.³⁸

Following the mechanism depicted in **Figure I.9**, the formation of a Pd⁰-acetylide intermediate capable to undergo an oxidative addition with the arylhalide seems to be key in the methodology.³⁸ In an unprecedented approach, they envisaged that the Pd⁰ intermediate could be also formed photochemically.³⁷ They noticed that the photocatalytic transformation using [Ru(bpy)₃]Cl₂ not only formed the desired product but also it was formed in higher yield than under dark conditions (from 11 to 91 % of yield), proving that a photoredox *Sonogashira* reaction could replace the typical copper-based *Sonogashira* procedure (**Figure I.10**).

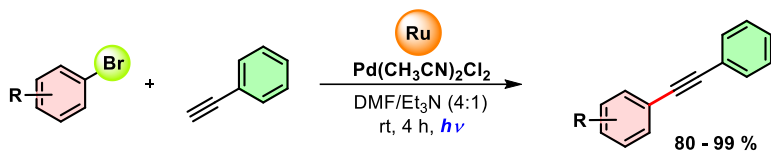


Figure I.10 Light-promoted copper-free Sonogashira coupling reaction.

Since 2008, a dramatic increase in the application of photoredox transformations for organic synthesis has been developed thanks to the studies of MacMillan³⁹⁻⁴¹, Yoon,⁴²⁻⁴⁵ Stephenson,⁴⁶⁻⁵² Koike and Akita,⁵³ Gagné,⁵⁴ Zeitler⁵⁵ and Rueping (Figure I.11).⁵⁶ From these initial studies, historically organic transformations have been developed under photocatalytic conditions. For example, α -amination of aldehydes, by Koike and Akita, and the [2+2] and [3+2] cycloadditions by Yoon and co-workers. Furthermore, the aza-Henry reaction for the formation of C–C bonds from tertiary amines and nitroalkanes,⁵⁰ the Mannich reaction for the condensation of non-enolizable aldehydes or amines and carbonyls⁵⁶ or the Apple reaction for the conversion of alcohols into halides,^{51,57} were developed under photocatalytic conditions (Figure I.12).

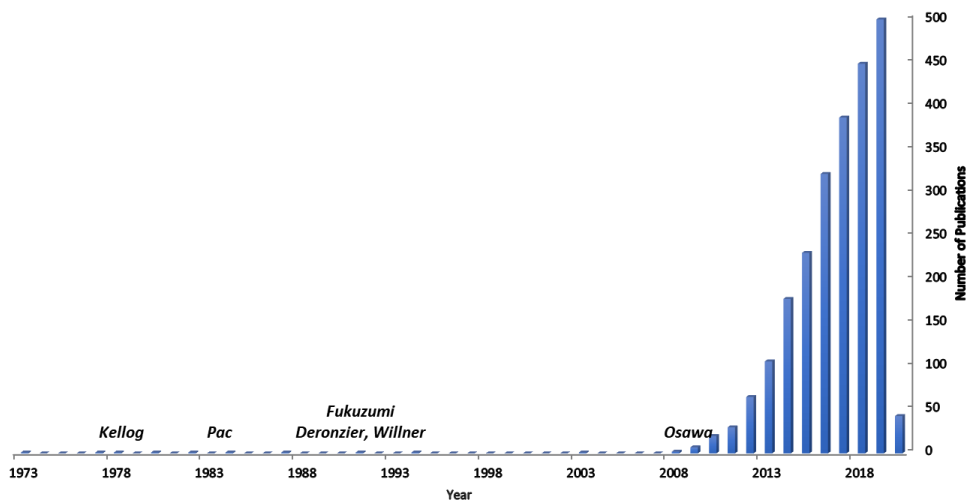


Figure I.11 Papers published per year in the field of organic photoredox catalysis.

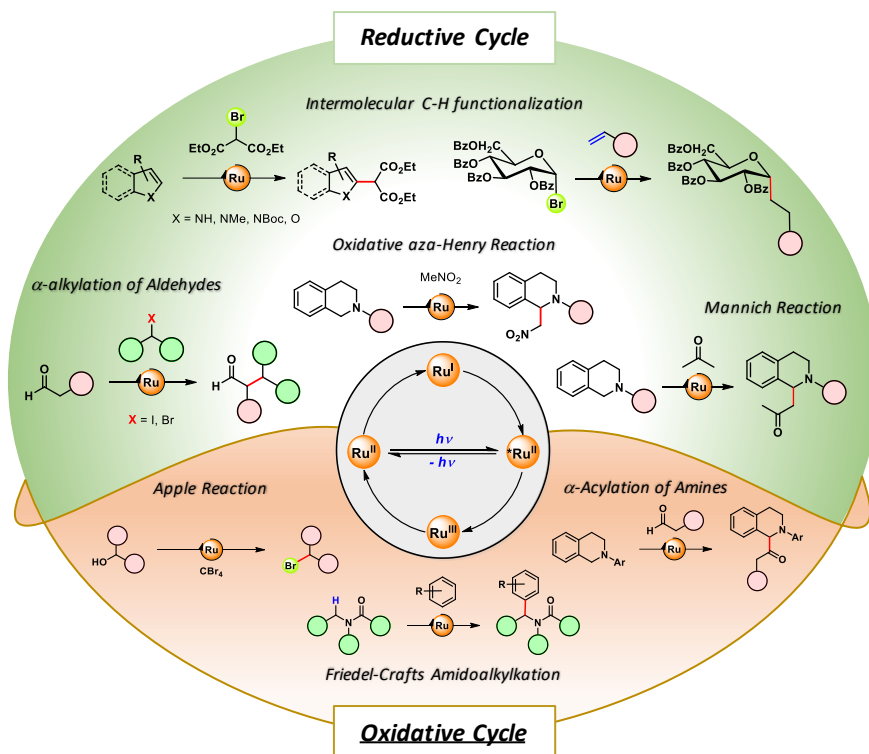


Figure I.12 Recent photoredox transformation for organic synthesis via reductive (green) or oxidative (orange) $[Ru(bpy)_3]^{2+}$ quenching cycles.^{39,48,50,51,54,56,58,59}

1.3. Fundamentals on Photophysical Features.

The basis of photoredox catalysis follows the absorption of a photon by a catalyst in UV or visible range and the promotion of an electron from its ground state energy level to an excited energy level. The essential photophysical features involved in an octahedral transition metal complex upon light excitation can be followed by the molecular orbital description and Jablonsky diagram. Simplified *molecular orbital (MO)* diagram (**Figure I.13**) can be used to rationalize the electronic structure of photoredox catalysts (PCs). As shown in **Figure I.13**, for octahedral metallorganic complex possible σ -donor, π -donor, and π -acceptor orbitals are included. In that, the subscripts indicate whether the MO is predominantly metal (*M*) or ligand (*L*) centered in character. The degenerated *d*-

orbitals of the free metal ion combine with the bonding orbitals of the ligands (σ_L and π_L), destabilizing and splitting into two sets with an energy difference (orbitals with t_{2g} and e_g symmetry). As a result, the π_M and σ_M^* orbitals in the center of the *MO* diagram are predominantly metal *d*-orbitals with t_{2g} and e_g symmetry respectively, being lower in energy than the π_L^* orbitals of the metal complex. The magnitude of the *d*-orbitals destabilization and ligand *field splitting* (Δ) depends mainly on the electronic configuration of the metal. In first-row transition metal complexes, Δ is smaller than for second and third-row transition metals. Nonetheless, the nature of the ligands surrounding the metal ion importantly affects the field splitting. Therefore, according to the spectrochemical series, ligands producing the most splitting are those that can engage in metal to ligand back-bonding. The spectrochemical series is an empirically-derived list of ligands ordered by the size of Δ ($I^- < Br^- < S^{2-} < SCN^-(S\text{-bonded}) < Cl^- < NO_3^- < N_3^- < F^- < OH^- < C_2O_4^{2-} < H_2O < NCS^-(N\text{-bonded}) < CH_3CN < py < NH_3 < en < 2,2'\text{-bipyridine} < phen < NO_2^- < PPh_3 < CN^- < CO$).⁶⁰

1.3.1 Types of Electronic Transitions.

The light absorption in a UV-Vis range promotes the electronic excitation from the lowest electronic state (ground state) to a state higher in energy (excited state) in their different excited vibrational states. This light absorption does not generate any nuclei position change and follows the semi-classical *Frank-Condon* principle being in the range of 10^{-15} s. At lower energy, it is to be assumed that the transitions occur from *highest occupied molecular orbital (HOMO)* (t_{2g} , π_M) to *lowest unoccupied molecular orbital (LUMO)* (e_g , σ_M). This transition is called *metal centered (MC)* or *d-d* transition and are commonly lower in energy for first-row transition metals than the second and third-row ones. When the *MC* electronic transition populates a σ_M^* , the strongly antibonding character of the orbital decreases the strength of some metal-ligand bonds, facilitating the ligand substitution reaction,

while the excitation with light predominantly promotes excitations between ligand centered (*LC*) orbitals ($\pi_L \rightarrow \pi_L^*$) or *intra-ligand* transitions. They are common in coordination complexes with ligands having extended π orbitals.

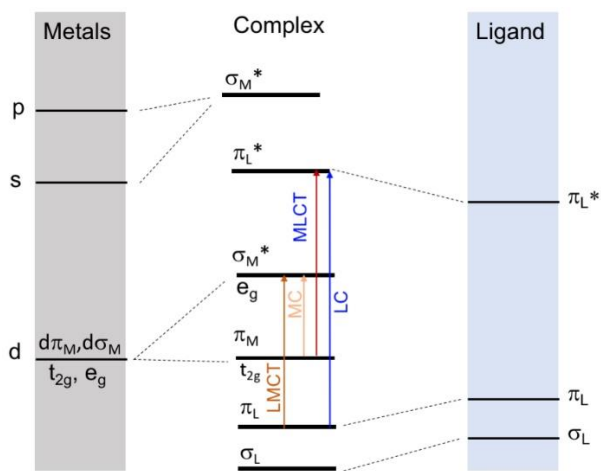


Figure I.13 Representation of molecular orbital diagram of an octahedral complex of a transition metal and its field splitting with ligands. The arrow indicates the direction of photoinduced-electron transfer (PET) into different molecular orbitals.

The variety of ligands makes it difficult to define general rules, however a common feature is that the transitions occur without significant charge redistribution. Nonetheless, they can cause important changes in the bonding properties of the ligands (donor/acceptor), and consequently, in its equilibrium geometry. Further major electronic transitions are *charge-transfer (CT)* transitions that are usually *metal-centered to ligand-centered (MLCT)* or *ligand-centered to metal-centered orbitals (LMCT)*. This transition promotes an important redistribution of the electric charges in the metal complex. The nature of the *CT* transition depends on the relative metal-ligand redox potentials. Thus, an *MLCT* will be favoured when it is easier to oxidize the metal center rather than the ligand, and in contrast, *LMCT* will be favoured when it is easier to oxidize the ligand instead the metal center. The *CT* excited states mainly govern the photoredox properties of the *PCs* and therefore a great number of the catalytic applications. As expected, after the promotion of the *CT*, the properties of the metal complex completely change. For

instance, in the case of *MLCT*, the oxidation of the metal strengthens the metal-ligand coordination for hard ligands (nitrogenated heteroaromatic, halides, amines, OH...) while it weakens it for soft ligands (CO, phosphines, alkenes...) facilitating a nucleophilic attack to the metal center. In the case of “protogenic” ligands (H₂O, NH₃, NRH₂, protonated imizadol, etc.), the pK_a of the complex decreases. The contrary happens for the *LMCT* excited state when the metal center is reduced. An example of this is the photochemical response of [Co(NH₃)₆]³⁺ complex (or Co^{III} complexes with amine type ligands). Its photoexcitation at 254 nm promotes an *LMCT* transition causing ligand dissociation and decomposition. Characteristically, cobalt complexes with amines ([Co(NH₃)₆]³⁺, [Co(en)₃]³⁺) that are stable in oxidation state III are not stable in II.⁶¹ Additionally, intermolecular *CT* transitions can also occur if an exogenous redox-active state can be reached and electronically populated. These transitions are frequently called *outer-sphere charge transfer (OSCT)*.

1.3.2 Selection rules.

The intensity of these transitions is modulated by the selection rules. Following the *orbital rule* (Laporte), the transition is allowed when $\Delta L = \pm 1$. The *spin rule* allows transitions $\Delta S = 0$ and the total angular momentum should follow $\Delta J = 0$ or ± 1 . Nevertheless, there are mechanisms that break these selection rules, such as *spin-coupling* and *desymmetrization* movements and vibrations. In general, the range of *extinction coefficients* (ϵ) for the combinations of forbidden and allowed spin and orbital selection rules are:⁶²⁻⁶⁴

- i) Orbital and spin allowed* 10³-10⁵ (mol⁻¹·cm⁻¹; typical *LMCT* or *MLCT*).
- ii) Orbital forbidden and spin allowed* 10⁰-10³ (mol⁻¹·cm⁻¹; typical *MC* or *d-d* transition).
- iii) Orbital allowed and spin forbidden* 10⁻⁵-10⁰ (mol⁻¹ cm⁻¹).

I.3.3 Deactivation Pathways.

From this initial excited state, after the photon absorption, the system decays through radiative (photon emission, luminescence) or non-radiative transition processes to existing lower energy excited states, until finally reaches again back to the ground state. Each of the deactivation processes presented below are unimolecular and therefore follow first-order kinetics (k_i), with a specific lifetime $[\tau_i = 1/k_i]$, half-lifetime $[t_{1/2} = \ln 2/k_i]$ and quantum yield $[\Phi_i = k_i/\sum_j k_j = k_i/k_{deact}]$. To better illustrate the possible deactivation pathways, the Jablonski diagram shows the electronic states of a molecule and the transitions between them (Figure I.14). The states are organized vertically by energy and assembled horizontally by the spin multiplicity of the state. Jablonski diagrams help to exemplify the electronic transitions between ground-state and excited states, and the excited state dynamics of the system in a simplified manner.

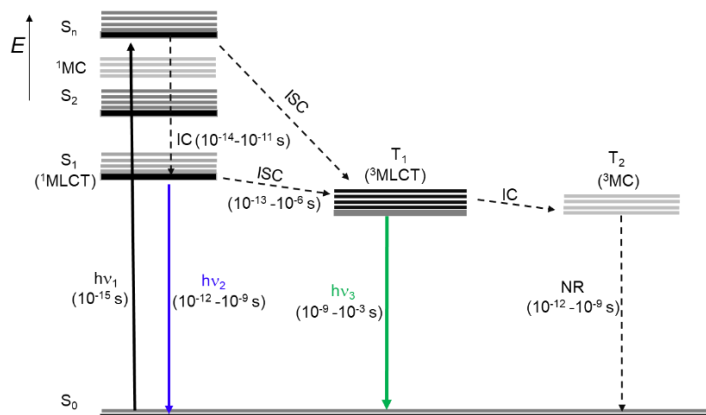


Figure I.14 General Jablonski diagram ($h\nu_1$ = photon absorption, $h\nu_2$ = fluorescence, $h\nu_3$ = phosphorescence).

Non-radiative transitions (dashed arrows) could proceed by several different mechanisms differentiated by the speed of that process. The *non-adiabatic vibrational relaxation* is in the range of 10^{-14} to 10^{-11} s and takes place in the same electronic state to the lowest vibrational level. In the same time-range takes place the *internal conversion* (IC), which promotes an electron from a vibrational state of an electronically excited state to a vibrational state of a lower electronic state (10^{-14} - 10^{-

¹¹ s). Ultimately, *intersystem crossing (ISC)*, which is a transition to an electronic state with a different spin multiplicity, takes place in the range of 10^{-13} to 10^{-6} s. *Radiative transitions* (solid arrows) are the transitions from electronically excited states to the ground state. When this process takes place after an *ISC*, it is called *phosphorescence* (10^{-9} - 10^{-3} s) whereas if it happens before that, is called *fluorescence* (10^{-12} - 10^{-9} s). In general terms, phosphorescent transitions are slower in comparison with fluorescence. The reason for this is that after an *ISC*, the following transition is spin forbidden. Therefore, the lifetime of the electronically excited state generated after the *ISC* is typically longer than 10^{-7} s. This time is sufficient to be engaged into bimolecular diffusive reactivity (10^{-8} s). In general, excited states that live longer than the bimolecular diffusion time can find other reactive species with an appropriate redox potential to participate in an electron transfer process (or energy transfer process). Indeed, most of the photoredox catalytic cycles are mediated by bimolecular electron transfer reactions, which have to be considered as deactivation pathways rather than quenching processes. Allowed *CT* absorptions will generate a variety of excited states depending on the ligand and metal nature. Maximizing the excited-state lifetime and decreasing the rate of the deactivation pathway (*via ISC/IC* or *MC*) to the ground state, favours the electron transfer process.

The most studied examples in literature are second and third-row transition metal complexes with a d^6 electronic configuration (Ir^{3+} , Ru^{2+} , Os^{2+}). Upon photon absorption in the visible range, these metals typically shift one electron from a metal centered orbital (t_{2g} or π_M ; S_0 , ground state) to a ligand centered π^* orbital. This process is commonly called ¹*MLCT* electronically excited state (S_1 ; singlet state). The reverse transition from ¹*MLCT* to the ground state is also allowed ($\Delta L = \pm 1$, $\Delta S = 0$) and therefore will decay quickly. However, if there is an accessible *ISC* to a ³*MLCT*, giving rise to a *spin-flip*, a long-lived excited state (T_1 ; triplet state) will be formed and then can engage in electron transfer processes. For first-row d^6 transition metal complexes, the crystal field splitting is smaller which place ¹*MC* and ³*MC* states at energies usually lower than ¹*MLCT* and ³*MLCT* states.

I.3.4 General Photoredox Catalytic Cycle.

The existence of long-lived excited-states ($\tau_{\text{deact}} > 10$ ns) is required to engage photocatalytic transformation in an electron transfer process to a second molecule. This bimolecular reaction is facilitated by the delocalization and simultaneous formation of an oxidant and reductant in the photocatalyst in the excited state (metal and ligand centered or *vice versa*). In the absence of any second electron-donating/accepting molecules, the excited state can decay back to the ground state by luminescence or *via* other non-radiative processes ($*PC^n \rightarrow PC^n$). Likewise, in the presence of second molecule as electron donor/acceptor, the excited state emission undergoes rapid decrease in its emission quantum yield, what is called *quenching*. This process could occur through oxidative ($*PC^n \rightarrow PC^{n+1}$) or reductive ($*PC^n \rightarrow PC^{n-1}$) quenching depending on how the PC gives or receives the electron respectively. Consequently the reduced photoredox catalyst (PC^{n-1} , or oxidized PC^{n+1}) can be oxidized (or reduced) back to the ground state (PC^n) in the presence of a suitable electron-accepting molecule (A, or an electron donor D), and thereby close the cycle of photoredox catalysis (Figure I.15).

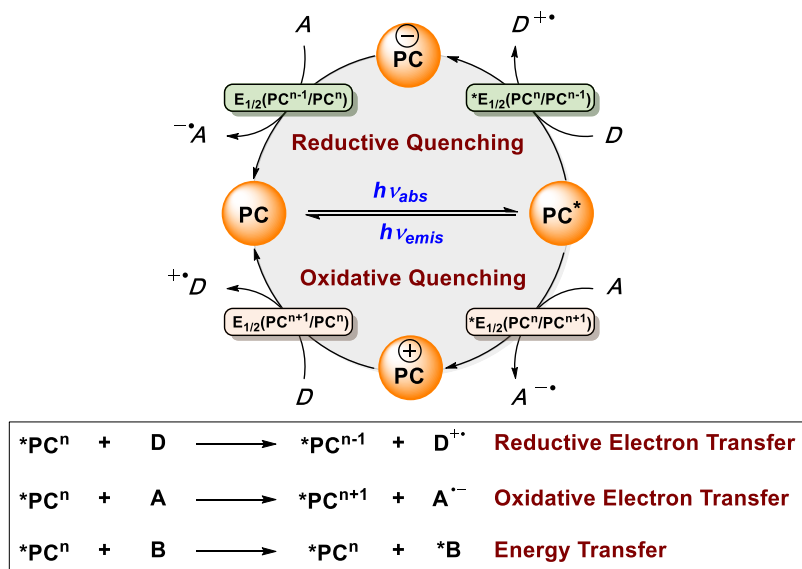


Figure I.15 General photocatalytic cycle including reductive and oxidative electron-transfer quenching processes from the photoexcited state (D and A stands for donor and acceptor molecules).

Although a quenching process could occur through energy transfer or electron-transfer, most of the photoredox transformations with first-row transition metal complexes imply an electron-transfer process. In this way, bimolecular quenching could be static *via* the formation of a ground state adduct between donor-acceptor molecules, that is maintained in the excited-state, or dynamic, when the bimolecular quenching occurs by collisional encounter between the donor and the acceptor.⁶⁵ First-row transition metal catalysis, often occur *via* dynamic quenching. Since the reaction is bimolecular, the lifetime of the excited state (first-order kinetics) should be longer than the time needed to encounter, collision and produce an effective electron transfer to the molecule to be transformed. The electron transfer (*ET*) kinetics can be estimated using *Marcus Theory* and its quadratic relationship.^{66,67} In this theory, it is correlated the free activation energy of the electron transfer (ΔG^\ddagger) and the change in free energy by the *ET* or driving force of the reaction (ΔG^0) as a function of the nuclear reorganization energy (λ) (eq. 1). Usually, although the *ET* barriers are lower in energy than for other processes occurring in solution, the *ET* could be involved in the series of elemental steps that controls the overall rate of the reaction.

$$\Delta G^\ddagger = \frac{1}{4\lambda} (\Delta G^0 + \lambda)^2 \quad (1)$$

Besides kinetics, thermodynamics is also key for an effective photoredox catalysis. In this regard, a desirable property for a photoredox catalyst is to have stable oxidized and reduced ground and excited states ensuring overall stability during catalysis. To have a proper electron transfer process, the redox potential of the excited state should match with the redox potential of the reaction to be carried out. The redox potentials, defined at thermally equilibrated states, can be obtained as an estimation for a given excited state of a photoredox catalyst, with the ground state redox potentials ($E_{1/2}^{ox}$ and $E_{1/2}^{red}$) and the excited state energy (E_{00}) (**Figure I.16**).

$$E^o(PC^+ / *PC) = E^o(PC^+ / PC) - E_{00} \quad (\text{Oxidative Quenching}) \quad (2)$$

$$E^o(*PC / PC^-) = E^o(PC / PC^-) + E_{00} \quad (\text{Reductive Quenching}) \quad (3)$$

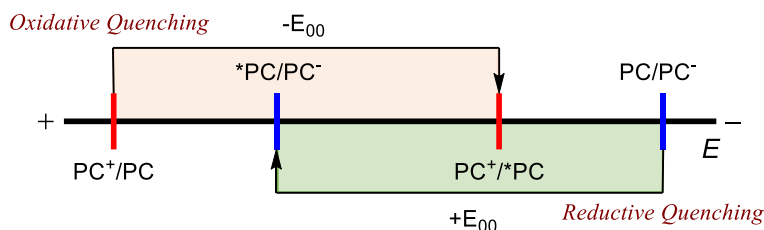


Figure I.16 Schematic representation of ground states and excited states redox potentials and its connection with E_{00} .

The excited state reduction potential is usually lower than the ground state by the excited state energy (E_{00}), making it a better oxidant at the excited state. Likewise, the oxidation potential is higher than its ground state, making it a better reductant at excited state (**Figure I.16**). It should be noticed that the redox values obtained by the equations 2 and 3 are $E_{1/2}$ values. Therefore, under catalytic conditions, the real redox potential of the solution will depend on the concentration of oxidized and reduced species, which is much lower than the initial PC concentration due to thermodynamic equilibria. In the case that redox events are equilibrated at the steady-state, *Nernst equation* can be applied to estimate the equilibrium concentration species. That means that photoredox catalysis could take place even when the redox potential of a PC is lower than the redox potential of the molecule to transform if a subsequent exergonic transformation is kinetically fast and thermodynamics allows the overall process.

1.3.5 Quantification of Excited-State Processes in Photocatalysis.

The total reduction of emission quantum yield and rate of deactivation of photocatalyst with a quencher (under reductive/oxidative quenching process) can be easily quantified by Stern-Volmer quenching studies.⁶⁸ For example, the total decrease in radiative quantum yield in the presence of quencher can be calculated by Stern-Volmer equation.

$$\frac{I_0}{I} = 1 + K_{SV}[Q] \quad (4)$$

$$\frac{\tau_0}{\tau} = 1 + K_{SV}[Q] \quad (5)$$

Where I_0 , I and τ_0 , τ are the luminescence intensity and lifetime of the emitter in the absence or in the presence of quencher concentration $[Q]$ and K_{SV} is the Stern-Volmer rate quenching constant (eq. 4-5). In the case of a bimolecular quenching process at pseudo-first-order conditions, K_{SV} is calculated from the linear plot of the ratio of intensity *vs* $[Q]$. In the case of pure dynamic quenching, the same procedure is valid while taking the ratio of lifetime *vs* $[Q]$. Further, the K_{SV} can be correlated with bimolecular quenching constant K_q by the relation $K_{SV} = K_q \tau_0$. It is important to point out that Stern-Volmer analysis does not give any discrete analysis of the quenching mechanism. Moreover, it gives almost indistinguishable results on electron transfer or energy transfer quenching of the excited state of emitter. Only real-time detection of radical intermediates by transient spectroscopic techniques will provide a realistic picture of the catalytic cycle. Nonetheless, the Stern-Volmer analysis provides a simple way to understand whether catalysis follows an oxidative or reductive quenching pathway between electron donor, photocatalyst and substrates.⁶⁹

1.4. First-Row Transition Metal Photocatalysts.

Although most of the studies related to photoredox catalysis have focused on both second and third-row transition metal complexes, during the last 20 years, the progress in photoredox catalysis with first-row transition metal complexes has been extraordinary. At the early stages of this development, thoughtful studies created the essential photophysics and photochemistry knowledge to understand the electronic structures of excited states. To this end, ligand design is at the core of obtained desired properties, and metals offer an extensive palette of potentially accessible excited states to be investigated. Certainly, first-row transition metals offer an opportunity to challenge the current state of the art of the coordination chemistry, photochemistry and photoinduced electron transfer processes.

Notwithstanding the fact that photochemistry of metal complexes with d^7 electronic configuration (Co^{2+} , Ni^{3+}) is less rich than the d^6 , it also exhibits interesting photochemical features. For instance, *LMCT* excited states are internally promoted between the metal and exchangeable ligands by inner-sphere electron transfer upon light irradiation which leads to dissociation or interesting ligand-based reactivity. Likewise, examples of d^8 configuration (Ni^{2+}) also illustrate the synthetic capacity of *LMCT* transitions.

Finally, photosensitizers based on $3d^{10}$ electronic configuration, in particular based on Cu^+ are quite effective photoredox catalysts rivalling well-established second and third-row transition metal-based *PCs*. They take advantage of the filled electronic shell, which eliminates the *MC* states providing photophysical features dominated by *MLCT* states with long-lived $^3\text{MLCT}$ excited states. Truly, the photophysics and photochemistry of metal complexes are intricate. The multitude of potential excited-states complicates the elaboration of general rules. Nevertheless, there are several valuable strategies to provide effective photoredox catalysts based on first-row transition metal complexes. In fact, Cu-photosensitizers are attracting more and more attention during last decades due to the similar photophysical properties to the well-established Ru^{II} and Ir^{III} complexes: strong absorption in visible-light region, long-lived *MLCT* excited states, tunable redox properties and high luminescence quantum yields.⁷⁰⁻⁷⁴

In particular, homoleptic or heteroleptic Cu^{I} complexes, with a preferred pseudo-tetrahedral D_{2d} geometry in the ground-state, rely on the drastic geometric changes taking place upon photoexcitation. The transient Cu^{II} ion assumes a more planar structure from the susceptibility to *pseudo Jahn-Teller* distortions (geometrical flattening). These geometric rearrangements have substantial effects on the stability of the excited state and reduce considerably the energy stored in this long-lived excited state (**Figure I.17**).

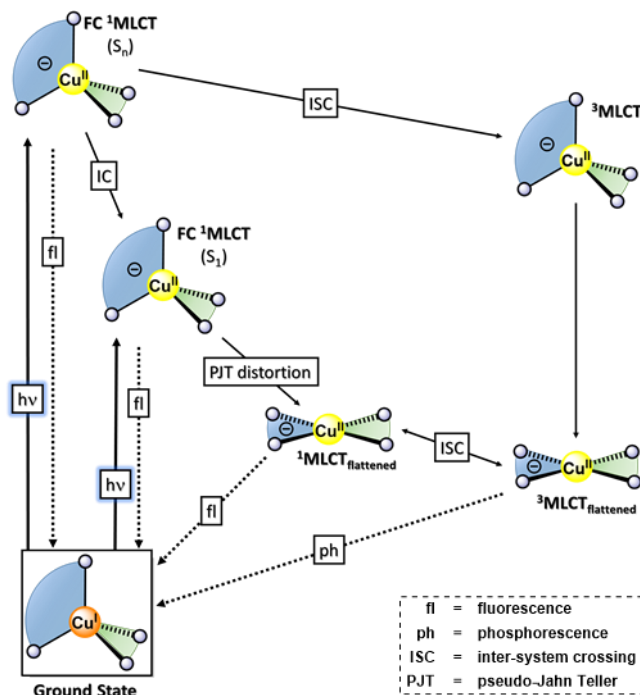


Figure I.17 Simplified Jablonski diagram showing photoexcitation dynamics and associated structural changes occurring in Cu^{I} homoleptic complexes between the ground state and MLCT excited states (bottom). Solid lines are absorption and dotted lines are fluorescence (fl) and phosphorescence (Ph).

Upon visible-light excitation of the Cu^{I} complexes, a $^1\text{MLCT}$ transition band results from the oxidation of the metal center and the reduction in one electron of the diamine ligand. The oxidized metal center Cu^{II} , with a d^9 electronic configuration in its MLCT excited state, undergoes a geometrical distortion by the *pseudo-Jahn-Teller* effect.⁷⁵ As a consequence, the geometry shifts from pseudotetrahedral (D_{2d}) to a distorted d^9 “flattened” MLCT excited-state structure, featuring a D_2 geometry. The light-induced flattening leads to a stabilized $^1\text{MLCT-flattened}$ state with respect to the Franck-Condon (FC) state, which can undergoes a *non-radiative* decay to the ground state (favoured according to the energy gap law) or weakened spin-orbital coupling between the $^1\text{MLCT-flattened}$ and $^3\text{MLCT-flattened}$ states, which in turn slows down the intersystem crossing (ISC) from the $^1\text{MLCT-flattened}$ state to the $^3\text{MLCT-flattened}$ state (on a picosecond timescale). Moreover, the high-lying FC

1MLCT can also undergo *ISC* into 3MLCT -flattened state bypassing the 1MLCT -flattened state, where the absence of flattening distortion enables large spin-orbital coupling and thus allows fast *ISC* (on a sub-picosecond timescale).

The flattened geometry of these *MLCT* states, opens the possibility for reactivity that can be quenched by donor solvent molecules forming non-emissive excited state complexes (exciplexes) with coordination solvents.^{76,77} However, tuning the steric and electronic properties of the coordinating ligands can enhance and stabilize an excited emissive *MLCT* state. Based on this understanding, McMillin group introduced in 2002 the heteroleptic Cu^I complexes $[Cu(N^{\wedge}N)(P^{\wedge}P)]^+$ using bulky bidentate phosphine ligands as $P^{\wedge}P$.^{72,73} The steric effect of these diphosphines relies on the three-dimensional orientation of the phosphorus-bound (aryl)-substituents inducing steric effects in the pseudotetrahedral C_{2v} structure facilitating the *ISC* to the 3MLCT state and reducing the solvent accessibility to the copper center. From that point on, numerous studies have confirmed the enormous potential of this strategy in different catalytic procedures.⁷⁸⁻⁸¹ It should be noted, however, that heteroleptic $[Cu(N^{\wedge}N)(P^{\wedge}P)]^+$ complexes can suffer disproportionation and dynamic ligand exchange to generate their respective homoleptic $[Cu(N^{\wedge}N)_2]^+$ and $[Cu(P^{\wedge}P)_2]^+$ counterparts in the case of small and labile phosphine ligands (diphosphines can act as σ -Lewis bases by donating the lone pair on the phosphorous atom to the metal center, and also as π -acceptor ligands through π backbonding).⁸² In this context, McMillin and co-workers demonstrated that the introduction of rigid DPEphos or Xantphos type-ligands allows the significant suppression of ligand dissociation and solvent-induced luminescence quenching (**Figure I.18**).⁸³⁻⁸⁵

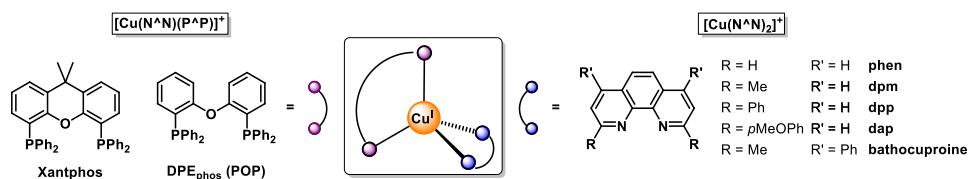


Figure I.18 General caption for heteroleptic $[Cu(N^{\wedge}N)(P^{\wedge}P)]^+$ (left) and homoleptic $[Cu(N^{\wedge}N)_2]^+$ photoredox catalysts (top).

In this regard, copper presents an attractive alternative to traditional noble-metal photocatalysts (e.g. Ru^{II} and Ir^{III}). This first-row transition metal PC can undergo both oxidative and reductive quenching pathways, the latter being more challenging.⁸⁶ The barrier to reductive quenching is further attributed to the difference in the equilibrium geometries of the ground and excited states of the copper system. This kinetic imposition arises from the structural reorganization and formal oxidation changes of the metal center (Cu^I to Cu^{II}) during $MLCT$ transitions that makes the electron transfer from the quencher Q to the excited hole of metal center an uphill energetic process.^{87,88} Reorganization by substitution of the 2, 9 positions of the phenanthroline ligand can enhance the reductive quenching of the $MLCT$ process. In this regard, Beller *et al.* reported many different kinds of heteroleptic $[Cu(N^{\wedge}N)(P^{\wedge}P)]^+$ complexes as photosensitizers in a noble metal-free water reduction system with suitable photocatalysts.^{74,83,89,90} Furthermore, they undergo both reductive and oxidative electron transfer with sacrificial electron donor or acceptor owing to the bulky substituents at 2, 9 positions of coordinating ligands (**Figure I.19**). However, the mechanism of water reduction mainly proceeds *via* oxidative electron transfer. During catalysis, these heteroleptic complexes undergo disproportionation reactions by ligand exchange into their respective homoleptic complexes and their spectral signature is monitored by UV/Vis *in situ* spectroelectrochemistry studies.⁹¹

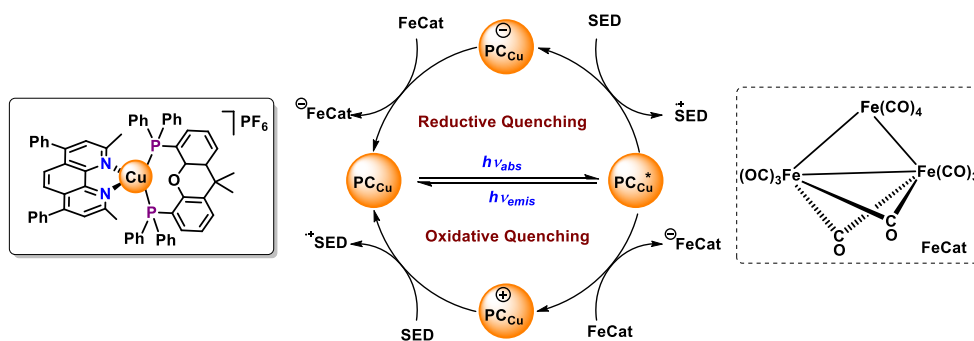


Figure I.19 The use of PC_{Cu} in reductive and oxidative electron transfer pathway and its molecular structure together with H_2 evolving molecular catalysts, $FeCat$.

As an alternative to copper, which is the most studied metal of the first series in photocatalysis, biologically active compounds, such as native cofactors derived from vitamin B₁₂, have been also extensively studied in photocatalysis.

1.5. B₁₂-Derivates in Reductive Organic Reactions

Coenzyme B₁₂ (5'-deoxy-5'-adenosylcobalamin, *AdoCbl*) and methylcobalamin (*MeCbl*) represent the only organometallic alkyl cofactors in biological systems that contain a stable metal-carbon bond (*M-C*).⁹² Their structure and reactivity were extensively studied observing that many of the biological functions of B₁₂-dependent enzymes, such as rearrangements, methyl transfer reactions and dehalogenations, involve the cleavage and formation of the *M-C* bond of the cobalt corrin cofactor.⁹³ The homolytic formation/cleavage of the *M-C* bond determines the one electron nature of the reactions occurring at coenzyme B₁₂. Thus, the *Co^{II}* form (*B₁₂r*) can be considered as an efficient radical trap that generates the corresponding alkylCob(III)alamin upon reaction with alkyl radicals. The *M-C* bond in coenzyme B₁₂ is relatively weak, with an estimated *BDE* of the *Co-C* bond of 26 kcal/mol.⁹³ Thus, coenzyme B₁₂ serves as a reversible source of the 5'-deoxy-5'-adenosyl radical in the enzymatic isomerization at, for instance, methyl-malonyl-CoA mutase (*MMCM*) or glutamate mutase enzymes. Alternatively, the heterolytic cleavage of the *M-C* bond is well-showcased at enzyme-catalysed methyl-transfer reactions. In this case, the reduced *Co^I* cobalamine (*B₁₂s*), considered a strong nucleophile, reacts with electrophilic alkylating agents by a formal bimolecular nucleophilic substitution (*S_N2*) reaction to form the corresponding alkylCob(III)alamin (**Figure I.20**). The *M-C* bond formed is involved in a nucleophile-induced demethylation of the methyl-Co(III)-corrin that regenerates the reduced *Co^I* center. Another biologically relevant cofactor is the nickel-based F₄₃₀ at methyl coenzyme M reductase (*MCR*).⁹⁴ In this nickel cofactor, the corresponding organonickel(III) complex is formed upon activation of alkyl halides by the highly nucleophilic Ni^I complex.^{95,96}

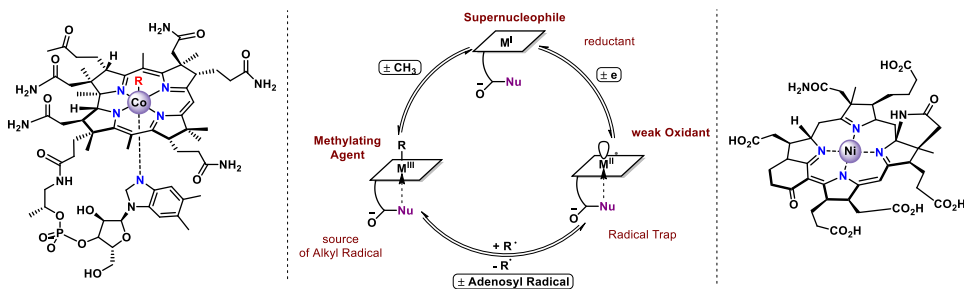


Figure I.20 Structure (left) and proposed mechanism of *B*₁₂ derivatives (center)⁹⁷ and Ni-corphin *F*₄₃₀ (right).^{94,98}

Taking advantage of the dual role of these cobalt and nickel complexes as supernucleophiles, authors like Scheffold or Pattenden showed the efficiency of these compounds as catalysts for reductive reactions under both electrochemical conditions or with chemical reductants.^{99,100} Thus, several electrophiles such as alkyl halides, acyl halides, epoxides, among others, can be activated by the reduced monovalent metal complexes bearing highly nucleophilic ligands. The homolytic cleavage of the *M*–*C* bond of the resulting organometallic *M*^{III} complexes (*M* = Co, Ni) under electrolytic,¹⁰¹ photolytic or thermolytic conditions generates carbon-centered radicals,^{102,103} which can further engage in *C*–*C* bond forming reactions.^{99,104} In seminal studies, Hisaeda's group demonstrated photochemically driven organic reactions catalysed vitamin *B*₁₂-derivatives. They utilized a heterogeneous platform based on cobaloxime coupled with titanium dioxide (*TiO*₂) as photoredox catalyst (which absorbs UV light at 365 nm), and methanol as solvent and sacrificial electron donor (**Figure I.21**).

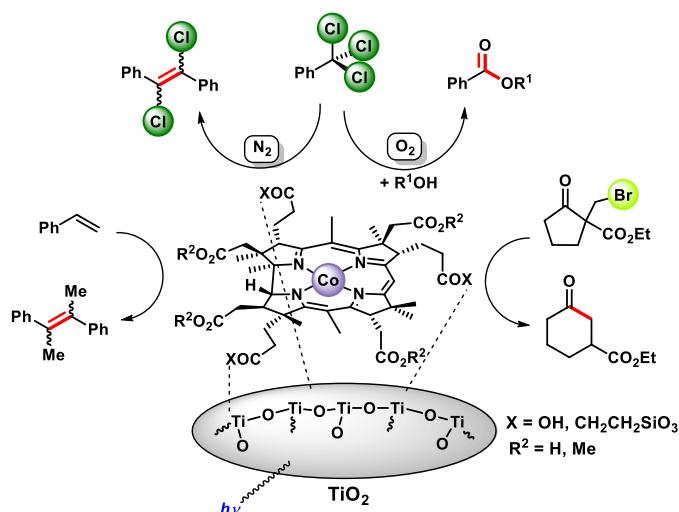


Figure I.21 Reactivity of heterogeneous and hybrid B_{12} - TiO_2 catalysts for reductive transformations in alcoholic solvents under UV-light irradiation.

The heterogeneous and hybrid B_{12} - TiO_2 catalyst has been employed in the hydrogenation and reductive dimerization of styrenes,¹⁰⁵ dehalogenation and ring expansion reactions of alkyl bromides^{106,107} and dechlorination of benzotrichloride.¹⁰⁸ Remarkably, under anaerobic conditions, B_{12} - TiO_2 reacts with benzotrichloride to form the corresponding 1,2-dichlorostilbenes (**Figure I.21**). On the other hand, when the reaction is carried out under aerobic conditions, methyl benzoate is obtained quantitatively. The ester product is formed by reaction of the resulting benzoyl chloride intermediate with the solvent (methanol). Thus, in the presence of amines in the reaction media, amides can be also prepared starting from benzotrichlorides derivatives. Very recently, a visible-light methodology for the dechlorination of 1-bis(4-chlorophenyl)-2,2,2-trichloroethane (*DDT*) catalyzed by iridium photosensitizer in combination with a cobalt corrinoid complex derived from vitamin B_{12} has been reported.¹⁰⁹ From these earliest studies from Hisaeda's group, many other authors used this idea of using cobaloximes as catalyst under visible-light irradiation for the coupling of alkyl iodides and alkenes to form *Heck-type* cyclization products¹¹⁰ or decarboxyolefination of carboxylic acids catalyzed by

iridium photoredox catalyst and cobaloxime $\text{Co}(\text{dmgH})_2(4\text{-OMe-py})$ (Figure I.22).¹¹¹

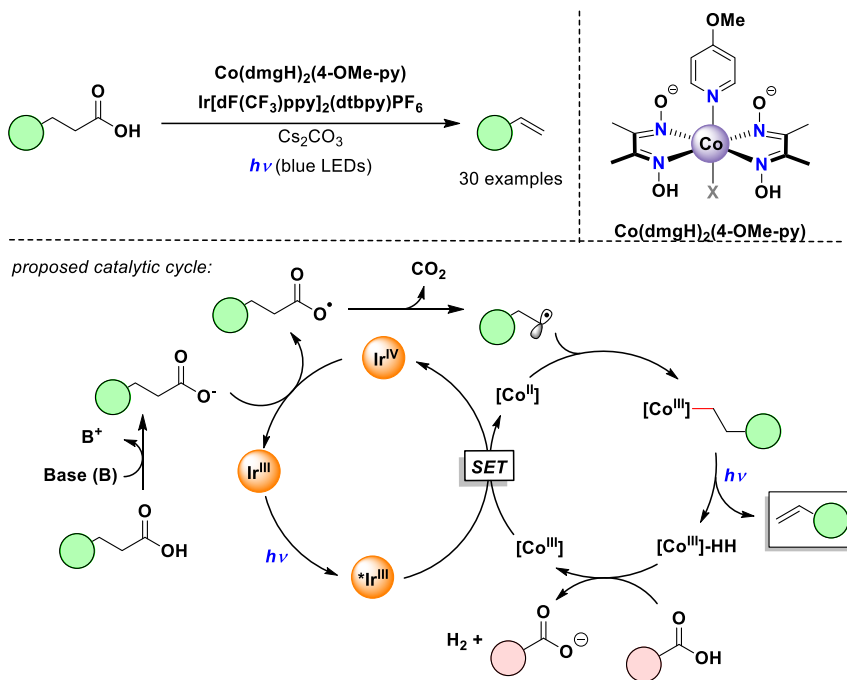


Figure I.22 Light-driven decarboxyolefination of carboxylic acids catalyzed by a dual Ir/Co catalytic system.¹¹¹

Successive studies were performed by the groups of Peters, Fujita, Polyansky and Fukuzumi among others to develop systems based on aminopyridine cobalt complexes for the reduction of protons to hydrogen (Figure I.23, left). Following this research line, in 2014, our group showed a photocatalytic reduction of water for hydrogen production by first-row transition-metal complexes based on aminopyridyl ligands.^{112,113} In the proposed mechanism a low-valent M^I complex is formed by a SET from the reduced iridium photocatalyst (Figure I.23, right). A subsequent protonation generates a $M^{\text{III}}\text{-H}$ intermediate and further reduction and protonation releases H_2 as product.

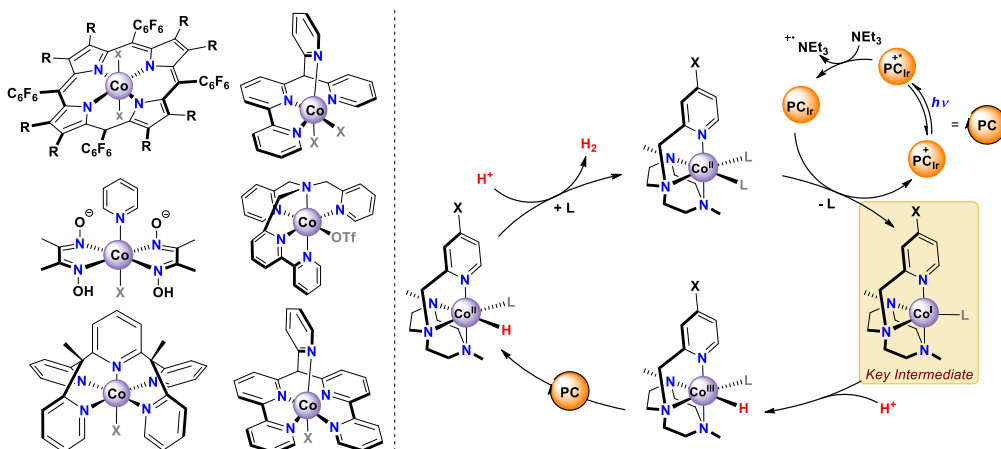


Figure I.23 Aminopyridine-cobalt complexes used in water reduction (left) and proposed mechanism for water reduction catalyzed by 2^XCo complexes (right).

Further studies showed the effectivity of the aminopyridil cobalt complexes in the photocatalysed reduction of organic substrates such as ketones or aldehydes^{114,115} using light as a source of energy and water as the source of protons. The photogenerated Co^I intermediate upon reaction with the copper photocatalyst was found to be key for the reaction to engage protons from water, that then will be transfer to the carbonyl *via* hydride transfer mechanism involving [C-H] species or *via* SET + HAT mechanism (Figure I.24).

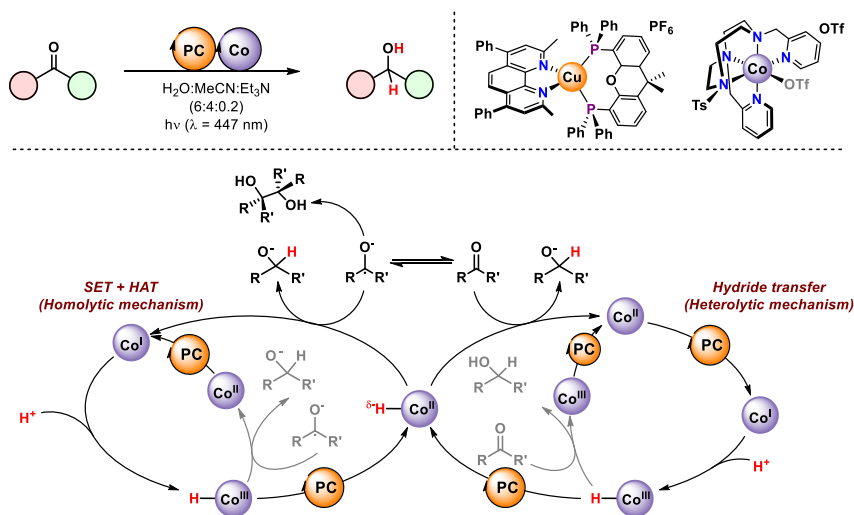


Figure I.24 Proposed mechanistic scenarios for the photoreduction of aromatic ketones and aldehydes.

I.6. *References of the Chapter.*

- (1) Ciamician, G. The Photochemistry of the Future. *Science* **1912**, *36*, 385, doi: 10.1126/science.36.926.385.
- (2) Ciamician, G.; Silber, P. Chemische Lichtwirkungen *Berichte der deutschen chemischen Gesellschaft* **1900**, *33*, 2911, doi: 10.1002/cber.19000330326.
- (3) Ciamician, G.; Silber, P. Chemische Lichtwirkungen *Berichte der deutschen chemischen Gesellschaft* **1908**, *41*, 1928, doi: 10.1002/cber.19080410272.
- (4) Saltiel, J.; Charlton, J. L.: *Essay 14 - Cis-Trans Isomerization of Olefins*; Academic Press, 1980; Vol. 42.
- (5) Hammond, G. S.; Saltiel, J. Photosensitized *Cis-Trans* Isomerization of the Stilbenes. *J. Am. Chem. Soc.* **1962**, *84*, 4983, doi: 10.1021/ja00883a075.
- (6) Sharma, R. K.; Kharasch, N. The Photolysis of Iodoaromatic Compounds. *Angew. Chem. Int. Ed.* **1968**, *7*, 36, doi: 10.1002/anie.196800361.
- (7) Adam, G.; Schreiber, K. Photochemical Reactions - III. The Photochemical Fragmentation of a Steroidal N-Chloroamine. *Tetrahedron Lett.* **1965**, *6*, 923, doi: 10.1016/S0040-4039(01)99500-0.
- (8) Yates, P. Photochemistry of Cyclic Ketones in Solution. *Pure Appl. Chem.* **1968**, *16*, 93, doi: 10.1351/pac196816010093.
- (9) Turro, N. J.; Dalton, J. C.; Dawes, K.; Farrington, G.; Hautala, R.; Morton, D.; Niemczyk, M.; Schore, N. Molecular Photochemistry. L. Molecular Photochemistry of Alkanones in Solution. .Alpha.-Cleavage, Hydrogen Abstraction, Cycloaddition, and Sensitization Reactions. *Acc. Chem. Res.* **1972**, *5*, 92, doi: 10.1021/ar50051a002.
- (10) Darling, T. R.; Turro, N. J.; Hirsch, R. H.; Lewis, F. D. Photochemistry Of .Alpha.-Cycloalkoxyacetophenones. Type II and Vibronic Pathways for Radiationless Triplet Decay. *J. Am. Chem. Soc.* **1974**, *96*, 434, doi: 10.1021/ja00809a019.
- (11) Woodward, R. B.; Hoffmann, R.: *The Conservation of Orbital Symmetry*; Elsevier Science, 2013.
- (12) Hixson, S. S.; Mariano, P. S.; Zimmerman, H. E. Di-.Pi.-Methane and Oxa-Di-.Pi.-Methane Rearrangements. *Chem. Rev.* **1973**, *73*, 531, doi: 10.1021/cr60285a005.
- (13) Kärkäs, M. D.; Porco, J. A.; Stephenson, C. R. J. Photochemical Approaches to Complex Chemotypes: Applications in Natural Product Synthesis. *Chem. Rev.* **2016**, *116*, 9683, doi: 10.1021/acs.chemrev.5b00760.
- (14) Müller, C.; Bauer, A.; Bach, T. Light-Driven Enantioselective Organocatalysis. *Angew. Chem. Int. Ed.* **2009**, *48*, 6640, doi: 10.1002/anie.200901603.
- (15) Burstall, F. H. 34. Optical Activity Dependent on Coordinated Bivalent Ruthenium. *J. Chem. Soc.* **1936**, 173, doi: 10.1039/JR9360000173.
- (16) Balzani, V.; Bolletta, F.; Gandolfi, M. T.; Maestri, M.: *Bimolecular electron-transfer Reactions of the Excited States of Transition Metal Complexes*; Springer Berlin Heidelberg: Berlin, Heidelberg, 1978.
- (17) Kalyanasundaram, K. Photophysics, Photochemistry and Solar Energy Conversion with Tris(Bipyridyl)Ruthenium(II) and Its Analogues. *Coord. Chem. Rev.* **1982**, *46*, 159, doi: 10.1016/0010-8545(82)85003-0.

- (18) Blau, F. Über Neue Organische Metallverbindungen. *Monatsh. Chem.* **1898**, *19*, 647, doi: 10.1007/BF01517438.
- (19) Juris, A.; Balzani, V.; Barigelletti, F.; Campagna, S.; Belser, P.; von Zelewsky, A. Ru^{II} Polypyridine Complexes: Photophysics, Photochemistry, Electrochemistry, and Chemiluminescence. *Coord. Chem. Rev.* **1988**, *84*, 85, doi: 10.1016/0010-8545(88)80032-8.
- (20) Prier, C. K.; Rankic, D. A.; MacMillan, D. W. C. Visible-Light Photoredox Catalysis with Transition Metal Complexes: Applications in Organic Synthesis. *Chem. Rev.* **2013**, *113*, 5322, doi: 10.1021/cr300503r.
- (21) Schultz, D. M.; Yoon, T. P. Solar Synthesis: Prospects in Visible-Light Photocatalysis. *Science* **2014**, *343*, 1239176, doi: 10.1126/science.1239176.
- (22) Narayanam, J. M. R.; Stephenson, C. R. J. Visible-Light Photoredox Catalysis: Applications in Organic Synthesis. *Chem. Soc. Rev.* **2011**, *40*, 102, doi: 10.1039/B913880N.
- (23) Corrigan, N.; Shanmugam, S.; Xu, J.; Boyer, C. Photocatalysis in Organic and Polymer Synthesis. *Chem. Soc. Rev.* **2016**, *45*, 6165, doi: 10.1039/C6CS00185H.
- (24) Pitre, S. P.; McTiernan, C. D.; Scaiano, J. C. Understanding the Kinetics and Spectroscopy of Photoredox Catalysis and Transition-Metal-Free Alternatives. *Acc. Chem. Res.* **2016**, *49*, 1320, doi: 10.1021/acs.accounts.6b00012.
- (25) Hedstrand, D. M.; Kruizinga, W. H.; Kellogg, R. M. Light Induced and Dye Accelerated Reductions of Phenacyl Onium Salts by 1,4-Dihydropyridines. *Tetrahedron Lett.* **1978**, *19*, 1255, doi: 10.1016/S0040-4039(01)94515-0.
- (26) Van Bergen, T. J.; Hedstrand, D. M.; Kruizinga, W. H.; Kellogg, R. M. Chemistry of Dihydropyridines. 9. Hydride Transfer from 1,4-Dihydropyridines to Sp³-Hybridized Carbon in Sulfonium Salts and Activated Halides. Studies with Nad(P)H Models. *J. Org. Chem.* **1979**, *44*, 4953, doi: 10.1021/jo00394a044.
- (27) Pac, C.; Ihama, M.; Yasuda, M.; Miyauchi, Y.; Sakurai, H. Tris(2,2'-Bipyridine)Ruthenium(2+)-Mediated Photoreduction of Olefins with 1-Benzyl-1,4-Dihydronicotinamide: A Mechanistic Probe for Electron-Transfer Reactions of Nad(P)H-Model Compounds. *J. Am. Chem. Soc.* **1981**, *103*, 6495, doi: 10.1021/ja00411a040.
- (28) Pac, C.; Miyauchi, Y.; Ishitani, O.; Ihama, M.; Yasuda, M.; Sakurai, H. Redox-Photosensitized Reactions. 11. Ru(Bpy)₃²⁺-Photosensitized Reactions of 1-Benzyl-1,4-Dihydronicotinamide with Aryl-Substituted Enones, Derivatives of Methyl Cinnamate, and Substituted Cinnamionitriles: Electron-Transfer Mechanism and Structure-Reactivity Relationships. *J. Org. Chem.* **1984**, *49*, 26, doi: 10.1021/jo00175a006.
- (29) Ishitani, O.; Yanagida, S.; Takamuku, S.; Pac, C. Redox-Photosensitized Reactions. 13. Ru(Bpy)₃²⁺-Photosensitized Reactions of an Nadh Model, 1-Benzyl-1,4-Dihydronicotinamide, with Aromatic Carbonyl Compounds and Comparison with Thermal Reactions. *J. Org. Chem.* **1987**, *52*, 2790, doi: 10.1021/jo00389a027.
- (30) Willner, I.; Tsfania, T.; Eichen, Y. Photocatalyzed and Electrocatalyzed Reduction of Vicinal Dibromides and Activated Ketones Using Ruthenium(I) Tris(Bipyridine) as Electron-Transfer Mediator. *J. Org. Chem.* **1990**, *55*, 2656, doi: 10.1021/jo00296a023.
- (31) Cano-Yelo, H.; Deronzier, A. Photocatalysis of the Pschorr Reaction by Tris-(2,2'-Bipyridyl)Ruthenium(II) in the Phenanthrene Series. *J. Chem. Soc. Perk. Trans. 2* **1984**, 1093, doi: 10.1039/P29840001093.

- (32) Cano-Yelo, H.; Deronzier, A. Photo-Oxidation of Some Carbinols by the Ru^{II} Polypyridyl Complex-Aryl Diazonium Salt System. *Tetrahedron Lett.* **1984**, *25*, 5517, doi: 10.1016/S0040-4039(01)81614-2.
- (33) Balzani, V.; Moggi, L.; Manfrin, M. F.; Bolletta, F.; Gleria, M. Solar Energy Conversion by Water Photodissociation. *Science* **1975**, *189*, 852, doi: 10.1126/science.189.4206.852.
- (34) Creutz, C.; Sutin, N. Reaction of Tris(Bipyridine)Ruthenium(III) with Hydroxide and Its Application in a Solar Energy Storage System. *Proc. Natl. Acad. Sci. U. S. A.* **1975**, *72*, 2858, doi: 10.1073/pnas.72.8.2858.
- (35) Lehn, J.-M.; Ziessel, R. Photochemical Generation of Carbon Monoxide and Hydrogen by Reduction of Carbon Dioxide and Water under Visible-Light Irradiation. *Proc. Natl. Acad. Sci. U. S. A.* **1982**, *79*, 701, doi: 10.1073/pnas.79.2.701.
- (36) Maidan, R.; Willner, I. Photoreduction of Carbon Dioxide to Methane in Aqueous Solutions Using Visible-light. *J. Am. Chem. Soc.* **1986**, *108*, 8100, doi: 10.1021/ja00285a043.
- (37) Osawa, M.; Nagai, H.; Akita, M. Photo-Activation of Pd-Catalyzed Sonogashira Coupling Using a Ru/Bipyridine Complex as Energy Transfer Agent. *Dalton Trans.* **2007**, 827, doi: 10.1039/B618007H.
- (38) Sonogashira, K.; Tohda, Y.; Hagihara, N. A Convenient Synthesis of Acetylenes: Catalytic Substitutions of Acetylenic Hydrogen with Bromoalkenes, Iodoarenes and Bromopyridines. *Tetrahedron Lett.* **1975**, *16*, 4467, doi: 10.1016/S0040-4039(00)91094-3.
- (39) Nicewicz, D. A.; MacMillan, D. W. C. Merging Photoredox Catalysis with Organocatalysis: The Direct Asymmetric Alkylation of Aldehydes. *Science* **2008**, *322*, 77, doi: 10.1126/science.1161976.
- (40) Nagib, D. A.; Scott, M. E.; MacMillan, D. W. C. Enantioselective α -Trifluoromethylation of Aldehydes Via Photoredox Organocatalysis. *J. Am. Chem. Soc.* **2009**, *131*, 10875, doi: 10.1021/ja9053338.
- (41) Shih, H.-W.; Vander Wal, M. N.; Grange, R. L.; MacMillan, D. W. C. Enantioselective α -Benzylation of Aldehydes Via Photoredox Organocatalysis. *J. Am. Chem. Soc.* **2010**, *132*, 13600, doi: 10.1021/ja106593m.
- (42) Ischay, M. A.; Anzovino, M. E.; Du, J.; Yoon, T. P. Efficient Visible-Light Photocatalysis of [2+2] Enone Cycloadditions. *J. Am. Chem. Soc.* **2008**, *130*, 12886, doi: 10.1021/ja805387f.
- (43) Du, J.; Yoon, T. P. Crossed Intermolecular [2+2] Cycloadditions of Acyclic Enones Via Visible-Light Photocatalysis. *J. Am. Chem. Soc.* **2009**, *131*, 14604, doi: 10.1021/ja903732v.
- (44) Ischay, M. A.; Lu, Z.; Yoon, T. P. [2+2] Cycloadditions by Oxidative Visible-Light Photocatalysis. *J. Am. Chem. Soc.* **2010**, *132*, 8572, doi: 10.1021/ja103934y.
- (45) Lu, Z.; Shen, M.; Yoon, T. P. [3+2] Cycloadditions of Aryl Cyclopropyl Ketones by Visible-Light Photocatalysis. *J. Am. Chem. Soc.* **2011**, *133*, 1162, doi: 10.1021/ja107849y.
- (46) Narayanam, J. M. R.; Tucker, J. W.; Stephenson, C. R. J. Electron-Transfer Photoredox Catalysis: Development of a Tin-Free Reductive Dehalogenation Reaction. *J. Am. Chem. Soc.* **2009**, *131*, 8756, doi: 10.1021/ja9033582.
- (47) Tucker, J. W.; Narayanam, J. M. R.; Krabbe, S. W.; Stephenson, C. R. J. Electron-transfer Photoredox Catalysis: Intramolecular Radical Addition to Indoles and Pyrroles. *Org. Lett.* **2010**, *12*, 368, doi: 10.1021/ol902703k.

- (48) Furst, L.; Matsuura, B. S.; Narayanam, J. M. R.; Tucker, J. W.; Stephenson, C. R. J. Visible-Light-Mediated Intermolecular C–H Functionalization of Electron-Rich Heterocycles with Malonates. *Org. Lett.* **2010**, *12*, 3104, doi: 10.1021/ol101146f.
- (49) Tucker, J. W.; Nguyen, J. D.; Narayanam, J. M. R.; Krabbe, S. W.; Stephenson, C. R. J. Tin-Free Radical Cyclization Reactions Initiated by Visible-Light Photoredox Catalysis. *Chem. Commun.* **2010**, *46*, 4985, doi: 10.1039/C0CC00981D.
- (50) Condie, A. G.; González-Gómez, J. C.; Stephenson, C. R. J. Visible-Light Photoredox Catalysis: Aza-Henry Reactions Via C–H Functionalization. *J. Am. Chem. Soc.* **2010**, *132*, 1464, doi: 10.1021/ja909145y.
- (51) Dai, C.; Narayanam, J. M. R.; Stephenson, C. R. J. Visible-Light-Mediated Conversion of Alcohols to Halides. *Nat. Chem.* **2011**, *3*, 140, doi: 10.1038/nchem.949.
- (52) Nguyen, J. D.; Tucker, J. W.; Konieczynska, M. D.; Stephenson, C. R. J. Intermolecular Atom Transfer Radical Addition to Olefins Mediated by Oxidative Quenching of Photoredox Catalysts. *J. Am. Chem. Soc.* **2011**, *133*, 4160, doi: 10.1021/ja108560e.
- (53) Takashi, K.; Munetaka, A. Photoinduced Oxyamination of Enamines and Aldehydes with Tempo Catalyzed by [Ru(Bpy)₃]²⁺. *Chem. Lett.* **2009**, *38*, 166, doi: 10.1246/cl.2009.166.
- (54) Andrews, R. S.; Becker, J. J.; Gagné, M. R. Intermolecular Addition of Glycosyl Halides to Alkenes Mediated by Visible-Light. *Angew. Chem. Int. Ed.* **2010**, *49*, 7274, doi: 10.1002/anie.201004311.
- (55) Neumann, M.; Földner, S.; König, B.; Zeitler, K. Metal-Free, Cooperative Asymmetric Organophotoredox Catalysis with Visible-Light. *Angew. Chem. Int. Ed.* **2011**, *50*, 951, doi: 10.1002/anie.201002992.
- (56) Rueping, M.; Vila, C.; Koenigs, R. M.; Poschamy, K.; Fabry, D. C. Dual Catalysis: Combining Photoredox and Lewis Base Catalysis for Direct Mannich Reactions. *Chem. Commun.* **2011**, *47*, 2360, doi: 10.1039/C0CC04539J.
- (57) Appel, R. Tertiary Phosphane/Tetrachloromethane, a Versatile Reagent for Chlorination, Dehydration, and P–N Linkage. *Angew. Chem. Int. Ed.* **1975**, *14*, 801, doi: 10.1002/anie.197508011.
- (58) Dai, C.; Meschini, F.; Narayanam, J. M. R.; Stephenson, C. R. J. Friedel–Crafts Amidoalkylation Via Thermolysis and Oxidative Photocatalysis. *J. Org. Chem.* **2012**, *77*, 4425, doi: 10.1021/jo300162c.
- (59) DiRocco, D. A.; Rovis, T. Catalytic Asymmetric α -Acylation of Tertiary Amines Mediated by a Dual Catalysis Mode: N-Heterocyclic Carbene and Photoredox Catalysis. *J. Am. Chem. Soc.* **2012**, *134*, 8094, doi: 10.1021/ja3030164.
- (60) Housecroft, C. E.; Sharpe, A. G.: *Inorganic Chemistry*; Pearson, 2012.
- (61) Balzani, V.; Bergamini, G.; Campagna, S.; Puntoriero, F.: Photochemistry and Photophysics of Coordination Compounds: Overview and General Concepts. In *Photochemistry and Photophysics of Coordination Compounds I*; Springer, 2007.
- (62) Harris, D. C.; Bertolucci, M. D.: *Symmetry and Spectroscopy: An Introduction to Vibrational and Electronic Spectroscopy*; Courier Corporation, 1989.
- (63) Laporte, O.; Meggers, W. F. Some Rules of Spectral Structure. *J. Opt. Soc. Am.* **1925**, *11*, 459, doi: 10.1364/JOSA.11.000459.
- (64) Rao, C. N. R.: *Ultra-Violet and Visible Spectrometry. Chemical Applications*; Butterworth, 1961.

- (65) Arias-Rotondo, D. M.; McCusker, J. K. The Photophysics of Photoredox Catalysis: A Roadmap for Catalyst Design. *Chem. Soc. Rev.* **2016**, *45*, 5803, doi: 10.1039/C6CS00526H.
- (66) Marcus, R. A. Electron-transfer Reactions in Chemistry: Theory and Experiment (Nobel Lecture). *Angew. Chem. Int. Ed.* **1993**, *32*, 1111, doi: 10.1002/anie.199311113.
- (67) Silverstein, T. P. Marcus Theory: Thermodynamics Can Control the Kinetics of electron-transfer Reactions. *J. Chem. Educ.* **2012**, *89*, 1159, doi: 10.1021/ed1007712.
- (68) Evans, R. C.; Douglas, P.; Burrow, H. D.: *Applied Photochemistry*; Springer, 2013.
- (69) Turro, N. J.: *Modern Molecular Photochemistry*; University science books, 1991.
- (70) Paria, S.; Reiser, O. Copper in Photocatalysis. *ChemCatChem* **2014**, *6*, 2477, doi: 10.1002/cctc.201402237.
- (71) Lazorski, M. S.; Castellano, F. N. Advances in the Light Conversion Properties of Cu^I-Based Photosensitizers. *Polyhedron* **2014**, *82*, 57, doi: 10.1016/j.poly.2014.04.060.
- (72) Kuang, S.-M.; Cuttell, D. G.; McMillin, D. R.; Fanwick, P. E.; Walton, R. A. Synthesis and Structural Characterization of Cu^I and Ni^{II} Complexes That Contain the Bis[2-(Diphenylphosphino)Phenyl]Ether Ligand. Novel Emission Properties for the Cu^I Species. *Inorg. Chem.* **2002**, *41*, 3313, doi: 10.1021/ic0201809.
- (73) Cuttell, D. G.; Kuang, S.-M.; Fanwick, P. E.; McMillin, D. R.; Walton, R. A. Simple Cu^I Complexes with Unprecedented Excited-State Lifetimes. *J. Am. Chem. Soc.* **2002**, *124*, 6, doi: 10.1021/ja012247h.
- (74) Luo, S.-P.; Mejía, E.; Friedrich, A.; Pazidis, A.; Junge, H.; Surkus, A.-E.; Jackstell, R.; Denurra, S.; Gladiali, S.; Lochbrunner, S.; Beller, M. Photocatalytic Water Reduction with Copper-Based Photosensitizers: A Noble-Metal-Free System. *Angew. Chem. Int. Ed.* **2013**, *52*, 419, doi: 10.1002/anie.201205915.
- (75) Siddique, Z. A.; Yamamoto, Y.; Ohno, T.; Nozaki, K. Structure-Dependent Photophysical Properties of Singlet and Triplet Metal-to-Ligand Charge Transfer States in Copper(I) Bis(Diimine) Compounds. *Inorg. Chem.* **2003**, *42*, 6366, doi: 10.1021/ic034412v.
- (76) Armaroli, N. Photoactive Mono- and Polynuclear Cu^I-Phenanthrolines. A Viable Alternative to Ru^{II}-Polypyridines? *Chem. Soc. Rev.* **2001**, *30*, 113, doi: 10.1039/B000703J.
- (77) Moudam, O.; Kaeser, A.; Delavaux-Nicot, B.; Duhayon, C.; Holler, M.; Accorsi, G.; Armaroli, N.; Séguy, I.; Navarro, J.; Destruel, P.; Nierengarten, J.-F. Electrophosphorescent Homo- and Heteroleptic Copper(I) Complexes Prepared from Various Bis-Phosphine Ligands. *Chem. Commun.* **2007**, 3077, doi: 10.1039/B707398D.
- (78) Zhang, Q.; Zhou, Q.; Cheng, Y.; Wang, L.; Ma, D.; Jing, X.; Wang, F. Highly Efficient Green Phosphorescent Organic Light-Emitting Diodes Based on Cu^I Complexes. *Adv. Mater.* **2004**, *16*, 432, doi: 10.1002/adma.200306414.
- (79) Czerwieńiec, R.; Kowalski, K.; Yersin, H. Highly Efficient Thermally Activated Fluorescence of a New Rigid Cu^I Complex [Cu(Dmp)(Phanephos)]⁺. *Dalton Trans.* **2013**, *42*, 9826, doi: 10.1039/C3DT51006A.
- (80) Czerwieńiec, R.; Yu, J.; Yersin, H. Blue-Light Emission of Cu^I Complexes and Singlet Harvesting. *Inorg. Chem.* **2011**, *50*, 8293, doi: 10.1021/ic200811a.
- (81) Kim, J.; Whang, D. R.; Park, S. Y. Designing Highly Efficient Cu^I Photosensitizers for Photocatalytic H₂ Evolution from Water. *ChemSusChem* **2017**, *10*, 1883, doi: 10.1002/cssc.201700389.

- (82) Crabtree, R. H.: *The Organometallic Chemistry of the Transition Metals*; John Wiley & Sons, 2009.
- (83) Lennox, A. J. J.; Fischer, S.; Jurrat, M.; Luo, S.-P.; Rockstroh, N.; Junge, H.; Ludwig, R.; Beller, M. Copper-Based Photosensitisers in Water Reduction: A More Efficient in Situ Formed System and Improved Mechanistic Understanding. *Chem. Eur. J.* **2016**, *22*, 1233, doi: 10.1002/chem.201503812.
- (84) Femoni, C.; Muzzioli, S.; Palazzi, A.; Stagni, S.; Zacchini, S.; Monti, F.; Accorsi, G.; Bolognesi, M.; Armaroli, N.; Massi, M.; Valenti, G.; Marcaccio, M. New Tetrazole-Based Cu^I Homo- and Heteroleptic Complexes with Various P[^]P Ligands: Synthesis, Characterization, Redox and Photophysical Properties. *Dalton Trans.* **2013**, *42*, 997, doi: 10.1039/C2DT32056H.
- (85) Kaeser, A.; Delavaux-Nicot, B.; Duhayon, C.; Coppel, Y.; Nierengarten, J.-F. Heteroleptic Silver(I) Complexes Prepared from Phenanthroline and Bis-Phosphine Ligands. *Inorg. Chem.* **2013**, *52*, 14343, doi: 10.1021/ic402342y.
- (86) Zhang, Y.; Schulz, M.; Wächtler, M.; Karnahl, M.; Dietzek, B. Heteroleptic Diimine–Diphosphine Cu^I Complexes as an Alternative Towards Noble-Metal Based Photosensitizers: Design Strategies, Photophysical Properties and Perspective Applications. *Coord. Chem. Rev.* **2018**, *356*, 127, doi: 10.1016/j.ccr.2017.10.016.
- (87) Cunningham, K. L.; McMillin, D. R. Reductive Quenching of Photoexcited Cu(Dipp)²⁺ and Cu(Tptap)²⁺ by Ferrocenes (Dipp = 2,9-Diisopropyl-1,10-Phenanthroline and Tptap = 2,3,6,7-Tetraphenyl-1,4,5,8-Tetraazaphenanthrene). *Inorg. Chem.* **1998**, *37*, 4114, doi: 10.1021/ic980213d.
- (88) Cunningham, K. L.; Hecker, C. R.; McMillin, D. R. Competitive Energy-Transfer and Reductive Quenching of the Ct Excited States of Copper(L) Phenanthrolines. *Inorg. Chim. Acta* **1996**, *242*, 143, doi: 10.1016/0020-1693(95)04859-6.
- (89) Karnahl, M.; Mejía, E.; Rockstroh, N.; Tschierlei, S.; Luo, S.-P.; Grabow, K.; Kruth, A.; Brüser, V.; Junge, H.; Lochbrunner, S.; Beller, M. Photocatalytic Hydrogen Production with Copper Photosensitizer–Titanium Dioxide Composites. *ChemCatChem* **2014**, *6*, 82, doi: 10.1002/cctc.201300459.
- (90) Mejía, E.; Luo, S.-P.; Karnahl, M.; Friedrich, A.; Tschierlei, S.; Surkus, A.-E.; Junge, H.; Gladiali, S.; Lochbrunner, S.; Beller, M. A Noble-Metal-Free System for Photocatalytic Hydrogen Production from Water. *Chem. Eur. J.* **2013**, *19*, 15972, doi: 10.1002/chem.201302091.
- (91) Fischer, S.; Hollmann, D.; Tschierlei, S.; Karnahl, M.; Rockstroh, N.; Barsch, E.; Schwarzbach, P.; Luo, S.-P.; Junge, H.; Beller, M.; Lochbrunner, S.; Ludwig, R.; Brückner, A. Death and Rebirth: Photocatalytic Hydrogen Production by a Self-Organizing Copper–Iron System. *ACS Catal.* **2014**, *4*, 1845, doi: 10.1021/cs500387e.
- (92) Kräutler, B.: *Vitamin B₁₂: Chemistry and Biochemistry*. Portland Press Ltd., 2005.
- (93) Halpern, J. Mechanisms of Coenzyme B₁₂-Dependent Rearrangements. *Science* **1985**, *227*, 869, doi: 10.1126/science.2857503.
- (94) Jaun, B.; Thauer, R.: Methyl-Coenzyme M Reductase and Its Nickel Corphin Coenzyme F₄₃₀ in Methanogenic Archaea. In *Nickel and Its Surprising Impact in Nature*, 2007.
- (95) Helvenston, M. C.; Castro, C. E. Nickel(I) Octaethylisobacteriochlorin Anion. An Exceptional Nucleophile. Reduction and Coupling of Alkyl Halides by Anionic and Radical

- Processes. A Model for Factor F_{430} . *J. Am. Chem. Soc.* **1992**, *114*, 8490, doi: 10.1021/ja00048a021.
- (96) Dey, M.; Li, X.; Kunz, R. C.; Ragsdale, S. W. Detection of Organometallic and Radical Intermediates in the Catalytic Mechanism of Methyl-Coenzyme M Reductase Using the Natural Substrate Methyl-Coenzyme M and a Coenzyme B Substrate Analogue. *Biochemistry* **2010**, *49*, 10902, doi: 10.1021/bi101562m.
- (97) Randaccio, L.; Furlan, M.; Geremia, S.; Šlouf, M.; Srnova, I.; Toffoli, D. Similarities and Differences between Cobalamins and Cobaloximes. Accurate Structural Determination of Methylcobalamin and of LiCl- and KCl-Containing Cyanocobalamins by Synchrotron Radiation. *Inorg. Chem.* **2000**, *39*, 3403, doi: 10.1021/ic0001199.
- (98) Healy, K. P.; Pletcher, D. The Chemistry of Electrogenerated Transition Metals Species - the Insertion of Olefins into a Nickel-Carbon Bond. *J. Organomet. Chem.* **1978**, *161*, 109, doi: 10.1016/S0022-328X(00)80916-X.
- (99) Scheffold, R.; Abrecht, S.; Orlinski, R.; Ruf, H. R.; Stamouli, P.; Tinembart, O.; Walder, L.; Weymuth, C.: Vitamin B₁₂-Mediated Electrochemical Reactions in the Synthesis of Natural Products. In *Pure Appl. Chem.*, 1987; Vol. 59.
- (100) Pattenden, G. Simonsen Lecture. Cobalt-Mediated Radical Reactions in Organic Synthesis. *Chem. Soc. Rev.* **1988**, *17*, 361, doi: 10.1039/CS9881700361.
- (101) Hill, H.; Pratt, J.; O'Riordan, M.; Williams, F.; Williams, R. The Chemistry of Vitamin B₁₂. Part XV. Catalysis of Alkyl Halide Reduction by Vitamin B₁₂: Studies Using Controlled Potential Reduction. *J. Chem. Soc. A: I, P, T* **1971**, doi: 10.1039/j19710001859.
- (102) Schrauzer, G. N.; Lee, L.-P.; Sibert, J. W. Alkylcobalamins and Alkylcobaloximes. Electronic Structure, Spectra, and Mechanism of Photodealkylation. *J. Am. Chem. Soc.* **1970**, *92*, 2997, doi: 10.1021/ja00713a012.
- (103) Schrauzer, G. N.; Sibert, J. W.; Windgassen, R. J. Photochemical and Thermal Cobalt-Carbon Bond Cleavage in Alkylcobalamins and Related Organometallic Compounds. Comparative Study. *J. Am. Chem. Soc.* **1968**, *90*, 6681, doi: 10.1021/ja01026a021.
- (104) Tada, M.; Kaneko, K. (Triphenyltin)Cobaloxime as a Reagent for Radical Generation from Bromides. *J. Org. Chem.* **1995**, *60*, 6635, doi: 10.1021/jo00125a067.
- (105) Shimakoshi, H.; Hisaeda, Y. B₁₂-TiO₂ Hybrid Catalyst for Light-Driven Hydrogen Production and Hydrogenation of C-C Multiple Bonds. *ChemPlusChem* **2014**, *79*, 1250, doi: 10.1002/cplu.201402081.
- (106) Shimakoshi, H.; Abiru, M.; Izumi, S.-i.; Hisaeda, Y. Green Molecular Transformation by a B₁₂-TiO₂ Hybrid Catalyst as an Alternative to Tributyltin Hydride. *Chem. Commun.* **2009**, 6427, doi: 10.1039/B913255D.
- (107) Izumi, S.-i.; Shimakoshi, H.; Abe, M.; Hisaeda, Y. Photo-Induced Ring-Expansion Reactions Mediated by B₁₂-TiO₂ Hybrid Catalyst. *Dalton Trans.* **2010**, *39*, 3302, doi: 10.1039/B921802E.
- (108) Shimakoshi, H.; Hisaeda, Y. Oxygen-Controlled Catalysis by Vitamin B₁₂-TiO₂: Formation of Esters and Amides from Trichlorinated Organic Compounds by Photoirradiation. *Angew. Chem.* **2015**, *127*, 15659, doi: 10.1002/ange.201507782.
- (109) Tian, H.; Shimakoshi, H.; Park, G.; Kim, S.; You, Y.; Hisaeda, Y. Photocatalytic Function of the B₁₂ Complex with the Cyclometalated Iridium(III) Complex as a Photosensitizer under Visible-Light Irradiation. *Dalton Trans.* **2018**, *47*, 675, doi: 10.1039/C7DT03742B.

- (110) Weiss, M. E.; Kreis, L. M.; Lauber, A.; Carreira, E. M. Cobalt-Catalyzed Coupling of Alkyl Iodides with Alkenes: Deprotonation of Hydridocobalt Enables Turnover. *Angew. Chem. Int. Ed.* **2011**, *50*, 11125, doi: 10.1002/anie.201105235.
- (111) Sun, X.; Chen, J.; Ritter, T. Catalytic Dehydrogenative Decarboxyolefination of Carboxylic Acids. *Nat. Chem.* **2018**, *10*, 1229, doi: 10.1038/s41557-018-0142-4.
- (112) Call, A.; Codolà, Z.; Acuña-Parés, F.; Lloret-Fillol, J. Photo- and Electrocatalytic H₂ Production by New First-Row Transition-Metal Complexes Based on an Aminopyridine Pentadentate Ligand. *Chem. Eur. J.* **2014**, *20*, 6171, doi: 10.1002/chem.201303317.
- (113) Call, A.; Franco, F.; Kandoth, N.; Fernández, S.; González-Béjar, M.; Pérez-Prieto, J.; Luis, J. M.; Lloret-Fillol, J. Understanding Light-Driven H₂ Evolution through the Electronic Tuning of Aminopyridine Cobalt Complexes. *Chem. Sci.* **2018**, *9*, 2609, doi: 10.1039/C7SC04328G.
- (114) Call, A.; Casadevall, C.; Acuña-Parés, F.; Casitas, A.; Lloret-Fillol, J. Dual Cobalt–Copper Light-Driven Catalytic Reduction of Aldehydes and Aromatic Ketones in Aqueous Media. *Chem. Sci.* **2017**, *8*, 4739, doi: 10.1039/C7SC01276D.
- (115) Call, A.; Lloret-Fillol, J. Enhancement and Control of the Selectivity in Light-Driven Ketone Versus Water Reduction Using Aminopyridine Cobalt Complexes. *Chem. Commun.* **2018**, *54*, 9643, doi: 10.1039/C8CC04239J.

UNIVERSITAT ROVIRA I VIRGILI
DEVELOPMENT OF VISIBLE LIGHT PHOTOREDOX METHODOLOGIES TOWARDS THE ACTIVATION
OF CARBON-HALOGEN BONDS
Miguel Claros Casielles

UNIVERSITAT ROVIRA I VIRGILI
DEVELOPMENT OF VISIBLE LIGHT PHOTOREDOX METHODOLOGIES TOWARDS THE ACTIVATION
OF CARBON-HALOGEN BONDS
Miguel Claros Casielles

Chapter II



Thesis Objectives

UNIVERSITAT ROVIRA I VIRGILI
DEVELOPMENT OF VISIBLE LIGHT PHOTOREDOX METHODOLOGIES TOWARDS THE ACTIVATION
OF CARBON-HALOGEN BONDS
Miguel Claros Casielles

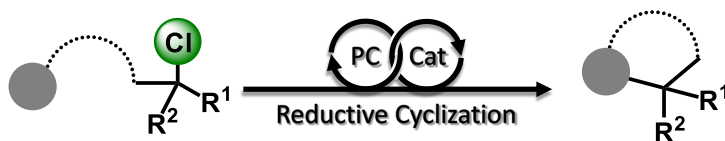
Organic halides scaffolds are predominant in both available feedstocks and biologically active molecules. Continuous development of photoredox methodologies has expanded the use of bench-stable radical precursors enabling the generation of new *Carbon–Carbon* and *Carbon–Heteroatom* bonds. This concept has been recently expanded for the activation of aryl chlorides. The chemical inertness of alkyl chlorides precludes their widespread use as electrophilic coupling partners in synthetic methodologies such as hydrodehalogenation or *Carbon–Carbon* and *Carbon–Heteroatom* bond-forming reactions.

Based on these premises, and the previous studies of the group for the reduction of ketones with a dual catalyst system based on PC_{Cu}/L^HCo , the main objectives of the thesis are:

- 1) Exploring the catalytic activity of the dual catalyst system (PC_{Cu}/L^HCo and PC_{Cu}/L^HNi) towards hydro-dehalogenation reactions of non-activated C–Halogen bonds, including C–Br, C–Cl and C–F bonds. Besides, we will apply this methodology for the hydro-dehalogenation of chlorinated and brominated pesticides and pharmaceuticals (*Chapter III*).



- 2) The development of the visible-light intramolecular cyclization reactions of non-activated alkyl chlorides containing tethered alkenes or alkynes catalyzed by the systems PC/M_{Cat} ($M = Co, Ni$) (*Chapter IV*). This would enable the construction of 5-membered carbocycles employing earth-abundant metals and using light as a source of energy.



- 3) Finally, we will study the mechanism of the activation of *Carbon-Chloride* bonds with the more active coordination *Co* and *Ni* catalysts (*Chapter V*). To this end, we will question the formation of radical intermediates by studying the reactivity of radical clocks and deuterated labelling experiments. In addition, we will investigate the putative formation of low valent Ni^I species by spectroscopic methods and spectroelectrochemical techniques.



UNIVERSITAT ROVIRA I VIRGILI
DEVELOPMENT OF VISIBLE LIGHT PHOTOREDOX METHODOLOGIES TOWARDS THE ACTIVATION
OF CARBON-HALOGEN BONDS
Miguel Claros Casielles

UNIVERSITAT ROVIRA I VIRGILI
DEVELOPMENT OF VISIBLE LIGHT PHOTOREDOX METHODOLOGIES TOWARDS THE ACTIVATION
OF CARBON-HALOGEN BONDS
Miguel Claros Casielles

Chapter III



Photocatalytic Activation of Carbon-Halogen Bonds

UNIVERSITAT ROVIRA I VIRGILI
DEVELOPMENT OF VISIBLE LIGHT PHOTOREDOX METHODOLOGIES TOWARDS THE ACTIVATION
OF CARBON-HALOGEN BONDS
Miguel Claros Casielles

III.1.	Contents	
III.2.	State-of-the-art.....	95
III.2. 1	Early Examples of Activation of Carbon–Halogen Bonds.....	99
III.3.	Results and Discussion	107
III.3. 1	Screening of the Conditions for the Activation of C–Cl Bonds	107
III.3. 2	Photoredox Activation of Halogenated Drugs and Derivatives.....	110
III.3. 3	Photoredox Activation of Organohalide Pesticides	113
III.3. 4	Photoredox Activation of Alkyl Fluorides.....	115
III.4.	Conclusions.	125
III.5.	Experimental Section.	127
III.5. 1	Material and Reagents.....	127
III.5. 2	Instrumentation.	127
III.5. 3	Experimental Procedures.	129
III.5. 4	Synthesis of Metal Complexes.....	130
III.5. 5	Synthesis and Characterization of Substrates.	140
III.5. 6	Characterization of Products.....	142
III.6.	References of the Chapter.....	145

Figure III.1 General mechanism for carbon-centered radical formation by visible-light photocatalysis.....	95
Figure III.2 Selected carbon-centered radical precursors for visible-light photocatalysis.	96
Figure III.3 Generation of alkyl and aryl radicals upon <i>SET</i> event. X = Cl, Br, I.	97
Figure III.4 Generation of alkyl radicals by the formation of <i>EDA</i> complex.	98
Figure III.5 Reduction of alkyl halides by <i>SET</i> process through the formation of radical-anion species.	98
Figure III.6 Light-driven reactivity of benzyl bromide with [Ru(bpy) ₃]Cl ₂ and BNAH photosensitizers.....	99
Figure III.7 Debromination of meso-1,2-dibromostilbene in a two-phase system.	100
Figure III.8 Kellogg's photoreduction at saturated carbon atoms using 3-methyl-2,3-dihydrobenzothiazole reductant.	101
Figure III.9 [Ru(bpy) ₃]Cl ₂ -photosensitized reduction of phenacyl bromide by a NADH analogue in the absence (left) and presence (right) of acid additive.....	101
Figure III.10 Photocatalytic reductive dehalogenation via photoredox catalysis.	102
Figure III.11 Photocatalytic dehalogenation of vicinal dibromocarbonyl compounds.....	103
Figure III.12 Selected halo-compounds and photocatalyst.....	104
Figure III.13 Reduction of aryl halides by consecutive visible-light-induced electron transfer processes (right) and lanthanide coupled photoinduced electron transfer (left).....	105

Figure III.14 UV-light-mediated generation of carbon radicals from organochlorides.	105
Figure III.15 Plot of the yield of the desired dehalogenated product vs the equivalents of ethanol respect to the initial amount of substrate.....	110
Figure III.16 Visible-light photocatalytic reduction of aryl halides.	111
Figure III.17 Selected drugs-containing aryl halides.	112
Figure III.18 Classification of organochlorinated pesticides.	113
Figure III.19 DDT dehalogenation reaction with iron porphyrin (top) and lindane dehalogenation with cobalt porphyrins (bottom).....	115
Figure III.20 First catalytic C–C bond formation involving a C–F bond cleavage reported.....	116
Figure III.21 Catalytic activation of C–F bonds by β -diketimate iron(II) complexes (left) and [Ni(acac) ₂] in the presence of N,N-dimesitylimidazolium chloride and NaO ⁱ Pr (right).	117
Figure III.22 Ni-catalyzed coupling of aryl and alkyl fluorides with Grignard reagents.....	117
Figure III.23 C–F bond cleavage reactions catalyzed by zirconocen complexes.	118
Figure III.24 Reactivity and proposed mechanism for the functionalization of unactivated trifluoromethylarenes.	118
Figure III.25 In-house developed parallel photoreactors.	129

Table III.1 Solvent screening for the photo-hydro-dehalogenation of alkyl chlorides.	108
Table III.2 Screening of equivalents of EtOH as protic solvent.	109
Table III.3 Solvent screening for the hydro-defluorination reaction.....	119
Table III.4 Control experiments for the hydro-defluorination reaction.	120
Table III.5 Screening of the reaction conditions	121
Table III.6 Catalyst screening	122
Table III.7 Comparison between copper and iridium based photocatalyst.	123
Table III.8 Substrate scope for hydro-defluorination reaction.	124

III.2. State-of-the-art.

In the search for more sustainable synthetic methodologies, over the last decades, chemists have been making great efforts to avoid the extensive use of toxic and hazardous reagents, harsh reaction conditions and expensive and sophisticated catalysts. Chemists have been attempting the development of energy-efficient processes that minimize energy consumption, the use of expensive metals (i.e. palladium, platinum) and waste products.¹⁻⁴ In this regard, photocatalysis has emerged as an eco-friendly synthetic protocol.

Nowadays, visible-light photoredox catalysis is a powerful tool for carbon-carbon ($C-C$) and carbon-heteroatom ($C-Het$) bond-forming or bond-scission reactions. A large number of photocatalytic reactions proceed through the formation of short-lived radical intermediates that are initiated through single-electron transfer (SET) processes from a photoredox mediator under visible-light irradiation (**Figure III.1**).⁵⁻⁷

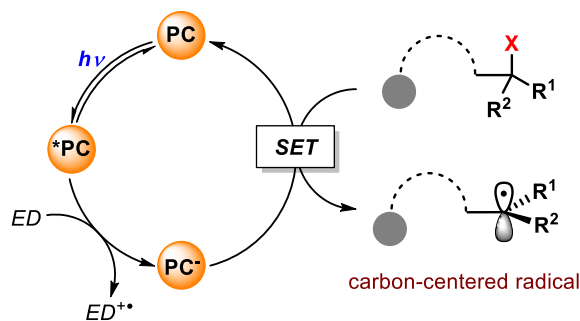


Figure III.1 General mechanism for carbon-centered radical formation by visible-light photocatalysis.

Radicals are highly reactive species against most organic molecules. For instance, radicals can be oxidized or reduced, they can abstract univalent atoms or even whole functional groups (transfer reactions),⁸ and they can be added to π -bonds or aromatic rings. Usually, their inherently high reactivity nature would compromise the reaction selectivity. Thus, gaining control over the selectivity in radical based

reactions is still challenging in both conventional catalysis and modern photocatalysis. One successful strategy to obtain selectivity is to employ bench-stable chemicals that serve as radical precursors, in such a way that in the process of the radical generation low concentrations are maintained. Therefore, the low concentration of radicals minimizes lateral reactivity such as radical dimerization processes. This control in the concentration can be achieved by regulating the rate of radical formation. To this end, carboxylic acids,⁹ potassium alkyltrifluoroborates,^{10,11} ammonium alkyl silicates,^{12,13} redox-active esters,¹⁴ dihydropyridines,^{15,16} and organic halides⁵ (**Figure III.2**) serve as useful radical precursors using photocatalysis. The activation modes of these precursors will depend on their specific nature, and can generally be classified as i) direct activation by light, ii) via the formation of *electron donor-acceptor (EDA)* complexes,¹⁷ and iii) via a *SET* process from a photocatalyst via either an oxidative or reductive quenching cycle.

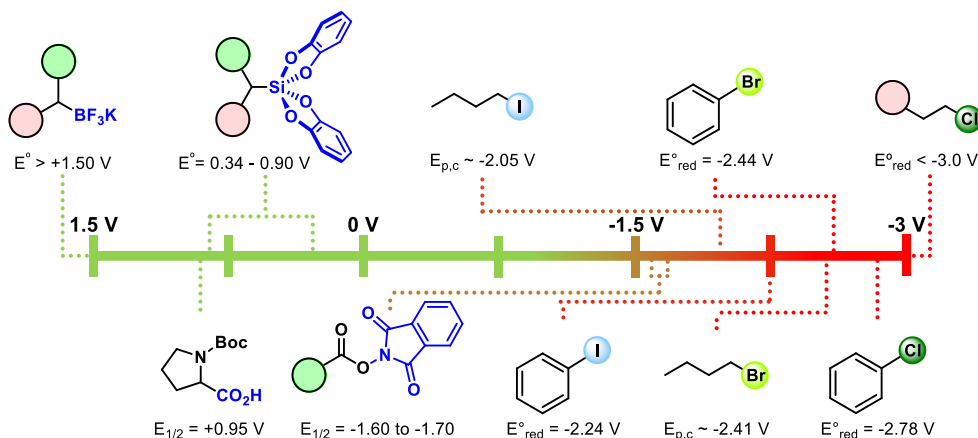


Figure III.2 Selected carbon-centered radical precursors for visible-light photocatalysis. Redox potentials are given in V vs SCE.

For the organic halides, the nature of the halide, and functional groups that electronically affect the carbon-halide (*C-Hal*) bond will dictate the reactivity. But in general, the reactivity trend for *C-Hal* bond activation follows $I > Br > Cl \gg F$. This order can be related to the bond dissociation energy (*BDE*) of the *C-Hal* bond (*BDE* for *C-I*, *C-Br*, *C-Cl*, *C-F* are 53, 67, 81, 109 kcal·mol⁻¹, respectively).¹⁸

Concerning the structure of the organohalides, the following general reactivity trend, from more reactive to less reactive, can be found: benzylic > allylic > vinylic > aromatic > aliphatic.¹⁹

For the usual redox reduction processes, the activation mechanism follows a concerted dissociative pathway where the C–Hal bond homolytically cleaves when an electron is transferred (**Figure III.3**, top).^{20,21} The dissociation of aromatic halides proceeds through a stepwise mechanism to form a radical anion intermediate (**Figure III.3**, bottom). Then, the generated reactive radical can be coupled with other transformations, such as hydrogen atom abstraction to form the dehalogenated product, or coupling with a radical acceptor to generate a carbon-carbon (C–C) or carbon-heteroatom (C–Het) bonds. The redox reduction event of the organic halide can be produced *via* a photoredox process.

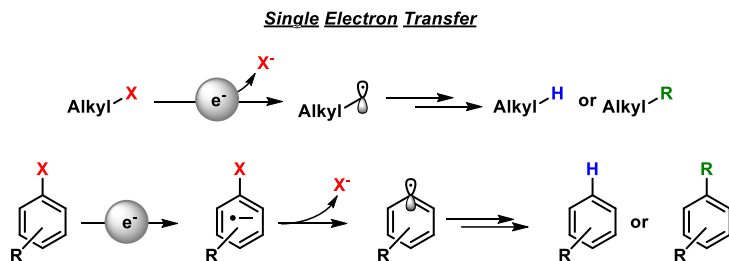


Figure III.3 Generation of alkyl and aryl radicals upon SET event. X = Cl, Br, I.

It is also valuable to note that, alkyl and aryl iodides can be directly activated by light if the wavelength and light flux are strong enough. They can also produce carbon centered radicals *via electron donor-acceptor (EDA) complexes* (**Figure III.4**), but commonly, a SET process from a photosensitizer accelerates this type of reaction significantly. The alkyl radical and aryl bromides behave similarly, however in this case, direct light activation is not likely, and EDA complexes are scarce. As illustrated by the BDE and redox potentials in **Figure III.2**, the activation of alkyl and aryl chlorides is more difficult, especially for the non-activated ones. They usually do not absorb visible-light directly, and even if they do, the BDE is larger than the energy of a 380 nm photon (84 vs 75 kcal·mol⁻¹, respectively). Therefore,

alkyl and aryl chlorides are unlikely to be activated by a single visible photon process, nor by an *EDA* complex.

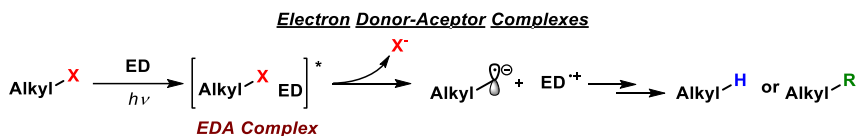


Figure III.4 Generation of alkyl radicals by the formation of *EDA* complex.

Although much time and effort has been devoted to the electrochemical reduction of alkyl halides,^{22,23} no precise data has been obtained due to the highly reactive nature of the radical anion intermediates formed. As a general trend, tertiary halides are more easily reduced than secondary, followed by primary ones.¹⁹ Then, the radical-anion usually suffers an irreversible fragmentation forming a halide anion and the corresponding carbon center radical (**Figure III.5**). Since the stability of the radical-anion is low, many authors consider this two-step process as a concerted electron-transfer-bond cleavage process.

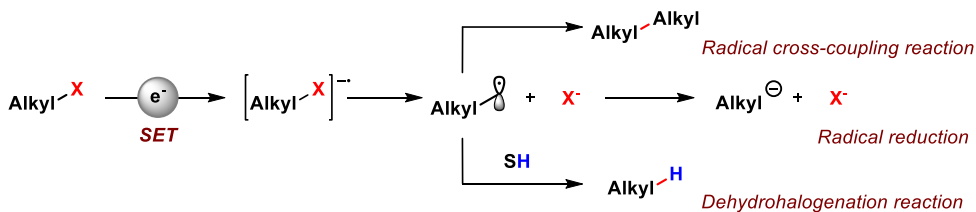


Figure III.5 Reduction of alkyl halides by SET process through the formation of radical-anion species.

In some cases, the redox potential of both alkyl iodides and bromides can be measured, although with compromised accuracy. In contrast, the reduction of alkyl chlorides is usually close to the discharge of the supporting electrolyte. Therefore, most of the tabulated standard potentials for the reaction $R - Cl + e^- \leftrightarrow R \cdot + X^-$ are estimated based on thermodynamic cycles similar to previously described procedures.^{24,25}

III.2.1 Early Examples of Activation of Carbon-Halogen Bonds.

Although there are a large variety of developed reducing methods, they usually require the use of highly toxic, environmentally hazardous or explosive reagents such as alkyl-stannanes or boranes.²⁶ The number of photoredox hydro-dehalogenation procedures is still small. In this context, Tanaka and co-workers published in 1984 the first example of a photoredox promoted hydro-dehalogenation reaction of benzyl bromide with 1-benzyl-1,4-dihyronicotinamide (*BNAH*) photocatalyzed by $[\text{Ru}(\text{bpy})_3]^{2+}$.²⁷ In the presence of ruthenium *PC*, the reaction involves a reductive quenching mechanism by the *BNAH* forming a reduced $[\text{Ru}^{\text{I}}]$ intermediate which undergoes a *SET* event forming the alkyl radical species. This reactive intermediate is further reduced *via* a *SET* yielding a benzyl anion which undergoes an $\text{S}_{\text{N}}2$ type reaction with another benzyl bromide equivalent to form the homocoupling 1,2-diphenylethane product (**Figure III.6**, left). Otherwise, in the absence of $[\text{Ru}(\text{bpy})_3]^{2+}$ irradiation with UV-Vis light gives rise to the photoinduced electron transfer (*ET*) process from *BNAH* leading to dehalogenation of the benzyl bromide. In this case, the reaction is postulated to proceed through a radical chain mechanism involving benzyl radical as a chain carrier (**Figure III.6**, right).

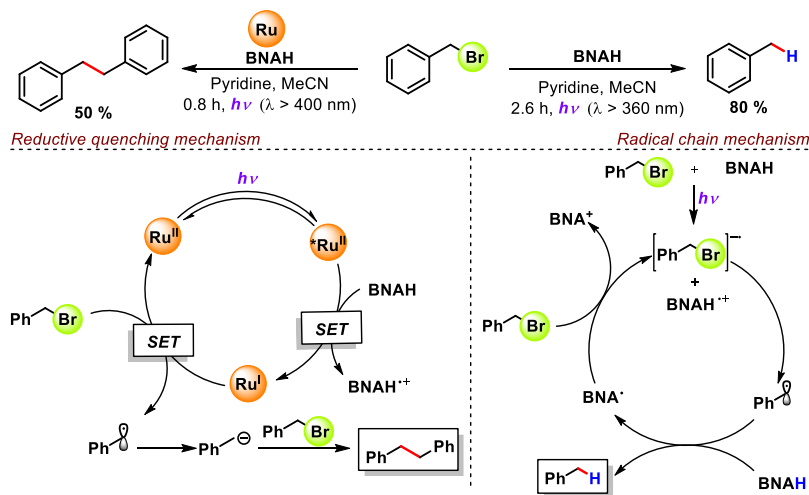


Figure III.6 Light-driven reactivity of benzyl bromide with $[\text{Ru}(\text{bpy})_3]\text{Cl}_2$ and *BNAH* photosensitizers.

Almost at the same time, Wilner and co-workers showed a biphasic ethyl acetate/water system using $[\text{Ru}(\text{bpy})_3]\text{Cl}_2$ as photocatalyst, $(\text{NH}_4)_3\text{EDTA}$ as electron donor and viologen (C_8V^{2+}) as a phase-transfer reduction co-catalyst for the photocatalytic debromination of dibromostilbene (**Figure III.7**).²⁸

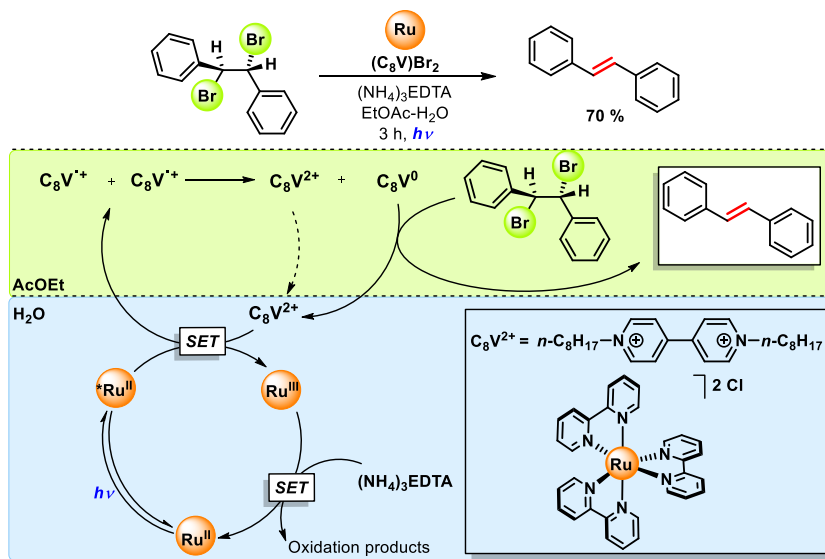


Figure III.7 Debromination of meso-1,2-dibromostilbene in a two-phase system.

Later on, the same authors showed that the $[\text{Ru}(\text{bpy})_3]\text{Cl}_2/\text{Et}_3\text{N}$ system also enables debromination reactions in the absence of viologen co-catalyst as demonstrated for the reduction of ethyl dibromocinnamate to ethyl cinnamate.²⁹ A similar approach was explored by Kellogg's group for the reduction of phenacyl bromide, bromomalonates and related compounds. Among the several photocatalysts tested ($[\text{Ru}(\text{bpy})_3]\text{Cl}_2$, mesotetraphenylporphyrin (TPP), eosin disodium salts or rose Bengal), best results were obtained with $[\text{Ru}(\text{bpy})_3]\text{Cl}_2$ as photocatalyst (**Figure III.8**).³⁰

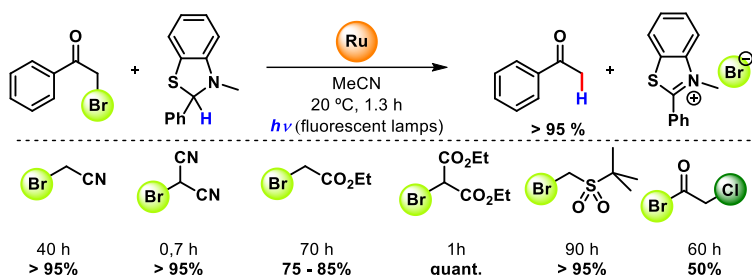


Figure III.8 Kellogg's photoreduction at saturated carbon atoms using 3-methyl-2,3-dihydrobenzothiazole reductant.

In 1990, another seminal example was reported by Fukuzumi and co-workers. They illustrated how the quenching process in the photocatalyzed reduction of phenacyl halides mediated by $[\text{Ru}(\text{bpy})_3]^{2+}$ could be simply switched with the pH. Interestingly, the redox potential of the ketone is reduced in the presence of HClO_4 , enabling the direct oxidative quenching to form the ketyl radical. In the absence of the acid, the 10-methyl-9,10-dihydroacridine (AcrH_2) reductively quenches the excited state $[\text{Ru}(\text{bpy})_3]^{2+*}$ forming a low-valent $[\text{Ru}^{\text{I}}]$ intermediate that engages into a SET to the ketone forming the ketyl radical before the debromination step (**Figure III.9**).

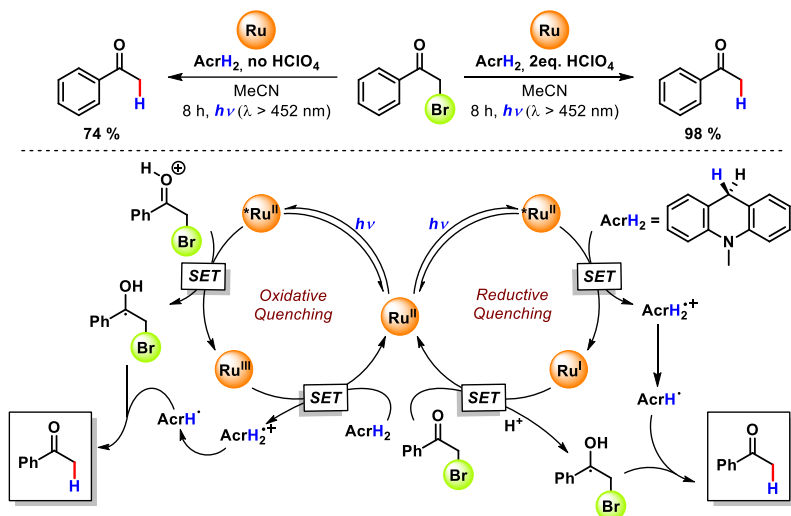


Figure III.9 $[\text{Ru}(\text{bpy})_3]\text{Cl}_2$ -photosensitized reduction of phenacyl bromide by a NADH analogue in the absence (left) and presence (right) of acid additive.

These pioneering works from the groups of Willner, Kellogg, Tanaka and Fukuzumi showed the potential of photoredox catalyzed hydro-dehalogenation reactions in organic chemistry. Nevertheless, it was not until 2008 when an increasing number of publications appeared in the literature. Many of the methodologies of photoinduced *SET* to organic halides published were used for the formation of new *C–C* or *C–Het* bonds, those examples will be discussed in *Chapter IV*. For the photo-hydro-dehalogenation reactions, Stephenson and co-workers showed in 2009 a simple procedure for the reduction of activated *C–Hal* bonds with excellent functional group tolerance and chemoselectivity over aryl and vinyl *C–Hal* bonds.³¹ In this case, the dehalogenation reaction was catalyzed by $[\text{Ru}(\text{bpy})_3]\text{Cl}_2$ in combination with *i*Pr₂NEt and HCO₂H or Hantzsch ester as the hydrogen atom donor (Figure III.10).

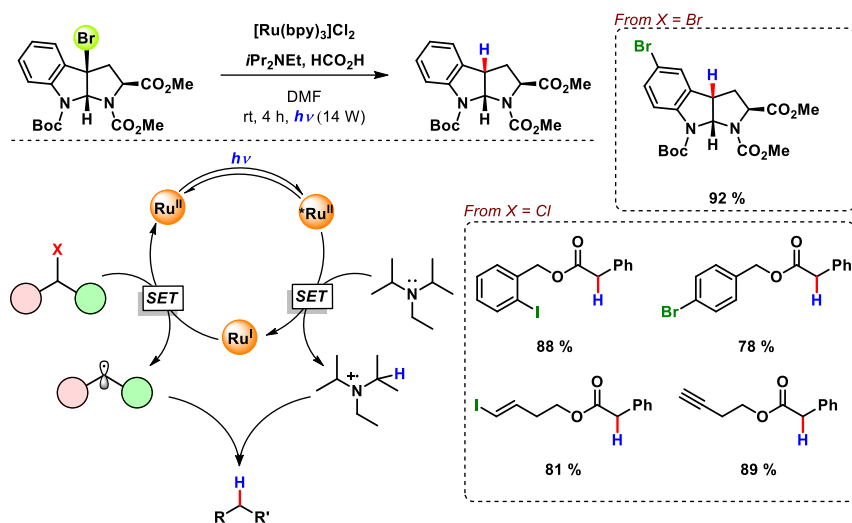


Figure III.10 Photocatalytic reductive dehalogenation via photoredox catalysis.³¹

Two years later, Reiser's group developed a photoreduction method catalyzed by $[\text{Ru}(\text{bpy})_3]\text{Cl}_2$ with ascorbic acid as the reductant and 1,5-dimethoxynaphthalene (DMN) as electron transporter to achieve dehalogenation of α -haloketones.³² In this example, sequential electron transfer processes allow the reductive debromination reaction of vicinal dibromo compounds to the corresponding (*E*)-alkenes and alkynes (Figure III.11, top). In this transformation,

carbonyl groups positioned in alpha to one halogen atom are required. Moreover, when both bromine atoms were located at the same carbon, they could obtain selective mono- or di-debromination reaction by modifying the reaction time, obtaining only mono-debromination at short reaction times and di-debromination at longer ones (Figure III.11, bottom).

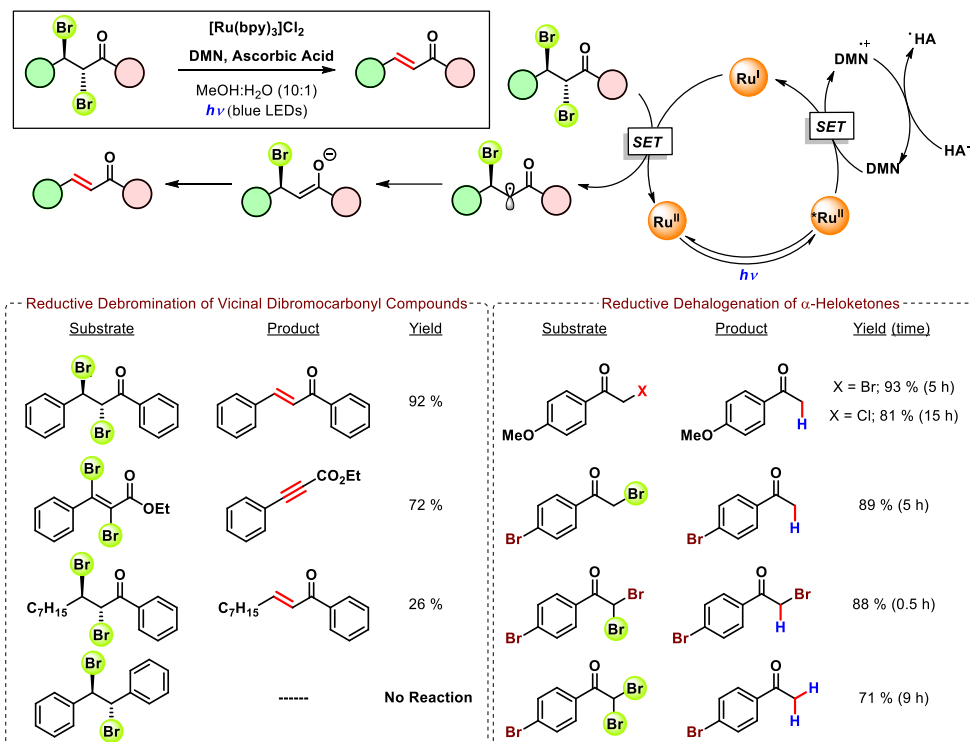


Figure III.11 Photocatalytic dehalogenation of vicinal dibromocarbonyl compounds.

In 2012, Stephenson and co-workers introduced iridium photoredox catalysts into the field of dehalogenation reactions for the radical reductive deiodination of alkyl, alkenyl and aryl iodides.³³ By increasing the redox potential of the photocatalyst, they could engage the activation of stronger C-Hal bonds as non-activated alkyl iodides (Figure III.12).

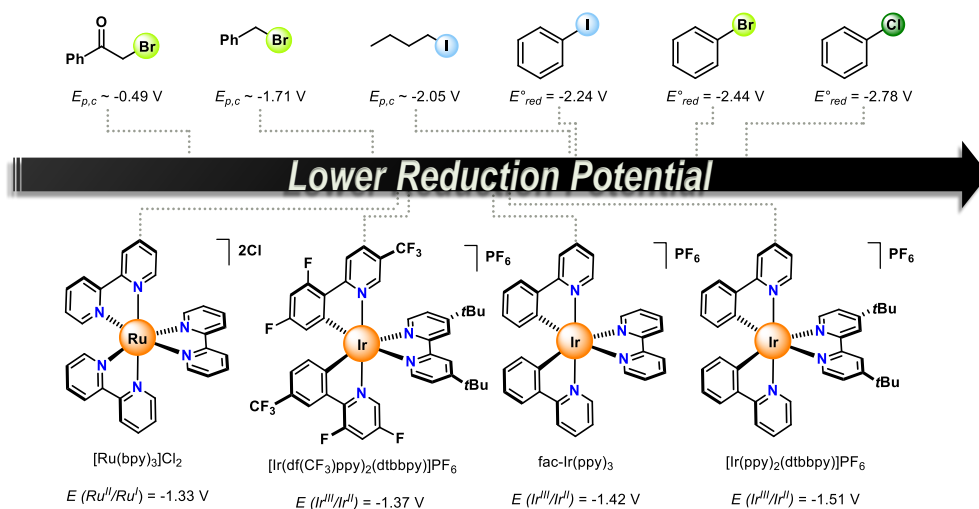


Figure III.12 Selected halo-compounds and photocatalyst. Redox potentials are given in V vs SCE.

Interestingly, a carbon-centered radical intermediate can be directly formed by the activation of a C–I bond *via* a photoinduced *SET* from the excited state of [Ir(ppy)₃] in an oxidative quenching pathway. A following H-atom abstraction step generates the final reduced product. Alternatively, the formed radical species can undergo intramolecular cyclizations when the substrate contains a π -acceptor group. This type of reductive cyclization reactions will be further discussed in the next chapter of this thesis. The versatility and simplicity of this protocol allows for an easy scale-up, low catalyst loading and short reaction times when the reaction is performed in a flow reactor. Moreover, flow chemistry facilitates the use of photoredox catalysis in the area of radical chemistry, previously dominated by tin, SmI₂ and trialkylborane reagents.^{8,34,35}

Continuous development of novel photoredox catalysts that provide higher reducing power has expanded the redox-potential window facilitating the cleavage of alkyl bromides *via* *SET* processes.^{36,37} In 2014, König and co-workers introduced the power of two photons in each catalytic cycle³⁸ and the reducing power of lanthanides³⁹ for the functionalization of the less reactive and more accessible aryl chlorides (**Figure III.13**).

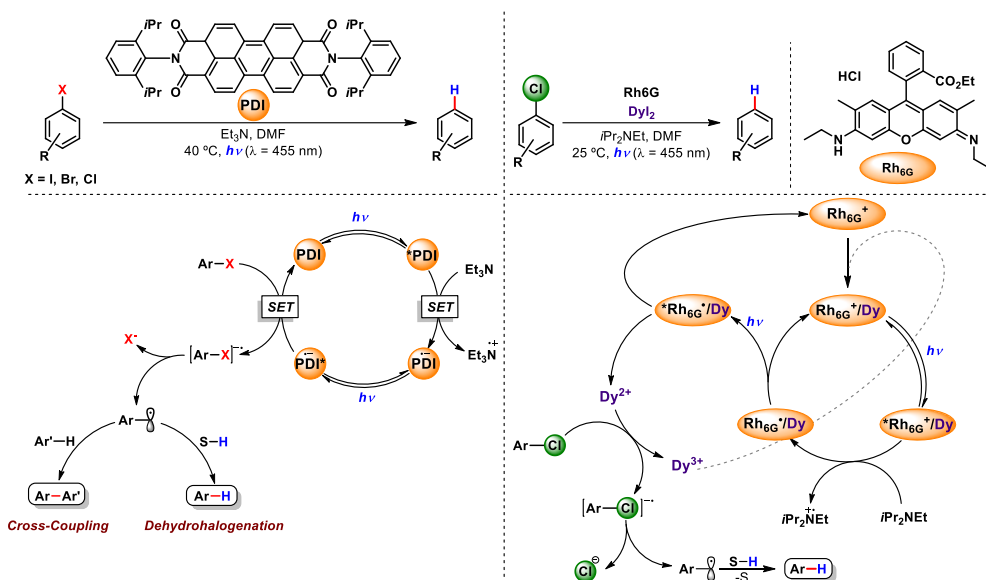


Figure III.13 Reduction of aryl halides by consecutive visible-light-induced electron transfer processes (left)³⁸ and lanthanide coupled photoinduced electron transfer (right).³⁹

The introduction of organic photocatalysts by König opened the window for more challenging transformations getting broadening the functional group tolerance with yields up to 82 % under really mild conditions (blue light, 25 °C).³⁹ Since these initial studies, organic photocatalysts have been used for this kind of transformations. In 2018, Matsubara and co-workers reported the first example of photoreduction of unactivated alkyl chlorides by using UV light in the presence of 1,4-cyclohexadiene (*CHD*) as hydrogen atom donor (**Figure III.14**).⁴⁰

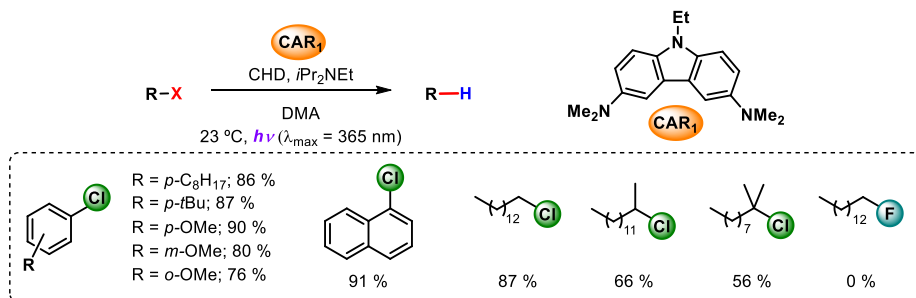


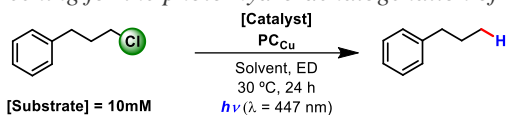
Figure III.14 UV-light-mediated generation of carbon radicals from organochlorides.

III.3. Results and Discussion

III.3.1 Screening of the Conditions for the Activation of C–Cl Bonds

Inspired by these precedents, we envisioned the *in situ* photogeneration of low-valent cobalt and nickel complexes that behave as supernucleophiles, capable of activating strong Csp^3-Cl bonds under visible-light irradiation. To test this hypothesis, we started by evaluating cobalt and nickel complexes in the reductive photo-hydro-dehalogenation reaction of (3-chloropropyl)benzene. Based on previous studies of the group (see **Section I.5** in the general introduction) we selected $[M(OTf)(Py_2T^stacn)](OTf)$, (where $M = Co$ (I^HCo), Ni (I^HNi)) in combination with $[Cu(bathocuproine)(Xantphos)](PF_6)$ (PC_{Cu}) as dual catalyst system in an acetonitrile solution. Running the reaction for 24 hours at 30 °C, low conversions were obtained with yields not higher than 13 % in the combination of I^HCo with PC_{Cu} and Et_3N or iPr_2NEt as *ED* (**Table III.1**, entries 1 and 2). Under similar reaction conditions employing the corresponding nickel complex, I^HNi affords higher conversions (24%) but lower yields (7 %) of the desired dehalogenated product (entries 3 and 4). The use of alternative solvents such as THF or toluene did not increase the yield of the dehalogenated product due to the insolubility of the catalyst (entries 6 and 7). On the other hand, the introduction of protic co-solvents in combination with MeCN into the reaction mixture increased the yield, reaching 83% and 92% for the reduced product by using I^HCo or I^HNi in combination with PC_{Cu} and Et_3N or iPr_2NEt as *ED* (entries 8 and 9). Finally, the combination of THF with EtOH as co-solvent gave the desired product in 65% yield but without achieving the full conversion of the initial substrate after 24 h (entry 12).

Table III.1 Solvent screening for the photo-hydro-dehalogenation of alkyl chlorides.



Entries	Catalyst (mol%)	Solvent	ED (eq)	Conv. (%)	Yield (%)
1	1^{H}Co (5)	MeCN	Et_3N (14.4)	22	13
2	1^{H}Co (5)	MeCN	$i\text{Pr}_2\text{NEt}$ (11.4)	15	9
3	1^{H}Ni (5)	MeCN	Et_3N (14.4)	24	7
4	1^{H}Ni (5)	MeCN	$i\text{Pr}_2\text{NEt}$ (11.4)	11	6
5 ^a	1^{H}Ni (5)	MeCN	$i\text{Pr}_2\text{NEt}$ (11.4)	26	9
6	1^{H}Ni (5)	THF	$i\text{Pr}_2\text{NEt}$ (11.4)	12	7
7	1^{H}Ni (5)	PhCH_3	$i\text{Pr}_2\text{NEt}$ (11.4)	10	4
8	1^{H}Co (5)	EtOH : MeCN (3:2)	Et_3N (14.4)	90	83
9	1^{H}Ni (5)	EtOH : MeCN (3:2)	$i\text{Pr}_2\text{NEt}$ (11.4)	94	92
10^a	1^{H}Ni (5)	EtOH : MeCN (3:2)	$i\text{Pr}_2\text{NEt}$ (11.4)	100	95
11^b	1^{H}Ni (5)	EtOH : MeCN (3:2)	$i\text{Pr}_2\text{NEt}$ (11.4)	96	95
12	1^{H}Ni (5)	THF:EtOH (2:3)	$i\text{Pr}_2\text{NEt}$ (11.4)	73	65

Conditions: substrate (10 mM), PCu (2 mol%), visible-light irradiation with blue LEDs (1 W, 447 nm) for 24 h at 30 °C. Conversion and yield were determined by GC using biphenyl as internal standard. ^aThe reaction was carried out in the presence of 10 eq. of NaOTf. ^bThe reaction was carried out in the presence of 10 eq. of THF.

It was hypothesized that the cleavage of the $\text{C}-\text{Hal}$ bond was reversible; thus, it has been reported in free radical polymerization the reversible cleavage of $\text{C}-\text{Hal}$ bonds to generate carbon centered radicals and halide anions. To avoid the potential reversibility of the reaction, some additives were tested to improve the yield by removing those chlorine atoms from the media. In apolar solvents, chlorine anions can be effectively removed by adding sodium salts with large and low polarized anions, forming insoluble NaCl. Meanwhile, chlorine radicals can be removed from the media by THF by HAT yielding HCl.⁴¹ Based on this, the presence of 10 equivalents of sodium salts in the reaction media improved the conversion of the starting chloroalkane from 11 to 26 % in pure acetonitrile solution without any improvement in the yield (entry 5). On the other hand, when ethanol is present, full

conversion was obtained with 95 % of yield for the desired product (improving the 94 % of conversion and 92 % of yield in the absence of additives; entry 10). Besides, the reaction in the presence of THF gave, as well, better results than in the absence of it (entry 11).

Sighting the crucial role of the protic solvent in the dehalogenation reaction of alkyl chlorides, we studied the impact of the equivalents of ethanol into the reaction yield. Surprisingly, we observed a drop of 30% in the yield by reducing the amount of ethanol to half (**Table III.2**, entry 2). **Table III.2** and **Figure III.15** show the results obtained with different amounts of ethanol as co-solvent in combination with acetonitrile. The presence of only 11 equivalents (or less) of ethanol gave between 6 and 7 % of yield (entries 7 to 11). We suggest that ethanol is the hydrogen atom donor that quenches the radical species after the activation of the Csp^3-Cl bond (**Figure III.5**). The amount of *ED* was also tested, observing as well, a detrimental effect on the yield when decreasing the equivalents of *ED* (entries 3, 6, 10).

Table III.2 Screening of equivalents of EtOH as protic solvent.

Entries	Eq. of EtOH*	ED (eq.)	Conv. (%)	Yield (%)
1	1063 (3/2)	<i>i</i>Pr₂NEt (11.4)	96	88
2	531	<i>i</i> Pr ₂ NEt (11.4)	70	59
3	531	<i>i</i> Pr ₂ NEt (5.7)	52	40
4	177	<i>i</i> Pr ₂ NEt (11.4)	36	28
5	106	<i>i</i> Pr ₂ NEt (11.4)	28	20
6	106	<i>i</i> Pr ₂ NEt (1.1)	13	6
7	11	<i>i</i> Pr ₂ NEt (11.4)	13	7
8	3	<i>i</i> Pr ₂ NEt (11.4)	13	7
9	2	<i>i</i> Pr ₂ NEt (11.4)	13	7
10	2	<i>i</i> Pr ₂ NEt (0.01)	13	6
11	0	<i>i</i> Pr ₂ NEt (11.4)	11	6

*Conditions: substrate (10 mM), I^HNi (5 mol%) PC_{Cu} (2 mol%), visible-light irradiation with blue LEDs (1 W, 447 nm) for 24 h at 30 °C. Conversion and yield were determined by GC using biphenyl as internal standard. *equivalents of EtOH respect to the substrate in combination with acetonitrile.*

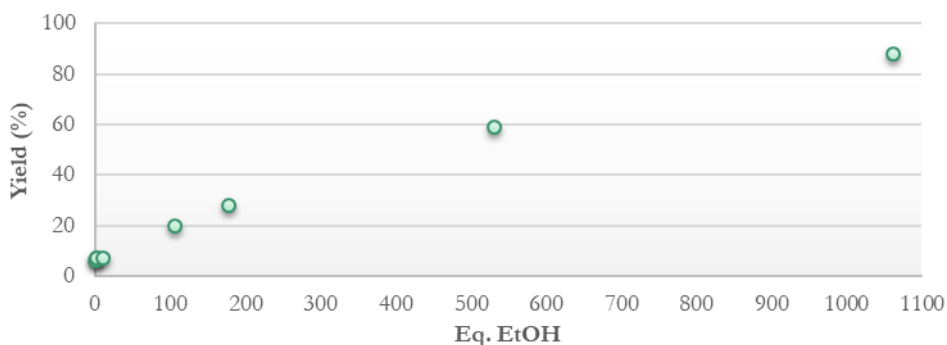


Figure III.15 Plot of the yield of the desired dehalogenated product vs the equivalents of ethanol respect to the initial amount of substrate.

Based on these studies, we could identify the pair $PC_{Cu}/I^H M$ as an efficient photocatalytic system for the reduction of non-activated alkyl chlorides in the presence of tri-alkyl amines as *ED* and protic solvents such as ethanol. Based on these results, we applied the developed catalytic dehalogenation methodology to reduce biologically active polyhalogenated molecules, such as drugs or pesticides, which cause environmental concerns due to their use and persistence in nature.

III.3. 2 Photoredox Activation of Halogenated Drugs and Derivatives

A large number of drugs and drugs precursors are based on halogenated structures. Halogen atoms are well known to play essential roles in non-covalent interactions such as halogen-bonding interactions, hydrogen-bond acceptors or as Lewis-acids.⁴² The anisotropic distribution of the charge density on the halogen atom induces them to participate in intermolecular interactions, which improves medicinal issues such as oral absorption, permeability, metabolic and chemical stability among others.^{43,44} Nowadays, many of the efforts of the chemical companies are to find straightforward and sustainable methodologies to perform halogenation reactions to design new drugs or unknown drug-receptors. Furthermore, many times, this installed halogen atom is used as a protecting or resilient group for late-stage functionalization. However, the presence of these halogen atoms also has the disadvantage of producing toxic molecules resilient in the environment, producing

unwanted waste that accumulates in the biosphere and propagates through the trophic chain. In this way, a sustainable protocol for the selective activation of carbon-halogen bonds could open the door for greener dehalogenation of complex molecules and the environmentally friendly treatment of the medical wastes.

In this regard, König and co-workers published in 2016 a fast colorimetric screening for visible-light photocatalytic oxidation and reduction reactions.⁴⁵ Of all photocatalysts tested in that study, (PDI, [Ir(ppy)₃] and [Ru(ppy)₃]Cl) only the iridium one gave, in all the cases, conversions higher than 60% and yielded up to 100 % for the dehalogenated product (**Figure III.16**, top). After showing that some simple aryl bromides and chlorides can be dehalogenated, the potential of this methodology is showcased by accomplishing the reduction of commercially available drugs such as bromazepam, hydrochlorothiazide and benzbromarone (**Figure III.16**, bottom).

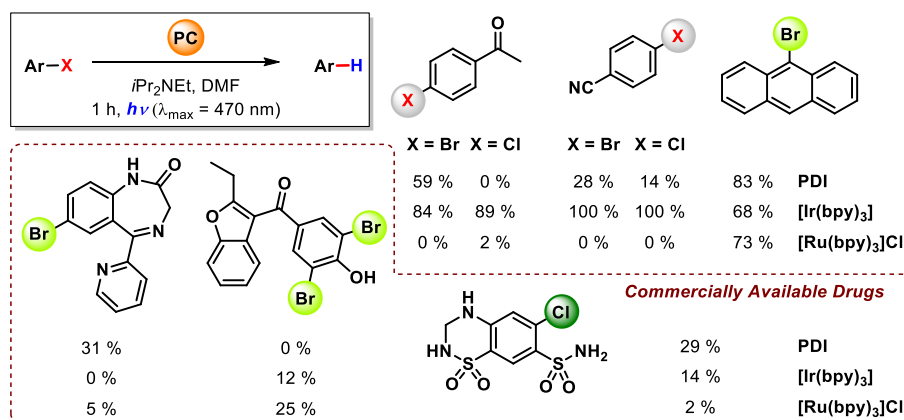


Figure III.16 Visible-light photocatalytic reduction of aryl halides.

Considering this precedent, we tested our dual catalyst *PC_{Cu}/LNi* developed for the activation of *Csp³-Cl* bonds towards the dehalogenation of relevant halogenated pharmaceuticals. Therefore, a family of commercially available drugs depicted in **Figure III.17** were submitted to our optimized photocatalytic conditions: 5 mol% of *I^HNi*, 2 mol% of *PC_{Cu}*, 11.4 equivalents of *iPr₂NEt* as *ED* in a 3/2 mixture of ethanol/acetonitrile as solvent. The reactions took place during 24 h at 30 °C under

blue light irradiation ($\lambda = 447$ nm) after which, a work-up based on aqueous extractions to remove the metallic salts was utilized.

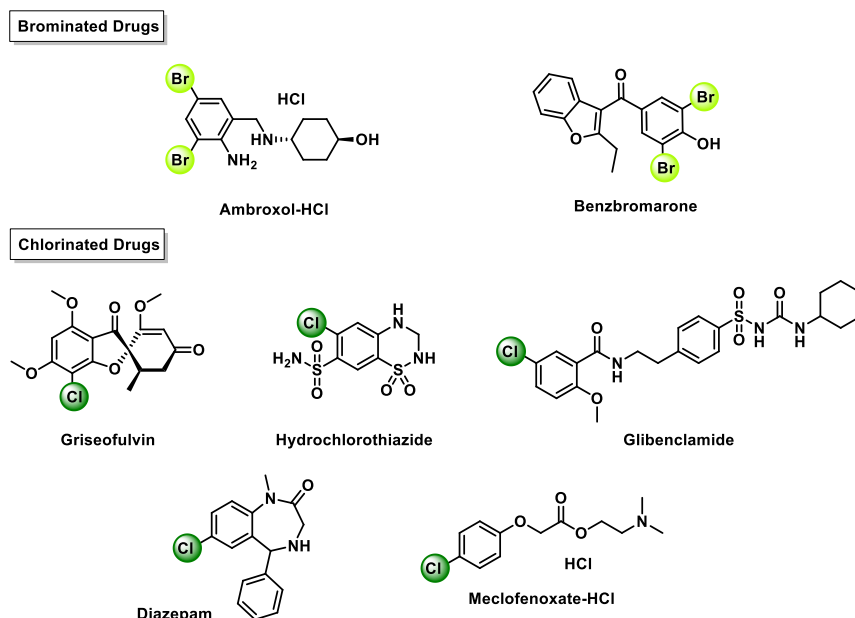


Figure III.17 Selected drugs-containing aryl halides.

Our study started with the exploration of drugs containing arylbromides such as Ambroxol or Benzbromarone. Under the previously optimized conditions for the dehalogenation reaction of alkyl halides, both drugs were entirely consumed after 24 h. When aryl chlorides were tested the complete consumption of the starting material was observed for Griseofulvin, Hydrochlorothiazide and Glibenclamide. The reactions produced a complex mixture of products that were not possible to identify in most of the cases. Otherwise, the photocatalytic reduction of Diazepam and Meclofenoxate gave the corresponding dehalogenated product.

III.3.3 Photoredox Activation of Organohalide Pesticides

Pesticides are defined as substances, or mixture of substances, intended for preventing or controlling attacks on products by destructive species. Within this kind of compounds, organohalides were the first and most widely used synthetic organic molecules. Most of them contain chlorine as the only halogen atom because they are relatively stable, and highly toxic to insects but not to human beings. On the other hand, pesticides are becoming an environmental problem due to their accumulation in the biosphere, in agricultural products (grain, pulse or vegetables) and animal products (meat, milk or eggs).

Structurally, we can organize them in four major chemical classes. The first of these consists of the chloroethylene derivatives, of which *DDT* and *Methoxychlor* are the prime examples. The second major class is composed of chlorinated cyclodiene compounds, including *Aldrin*, *Dieldrin*, and *Heptachlor*. The benzene hexachloride derivatives make up the third class of organochlorine insecticides, and toxaphenes constitute the fourth (Figure III.18).⁴⁶

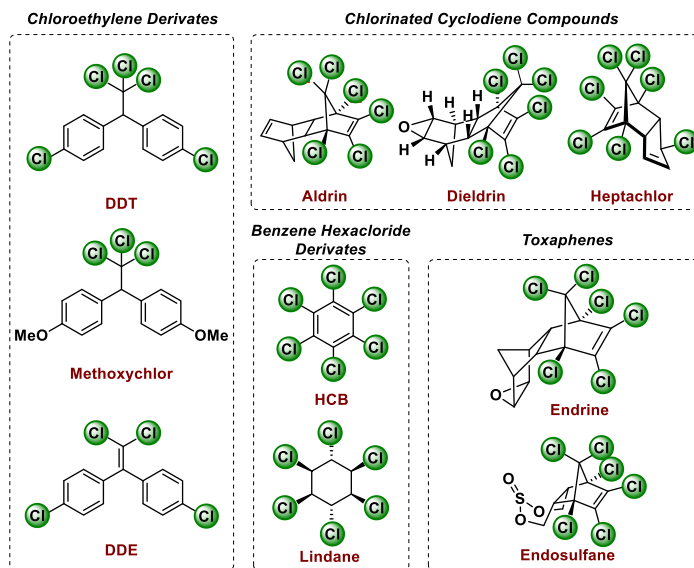


Figure III.18 Classification of organochlorinated pesticides.

Chlorinated pesticides exhibit a wide range of toxic effects. Due to the extensive use of these compounds, their accumulation in the environment only grows although many of them are biodegradable.⁴⁷ During the last few years, it has been reported an increasing number of problems caused by pesticides like lindane or *DDT*. Indeed, green and sustainable protocols should be found to solve these problems. Browsing literature, we can find several examples of the activation of different pesticides using iron⁴⁸ or cobalt⁴⁹ porphyrins as catalysts (**Figure III.19**).

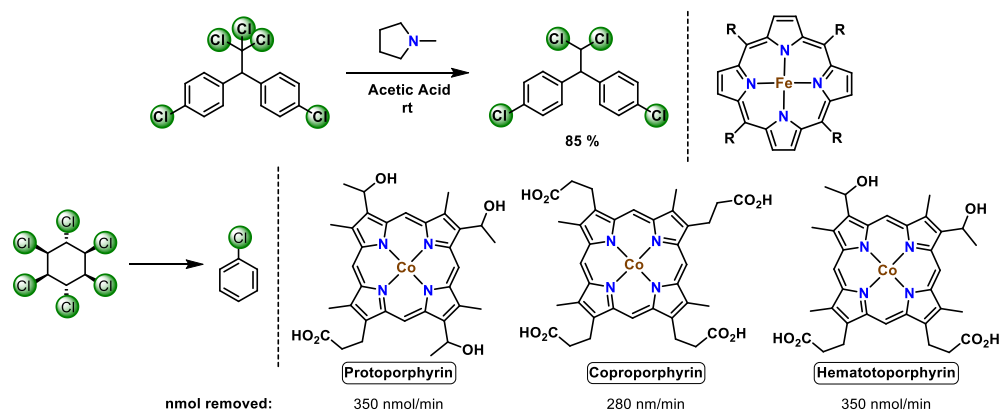


Figure III.19 *DDT* dehalogenation reaction with iron porphyrin (top) and lindane dehalogenation with cobalt porphyrins (bottom).

Taking this into account, we tested our system towards the activation of some halogenated pesticides. First, we focused on the degradation of lindane under optimized conditions for the dehalogenation reactions of alkyl halides (10 mM concentration of substrate, 5 mol% of catalyst, 2 mol% of photoredox catalyst, 11.4 equivalents of *ED*, MeCN:EtOH mixture as solvent, 30 °C and 24 hours). We observed the full conversion of lindane to a complex mixture of products which was not fully elucidated by our preliminary analytical data. HPLC–MS chromatogram indicates the formation of *n*-hexane, benzene, chlorobenzene as mayor products among others. Other pesticides such as *Aldrin*, *DDT* and *Dieldrin* were also consumed completely under our developed photocatalytic conditions to give a complex mixture of products again. Nevertheless, the product distribution did not contain chlorinated products.

To summarize sections **III.3. 2** and **III.3. 3**, reacting different organohalide drugs and pesticides under optimized conditions for the photo-hydro-dehalogenation reaction generates the complete consumption of the starting halogenated compound resulting in a complex mixture of products in most cases. The highly reactive conditions of the photochemical procedure used, and the complexity of the molecules tested, make the selectivity of the process the bottleneck of the presented methodology. In spite of that, for all molecules tested, the complete consumption of the starting compounds was observed, reaching the proposed goal; the destruction of halogenated drugs and pesticides.

III.3. 4 Photoredox Activation of Alkyl Fluorides

During the last decades, fluorinated compounds have received increasing attention from the scientific community, due to their unique properties (small size and high electronegativity). Fluorine is used in many different products as polymers (*PTFE*), freon, fluoro-liquid crystal, pharmaceutical and agrochemical compounds. At present, 30-40% of agrochemicals and 20% of pharmaceuticals on the market are estimated to contain fluorine, including half of the top 10 drugs sold in 2005.⁵⁰ Even though *C-F* bonds are present in many pharmaceutical molecules, these kind of halogenated bonds sometimes have lethal effects when acting as the substrate of an enzyme.⁵¹ Frequently the fluorinated analogue acts as an irreversible inhibitor of the enzyme through the formation of covalent bonds and loss of fluoride.⁵²

Fluorine is the only element that can completely replace hydrogen in hydrocarbons. With this substitution, many physical properties result significantly modified. The extremely high electronegativity of the fluorine atom results in weaker dipole forces. Indeed, the *Csp³-F* bond is much less polarizable than the corresponding *Csp³-H* bond. While the full H replacement by F atoms lowers the boiling points, although having higher molecular weight,⁵³ a partial replacement results in an increment of the boiling point. Nevertheless, perfluorated molecules are

highly volatile. Additionally the *H/F* exchange increases the densities and viscosities, while refractive indexes and surface tensions decrease.⁵³

The strength of the carbon-fluorine bond makes the *C–F* bond thermally, photochemically, electrochemically and even chemically very stable. These properties make fluorocarbons indispensable for many applications. On the other hand, their high stability generates long atmospheric lifetimes which can exceed 2000 years.⁵⁴

The first report of activation of *C–F* bonds was reported in 1947 by Miller and co-workers⁵⁵ by using sodium metal in liquid ammonia at -78 °C. At that point, no comments were made about the product formed, except the observation of fluoride ions. Remarkably, *C–F* bond activation has also been shown to occur in metal-containing systems dating as far back to 1954 using biological systems such as *Horseradish Peroxidase (HRP)*,⁵⁶ *Cytochrome P450* or *B₁₂-derivates* among others.⁵⁷ Although at that point, authors do not offer detailed mechanisms, they proposed the formation of radicals followed by the activation of the respective enzyme. A few years later, in 1973, Tamao and Kumada reported the first example of a catalytic *C–C* bond forming reaction from *C–F* bond scission by a nickel-catalysed cross-coupling reaction of *Grignard* reagents with aryl and alkenyl halides (**Figure III.20**).⁵⁸

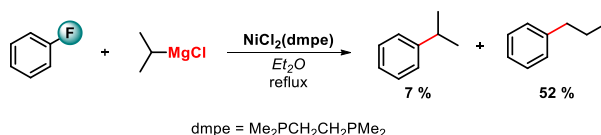


Figure III.20 First catalytic *C–C* bond formation involving a *C–F* bond cleavage reported.

Oxidative addition to carbon-fluorine bond is among the most studied pathways in transition-metal catalysed *C–F* bond activation. By this mechanism, the activation of aromatic fluorocarbons turns out to be relatively easy *via* η^2 -arene intermediate.⁵⁹ Moreover, the addition/elimination mechanism can also be feasible for this transformation.⁵⁹ The activation of aliphatic *Csp³–F* bonds usually involves

strong reducing conditions using ammonia, alkali metals or other metal salts.^{60,61} In this way, tertiary Csp^3-F bonds are usually required. However, secondary ones can also be reduced.⁶² Nonetheless, first-row transition metal complexes have been used for catalytic activation of $C-F$ bonds. Holland and co-workers demonstrated at the beginning of 21st century a catalytic hydro-defluorination of fluoroolefins by β -diketiminato iron(II) complexes (**Figure III.21**, left).⁶³ Additionally, hydro-defluorination of fluorobenzene was performed using $[Ni(acac)_2]$ in presence of N,N -dimesitylimidazolium chloride and $iPrONa$ (**Figure III.21**, right).⁶⁴

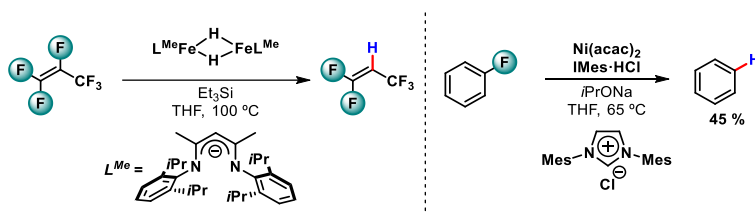


Figure III.21 Catalytic activation of $C-F$ bonds by β -diketiminato iron(II) complexes (left) and $[Ni(acac)_2]$ in the presence of N,N -dimesitylimidazolium chloride and $iPrONa$ (right).

Kumada-Corriu cross-coupling reactions have been accomplished using nickel(0) complexes bearing N -heterocyclic carbenes.⁶⁵ Furthermore, various nickel- and palladium-catalyzed cross-coupling reactions of aryl fluorides were developed.^{66,67} Additionally, Kambe and co-workers presented the use of fluoroalkanes for its coupling with *Grignard* reagents converting 1-fluorooctane into 2-octylbutenyl *Grignard* reagent that can be used for further transformation (**Figure III.22**).⁶⁸

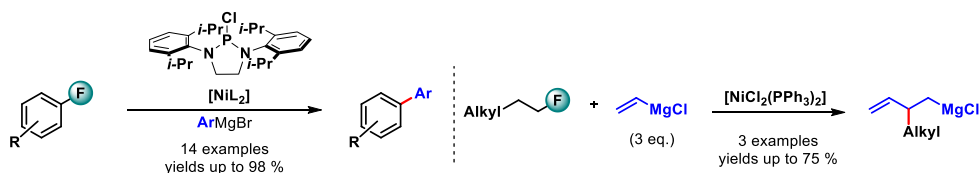


Figure III.22 Ni-catalyzed coupling of aryl and alkyl fluorides with *Grignard* reagents.

Radical pathways for the activation of $C-F$ bonds have also been successfully demonstrated utilizing zirconium and hafnium hydrides affording

quantitative yields for the hydro-defluorination of unactivated fluoroalkanes (**Figure III.23**).^{69,70}

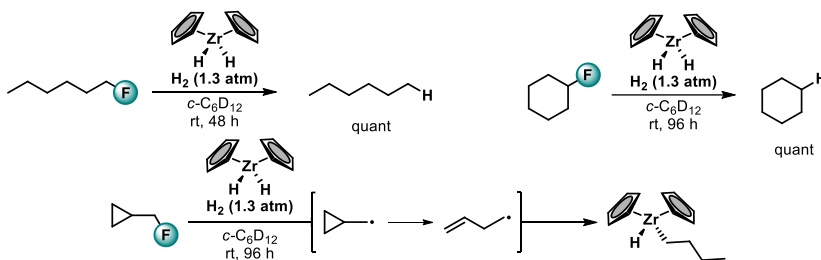


Figure III.23 C–F bond cleavage reactions catalyzed by zirconocen complexes.

More recently, the group of Nathan Jui published an elegant selective C–F functionalization of unactivated trifluoromethylarenes by mixing a hydrogen atom transfer (HAT) with a single electron transfer (SET) path in the presence of a base under visible-light irradiation.⁷¹ In this work, the photocatalytic system undergoes a SET reaction to afford a trifluoromethyl radical anion that loses a fluoride anion yielding a difluorobenzyl radical. This radical is then trapped by an olefin before being protonated in the catalytic cycle to form the final defluoroalkylated product (**Figure III.24**).

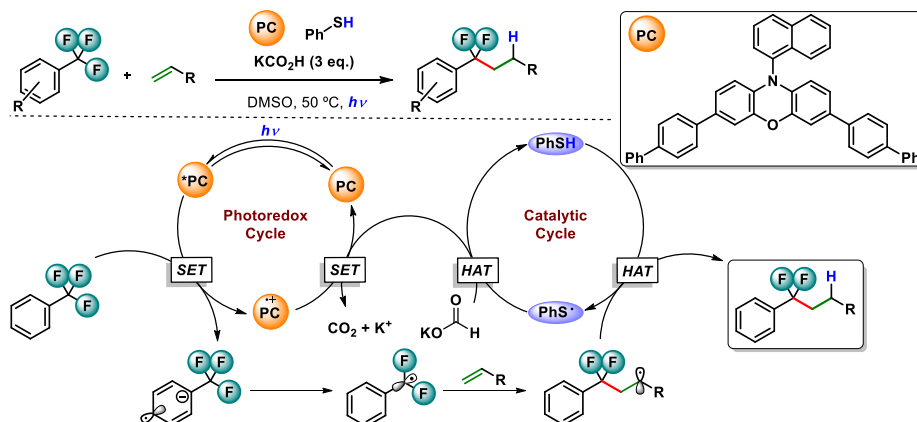
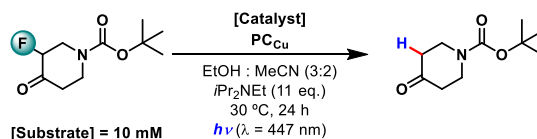


Figure III.24 Reactivity and proposed mechanism for the functionalization of unactivated trifluoromethylarenes.

Taking these examples into account, and knowing the potential of our system with the results from the hydro-dehalogenation in hand, we envisioned that our

system could also perform this activation photocatalytically. To test our hypothesis, we selected the commercially available *tert*-butyl 3-fluoro-4-oxopiperidine-1-carboxylate as a model substrate due to the presence of the fluorine atom in the alpha position to a carbonyl. Submitting the fluorinated substrate to the optimal conditions for the reductive dehalogenation reaction of alkyl chlorides, we could obtain complete consumption of the starting material for the defluorinated product in 63 % yield using I^HCo as catalyst and 60 % yield with I^HNi (Table III.3, entries 1 and 2). In contrast to hydro-dechlorination reactions shown in previous sections, in this case, the use of a more acidic protic solvent represents an improvement in the yield for the desired product (66 % of yield for the use of methanol instead of ethanol, entry 4). Moreover, the use of pure acetonitrile solution gave the best results under the experimental conditions obtaining a 73 % yield of the desired product using I^HCo as catalyst and 69 % yield with I^HNi (entries 6 and 7). Control experiments performed in the absence of one of the compounds of the mixture did not yield the consumption of the substrate (Table III.4) proving than all the components are needed for the transformation.

Table III.3 Solvent screening for the hydro-defluorination reaction.



Entries	Catalyst (mol%)	Solvent	ED (eq.)	Yield (%)
1	I^HCo (5)	EtOH : MeCN (3:2)	Et ₃ N (14.4)	63
2	I^HNi (5)	EtOH : MeCN (3:2)	<i>i</i> Pr ₂ NEt (11.4)	60
3	I^HCo (5)	<i>i</i> PrOH : MeCN (3:2)	Et ₃ N (14.4)	57
4	I^HCo (5)	MeOH : MeCN (3:2)	Et ₃ N (14.4)	66
5	I^HCo (5)	H ₂ O : MeCN (3:2)	Et ₃ N (14.4)	20
6	I^HCo (5)	MeCN	Et₃N (14.4)	73
7	I^HNi (5)	MeCN	<i>i</i>Pr₂NEt (11.4)	69

Conditions: substrate (10 mM), PC_{Cu} (2 mol%), visible-light irradiation with blue LEDs (1 W, 447 nm) for 24 h at 30 °C. Conversion and yield were determined by GC using biphenyl as internal standard. ^aReactions were carried out without PC_{Cu}. ^bExperiments done without irradiation.

Table III.4 Control experiments for the hydro-defluorination reaction.

Entries	Catalyst (mol%)	Solvent	ED (eq.)	Yield (%)
1	1^{H}Co (5) ^a	EtOH : MeCN (3:2)	Et ₃ N (14.4)	-
2	1^{H}Ni (5) ^a	EtOH : MeCN (3:2)	<i>i</i> Pr ₂ NEt (11.4)	2
3	-	EtOH : MeCN (3:2)	Et ₃ N (14.4)	6
4	1^{H}Co (5) ^b	EtOH : MeCN (3:2)	Et ₃ N (14.4)	-
5	1^{H}Ni (5) ^b	EtOH : MeCN (3:2)	<i>i</i> Pr ₂ NEt (11.4)	2
6	1^{H}Co (5)	EtOH : MeCN (3:2)	-	-
7	1^{H}Ni (5)	EtOH : MeCN (3:2)	-	-

Conditions: substrate (10 mM), PC_{Cu} (2 mol%), visible-light irradiation with blue LEDs (1 W, 447 nm) for 24 h at 30 °C. Conversion and yield were determined by GC using biphenyl as internal standard. ^aReactions were carried out without PC_{Cu}. ^bExperiments done without irradiation.

Utilizing a pure acetonitrile as solvent, we optimized the ratios between catalyst and photocatalyst (**Table III.5**, entries 1-10), equivalents of electron-donor (entries 11, 12), and concentration of the substrate (entries 13-16). None of the changes yielded an improvement in the results. Unfortunately, lower yields were obtained when both catalyst loadings were doubled (entries 3 and 4), the equivalents of electron donor were reduced (entries 11 and 12) and the concentration was decreased (entry 13) or increased (entries 14 to 16).

Table III.5 Screening of the reaction conditions.

Entries	[Substrate]	Catalyst (mol%)	PC (%)	ED (eq)	Yield (%)
1	10 mM	1^{H}Co (5)	PC_{Cu} (2)	Et_3N (14.4)	73
2	10 mM	1^{H}Ni (5)	PC_{Cu} (2)	<i>i</i> Pr ₂ NEt (11.4)	69
3	10 mM	1^{H}Co (10)	PC_{Cu} (4)	Et_3N (14.4)	50
4	10 mM	1^{H}Ni (10)	PC_{Cu} (4)	<i>i</i> Pr ₂ NEt (11.4)	60
5	10 mM	1^{H}Co (10)	PC_{Cu} (2)	Et_3N (14.4)	52
6	10 mM	1^{H}Ni (10)	PC_{Cu} (2)	<i>i</i> Pr ₂ NEt (11.4)	61
7	10 mM	1^{H}Co (3)	PC_{Cu} (3)	Et_3N (14.4)	56
8	10 mM	1^{H}Ni (3)	PC_{Cu} (3)	<i>i</i> Pr ₂ NEt (11.4)	52
9	10 mM	1^{H}Co (3)	PC_{Cu} (1)	Et_3N (14.4)	56
10	10 mM	1^{H}Ni (3)	PC_{Cu} (1)	<i>i</i> Pr ₂ NEt (11.4)	53
11	10 mM	1^{H}Co (5)	PC_{Cu} (2)	Et_3N (7.2)	57
12	10 mM	1^{H}Co (5)	PC_{Cu} (2)	Et_3N (3.6)	56
13	5 mM	1^{H}Co (5)	PC_{Cu} (2)	Et_3N (14.4)	57
14	20 mM	1^{H}Co (5)	PC_{Cu} (2)	Et_3N (14.4)	57
15	50 mM	1^{H}Co (5)	PC_{Cu} (2)	Et_3N (14.4)	46
16	100 mM	1^{H}Co (5)	PC_{Cu} (2)	Et_3N (14.4)	46

Conditions: Reactions carried out in pure acetonitrile solution under visible-light irradiation with blue LEDs (1 W, 447 nm) for 24 h at 30 °C. Conversion and yield were determined by GC using biphenyl as internal standard.

With the optimized conditions in hand, we performed the screening of different *N*-based cobalt and nickel complexes. Almost all the catalysts tested for the photoredox catalyzed hydro-defluorination reaction produced moderate to good yields (**Table III.6**). Surprisingly, the use of iron-based *Ts^HPy₂tacn* ligand (**1^{H}Fe** , entry 3) yielded the defluorinated product with 44% yield, showing iron as another potential metal to use in this methodology. Electronic effects introducing by utilizing the ligand *Ts^xPy₂tacn*, did not induce a remarkable improvement in the catalytic outcome, obtaining variations that can correspond to the experimental error (entries 5 to 6). Other pentacoordinate complexes such as *DPA* (entries 7 and 8) or *N4Py*

(entries 9 and 10) were tested, obtaining remarkable results for the combination of *DPA* with nickel (69 % yield, entry 8). *Salen*-based complexes showed not to be competent catalysts for this transformation (entries 11 and 12), while the tetracoordinate *Ni-cyclam* complex gave 66 % of the desired product (entry 13). This result indicates that *Ni-cyclam* is as efficient as the pentacoordinate metal derivatives for the defluorination reaction.

Table III.6 Catalyst screening.

Entries	Catalyst (mol%)	PC (%)	Solvent	ED (eq.)	Yield (%)
1	1^{H}Co (5)	PC_{Cu} (2)	MeCN	Et_3N (14.4)	73
2	1^{H}Ni (5)	PC_{Cu} (2)	MeCN	<i>i</i> Pr ₂ NEt (11.4)	69
3	1^{H}Fe (5)	PC_{Cu} (2)	MeCN	Et_3N (14.4)	44
5	1^{DMM}Co (5)	PC_{Cu} (2)	MeCN	Et_3N (14.4)	67
4	1^{DMM}Ni (5)	PC_{Cu} (2)	MeCN	<i>i</i> Pr ₂ NEt (11.4)	67
6	$1^{\text{CO}_2\text{Et}}\text{Co}$ (5)	PC_{Cu} (2)	MeCN	Et_3N (14.4)	72
7	Co- <i>DPA</i> (5)	PC_{Cu} (2)	MeCN	Et_3N (14.4)	55
8	Ni- <i>DPA</i> (5)	PC_{Cu} (2)	MeCN	<i>i</i> Pr ₂ NEt (11.4)	69
9	Co-N4Py (5)	PC_{Cu} (2)	MeCN	Et_3N (14.4)	61
10	Ni-N4Py (5)	PC_{Cu} (2)	MeCN	<i>i</i> Pr ₂ NEt (11.4)	57
11	Co- <i>Salen</i> (5)	PC_{Cu} (2)	MeCN	Et_3N (14.4)	3
12	Ni- <i>Salen</i> (5)	PC_{Cu} (2)	MeCN	<i>i</i> Pr ₂ NEt (11.4)	32
13	Ni-Cyclam (5)	PC_{Cu} (2)	MeCN	<i>i</i> Pr ₂ NEt (11.4)	66

Conditions: substrate (10 mM), PC_{Cu} (2 mol%), visible-light irradiation with blue LEDs (1 W, 447 nm) for 24 h at 30 °C. Conversion and yield were determined by GC using biphenyl as the internal standard.

With the objective in mind to reduce less-activated fluorinated substrates, we tested a more powerful photoredox catalyst such as $\text{PC}_{\text{Ir}}^{\text{NMe}_2}$ (-1.80 V vs SCE in MeCN). However, the combination of $\text{PC}_{\text{Ir}}^{\text{NMe}_2}$ with neither cobalt, nickel nor iron triazacyclononane catalysts improved the yield of the reaction (**Table III.7**).

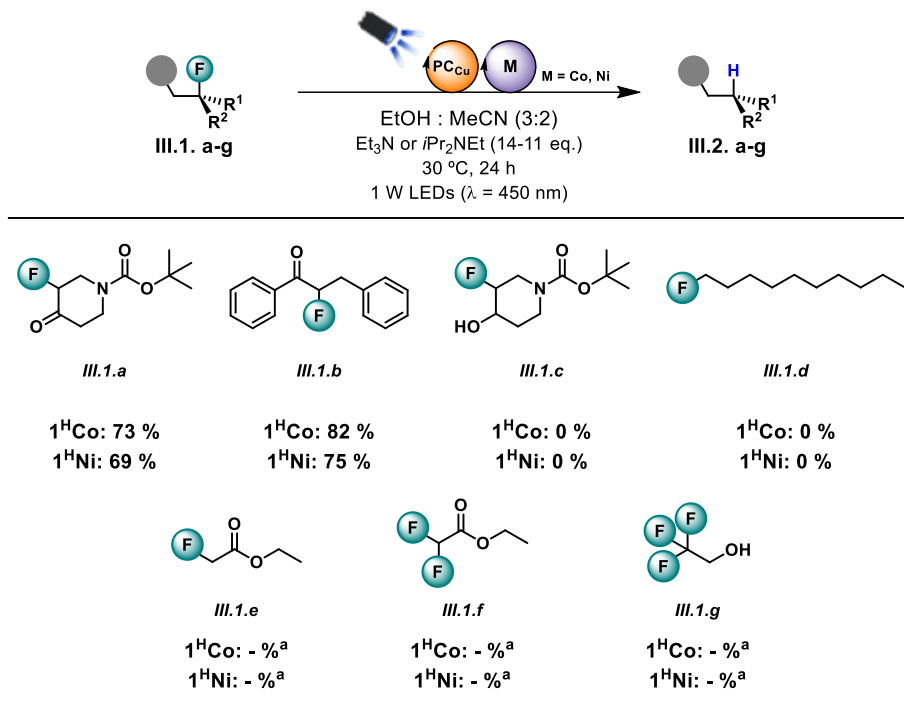
Table III.7 Comparison between copper and iridium based photocatalyst.

Entries	Catalyst (mol%)	PC (%)	Solvent	ED (eq)	Yield (%)
1	¹ HCo (5)	PC _{Cu} (2)	MeCN	Et ₃ N (14.4)	71
2	¹ HCo (5)	PC _{Ir^{MeC}} (2)	MeCN	Et ₃ N (14.4)	44
3	¹HNi (5)	PC_{Cu} (2)	MeCN	<i>i</i>Pr₂NEt (11.4)	69
4	¹ HNi (5)	PC _{Ir^{MeC}} (2)	MeCN	<i>i</i> Pr ₂ NEt (11.4)	41
5	¹ HFe (5)	PC _{Cu} (2)	MeCN	Et ₃ N (14.4)	44
6	¹ HFe (5)	PC _{Ir^{MeC}} (2)	MeCN	Et ₃ N (14.4)	39

Conditions: substrate (10 mM), visible-light irradiation with blue LEDs (1 W, 447 nm) for 24 h at 30 °C. Conversion and yield were determined by GC using biphenyl as internal standard.

Once finished the screening of the conditions, we were interested in testing other fluorine-containing substrates. We submitted activated and non-activated monofluorinated compounds to the developed photocatalytic conditions (**Table III.8**). Additionally, alpha di- and trifluoroketones and alcohols were also included as halogenated substrates. We observed that a ketone located in the alpha position was crucial for the reaction to succeed, obtaining 82 % yield for the dehalogenated product using 2-fluoro-1,3-diphenylpropan-1-one as substrate (**III.1. b**). *Tert*-butyl 3-fluoro-4-hydroxypiperidine-1-carboxylate (**III.1. c**) and 1-fluorodecane (**III.1. d**) did not give any conversion of the starting material. Furthermore, when substrates **III.1 e**, **III.1 f** and **III.1 g** were reacted under these catalytic conditions, any fluorine-containing compound was found standing for the total consumption of these fluorinated substrates.

Table III.8 Substrate scope for hydro-defluorination reaction.



Conditions: substrate (10 mM), ^1H M (5 mol%), PC_{Cu} (2 mol%), $\text{Et}_3\text{N}/i\text{Pr}_2\text{NEt}$ (14 or 11 eq.) in MeCN. The reactions were running 24 h at 30 °C under visible-light irradiation with blue LEDs (1 W, 447 nm). Conversions were determined by GC using biphenyl as internal standard.^a Complete conversion was observed for the starting material.

III.4. Conclusions.

To sum-up, we can conclude that the pair formed for [Cu(bathocuproine)(Xantphos)](PF₆) (**PC_{Cu}**) and [M(OTf)(Py₂T^stacn)](OTf) (**I^{HM}M**) in the presence of tri-alkyl amines as *ED* is a powerful system for the activation of *Csp³-Halogen* bonds. The presence of ethanol as protic solvent, proved to be of great importance for the dehalogenation of non-activated alkyl chlorides, whereas was not crucial in the case of alkyl fluorides, which were activated in pure acetonitrile solutions. This suggests that both activations could proceed through different mechanistic pathways.

All the components in the reaction (photocatalyst, catalyst, *ED*, and light) were demonstrated to be needed for the reaction to occur. *Tetra* and *penta*-coordinated *N*-based ligands were tested for the hydro-defluorination reaction obtaining good yields for the use of *Ni-DPA*, *Ni-Cyclam* in addition **I^{DMM}M**. For this reaction, the use of a more powerful photocatalyst such as **PCIr^{NMe₂}** did not give any improvement in the yield.

Biologically relevant molecules such as drugs or pesticides were submitted to the photocatalytic protocol. The preliminary results showed that the substrates were utterly consumed. Nevertheless, to precisely identify products formed, additional studies are needed.

III.5. Experimental Section.

III.5.1 Material and Reagents.

Reagents and solvents were used as received from the commercial supplier unless otherwise stated. Triethylamine and di-*isopropylethylamine* were distilled over potassium hydroxide and were stored under argon. For the synthesis of reagents, the solvents (hexane, Et₂O, CH₂Cl₂, MeCN, DMF and toluene) were used from an SPS-400, Innovative Technology solvent purification system, and stored under argon with activated 4 Å molecular sieves.

Anhydrous acetonitrile was purchased from Sigma-Aldrich® and water was purified with a Milli-Q Millipore Gradient AIS system. Water, methanol, ethanol, isopropanol, butyronitrile, isobutyronitrile and trimethylacetonitrile used for photoreactions were degassed by freeze-pump-thaw method (repeated 3 cycles) and were stored under argon.

The synthesis of air-sensitive reagents, as well as the preparation of visible-light photocatalytic reactions, were conducted inside a nitrogen-filled glove box (mBraun Unilab) with concentrations of O₂ and H₂O lower than 0.5 ppm and using Schlenk techniques under argon atmosphere.

III.5.2 Instrumentation.

NMR spectra were recorded on a Bruker 300 MHz, 400 MHz or 500 MHz spectrometers at room temperature. ¹H and ¹³C NMR chemical shifts are reported in parts per million (ppm), relative to the residual solvent peak as the internal reference. Multiplicities are reported as follows: singlet (s), doublet (d), doublet of doublet (dd), triplet of doublets (td), triplet (t), broad signal (br) and multiplet (m). Deuterated solvents (CDCl₃, CD₃CN, EtOD) were stored with activated 4 Å molecular sieves and they were degassed by the freeze-pump-thaw method when it was required for photocatalytic reactions.

High-resolution Mass Spectrometry (HRMS) data was collected on an HPLC-QqTOF (Maxis Impact, Bruker Daltonics) or HPLC-TOF (MicroTOF Focus, Bruker Daltonics) mass spectrometer using 1 mM solution of the analyzed compound.

Gas chromatography analysis and quantification of the starting materials and products were carried out on an Agilent 7820A gas chromatograph (HP5 capillary column, 30 m x 320 μm x 0.25 μm or Sapiens 5MS capillary column, 30 m x 250 μm x 0.25 μm) and a flame ionization detector (FID). GC-MS spectral analyses were performed on an Agilent 7890A gas chromatograph (HP5 capillary column, 30 m x 320 μm x 0.25 μm) interfaced with an Agilent 5975c MS mass spectrometer.

Gas chromatography identification gases at the headspace was analyzed with an Agilent 7820A GC System equipped with columns Washed Molecular Sieve 5A, 2m x 1/8'' OD, Mesh 60/80 SS and Porapak Q, 4m x 1/8'' OD, SS, Mesh: 80/100 SS and a Thermal Conductivity Detector. The H_2 amount obtained was calculated through the interpolation of the previous calibration using different H_2/N_2 mixtures.

III.5. 2.1 In-house Developed Parallel Photoreactor.

Light source: The reactions were performed using Royal-Blue ($\lambda = 447 \pm 20$ nm) LUXEON Rebel ES LED - 1030 mW @ 700mA (Datasheet: <https://www.luxeonstar.com/assets/downloads/ds68.pdf>) as a light source.

Temperature Control: Reaction temperature was controlled by a high precision thermoregulation Hubber K6 cryostat. Likewise, aiming at ensuring stable irradiation, the temperature of the LEDs was controlled and set at 22 $^\circ\text{C}$.

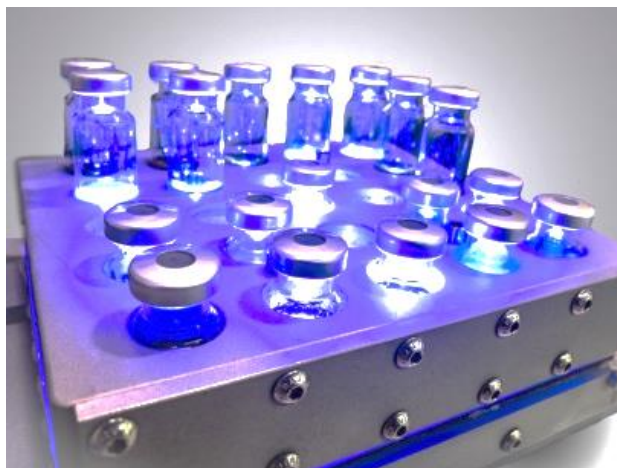


Figure III.25 In-house developed parallel photoreactors.

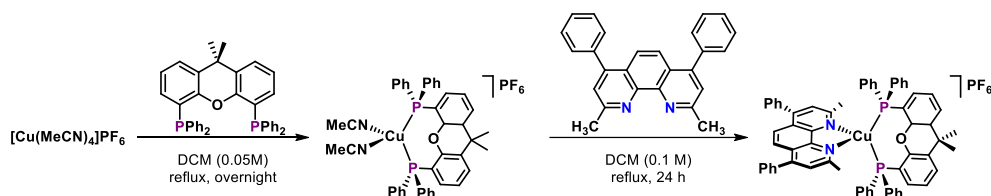
III.5.3 Experimental Procedures.

General procedure for hydro-dehalogenation reactions: Inside an anaerobic box, aliquots from stock solutions of haloalkane (0.2 mL, 0.02 mmol, 1.0 eq.), catalyst (0.1 mL, 0.001 mmol, 5 mol %), PC_{Cu} (0.1 mL, 4×10^{-4} mmol, 2 mol %) and acetonitrile (0.4 mL) were equally distributed into a vial (10 mL of headspace) that contained glass beads. The vial was sealed with a septum and removed from the anaerobic box. The degassed protic solvent was added to the vial to reach a total volume of 2 mL (total concentration of substrate 10 mM). Et_3N (40 μ L, 0.286 mmol, 14.4 eq.) or iPr_2NEt (40 μ L, 0.229 mmol, 11.4 eq.) was added to each vial, which

was placed in the photoreactor at the indicated temperature (30 °C). After irradiating for 24 h with blue LEDs ($\lambda = 447$ nm), the sample was diluted with ethyl acetate (2 mL). A solution of biphenyl in ethyl acetate was added as internal standard (8.7×10^{-3} mmol in 0.25 mL). Then, the addition of 1 mL of H₂O formed a biphasic solution, and an aliquot of the organic phase was passed through a plug of MgSO₄ and eluted with EtOAc. The resulting solution was analyzed by gas chromatography. The yields reported for each reaction are given as an average of at least two runs.

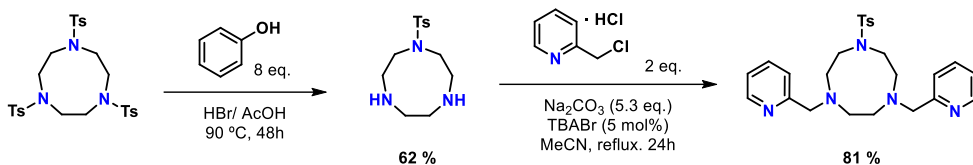
III.5. 4 Synthesis of Metal Complexes.

Synthesis of PCu.



PCu was synthesized following a reported procedure³⁶ yielding 3 g of the corresponding copper salt as a light-yellow solid (78% of yield). ¹H NMR (400 MHz, CDCl₃) $\delta = 7.78$ (s, 2H), 7.66 (dd, $J = 7.8, 1.4$ Hz, 2H), 7.61 – 7.51 (m, 6H), 7.50 – 7.43 (m, 6H), 7.27 (d, $J = 4.5$ Hz, 6H), 7.22 (t, $J = 7.7$ Hz, 2H), 7.13 – 7.03 (m, 15H), 6.96 (dt, $J = 6.2, 3.9$ Hz, 2H), 2.33 (s, 6H), 1.75 (s, 6H). ¹³C NMR (101 MHz, CDCl₃) $\delta = 157.8, 155.2, 155.1, 155.0, 150.2, 143.6, 136.3, 133.7, 133.1, 133.0, 132.9, 131.4, 130.3, 130.0, 129.4, 129.0, 128.6, 128.6, 128.6, 127.6, 125.6, 125.4, 123.6, 121.6, 121.5, 77.3, 77.0, 76.7, 36.1, 28.6, 27.4$. ³¹P NMR (162 MHz, CDCl₃) $\delta = -9.31, 141.23$.

Synthesis of ligand Ts^H Py₂tacn.

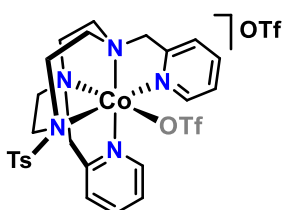


1-(p-toluenesulfonyl)-1,4,7-triazacyclononane (H tacn): Ts tacn (27,26g, 46,1 mmol) and phenol (35, 372 mmol) were mixed in a 1L flask. A solution of HBr (33% in AcOH, 380 mL) was added carefully and the mixture was refluxed for 48 h at 90 °C. The suspension was allowed to reach ambient temperature and then filtered through sintered glass. The filter cake was washed with Et₂O until obtaining a nearly colourless filter cake. The solid was slowly dissolved in 300 mL in 2 M aq. NaOH at 0 °C and stirred until a strong basic pH was reached (pH 12-14). The aqueous phase was then extracted with DCM (5 x 50 mL) and the combined organic extracts (slightly pink) were dried over MgSO₄. The solvent was removed under reduced pressure and the light pink oil was dried on high vacuum to obtain a pale pink/white solid 8.26g (62%).

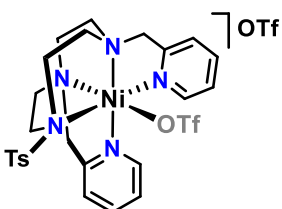
1,4-bis(pyridin-2-ylmethyl)-7-tosyl-1,4,7-triazonane (Ts^H Py₂tacn): 2-Picolyl chloride hydrochloride (1.18 g, 7.20 mmol), H tacn (1.02 g, 3.60 mmol) and anhydrous acetonitrile (40 mL) were mixed in a 100 mL flask. Na₂CO₃ (2.05 g) and tetrabutylammonium bromide (TBABr, 1.16g) were added directly as solids, and the resulting mixture was heated at reflux under N₂ for 24 hours. After cooling to room temperature, the resulting orange mixture was filtered, and the filter cake was washed with DCM. The combined filtrates were evaporated under reduced pressure. To the resulting residue, 2 M NaOH (20 mL) was added, and the mixture was extracted with CH₂Cl₂ (4 x 40 mL). The oil residue was extracted with ether. The combined organic layers were dried over MgSO₄, and the solvent was removed under reduced pressure. The resulting residue was treated with *n*-hexane (100 mL) and stirred for 12 hours. Then, extractions with DCM:Hexane were done until having a

clean product. The solvent from the orange filtrates was removed under reduced pressure to yield 1.4 g of a brownish solid (3.6 mmol, 81 %).

Synthesis of I^HCo and I^HNi .

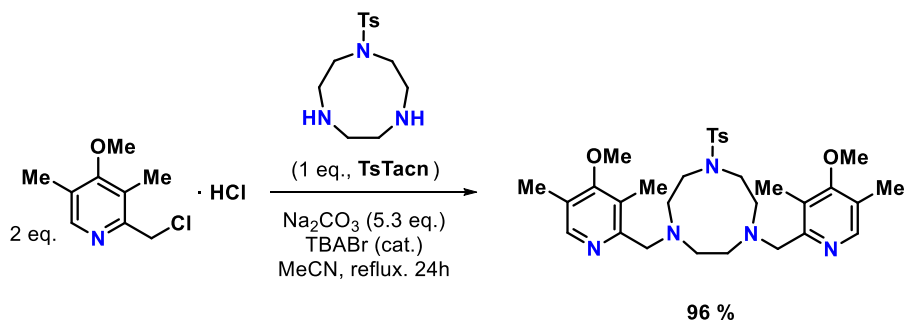


I^HCo was synthesized following the reported procedure.^[6] A solution of $Co(OTf)_2(MeCN)_2$ (374 mg, 0.851 mmol) in anhydrous tetrahydrofuran (1 mL) was added dropwise to a vigorously stirred solution of $^{DMM}Py_2Tstacn$ (550 mg, 0.945 mmol) in THF (1 mL). After stirring for 2 h, the solution was filtered off and the resulting solid dried under vacuum. This solid was dissolved in CH_2Cl_2 , and the slow diffusion of diethyl ether into this solution gave 0.273 g of the title complex as a pale pink solid (77 %). The spectroscopic data is in agreement with previously reported data for this compound.⁷²



I^HNi was synthesized following an analogous synthetic procedure as described for complex I^HCo , obtaining 0.823 g of the targeted complex as a pale purple solid (68 %). The spectroscopic data is in agreement with previously reported data for this compound.⁷²

Synthesis of ligand $Ts^{DMM}Py_2tacn$.

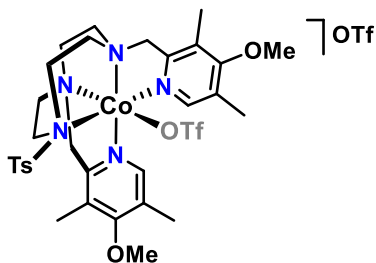


$Ts^{DMM}Py_2tacn$ was synthesized following a reported procedure with the introduction of small modifications in the purification steps.⁷³ 2-Chloromethyl-4-

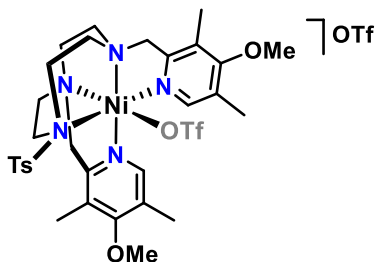
methoxy-3,5-dimethylpyridine hydrochloride (2.59 g, 11.64 mmol), Ts^+taccn (1.5 g, 5.29 mmol) and anhydrous acetonitrile (80 mL) were mixed in a 150 mL flask. Na_2CO_3 (3 g, 28.3 mmol) and tetrabutylammonium bromide (TBABr, 130 mg, 0.54 mmol) was added directly as solids, and the resulting mixture was heated at reflux for 24 h under N_2 atmosphere. After cooling at room temperature, the resulting orange mixture was filtered, and the filter cake was washed with CH_2Cl_2 . The combined filtrates were evaporated under reduced pressure. Then, a solution of HCl 1 M (20 mL) was added to the residue, and the aqueous phase was washed with dichloromethane (3 x 20 mL). The aqueous phase was basified to pH 10 with a solution of NaOH 2 M, and dichloromethane (30 mL) was added. The organic layer was separated, and the aqueous phase was extracted with dichloromethane (3 x 20 mL). The combined organic extracts were dried over $MgSO_4$, and the solvent was removed under reduced pressure. Finally, the oil residue was dissolved with 5 mL of dichloromethane, and the addition of hexane (20 mL) caused the precipitation of a brownish oil. The solution was decanted, and the solvent was removed under reduced pressure, which gave 1.78 g of the title compound. The remaining brownish oil was dissolved again in 3 mL of dichloromethane and the addition of hexane (10 mL) caused the formation of an oil residue. The organic solution was decanted, the solvent removed and another fraction of 1.10 g of the title compound was obtained (overall yield of the reaction 96%).

1H NMR (500 MHz, $CDCl_3$): δ = 8.11 (s, 2H), 7.56 (d, J = 8.1 Hz, 2H), 7.23 (d, J = 8.0 Hz, 2H), 3.72 (s, 10H), 3.09 - 2.97 (m, 8H), 2.64 (s, 4H), 2.39 (s, 3H), 2.29 (s, 6H), 2.21 (s, 6H) ppm. ^{13}C NMR (126 MHz, $CDCl_3$): δ = 164.2, 157.4, 148.5, 143.0, 135.9, 129.6, 127.2, 126.2, 125.2, 63.0, 59.9, 56.3, 56.1, 50.3, 21.6, 13.4, 11.3 ppm. IR (film): 2925, 2832, 1563, 1450, 1334, 1252, 1156, 1090, 998, 711, 694, 547 cm^{-1} . MS: m/z calcd. for $C_{31}H_{44}N_5O_4S$ $[M+H]^+$: 582.3114, found 582.3109. The spectroscopic data is in agreement with previously reported data for this compound.⁷³

Synthesis of $I^{DMM}Co$ and $I^{DMM}Ni$.

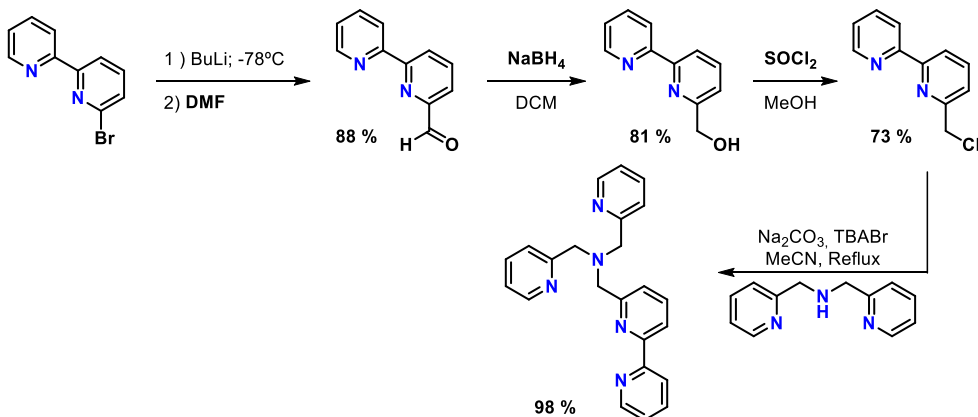


$I^{DMM}Co$ was synthesized following the reported procedure.^[6] A solution of $Co(OTf)_2(MeCN)_2$ (374 mg, 0.851 mmol) in anhydrous tetrahydrofuran (THF) (1 mL) was added dropwise to a vigorously stirred solution of $I^{DMM}Py_2Tstacn$ (550 mg, 0.945 mmol) in THF (1 mL). After stirring for 2 h, the solution was filtered off and the resulting solid dried under vacuum. This solid was dissolved in CH_2Cl_2 , and the slow diffusion of diethyl ether into this solution gave 0.672 g of the title complex as a pale pink solid (76 %). **Anal.** Calcd. for $C_{33}H_{47}CoF_6N_5O_{12}S_3$: C, 40.69; N, 7.19; H, 4.86 %. Found: C, 41.04; N, 7.20; H, 4.46 %. **MS** (m/z): 789.1882 [M - OTf]⁺.



$I^{DMM}Ni$ was synthesized following an analogous synthetic procedure as described for complex $I^{DMM}Co$, obtaining 0.213 g of the targeted complex as a pale blue solid (68 %). **Anal.** Calcd. for $C_{33}H_{45}NiF_6N_5O_{11}S_3$: C, 41.50; N, 7.33; H, 4.75 %. Found: C, 41.77; N, 7.28; H, 4.56 %. **MS** (m/z): 788.1904 [M - OTf]⁺.

Synthesis of 1-([2,2'-bipyridin]-6-yl)-N,N-bis(pyridin-2-ylmethyl)ethanamine (DPA-BPy).



DPA-BPy was synthesized following the reported procedure with slightly modifications.⁷⁴

Bpy-CH₂-OH: To an anhydrous solution of 6-bromo-2,2'-bipyridine (3 g, 12.8 mmol) in 36 mL of Et₂O:hexane:THF (18:6:6) was added dropwise *n*BuLi (8.29 mL, 13.27 mmol, 1.6 M in hexane) at -78 °C under argon atmosphere. After the addition was completed, the red mixture was stirred 2 hours at the same temperature. Then, a solution of DMF (1.97 mL, 25.5 mmol) in 15 mL of Et₂O was added slowly, and it was stirred for 1 h at -78 °C and an additional hour at room temperature. The reaction mixture was quenched by the addition of HCl 1M at 0 °C. NaOH (2M, 30 mL) was added to the resulting residue, and the mixture was extracted with DCM (3 x 20 mL). The combined organic layers were dried over MgSO₄, and the solvent was removed under reduced pressure yielding 2.06 g of the desired aldehyde (88% of yield). The obtained reddish oil was dissolved in MeOH (50 mL), and NaBH₄ (508 mg, 14.98 mmol) was added slowly directly as solid at 0 °C. After that, the ice bath was removed, and the solution was stirred overnight. The reaction was quenched by the addition of NH₄Cl (1M solution in water, 30 mL), and stirred for 10 min. After that, the solution was made alkaline with NaOH and extracted with DCM (3 x 50 mL). The combined organic layers were dried over MgSO₄ and the solvent evaporated under reduced pressure. The resulting oil product was purified by silica column chromatography (Hexane:AcOEt 1:1) to afford 1.7 g of the desired product (81 % yield) as a white solid.

¹H NMR (400 MHz, CDCl₃): δ = 8.69 (ddd, *J* = 4.8, 1.8, 0.9 Hz, 1H), 8.42 (dt, *J* = 8.0, 1.1 Hz, 1H), 8.33 (dd, *J* = 7.8, 0.9 Hz, 1H), 7.88 – 7.77 (m, 2H), 7.33 (ddd, *J* = 7.5, 4.8, 1.2 Hz, 1H), 7.25 (d, *J* = 7.1 Hz, 1H), 4.84 (s, 2H) ppm.

Bpy-CH₂-Cl: To neat *Bpy-CH₂-OH* (1 g, 5.37 mmol) was added SOCl₂ (6.23 mL, 86 mmol) dropwise with stirring at room temperature. The mixture was then refluxed for 2 h. The excess of SOCl₂ was evaporated under reduced pressure. Saturated Na₂CO₃ was used to neutralize the solution to pH = 7.5. The mixture was extracted with ether (3 x 15 mL), and the combined organic phases were washed with brine

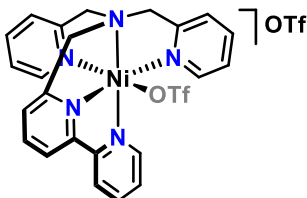
and dried over solid MgSO_4 . The solution was concentrated to yield a brownish oil, which was dissolved in the minimum quantity of DCM. After that, *n*-hexane was added. The DCM-containing solution was transferred to a clean flask where, after drying was obtained the product as a brownish solid.

$^1\text{H NMR}$ (400 MHz, CDCl_3): δ = 8.68 (dt, J = 4.9, 1.4 Hz, 1H), 8.48 – 8.42 (m, 1H), 8.39 – 8.33 (m, 1H), 7.83 (dt, J = 10.0, 7.8 Hz, 2H), 7.51 (dd, J = 7.6, 1.0 Hz, 1H), 7.32 (ddd, J = 7.6, 4.8, 1.3 Hz, 1H), 4.76 (s, 2H) ppm.

DPA-Bpy: *Bpy-CH₂-Cl* (0.8 g, 3.91 mmol), di-(2-picolyl)amine (0.78 g, 3.91 mmol) and anhydrous acetonitrile (40 mL) were mixed in a 100 mL flask. Na_2CO_3 (5 g) and tetrabutylammonium bromide (TBABr) (0.5 g) were added directly as solids, and the resulting mixture was heated at reflux temperature for 24 hours. After cooling to room temperature, the resulting orange solution was filtered, and the filter cake was washed three times with DCM. The combined filtrates were evaporated under reduced pressure. NaOH (2 M, 30 mL) was added to the resulting residue, and the mixture was extracted with DCM (3 x 15 mL). The combined organic layers were dried over MgSO_4 , and the solvent was removed under reduced pressure. The resulting oil product was dissolved in DCM and, in an ice-cooled flask, *n*-hexane was added. The solution was filtered off, and the clean product was obtained 1.41 g, 3.91 mmol, 98 % yield) as a yellow solid.

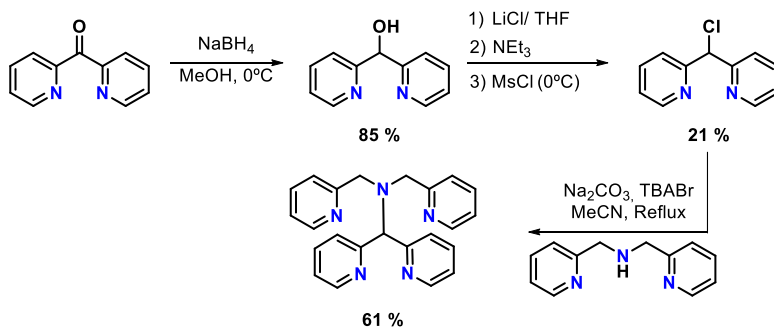
$^1\text{H NMR}$ (400 MHz, CDCl_3): δ = 8.60 (d, J = 2.2 Hz, 1H), 8.52 – 8.46 (m, 1H), 8.39 (dd, J = 7.9, 2.1 Hz, 2H), 8.21 (dd, J = 7.9, 2.0 Hz, 2H), 7.80 – 7.68 (m, 3H), 7.58 (dt, J = 3.3, 1.8 Hz, 5H), 7.08 (dd, J = 5.4, 2.9 Hz, 1H), 3.98 – 3.87 (m, 6H) ppm.
 $^{13}\text{C NMR}$ (400 MHz, CDCl_3): δ = 159.7, 159.6, 158.7, 156.3, 155.4, 149.3, 149.1 (2C), 137.2, 136.8, 136.4, 123.5, 122.9 (2C), 122.9, 122.2, 122.0, 121.9, 121.2, 119.2, 60.3, 60.1, 54.8 ppm.

Synthesis of Ni-DPA.



In a glovebox, a suspension of $\text{Ni}(\text{OTf})_2(\text{MeCN})_2$ (400 mg, 1.089 mmol) in anhydrous THF (2 mL) was added dropwise to a vigorously stirred solution of DPA-Bpy ligand (430 mg, 0.980 mmol) in THF (2 mL). After few minutes, a brown solution appeared. After stirring for an additional 5 hours, Et_2O (3 mL) was added, and the resulting solid was filtered off and dried under vacuum. The solid was dissolved in DCM, filtered through Celite, and the slow diffusion of diethyl ether into the solution produced a pale brown solid (631 mg, 1.089 mmol, 80 %). **Anal.** Calcd. for $\text{C}_{25}\text{H}_{23}\text{NiF}_6\text{N}_5\text{O}_7\text{S}_2$: C, 41.45; N, 9.66; H, 2.92; S, 8.85 %. Found: C, 41.27; N, 9.43; H, 3.00; S, 8.82 %. **MS** (m/z): 574.0663 [$\text{M} - \text{OTf}$]⁺.

Synthesis of 1,1-di(pyridin-2-yl)-N,N-bis(pyridin-2-ylmethyl)methanamine (N4Py).



N4Py was synthesized following the reported procedure with slightly modifications.^{75,76}

Py₂CHOH: To a mixture of di-2-pyridyl ketone (4.4 g, 23.89 mmol) in MeOH (50 mL), 1.0 g of NaBH_4 (26.4 mmol) was slowly added as solid at 0 °C. Then, the ice bath was removed and stirring continued overnight. Removal of the solvent under reduced pressure was followed by addition of water (20 mL), and the mixture was acidified with 2 M HCl and stirred for 10 min. The clear solution was made alkaline

with dilute ammonia and extracted with DCM (3 x 50 mL). The combined DCM layers were dried over MgSO₄, and the solvent was evaporated to give di(2-pyridyl)methanol (3.8 g, 27.1 mmol, 85 %) as a yellow oil, which was used without further purification.

¹H NMR (400 MHz, CDCl₃): δ = 8.55 (dd, *J* = 4.9, 0.8 Hz, 2H), 7.65 (td, *J* = 7.7, 1.8 Hz, 2H), 7.57 – 7.50 (m, 2H), 7.18 (ddd, *J* = 7.4, 4.9, 1.2 Hz, 2H), 5.89 (s, 1H) ppm.

Py₂CHCl: A 100 mL flame dried round bottom flask was charged with 7.3 g of LiCl (172 mmol) absolutely dried and 2 g of di(2-pyridyl)methanol (10.7 mmol). Around 50 mL of dry THF was added under N₂ to obtain a pale yellow solution. Then, Et₃N (4.49 mL, 32.2 mmol) was added carefully, and the mixture was cooled to 0 °C. After 10 minutes, MeSO₂Cl (2.5 mL, 32.2 mmol) was added dropwise at 0 °C and the mixture continued stirring for 2 hours at the same temperature and then for 1 day at room temperature. The reaction was quenched by the addition of H₂O (15 mL) and neutralized using NaHCO₃. The resulting solution was extracted 3 times with DCM, and the combined organic layers were then washed with a saturated NaCl solution. The red organic phase was then dried over MgSO₄, filtered, and the solvent removed under vacuum. The crude mixture was purified by column chromatography (Hexane:AcOEt 1:1) to provide 0.5 g (10.74 mmol, 21 %) of the desired product.

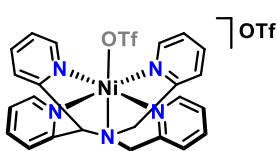
¹H NMR (400 MHz, CDCl₃): δ = 8.57 (d, *J* = 4.7 Hz, 2H), 7.80 – 7.67 (m, 2H), 7.29 – 7.14 (m, 2H), 6.30 (d, *J* = 1.5 Hz, 1H) ppm.

N4Py: Di-(2-picolyl)amine (292 mg, 1.466 mmol), di(2-pyridyl)methyl chloride (300 mg, 1.466 mmol) and anhydrous acetonitrile (50 mL) were mixed in a 100 mL flask. Na₂CO₃ (3 g) and tetrabutylammonium bromide (TBABr) (200 mg) were added directly as solids, and the resulting mixture was heated at reflux temperature for 24 h. After cooling to room temperature, the resulting orange solution was filtered, and the filter cake was washed with DCM. The combined filtrated were evaporate under reduced pressure. NaOH (2M, 30 mL) was added to the resulting

residue, and the mixture was extracted with DCM (3 x 15 mL). The combined organic layers were dried over MgSO_4 , and the solvent was removed under reduced pressure. The resulting oil product was purified by silica column chromatography (DCM:MeOH 30:1) to afford 0.326 g of the desired product (61 % yield) as a yellow oil.

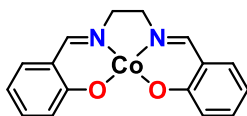
$^1\text{H NMR}$ (300 MHz, CDCl_3): δ = 8.46 (ddt, J = 22.7, 4.8, 1.5 Hz, 4H), 7.70 – 7.46 (m, 8H), 7.13 – 6.97 (m, 4H), 5.31 (s, 1H), 3.93 (s, 4H) ppm. $^{13}\text{C NMR}$ (126 MHz, CDCl_3): δ = 160.4, 160.2, 160.10 (2C), 149.7, 149.6, 149.4, 148.7, 137.6, 136.8, 136.6, 136.6, 126.8, 124.3, 123.3, 122.8, 122.6, 122.4, 122.3, 122.1, 59.3, 57.7, 55.1 ppm.

Synthesis of Ni- N4Py.



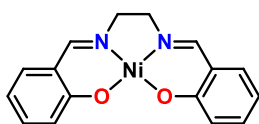
Inside a glovebox, a suspension of $\text{Ni}(\text{OTf})_2(\text{MeCN})_2$ (269 mg, 0.612 mmol) in anhydrous THF (2 mL) was added dropwise to a vigorously stirred solution of N4Py ligand (250 mg, 0.680 mmol) in THF (2 mL), causing a colour change from light yellow to brown after few minutes. After stirring overnight, Et_2O (3 mL) was added, causing the precipitation of a brown solid. The supernatant was removed, and the solid was dried under vacuum. This solid was dissolved in CH_2Cl_2 , filtered through Celite[®], and the slow diffusion of diethyl ether into a saturated solution of complex caused the formation of a pale brown solid, which was dried under vacuum to give 282 mg of the title compound (0.489 mmol, 72 %). **Anal.** Calcd. for $\text{C}_{25}\text{H}_{23}\text{NiF}_6\text{N}_5\text{O}_7\text{S}_2$: C, 40.84; N, 9.52; H, 3.04; S, 8.72 %. Found: C, 40.84; N, 10.05; H, 3.23; S, 8.35 %. **MS** (m/z): 574.0665 [$\text{M} - \text{OTf}$]⁺.

Synthesis of Co-salen and Ni-salen.



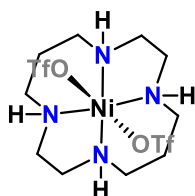
Co-salen: $\text{H}_2(\text{salen})$ 1.0 g (3.73 mmol) and ethanol (6 mL) were mixed under an Ar atmosphere, and the solution was heated to 90 °C in an oil bath. CoCl_2 (3.35 mmol, 0.9 eq.) as

a metal precursor in ethanol (6 mL) was added to the solution. After stirring for 24 h, the solution was cooled to room temperature and filtered to remove the remaining $H_2(\text{salen})$ and M^{2+} ions, followed by drying under vacuum for a day yielded 0.873 g of the *Co-salen* complex as an orange powder (72% of yield). **Anal.** Calcd. for $C_{16}H_{14}CoN_2O_2$: C, 44.34; N, 8.43; H, 6.04%. Found: C, 44.13; N, 12.32; H, 5.26 %. **HPLC-MS** (m/z): 325.0 $[M]^+$.



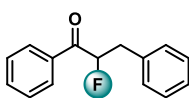
Ni-salen was synthesized following the analogous procedure to the described for complex *Co-salen* obtaining 0.896 g of the desired product as a brown crystalline solid (83 %). **Anal.** Calcd. for $C_{16}H_{14}NiN_2O_2$: C, 44.37; N, 6.46; H, 6.05%. Found: C, 44.98; N, 8.61; H, 5.34 %. **MS** (m/z): 325.0 $[M]^+$.

Synthesis of Ni-cyclam.



$Ni(OTf)_2(MeCN)_2$ (0.65 g, 1.415 mmol) was dissolved in warm ethanol (20 mL) and added to a solution of the ligand (0.289 g, 1.443 mmol) in ethanol (10 mL). The resulting light brown solution was warmed for a one hour in a sealed tube before ether was added. The resultant dark yellow precipitate was filtered off and washed with ether yielded a yellow solid (597 mg, 1.115 mmol, 76 %). **Anal.** Calcd. for $C_{12}H_{24}F_6N_4NiO_6S_2$: C, 26.05; N, 10.13; H, 4.37 %. Found: C, 25.94; N, 10.18; H, 4.24 %. **MS** (m/z): 407.1 $[M - OTf]^+$, 129.1 $[M-2 \cdot OTf]^{2+}$.

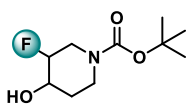
III.5.5 Synthesis and Characterization of Substrates.



Substrate (III.1. b): A solution of the ketone (0.3 g, 1.4 mmol) in THF (1 mL) was added over 5 min to a solution of LDA (1M, 1.6 mL, 1.6 mmol, 1.1 eq) in THF (1.1 mL) at $-78^\circ C$. The mixture was stirred at $-78^\circ C$ for 1.5 h. Then a solution of N-fluorobenzenesulfonimide

(NFSI; 0.54 g, 1.7 mmol) in THF (1.8 mL) was added over 5 min to the solution of the enolate at $-78\text{ }^{\circ}\text{C}$. The mixture was allowed to stir at $-78\text{ }^{\circ}\text{C}$ for 5 min, and then it was allowed to warm to r.t. (white or light yellow suspension) and stirred for 6–12 h. Next, aqueous solutions of NH_4Cl (saturated; 20 mL) and of HCl (1 N; 50 mL) were added in turn. The mixture was extracted with DCM ($3 \times 70\text{ mL}$), and the organic layers were combined, dried over MgSO_4 , and concentrated. The desired product was purified by flash chromatography (Hexane: Et_2O 95:5) to yield the desired product (0.198 mg, 61 % of yield) as a colorless oil.

$^1\text{H NMR}$ (400 MHz, CDCl_3): δ = 7.94 (dt, J = 8.5, 1.1 Hz, 2H), 7.65 – 7.57 (m, 1H), 7.48 (dd, J = 8.4, 7.2 Hz, 1H), 7.34 – 7.25 (m, 4H), 5.74 (ddd, J = 49.0, 8.2, 4.0 Hz, 1H), 3.41 – 3.18 (m, 2H) ppm. $^{19}\text{F NMR}$ (376 MHz, CDCl_3): δ = -186.37 ppm.

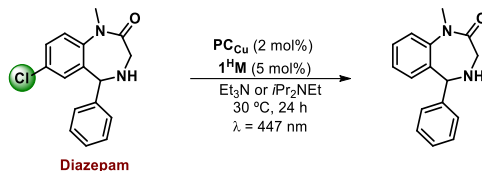


Substrate (III.1. c): To the solution of *tert*-butyl 3-fluoro-4-oxopiperidine-1-carboxylate (350 mg, 1.611 mmol) in MeOH (3 mL), NaBH_4 (91 mg, 2.417 mmol) was slowly added at $0\text{ }^{\circ}\text{C}$. The reaction mixture was stirred at room temperature for 4 h. After diluting with water (80 mL), the mixture was extracted with ethyl acetate (100 mL x 2). The combined organic layers were washed with brine, dried, concentrated and purified by silica gel column chromatography (Hexane: Et_2O 80:20) to give *tert*-butyl 3-fluoro-4-hydroxypiperidine-1-carboxylate (318 mg, 90 % of yield) as a yellow solid.

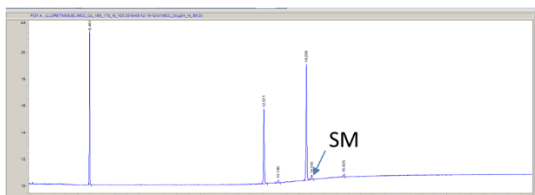
$^1\text{H NMR}$ (400 MHz, CDCl_3): δ = 4.61 (ddt, J = 48.0, 6.2, 2.8 Hz, 1H), 4.05 – 3.85 (m, 1H), 3.82 – 3.10 (m, 4H), 1.81 (tdd, J = 19.5, 9.3, 4.4 Hz, 2H), 1.47 (s, 9H) ppm. $^{19}\text{F NMR}$ (376 MHz, CDCl_3): δ = -186.36 ppm.

III.5.6 Characterization of Products.

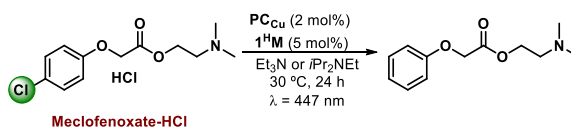
Hydro-dehalogenation reaction of Diazepam.



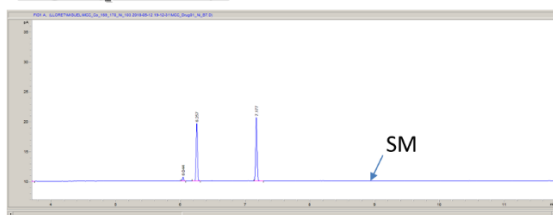
Using $\text{Ni}^{\text{II}}\text{Py}_2\text{tacn}$ as Catalyst



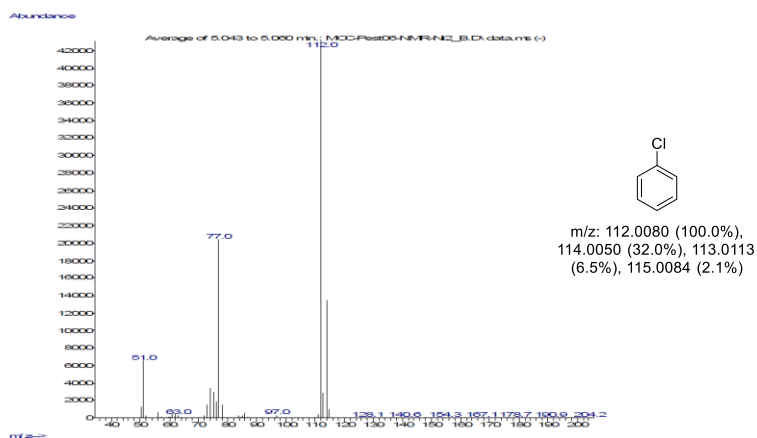
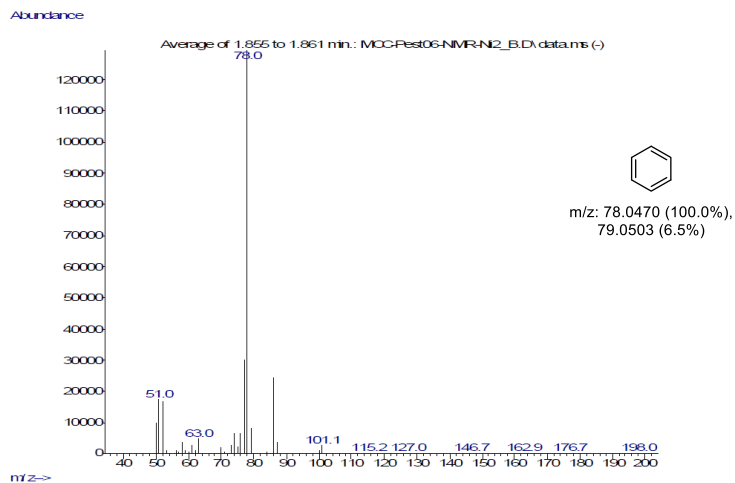
Hydro-dehalogenation reaction of Meclofenoxate.

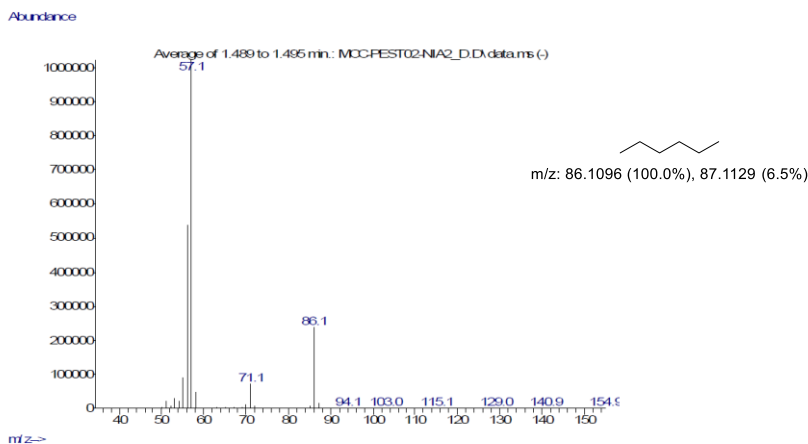


Using $\text{Ni}^{\text{II}}\text{Py}_2\text{tacn}$ as Catalyst

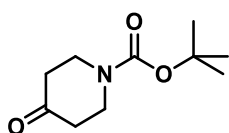


Hydro-dehalogenation reaction of Lindane.



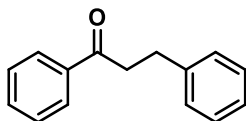


Hydro-defluorination reactions.



Product (III.2.a): Dehalogenation according to general procedure: scale 0.24 mmol, flash chromatography (SiO₂, 5 % → 10 % → 20 % Et₂O in Hexane).

¹H NMR (400 MHz, CDCl₃): δ = 3.71 (t, *J* = 6.2 Hz, 4H), 2.43 (t, *J* = 6.2 Hz, 4H), 1.48 (s, 9H) ppm. ¹³C NMR (126 MHz, CDCl₃): δ = 207.8, 154.47, 80.5, 43.0 (2C), 41.3 (2C), 28.4 (3C) ppm.



Product (III.2.b): Dehalogenation according to general procedure: scale 0.24 mmol, flash chromatography (SiO₂, 5 % → 10 % → 20 % Et₂O in Hexane).

¹H NMR (300 MHz, CDCl₃): δ = 7.61 (d, *J* = 7.3 Hz, 2H), 7.37 (d, *J* = 4.4 Hz, 3H), 7.31 (d, *J* = 8.4 Hz, 2H), 7.22 (s, 2H), 7.18 (d, *J* = 7.5 Hz, 1H), 2.18 (m, 2H), 2.06 (m, 2H) ppm.

III.6. *References of the Chapter*

- (1) Chirik, P. J. Carbon–Carbon Bond Formation in a Weak Ligand Field: Leveraging Open-Shell First-Row Transition-Metal Catalysts. *Angew. Chem. Int. Ed.* **2017**, *56*, 5170, doi: 10.1002/anie.201611959.
- (2) De Abreu, M.; Belmont, P.; Brachet, E. Synergistic Photoredox/Transition-Metal Catalysis for Carbon–Carbon Bond Formation Reactions. *Eur. J. Org. Chem.* **2019**, doi: 10.1002/ejoc.201901146.
- (3) Brahmachari, G. Design for Carbon–Carbon Bond Forming Reactions under Ambient Conditions. *RSC Advances* **2016**, *6*, 64676, doi: 10.1039/C6RA14399G.
- (4) Brahmachari, G.: *Green Synthetic Approaches for Biologically Relevant Heterocycles*; Elsevier Science, 2014.
- (5) Twilton, J.; Le, C.; Zhang, P.; Shaw, M. H.; Evans, R. W.; MacMillan, D. W. C. The Merger of Transition Metal and Photocatalysis. *Nat. Rev. Chem* **2017**, *1*, 0052, doi: 10.1038/s41570-017-0052.
- (6) Romero, N. A.; Nicewicz, D. A. Organic Photoredox Catalysis. *Chem. Rev.* **2016**, *116*, 10075, doi: 10.1021/acs.chemrev.6b00057.
- (7) Matsui, J. K.; Lang, S. B.; Heitz, D. R.; Molander, G. A. Photoredox-Mediated Routes to Radicals: The Value of Catalytic Radical Generation in Synthetic Methods Development. *ACS Catal.* **2017**, *7*, 2563, doi: 10.1021/acscatal.7b00094.
- (8) Studer, A.; Curran, D. P. Catalysis of Radical Reactions: A Radical Chemistry Perspective. *Angew. Chem. Int. Ed.* **2016**, *55*, 58, doi: 10.1002/anie.201505090.
- (9) Zuo, Z.; Ahneman, D. T.; Chu, L.; Terrett, J. A.; Doyle, A. G.; MacMillan, D. W. C. Merging Photoredox with Nickel Catalysis: Coupling of A-Carboxyl Sp³-Carbons with Aryl Halides. *Science* **2014**, *345*, 437, doi: 10.1126/science.1255525.
- (10) Tellis, J. C.; Kelly, C. B.; Primer, D. N.; Jouffroy, M.; Patel, N. R.; Molander, G. A. Single-Electron Transmetalation Via Photoredox/Nickel Dual Catalysis: Unlocking a New Paradigm for Sp³–Sp² Cross-Coupling. *Acc. Chem. Res.* **2016**, *49*, 1429, doi: 10.1021/acs.accounts.6b00214.
- (11) Tellis, J. C.; Primer, D. N.; Molander, G. A. Single-Electron Transmetalation in Organoboron Cross-Coupling by Photoredox/Nickel Dual Catalysis. *Science* **2014**, *345*, 433, doi: 10.1126/science.1253647.
- (12) Jouffroy, M.; Primer, D. N.; Molander, G. A. Base-Free Photoredox/Nickel Dual-Catalytic Cross-Coupling of Ammonium Alkylsilicates. *J. Am. Chem. Soc.* **2016**, *138*, 475, doi: 10.1021/jacs.5b10963.
- (13) Corcé, V.; Chamoreau, L.-M.; Derat, E.; Goddard, J.-P.; Ollivier, C.; Fensterbank, L. Silicates as Latent Alkyl Radical Precursors: Visible-Light Photocatalytic Oxidation of Hypervalent Bis-Catecholato Silicon Compounds. *Angew. Chem. Int. Ed.* **2015**, *54*, 11414, doi: 10.1002/anie.201504963.
- (14) Mao, R.; Frey, A.; Balon, J.; Hu, X. Decarboxylative C_{sp3}–N Cross-Coupling Via Synergetic Photoredox and Copper Catalysis. *Nat. Catal.* **2018**, *1*, 120, doi: 10.1038/s41929-017-0023-z.
- (15) Nakajima, K.; Nojima, S.; Sakata, K.; Nishibayashi, Y. Visible-Light-Mediated Aromatic Substitution Reactions of Cyanoarenes with 4-Alkyl-1,4-Dihydropyridines through

Double Carbon–Carbon Bond Cleavage. *ChemCatChem* **2016**, *8*, 1028, doi: 10.1002/cctc.201600037.

(16) Chen, W.; Liu, Z.; Tian, J.; Li, J.; Ma, J.; Cheng, X.; Li, G. Building Congested Ketone: Substituted Hantzsch Ester and Nitrile as Alkylation Reagents in Photoredox Catalysis. *J. Am. Chem. Soc.* **2016**, *138*, 12312, doi: 10.1021/jacs.6b06379.

(17) Lima, C. G. S.; de M. Lima, T.; Duarte, M.; Jurberg, I. D.; Paixão, M. W. Organic Synthesis Enabled by Light-Irradiation of Eda Complexes: Theoretical Background and Synthetic Applications. *ACS Catal.* **2016**, *6*, 1389, doi: 10.1021/acscatal.5b02386.

(18) Luo, Y.-R.: *Handbook of Bond Dissociation Energies in Organic Compounds*; CRC press, 2002.

(19) Trost, B. M.; Fleming, I.: *Comprehensive Organic Synthesis: Selectivity, Strategy, and Efficiency in Modern Organic Chemistry*; Elsevier Science, 1991; Vol. 8. pp. 793-991.

(20) Andrieux, C. P.; Gallardo, I.; Savaent, J. M.; Su, K. B. Dissociative Electron Transfer. Homogeneous and Heterogeneous Reductive Cleavage of the Carbon-Halogen Bond in Simple Aliphatic Halides. *J. Am. Chem. Soc.* **1986**, *108*, 638, doi: 10.1021/ja00264a013.

(21) Houmam, A. Electron Transfer Initiated Reactions: Bond Formation and Bond Dissociation. *Chem. Rev.* **2008**, *108*, 2180, doi: 10.1021/cr068070x.

(22) Bard, A. J.: *Encyclopedia of Electrochemistry of the Elements*; Marcel Dekker., 1982.

(23) Patai, S.: *The Chemistry of Halides Pseudo-Halides and Azides, Supplement D, Part 2*; Wiley, 1983.

(24) Hush, N. S.: *Electrode Reactions of the Methyl Halides*, 1957; Vol. 61.

(25) Ebersson, L. Electron Transfer Reactions in Organic Chemistry. II. An Analysis of Alkyl Halide Reduction by Electron Transfer Reagents on the Basis of the Marcus Theory. *Acta Chem. Scand.* **1982**, *36b*, 533, doi: 10.3891/acta.chem.scand.36b-0533.

(26) Studer, A.; Amrein, S. Silylated Cyclohexadienes: New Alternatives to Tributyltin Hydride in Free Radical Chemistry. *Angew. Chem. Int. Ed.* **2000**, *39*, 3080, doi: 10.1002/1521-3773(20000901)39:17<3080::Aid-anie3080>3.0.Co;2-e.

(27) Hironaka, K.; Fukuzumi, S.; Tanaka, T. Tris(Bipyridyl)Ruthenium(II)-Photosensitized Reaction of 1-Benzyl-1,4-Dihydronicotinamide with Benzyl Bromide. *J. Chem. Soc. Perk. Trans. 2* **1984**, 1705, doi: 10.1039/P29840001705.

(28) Maidan, R.; Goren, Z.; Becker, J. Y.; Willner, I. Application of Multielectron Charge Relays in Chemical and Photochemical Debromination Processes. The Role of Induced Disproportionation of N,N'-Dioctyl-4,4'-Bipyridinium Radical Cation in Two-Phase Systems. *J. Am. Chem. Soc.* **1984**, *106*, 6217, doi: 10.1021/ja00333a017.

(29) Willner, I.; Tsfania, T.; Eichen, Y. Photocatalyzed and Electrocatalyzed Reduction of Vicinal Dibromides and Activated Ketones Using Ruthenium(I) Tris(Bipyridine) as Electron-Transfer Mediator. *J. Org. Chem.* **1990**, *55*, 2656, doi: 10.1021/jo00296a023.

(30) Mashraqui, S. H.; Kellogg, R. M. 3-Methyl-2,3-Dihydrobenzothiazoles as Reducing Agent. Dye Enhanced Photoreactions. *Tetrahedron Lett.* **1985**, *26*, 1453, doi: 10.1016/S0040-4039(00)99069-5.

(31) Narayanam, J. M. R.; Tucker, J. W.; Stephenson, C. R. J. Electron-Transfer Photoredox Catalysis: Development of a Tin-Free Reductive Dehalogenation Reaction. *J. Am. Chem. Soc.* **2009**, *131*, 8756, doi: 10.1021/ja9033582.

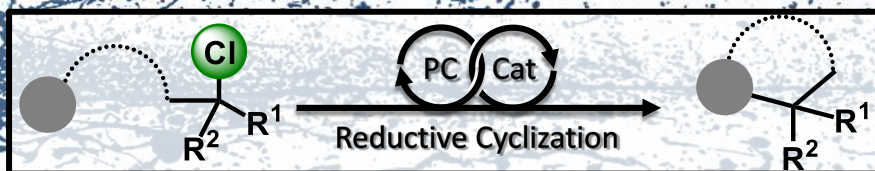
- (32) Maji, T.; Karmakar, A.; Reiser, O. Visible-Light Photoredox Catalysis: Dehalogenation of Vicinal Dibromo-, α -Halo-, and α,α -Dibromocarbonyl Compounds. *J. Org. Chem.* **2011**, *76*, 736, doi: 10.1021/jo102239x.
- (33) Nguyen, J. D.; D'Amato, E. M.; Narayanam, J. M. R.; Stephenson, C. R. J. Engaging Unactivated Alkyl, Alkenyl and Aryl Iodides in Visible-Light-Mediated Free Radical Reactions. *Nat. Chem.* **2012**, *4*, 854, doi: 10.1038/nchem.1452.
- (34) McCarroll, A. J.; Walton, J. C. Programming Organic Molecules: Design and Management of Organic Syntheses through Free-Radical Cascade Processes. *Angew. Chem. Int. Ed.* **2001**, *40*, 2224, doi: 10.1002/1521-3773(20010618)40:12<2224::Angewandte2224>3.0.Co;2-f.
- (35) Newcomb, M. Radical Kinetics and Clocks. *Encyclopedia of Radicals in Chemistry, Biology and Materials.* **2012**, doi: 10.1002/9780470971253.rad086
- (36) Revol, G.; McCallum, T.; Morin, M.; Gagosz, F.; Barriault, L. Photoredox Transformations with Dimeric Gold Complexes. *Angew. Chem. Int. Ed.* **2013**, *52*, 13342, doi: 10.1002/anie.201306727.
- (37) Chow, P.-K.; Cheng, G.; Tong, G. S. M.; To, W.-P.; Kwong, W.-L.; Low, K.-H.; Kwok, C.-C.; Ma, C.; Che, C.-M. Luminescent Pincer Platinum(II) Complexes with Emission Quantum Yields up to Almost Unity: Photophysics, Photoreductive C–C Bond Formation, and Materials Applications. *Angew. Chem. Int. Ed.* **2015**, *54*, 2084, doi: 10.1002/anie.201408940.
- (38) Ghosh, I.; Ghosh, T.; Bardagi, J. I.; König, B. Reduction of Aryl Halides by Consecutive Visible-Light-Induced Electron Transfer Processes. *Science* **2014**, *346*, 725, doi: 10.1126/science.1258232.
- (39) Meyer, A. U.; Slanina, T.; Heckel, A.; König, B. Lanthanide Ions Coupled with Photoinduced Electron Transfer Generate Strong Reduction Potentials from Visible-Light. *Chem. Eur. J.* **2017**, *23*, 7900, doi: 10.1002/chem.201701665.
- (40) Matsubara, R.; Yabuta, T.; Md Idros, U.; Hayashi, M.; Ema, F.; Kobori, Y.; Sakata, K. Uva- and Visible-Light-Mediated Generation of Carbon Radicals from Organochlorides Using Nonmetal Photocatalyst. *J. Org. Chem.* **2018**, *83*, 9381, doi: 10.1021/acs.joc.8b01306.
- (41) Begum, S.; Subramanian, R. Reaction of Chlorine Radical with Tetrahydrofuran: A Theoretical Investigation on Mechanism and Reactivity in Gas Phase. *J. Mol. Model.* **2014**, *20*, 2262, doi: 10.1007/s00894-014-2262-0.
- (42) Ibrahim, M. A. A. Molecular Mechanical Study of Halogen Bonding in Drug Discovery. *J. Comput. Chem.* **2011**, *32*, 2564, doi: 10.1002/jcc.21836.
- (43) Cavallo, G.; Metrangolo, P.; Milani, R.; Pilati, T.; Priimagi, A.; Resnati, G.; Terraneo, G. The Halogen Bond. *Chem. Rev.* **2016**, *116*, 2478, doi: 10.1021/acs.chemrev.5b00484.
- (44) Wilcken, R.; Zimmermann, M. O.; Lange, A.; Joerger, A. C.; Boeckler, F. M. Principles and Applications of Halogen Bonding in Medicinal Chemistry and Chemical Biology. *J. Med. Chem.* **2013**, *56*, 1363, doi: 10.1021/jm3012068.
- (45) Poznik, M.; König, B. Fast Colorimetric Screening for Visible-Light Photocatalytic Oxidation and Reduction Reactions. *React. Chem. Eng.* **2016**, *1*, 494, doi: 10.1039/C6RE00117C.
- (46) Manahan, S. E.: *Toxicological Chemistry and Biochemistry, Third Edition*; CRC Press, 2002.

- (47) Jeschke, P. Latest Generation of Halogen-Containing Pesticides. *Pest. Manag. Sci.* **2017**, *73*, 1053, doi: 10.1002/ps.4540.
- (48) Wade, R. S.; Castro, C. E. Oxidation of Iron(II) Porphyrins by Alkyl Halides. *J. Am. Chem. Soc.* **1973**, *95*, 226, doi: 10.1021/ja00782a040.
- (49) Marks, T. S.; Allpress, J. D.; Maule, A. Dehalogenation of Lindane by a Variety of Porphyrins and Corrins. *Appl. Environ. Microbiol.* **1989**, *55*, 1258.
- (50) Thayer, A. M. Fabulous Fluorine. *Chemical & Engineering News Archive* **2006**, *84*, 15, doi: 10.1021/cen-v084n023.p015.
- (51) Gould, R. F.: Biochemistry Involving Carbon-Fluorine Bonds, Copyright, Acs Symposium Series. In *Biochemistry Involving Carbon-Fluorine Bonds*; Robert, F. G., Ed.; Acs Symposium Series 28; American Chemical Society, 1976; Vol. 28.
- (52) Smith, F. A. Carbon-Fluorine Compounds. *Science* **1973**, *179*, 272, doi: 10.1126/science.179.4070.272.
- (53) Henne, A. Chemistry of Organic Fluorine Compounds. *J. Am. Chem. Soc.* **1963**, *85*, 490, doi: 10.1021/ja00887a042.
- (54) Ravishankara, A. R.; Solomon, S.; Turnipseed, A. A.; Warren, R. F. Atmospheric Lifetimes of Long-Lived Halogenated Species. *Science* **1993**, *259*, 194, doi: 10.1126/science.259.5092.194.
- (55) Miller, J. F.; Hunt, H.; McBee, E. T. Decomposition and Analysis of Organic Compounds Containing Fluorine and Other Halogens. *Anal. Chem.* **1947**, *19*, 148, doi: 10.1021/ac60003a003.
- (56) *The Enzymes: Part B. Oxidation and Reduction. Vol. 8*; Academic Press, 1963.
- (57) Mansuy, D.; Nastainczyk, W.; Ullrich, V. The Mechanism of Halothane Binding to Microsomal Cytochrome P₄₅₀. *Naunyn-Schmiedeberg's Arch. Pharmacol.* **1974**, *285*, 315, doi: 10.1007/BF00501461.
- (58) Kiso, Y.; Tamao, K.; Kumada, M. Effects of the Nature of Halides on the Alkyl Group Isomerization in the Nickel-Catalyzed Cross-Coupling of Secondary Alkyl Grignard Reagents with Organic Halides. *J. Organomet. Chem.* **1973**, *50*, C12, doi: 10.1016/S0022-328X(00)95063-0.
- (59) Kiplinger, J. L.; Richmond, T. G.; Osterberg, C. E. Activation of Carbon-Fluorine Bonds by Metal Complexes. *Chem. Rev.* **1994**, *94*, 373, doi: 10.1021/cr00026a005.
- (60) McAlexander, L. H.; Beck, C. M.; Burdeniuc, J. J.; Crabtree, R. H. Fluoroalkane Aromatization over Hot Sodium Oxalate. *J. Fluorine Chem.* **1999**, *99*, 67, doi: 10.1016/S0022-1139(99)00113-X.
- (61) Burdeniuc, J.; Sanford, M.; Crabtree, R. H. Amine Charge Transfer Complexes of Perfluoroalkanes and an Application to Poly(Tetrafluoroethylene) Surface Functionalization. *J. Fluorine Chem.* **1998**, *91*, 49, doi: 10.1016/S0022-1139(98)00215-2.
- (62) Kiplinger, J. L.; Richmond, T. G. Group Iv Metallocene-Mediated Synthesis of Fluoroaromatics Via Selective Defluorination of Saturated Perfluorocarbons. *J. Am. Chem. Soc.* **1996**, *118*, 1805, doi: 10.1021/ja952563u.
- (63) Vela, J.; Smith, J. M.; Yu, Y.; Ketterer, N. A.; Flaschenriem, C. J.; Lachicotte, R. J.; Holland, P. L. Synthesis and Reactivity of Low-Coordinate Iron(II) Fluoride Complexes and Their Use in the Catalytic Hydro-defluorination of Fluorocarbons. *J. Am. Chem. Soc.* **2005**, *127*, 7857, doi: 10.1021/ja042672l.

- (64) Desmarets, C.; Kuhl, S.; Schneider, R.; Fort, Y. Nickel(0)/Imidazolium Chloride Catalyzed Reduction of Aryl Halides. *Organometallics* **2002**, *21*, 1554, doi: 10.1021/om010949+.
- (65) Böhm, V. P. W.; Gstöttmayr, C. W. K.; Weskamp, T.; Herrmann, W. A. Catalytic C–C Bond Formation through Selective Activation of C–F Bonds. *Angew. Chem. Int. Ed.* **2001**, *40*, 3387, doi: 10.1002/1521-3773(20010917)40:18<3387::Aid-anie3387>3.0.Co;2-6.
- (66) Dankwardt, J. W. Transition Metal Catalyzed Cross-Coupling of Aryl Grignard Reagents with Aryl Fluorides Via Pd- or Ni-Activation of the C–F Bond: An Efficient Synthesis of Unsymmetrical Biaryls – Application of Microwave Technology in Ligand and Catalyst Screening. *J. Organomet. Chem.* **2005**, *690*, 932, doi: 10.1016/j.jorganchem.2004.10.037.
- (67) Ackermann, L.; Born, R.; Spatz, J. H.; Meyer, D. Efficient Aryl–(Hetero)Aryl Coupling by Activation of C–Cl and C–F Bonds Using Nickel Complexes of Air-Stable Phosphine Oxides. *Angew. Chem. Int. Ed.* **2005**, *44*, 7216, doi: 10.1002/anie.200501860.
- (68) Terao, J.; Watabe, H.; Kambe, N. Ni-Catalyzed Alkylative Dimerization of Vinyl Grignard Reagents Using Alkyl Fluorides. *J. Am. Chem. Soc.* **2005**, *127*, 3656, doi: 10.1021/ja042565r.
- (69) Kraft, B. M.; Lachicotte, R. J.; Jones, W. D. Aliphatic Carbon–Fluorine Bond Activation Using (C₅Me₅)₂ZrH₂. *J. Am. Chem. Soc.* **2000**, *122*, 8559, doi: 10.1021/ja001006r.
- (70) Kraft, B. M.; Lachicotte, R. J.; Jones, W. D. Aliphatic and Aromatic Carbon–Fluorine Bond Activation with Cp*₂ZrH₂: Mechanisms of Hydro-defluorination. *J. Am. Chem. Soc.* **2001**, *123*, 10973, doi: 10.1021/ja016087l.
- (71) Vogt, D. B.; Seath, C. P.; Wang, H.; Jui, N. T. Selective C–F Functionalization of Unactivated Trifluoromethylarenes. *J. Am. Chem. Soc.* **2019**, *141*, 13203, doi: 10.1021/jacs.9b06004.
- (72) Call, A.; Codolà, Z.; Acuña-Parés, F.; Lloret-Fillol, J. Photo- and Electrocatalytic H₂ Production by New First-Row Transition-Metal Complexes Based on an Aminopyridine Pentadentate Ligand. *Chem. Eur. J.* **2014**, *20*, 6171, doi: 10.1002/chem.201303317.
- (73) Call, A.; Lloret-Fillol, J. Enhancement and Control of the Selectivity in Light-Driven Ketone Versus Water Reduction Using Aminopyridine Cobalt Complexes. *Chem. Commun.* **2018**, *54*, 9643, doi: 10.1039/C8CC04239J.
- (74) Radaram, B.; Ivie, J. A.; Singh, W. M.; Grudzien, R. M.; Reibenspies, J. H.; Webster, C. E.; Zhao, X. Water Oxidation by Mononuclear Ruthenium Complexes with Tpa-Based Ligands. *Inorg. Chem.* **2011**, *50*, 10564, doi: 10.1021/ic200050g.
- (75) Roelfes, G.; Lubben, M.; Hage, R.; Que, J., Lawrence; Feringa, B. L. Catalytic Oxidation with a Non-Heme Iron Complex That Generates a Low-Spin Fe^{III}OOH Intermediate. *Chem. Eur. J.* **2000**, *6*, 2152, doi: 10.1002/1521-3765(20000616)6:12<2152::Aid-chem2152>3.0.Co;2-o.
- (76) Lubben, M.; Meetsma, A.; Wilkinson, E. C.; Feringa, B.; Que Jr., L. Nonheme Iron Centers in Oxygen Activation: Characterization of an Iron(III) Hydroperoxide Intermediate. *Angew. Chem. Int. Ed.* **1995**, *34*, 1512, doi: 10.1002/anie.199515121.

UNIVERSITAT ROVIRA I VIRGILI
DEVELOPMENT OF VISIBLE LIGHT PHOTOREDOX METHODOLOGIES TOWARDS THE ACTIVATION
OF CARBON-HALOGEN BONDS
Miguel Claros Casielles

Chapter IV



Reductive Cyclizations from non-activated Alkyl-Halides

UNIVERSITAT ROVIRA I VIRGILI
DEVELOPMENT OF VISIBLE LIGHT PHOTOREDOX METHODOLOGIES TOWARDS THE ACTIVATION
OF CARBON-HALOGEN BONDS
Miguel Claros Casielles

IV.1. Contents	
IV.2. State-of-the-art.....	157
IV.2. 1 Light-Driven Intramolecular Reductive Cyclizations of Alkyl Halides with Pendant Alkenes.	161
IV.3. Results and Discussion.	165
IV.3. 1 Visible-Light Photoredox Reductive Cyclization from Non-Activated Alkyl Bromides with Tethered Alkenes.	165
IV.3. 2 Visible-Light Photoredox Reductive Cyclization from Non-Activated Alkyl Chlorides with Tethered Alkenes.	169
IV.3. 3 Visible-Light Photoredox Reductive Cyclization from Non-Activated Alkyl Chlorides with Tethered Alkynes.	185
IV.3. 4 Unsuccessful Substrates.	188
IV.4. Conclusions.	189
IV.5. Experimental Section.	191
IV.5. 1 Material and Reagents.	191
IV.5. 2 Instrumentation.	191
IV.5. 3 Experimental Procedures.	194
IV.5. 4 Synthesis and Characterization of Metal Complexes.	197
IV.5. 5 Synthesis and Characterization of Substrates.	201
IV.5. 6 Synthesis and Characterization of Products.	244
IV.6. References	261

Figure IV.1 General cyclization scheme	158
Figure IV.2 Radical chain reactions using tri- <i>n</i> -butyltin hydride as a prototypical reagent.	159
Figure IV.3 Selected examples of intramolecular radical cyclizations conducted with tri- <i>n</i> -butyltin hydride using halides, selenides, thionocarbonates and alkynes as radical precursors.	159
Figure IV.4 Radical chain mechanism initiated by mercury hydride.	160
Figure IV.5 Reductive cyclization reactions by Ti ^{III} (left) and Sm ^{II} (right) reagents.	160
Figure IV.6 General mechanism for carbon-centered radical formation by visible-light photocatalysis.	161
Figure IV.7 Photoredox promoted visible-light cyclization reactions from activated and non-activated alkyl halides.	162
Figure IV.8 Recent developed strategies for the functionalization of challenging aryl and alkyl bromides.	163
Figure IV.9 Recent developed strategies for the functionalization of challenging aryl and alkyl halides.	164
Figure IV.10 ¹ H-NMR spectrum for the mixture of products IV.2.b and IV.2.c of the 5-exo-trig cyclization reaction of alkyl bromide with disubstituted olefin (IV.1.b).	168
Figure IV.11 Proposed mechanism for the formation of IV.2.b and IV.2.c	169
Figure IV.12 Molecular structures of the photocatalysts tested in the screening.	172
Figure IV.13 Molecular structure of triazacyclononane based catalysts (1 ^x M, 2 ^x M and 3M), M-DPA and M-N4Py catalysts.	173

Figure IV.14 Molecular structure of M ^X MCP, M ^X PDP and M ^X TPA catalysts.	174
Figure IV.15 Molecular structure of M-Cyclam, M-Salen, M-TPP, M-Terpy, M-Terpy ₂ , Co(DMG) and Vitamin B ₁₂ catalysts.....	175
Figure IV.16 Single-point monitoring experiments of the reductive cyclization of IV.3.a.	179
Figure IV.17 Single-point monitoring experiment throughout light-dark cycles.	179
Figure IV.18 Single-point monitoring experiment of bromine/chlorine selectivity. Subsequent reaction of alkyl-chloride substrates after alkyl-bromide substrates (top) and concurrently reaction of methyl and ethyl malonate derivatives in alkyl chloride substrates (bottom left) and alkyl bromide substrates (bottom right).....	180
Figure IV.19 Hydrogen evolution monitoring in the optimized conditions for the cyclization reaction of substrate IV.3.a.	182
Figure IV.20 In-house developed parallel photoreactors coupled with parallel pressure transducer device.....	194

Table IV.1 Catalyst screening for the reductive cyclization of non-activated alkyl bromides.	166
Table IV.2 Screening of conditions for the reductive cyclization of non-activated alkyl bromides.	167
Table IV.3 Catalyst loading and photocatalyst screening for the cyclization reaction of non-activated alkyl bromides with pendant disubstituted alkenes.	168
Table IV.4 Initial screening of conditions for the reductive cyclization reaction of non-activated alkyl chlorides.	170
Table IV.5 Solvent screening for the cyclization reaction of non-activated alkyl chlorides.	171
Table IV.6 Photoredox catalyst screening for the cyclization of non-activated alkyl chlorides.	172
Table IV.7 Catalyst screening for the reductive cyclization of non-activated alkyl chlorides.	175
Table IV.8 Substrate scope of the cyclization of non-activated alkyl chlorides with tethered alkenes.	184
Table IV.9 Screening of the conditions for the cyclization of non-activated alkyl chlorides been tethered alkynes.	185
Table IV.10 Substrate scope of the cyclization of non-activated alkyl chlorides with tethered alkynes.	187
Table IV.11 Non-working substrates for the reductive cyclization methodology.	188

IV.2. *State-of-the-art.*

Carbocyclic or heterocyclic subunits are present in more than 90% of chemically individual molecules in nature.¹⁻³ Many of these are important medicinal compounds, components of food, pigments or fragrances such as terpenes or steroids.^{4,5} Due to symmetry and hindered rotation, cyclic compounds have higher boiling and melting points as well as higher densities comparing with the corresponding linear molecules. These differential properties are the result of the higher *London Dispersion* forces and the different packing density of the crystals of both series. Not surprisingly, the key cyclization step remains critical to the formation of the desired cyclic structure in a regio- and stereoselective manner. In the literature, it is possible to find several methods to build ring systems involving cationic, radical or anionic intermediates, as well as metal-catalyzed and pericyclic reactions (including cycloadditions, electrocyclic reactions and sigmatropic rearrangements).⁶ Setting aside pericyclic reactions, which are out of the scope of this thesis, cationic cyclizations reactions often lead to the thermodynamic product, whereas radical cyclizations usually proceed under kinetic control. Both kinetic and thermodynamic products can be obtained in both anionic and metal-catalyzed cyclization reactions. In such cases, the main side product is the corresponding alkene formed upon β -elimination step. Radical cyclization procedures allow the use of neutral conditions as well as broad functional group tolerance.⁷ Radical cyclization reactions have grown in importance due to the high functional group tolerance and high levels of regio-, chemo- and stereoselectivity.⁸⁻¹⁰ Generally, these reactions comprise three basic steps: selective radical generation, radical cyclization and conversion to the desired product (**Figure IV.1**).

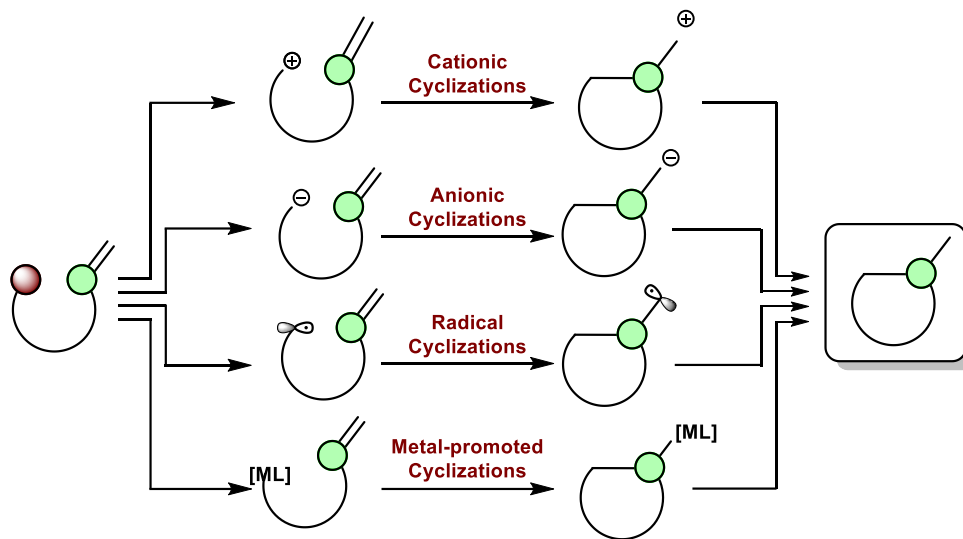


Figure IV.1 General cyclization scheme

As mentioned in *Chapter III*, a wide variety of functional groups can be employed as radical precursors (**Figure III.1**). The cyclization step usually involves the addition of the radical intermediate to a π -bond. However, radical scavengers, fragmentation or electron transfer reactions can also convert the radical intermediate into the final product.

The use of trialkyl tin hydride (R_3SnH) in combination with azobisisobutyronitrile (*AIBN*) as radical initiator is a common method to conduct radical reactions of alkyl halides as precursors. The reaction of R_3SnH with *AIBN* generates the chain carrier $R_3Sn\cdot$ (**Figure IV.2, B**), which enables the atom or group abstraction of the alkyl halide (*C*) to form a carbon-centered radical (*D*). This radical intermediate can be hydrogenated to form the proto-dehalogenated product (*E*), or it can engage into the cyclization step with a tethered π -bond (alkene, alkyne) to provide the cycloalkyl radical (*F*). Finally, the cyclized radical engages in a hydrogen atom abstraction with a molecule of tin hydride (radical chain step) yielding the desired reduced cyclized product (*G*) and the chain-carrying tin radical (*B*).¹¹ Dehalogenation is an important side-reaction in radical cyclizations promoted by Bu_3SnH and *AIBN*. This problem can be usually solved by employing low

concentrations of tin hydride due to the kinetic difference between both reactions, which favours the cyclization (intramolecular) over the hydride abstraction (intermolecular).

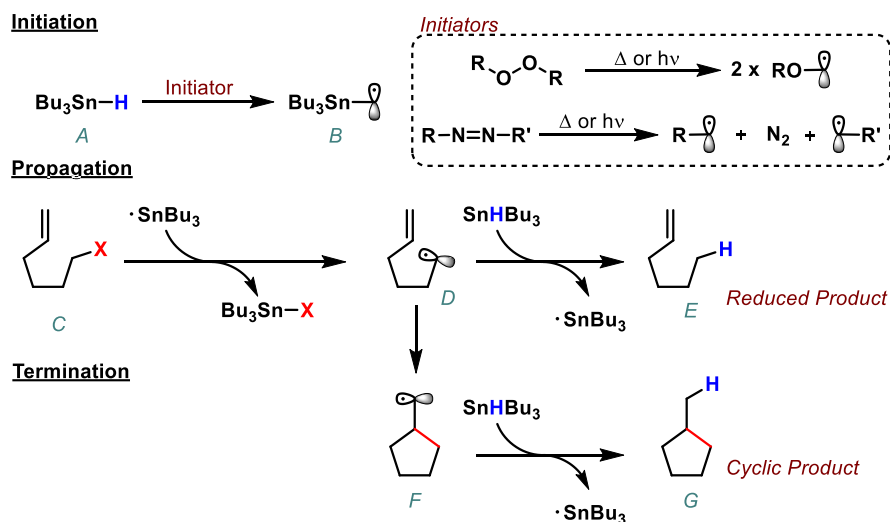


Figure IV.2 Radical chain reactions using tri-*n*-butyltin hydride as a prototypical reagent.

The versatility of radical cyclization methods is highlighted by the diversity of radical precursors that can be activated with trialkyltin hydride and AIBN, including acyl selenides, thionocarbonates and alkynes (Figure IV.3).

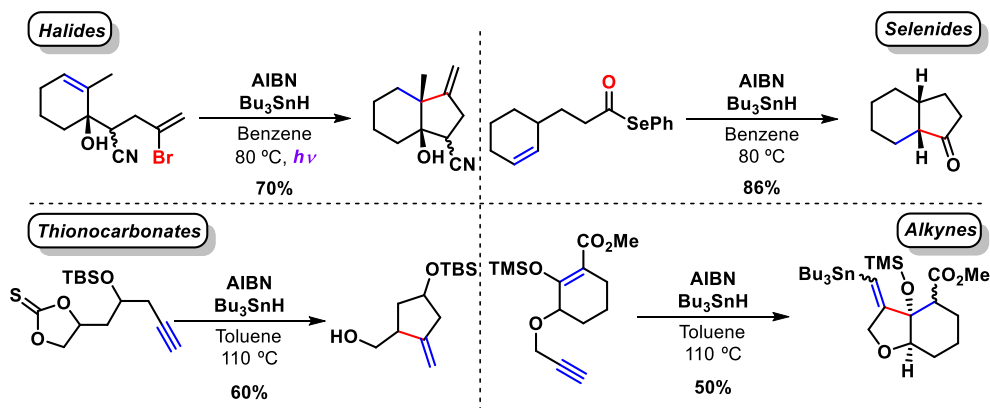


Figure IV.3 Selected examples of intramolecular radical cyclizations conducted with tri-*n*-butyltin hydride using halides,¹² selenides,¹³ thionocarbonates¹⁴ and alkynes¹⁵ as radical precursors.

Organomercury(II) halides or acetates have also been employed in cyclization reactions due to their ability to initiate radical chain mechanisms.⁷ In the

presence of hydride donors such as sodium borohydride, sodium cyanoborohydride or tin hydride, organomercury compounds are reduced to form alkylmercury(II) hydride species. These transient intermediates decompose to give Hg⁰ and alkyl radicals (**Figure IV.4**). Since mercury hydrides are better hydrogen donors than tin hydrides, dehalogenation competes strongly with the cyclization reaction, limiting the use of organomercury compounds to those favourable cases where the cyclization step is considerably faster.

Initiation



Figure IV.4 Radical chain mechanism initiated by mercury hydride.

As an alternative to metal hydride based reactions, fragmentation,^{16,17} radical/radical coupling¹⁸ or oxidative^{19,20}/reductive²¹⁻²³ (*redox*) methods can be employed for radical cyclization reactions. In order to design more selective methodologies, the use of stoichiometric amounts of chemical reductants, such as titanium(III) chloride^{21,24} and samarium(II)iodide were widely used for the activation of *Carbon-Halogen* bonds (**Figure IV.5**).²⁵ In these reductive methods, the initial radical is generated by one-electron transfer to the precursor. In this context, Curran and co-workers in 1990 employed SmI₂ for the radical cyclization of aryl iodides in the presence of hexamethylphosphoramide “HMPA” (the HMPA decreases the reduction potential of SmI₂).²⁶ Additionally, tandem cyclization reactions can be performed to form 5,5-bicyclic systems as demonstrated by Molander and co-workers in 1995.²⁷

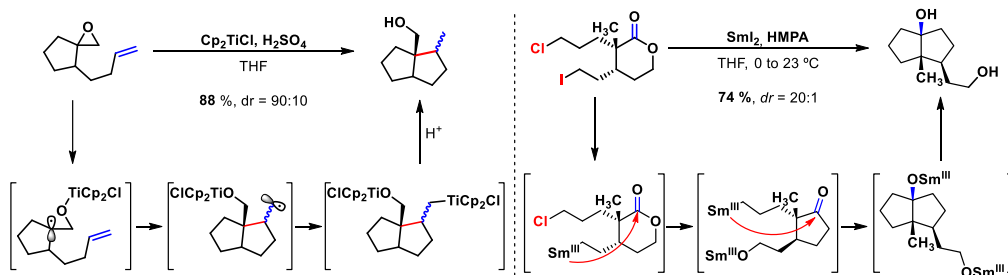


Figure IV.5 Reductive cyclization reactions by Ti^{III} (left) and Sm^{II} (right) reagents.

The methods mentioned above to perform cyclization reactions require the use of stoichiometric amounts of highly toxic, environmentally hazardous or explosive reagents. Alternatively, visible-light photocatalytic strategies have been recently developed that demonstrate more sustainable cyclization reactions. Visible-light can be used as a source of energy to activate organic molecules to trigger the formation of carbon-centered radicals, which ultimately can be trapped by tethered π -systems. Thus, a photoexcited photoredox mediator can enable the formation of radical species through single electron transfer (SET) processes (**Figure IV.6**). Commonly employed photosensitizers such as organic dyes (i.e. eosin Y, rhodamine B) and Ru^{II} and Ir^{III} polypyridyl complexes enable the cleavage of a variety of precursors such as alkyltrifluoroborates, carboxylic acids or weak C–Halogen bonds, mostly aryl and alkyl iodides or activated alkyl bromides.^{28,29} With appropriate substrates in hand, visible-light intramolecular reductive cyclization reactions to construct complex carbocyclic structures have been recently developed, which will be the focus of this chapter.

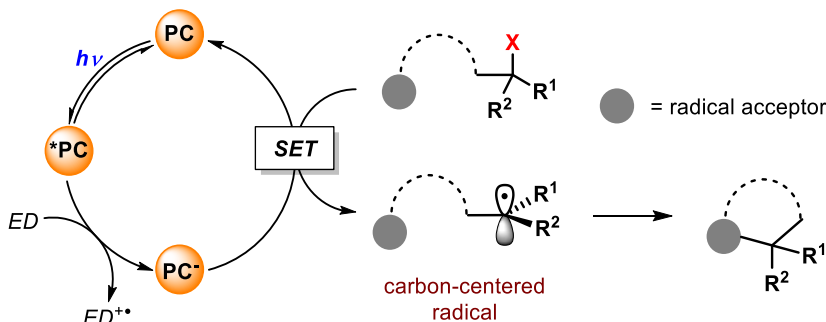


Figure IV.6 General mechanism for carbon-centered radical formation by visible-light photocatalysis.

IV.2. 1 Light-Driven Intramolecular Reductive Cyclizations of Alkyl Halides with Pendant Alkenes.

In 2010, Stephenson and co-workers first reported the intramolecular reductive cyclization of alkyl halides with pendant alkenes or alkynes in the

synthesis of 5 and 6-membered rings under visible-light photocatalysis.²⁸ Activated alkyl halides are alkyl radical precursors, which cyclize intramolecularly with an alkene or alkyne to give the kinetically favoured product *via 5-exo-trig* or *5-exo-dig* pathways, respectively. These light-driven cyclizations employed [Ru(bpy)₃]Cl₂ and [Ir(ppy)₂(dtbbpy)]PF₆ complexes as photoredox catalysts (PCs) for the cyclization of activated alkyl bromides and non-activated alkyl iodides respectively (**Figure IV.7**, top). Continuous development of novel photoredox catalysts that provide higher reducing power has expanded the redox potential window facilitating the cleavage of less activated functional groups, for example, alkyl bromides. In this context, Barriault and co-workers introduced the use of a dimeric gold complex [Au₂(μ-dppm)₂]²⁺ that absorbs light in the UV region (λ_{max} = 295 nm) aiming at using non-activated alkyl bromides in such transformations (**Figure IV.7**, bottom left).³⁰ Additionally, Che and co-workers have developed several visible-light noble-metal based PCs to reach enough reducing power to achieve the Csp³-Br bond cleavage (**Figure IV.7**, bottom right).³¹

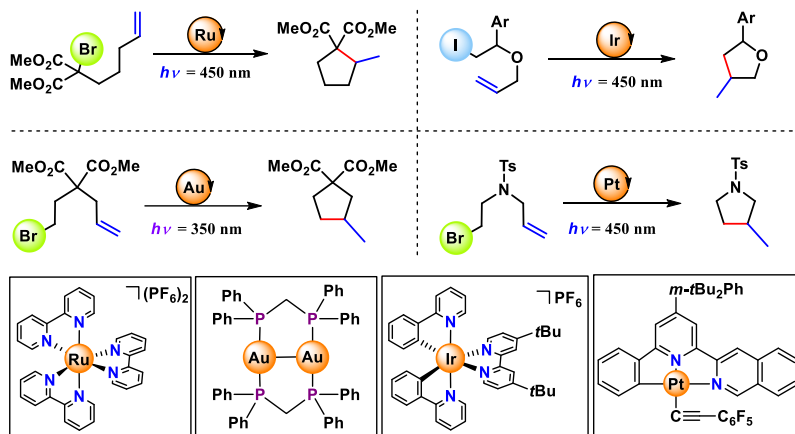


Figure IV.7 Photoredox promoted visible-light cyclization reactions from activated and non-activated alkyl halides.

However, aryl and alkyl chlorides are usually out of the scope of most C–C and C–Heteroatom bond-forming reactions due to the inherent chemical inertness of the Csp³–Cl bonds. Nevertheless, few seminal examples demonstrate the feasibility of using non-activated alkyl chlorides as electrophilic coupling partners

in transition metal-catalysed cross-coupling reactions.³²⁻³⁴ As an alternative, the synergistic merger of a photosensitizer that reduces the oxidation state of a coordination metal complex has enabled the employment of less reactive precursors in C–C bond forming reactions.^{35,36} In this regard, in 2016, MacMillan and co-workers reported the dehalogenation and intramolecular radical cyclization of aryl and alkyl bromides (Figure IV.8). They also reported the trifluoromethylation of aryl bromides^{37,38} triggered by the use of halogen abstractors as tris(trimethylsilyl)silane (*TTMSS*).

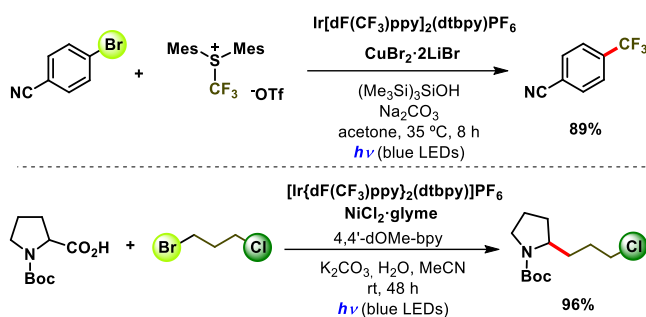


Figure IV.8 Recent developed strategies for the functionalization of challenging aryl and alkyl bromides.

Alternatively, the use of lanthanides in combination of organic dyes,³⁵ or a dual Ir/Pd catalytic system³⁹ has enabled the activation of *Csp*²–Cl bonds (Figure IV.9). Besides, activated aryl chlorides bearing electron-deficient substituents can serve as radical surrogates for hydroarylation reactions employing *N*-phenylphenothiazine (*PTH*) as photocatalyst in combination with a thiol and a stoichiometric amount of formate.⁴⁰ An *S_N2* reaction pathway was proposed for the activation of benzylic chlorides by using dithiocarbonyl anions as nucleophilic catalysts.⁴¹ The resulting dithiocarbamate undergoes photolytic C–S bond cleavage that generates a C-centered radical, which ultimately can react with electron-deficient olefins or heteroarematoms as radical acceptor coupling partners.

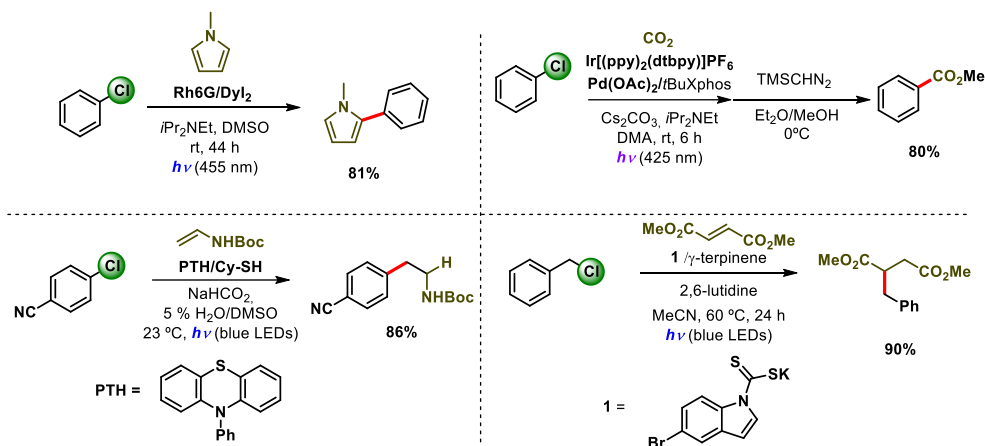


Figure IV.9 Recent developed strategies for the functionalization of challenging aryl and alkyl halides.

As a proof of concept, Fu, Peters and co-workers demonstrated that the photoluminescent copper-carbazolide complex is an efficient catalyst for $C-N$ bond-forming reactions between amines and alkyl halides (Cl and Br) upon UV irradiation.⁴² Following a similar strategy, they also reported a light-driven copper-catalyzed alkylation of amides with alkyl bromides.^{43,44} Remarkably, the copper-carbazolide complex bearing a chiral phosphine ligand catalyzes the visible-light photoinduced enantioconvergent $C-N$ cross-coupling of racemic tertiary α -chloroamides.⁴⁵ In the proposed mechanism, these activated alkyl chlorides engage in an electron transfer process with the excited chiral copper-carbazolide. The generated solvent-caged tertiary alkyl radical is coupled with the carbazolide ligand of the copper catalyst in an enantioconvergent bond-forming step.

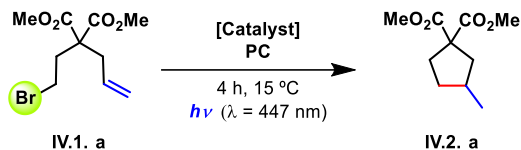
Taking into account the precedents above in $C-C$ bond forming reactions proceeding through carbon centered radicals, and the potential of the [Cu(bathocuproine)(Xantphos)](PF₆) (**PC_{Cu}**) and [M(OTf)(Py₂T^stacn)](OTf) (**I^HM**) as an efficient dual catalyst system towards the activation of Csp^3-Cl bonds under visible-light photocatalysis (see *Chapter III*), we envisioned the construction of carbocycles *via* reductive cyclization reactions of non-activated chloroalkanes.

IV.3. Results and Discussion.

IV.3.1 Visible-Light Photoredox Reductive Cyclization from Non-Activated Alkyl Bromides with Tethered Alkenes.

After demonstrating and then optimizing the conditions for dehalogenation reactions of non-activated alkyl halides as described in the previous chapter, we turned our attention to develop the intramolecular reductive cyclization reactions of alkyl halides (X = Br, Cl) containing tethered alkenes. First, we tested several alkyl bromides that contain two geminal substituents to favour the cyclization step by taking advantage of the *Thorpe-Ingold effect*.⁴⁶ We found that by utilizing dimethyl 2-allyl-2-(2-bromoethyl)malonate as a model substrate, it was cyclized from good to excellent yields when employing I^HCo catalyst in combination with [Cu(bathocuproine)(Xantphos)](PF₆) (PC_{Cu}) as photoredox catalyst (Table IV.1, entry 1), in a water/acetonitrile solvent mixture. In contrast, the formation of the desired product was obtained in low yields with the commercially available cobalt(dimethylglyoxime) ($Co(DMG)PyCl$) and *Vitamin B*₁₂, as well as with cobalt triflate salt (entries 2 to 4). Changing the protic solvent from water to ethanol, we observed a small improvement in the yield up to 87% of the desired cyclic product (entry 5). Pyridine chloride dimethylglyoxime (entry 6) and bis-chloro dimethylglyoxime (entry 8) did not give better results under these conditions. We found that the combination of PC_{Cu} with *in-situ* formed $Co-dtbbpy$ complex gave the product in 77% yield (entry 10). Changing the photoredox catalyst to [Ir(bpy)(ppy)₂](PF₆) (PC_{Ir2}) in combination with [$Co(DMG)PyCl$], [$Co(DMG)Cl_2$] and [$Co-dtbbpy$] yielded the product in 77%, 86% and 88% respectively (entries 7, 9 and 11).

Table IV.1 Catalyst screening for the reductive cyclization of non-activated alkyl bromides.



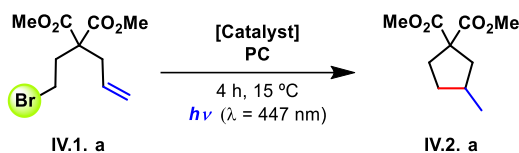
Entry	Catalyst (mol%)	PC (%)	Solvent	Conv. (%)	Yield (%)
1	1^{H}Co (5)	PC_{Cu} (1)	$\text{H}_2\text{O} : \text{MeCN}$ (3:2)	100	84
2	$\text{Co}(\text{OTf})_2(\text{CH}_3\text{CN})_2$ (5)	PC_{Cu} (1)	$\text{H}_2\text{O} : \text{MeCN}$ (3:2)	54	5
3	$\text{Co}(\text{DMG})\text{PyCl}$ (5)	PC_{Cu} (1)	$\text{H}_2\text{O} : \text{MeCN}$ (3:2)	100	13
4	Vitamin B ₁₂ (5)	PC_{Cu} (1)	$\text{H}_2\text{O} : \text{MeCN}$ (3:2)	7	-
5	1^{H}Co (5)	PC_{Cu} (1)	$\text{EtOH} : \text{MeCN}$ (3:2)	100	87
6	$\text{Co}(\text{DMG})\text{PyCl}$ (5)	PC_{Cu} (1)	$\text{EtOH} : \text{MeCN}$ (3:2)	95	5
7	$\text{Co}(\text{DMG})\text{PyCl}$ (5)	PC_{IrI} (1)	$\text{EtOH} : \text{MeCN}$ (3:2)	100	77
8	$\text{Co}(\text{DMG})\text{Cl}_2$ (5)	PC_{Cu} (1)	$\text{EtOH} : \text{MeCN}$ (3:2)	100	11
9	$\text{Co}(\text{DMG})\text{Cl}_2$ (5)	PC_{IrI} (1)	$\text{EtOH} : \text{MeCN}$ (3:2)	100	86
10	Co-dtbbpy (5)	PC_{Cu} (2)	$\text{EtOH} : \text{MeCN}$ (3:2)	87	80
11	Co-dtbbpy (5)	PC_{IrI} (2)	$\text{EtOH} : \text{MeCN}$ (3:2)	100	88

Conditions: 10 mM concentration of substrate, 14.4 eq of Et_3N as ED under visible-light irradiation with blue LEDs (1 W, 447 nm) for 4 h at 15 °C. Conversion and yield were determined by GC using biphenyl as internal standard.

After the short catalyst screening, and selecting 1^{H}Co as the best coordination catalyst, we investigated the effect of the solvent mixture and concentration in the reaction outcome. Although synthetic useful yields were obtained in pure acetonitrile solution (**Table IV.2**, entry 1), the yield improved from 84% to 93% by changing the protic solvent (entries 2 to 5). We observed that the less acidic the protic solvent, the better the yields. Interestingly, the radical cyclization reaction operates in competitive yields in aqueous solutions which corresponds to a non-classical media for this kind of transformations.⁴⁷ Higher or lower concentration gave lower yields (entries 6 to 8). Additionally, blank experiments were carried out in the absence of cobalt catalyst, obtaining low conversions (7%) when we employed only the copper photocatalyst (PC_{Cu}) (entry

9). In contrast, blank experiments with different iridium photocatalysts indicate that these photoredox catalysts are capable of activating the alkyl bromide towards the synthesis of cyclized products from moderate to good yields (entries 10 to 12). Moreover, PC_{Ir4} alone is highly efficient, giving the targeted cyclic product **IV.2.a** in 86% yield (entry 12).

Table IV.2 Screening of conditions for the reductive cyclization of non-activated alkyl bromides.



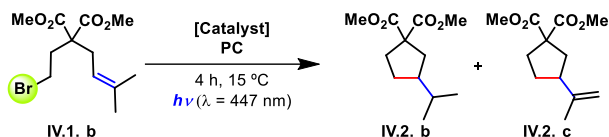
Entry	[] (mM)	Catalyst (mol%)	PC (%)	Solvent	Conv. (%)	Yield (%)
1	10	1^HCo (5)	PC_{Cu} (1)	MeCN	100	67
2	10	1^HCo (5)	PC_{Cu} (1)	H ₂ O : MeCN (3:2)	100	84
3	10	1^HCo (5)	PC_{Cu} (1)	MeOH : MeCN (3:2)	100	83
4	10	1^HCo (5)	PC_{Cu} (1)	EtOH : MeCN (3:2)	100	87
5	10	1^HCo (5)	PC_{Cu} (1)	<i>i</i>PrOH : MeCN (3:2)	100	93
6	8.7	1^HCo (5)	PC_{Cu} (1)	H ₂ O : MeCN (3:2)	100	72
7	15	1^HCo (5)	PC_{Cu} (1)	H ₂ O : MeCN (3:2)	100	54
8	20	1^HCo (5)	PC_{Cu} (1)	H ₂ O : MeCN (3:2)	100	38
9	10	-	PC_{Cu} (1)	EtOH : MeCN (3:2)	14	7
10	10	-	PC_{Ir1} (1)	EtOH : MeCN (3:2)	41	41
11	10	-	PC_{Ir3} (1)	EtOH : MeCN (3:2)	51	51
12	10	-	PC_{Ir4} (1)	EtOH : MeCN (3:2)	100	86

Conditions: 14.4 eq of Et_3N as ED under visible-light irradiation with blue LEDs (1 W, 447 nm) for 4 h at 15 °C. Conversion and yield were determined by GC using biphenyl as internal standard.

The reductive cyclization reactions of alkyl bromide **IV.1.b**, which contains a disubstituted alkene as radical acceptor, which being less activated, is more challenging. Under optimized conditions and only using PC_{Cu} or PC_{Ir} as photoredox catalyst (entries 1 to 4), it provides the cyclized product **IV.2.b** in low yields (20 - 27%). In contrast, the 5-*exo-trig* cyclization reaction occurs with excellent yields

when the reaction is carried out in the presence of both I^HCo and PC_{Cu} . This exemplifies the synergistic merger of both catalysts to achieve more difficult reductive cyclizations. The isolation of the formed products reveals the formation of two different cyclic products (**IV.2.b** and **IV.2.c**) in a 2:1 ratio. The major product is the expected 5-*exo-trig* cyclic product, whereas the minor one contains a terminal olefin in the isopropyl unit.

Table IV.3 Catalyst loading and photocatalyst screening for the cyclization reaction of non-activated alkyl bromides with pendant disubstituted alkenes.



Entry	Catalyst (mol%)	PC (%)	Solvent	Conv. (%)	Yield b/c (%)
1	-	PC _{Cu} (1.5)	EtOH : MeCN (3:2)	8	2/1
2	-	PC _{Ir2} (1.5)	EtOH : MeCN (3:2)	29	20/4
3	-	PC _{Ir3} (1.5)	EtOH : MeCN (3:2)	30	20/4
4	-	PC _{Ir4} (1.5)	EtOH : MeCN (3:2)	41	27/6
5	I^HCo (1.5)	PC_{Cu} (1.5)	EtOH : MeCN (3:2)	100	61/30
6	I^HCo (6)	PC_{Cu} (1.5)	EtOH : MeCN (3:2)	100	66/23

Conditions: 14.4 eq of Et₃N as ED under visible-light irradiation with blue LEDs (1 W, 447 nm) for 4 h at 15 °C. Conversion and yield were determined by GC using biphenyl as internal standard.

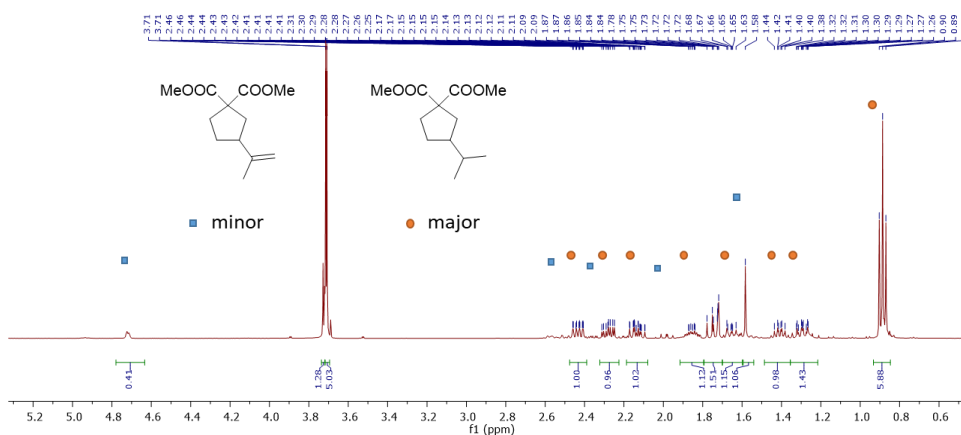


Figure IV.10 1H -NMR spectrum for the mixture of products **IV.2.b** and **IV.2.c** of the 5-*exo-trig* cyclization reaction of alkyl bromide with disubstituted olefin (**IV.1.b**).

Disubstituted alkenes in the designed substrate allow for the formation of a more stabilized tertiary radical species, which can proceed through two different pathways: A) the expected *HAT* to the solvent to generate the mayor *5-exo-trig* cyclic product or B) an alternative *HAT* from the oxidized *ED*^{28,48} or from the organoradical that is formed along the dominant A pathway. Pathway B might explain the formation of the minor the side-product observed (**Figure IV.11**).

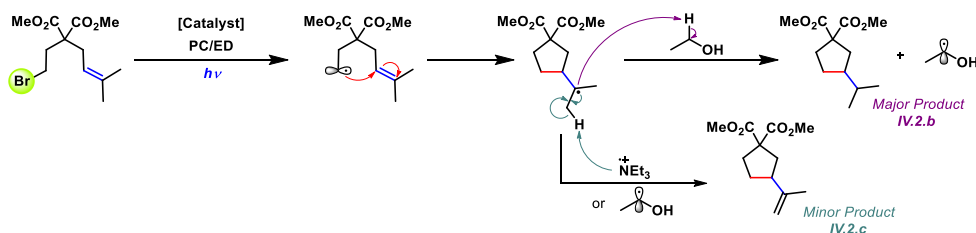


Figure IV.11 Proposed mechanism for the formation of **IV.2.b** and **IV.2.c**.

IV.3.2 Visible-Light Photoredox Reductive Cyclization from Non-Activated Alkyl Chlorides with Tethered Alkenes.

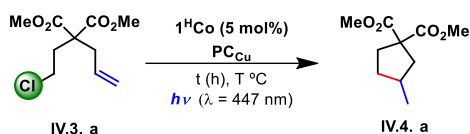
Immediately following the demonstration of our system's capacity to promote reductive cyclization reactions from non-activated alkyl bromides, we explored the analogous reaction with alkyl chlorides. The reduction potential of *n*Bu-Br is tabulated at -2.85 V (vs. SCE in MeCN) whereas the reduction potential of non-activated alkyl chlorides is measured lower than -3 V vs SCE. Previous work from MacMillan group for the metallaphotoredox cross-coupling reaction of carboxylic acids with alkyl halides, showed that the commonly used iridium photoredox catalyst (*PC_{Ir}*) in combination with [*Ni-dtbbpy*] is tolerant to alkyl chlorides (**Table IV.8**).³⁸ The dual catalytic system is able to activate *Csp*³-Br bonds in the presence of *Csp*³-Cl bonds with excellent selectivity, under visible-light irradiation, highlighting the robustness of alkyl chlorides to common photocatalytic conditions.

IV.3.2.1 Screening of the Conditions.

As it was shown in the previous chapter, our dual catalyst system based on first-row transition metals (copper/cobalt or nickel) in combination with an *ED* under

visible-light irradiation, is able to activate Csp^3-Cl bonds of non-activated alkyl chlorides in hydro-dehalogenation reactions. Therefore, we envisioned that our developed bimetallic system I^HCo/PC_{Cu} might also catalyze the cyclization of alkyl chlorides with pendant alkenes, similarly to the alkyl bromides presented in the previous section. To test this hypothesis, we selected dimethyl 2-allyl-2-(2-chloroethyl)malonate as a model substrate, I^HCo as catalyst and PC_{Cu} as photocatalyst in the presence of Et_3N as *ED* in acetonitrile (**Table IV.4**, entry 1). Under these conditions and using water as co-solvent, we observed the consumption of only 27% of the initial substrate after 18 h at 15 °C (entries 1 and 2). The replacement of H_2O by 2-propanol gives better results, reaching 64 % conversion and 63% yield after 30 h at 30 °C (entry 5). Replacement of 2-propanol by ethanol gives up to 83 % yield after one-day of reaction, with almost full conversion (entry 10).

Table IV.4 Initial screening of conditions for the reductive cyclization reaction of non-activated alkyl chlorides.



Entry	PC (%)	Solvent (mL)	T (°C)	t (h)	Conv. (%)	Yield (%)
1	PC _{Cu} (1)	MeCN	15	18	27	21
2	PC _{Cu} (1)	H ₂ O : MeCN (3:2)	15	18	27	14
3	PC _{Cu} (1)	<i>i</i> PrOH : MeCN (3:2)	15	18	52	40
4	PC _{Cu} (1)	MeCN	30	18	34	26
5	PC _{Cu} (1)	<i>i</i> PrOH : MeCN (3:2)	30	18	64	63
6	PC _{Cu} (1)	EtOH : MeCN(3:2)	30	18	73	70
7	PC _{Cu} (2)	MeCN	30	24	27	17
8	PC _{Cu} (2)	H ₂ O : MeCN (3:2)	30	24	67	22
9	PC _{Cu} (2)	<i>i</i> PrOH : MeCN (3:2)	30	24	85	70
10	PC_{Cu} (2)	EtOH : MeCN(3:2)	30	24	96	83

Conditions: 10 mM concentration of substrate with with 5 mol% of I^HCo and 14.4 eq of Et_3N as *ED* under visible-light irradiation with blue LEDs (1 W, 447 nm). Conversion and yield were determined by GC using biphenyl as internal standard.

After the optimization of the protic solvents (i.e. organic alcohols), we investigated the effect of combining ethanol with other solvents. As can be seen in **Table IV.5**, for instance, we found that the combination of *n*-butyronitrile / ethanol also gave excellent results (entry 7).

Table IV.5 Solvent screening for the cyclization reaction of non-activated alkyl chlorides.

Entry	Solvent (mL)	ED (eq.)	Conv. (%)	Yield (%)
1	MeCN	Et ₃ N (14.4)	24	17
2	H ₂ O : MeCN (3:2)	Et ₃ N (14.4)	67	22
3	MeOH : MeCN (3:2)	Et ₃ N (14.4)	39	27
4	<i>i</i> PrOH : MeCN (3:2)	Et ₃ N (14.4)	75	61
5	EtOH : MeCN (3:2)	Et₃N (14.4)	96	83
6	EtOH : MeCN (3:2)	<i>i</i> Pr ₂ NEt (11.4)	93	78
7	EtOH : <i>n</i>-BuCN (3:2)	Et₃N (14.4)	98	85
8	EtOH : <i>i</i> -BuCN (3:2)	Et ₃ N (14.4)	84	74
9	EtOH : <i>t</i> -BuCN (3:2)	Et ₃ N (14.4)	68	58

Conditions: 10 mM concentration of substrate with 5 mol% of I^HCo and 2 mol% of PC_{Cu} under visible-light irradiation with blue LEDs (1 W, 447 nm). Conversion and yield were determined by GC using biphenyl as internal standard.

Then, we screened several photoredox catalysts under optimized conditions (10 mM concentration of substrate with 5 mol% of I^HCo and 14.4 eq. of Et₃N as ED). In general, photocatalysts PC_{Ru} , PC_{Ir1} - PC_{Ir4} (**Table IV.6**, entries 1 to 5) gave rise to lower conversions and yields than PC_{Cu} . Interestingly, the more reducing PC_{IrNMe2} provided comparable results (entry 7). At this point, we also showed that all the components in the reaction were needed for the cyclization to proceed, observing no formation of the product in the absence of photocatalyst (entry 8), catalyst (entry 9), ED (entry 10) or light.

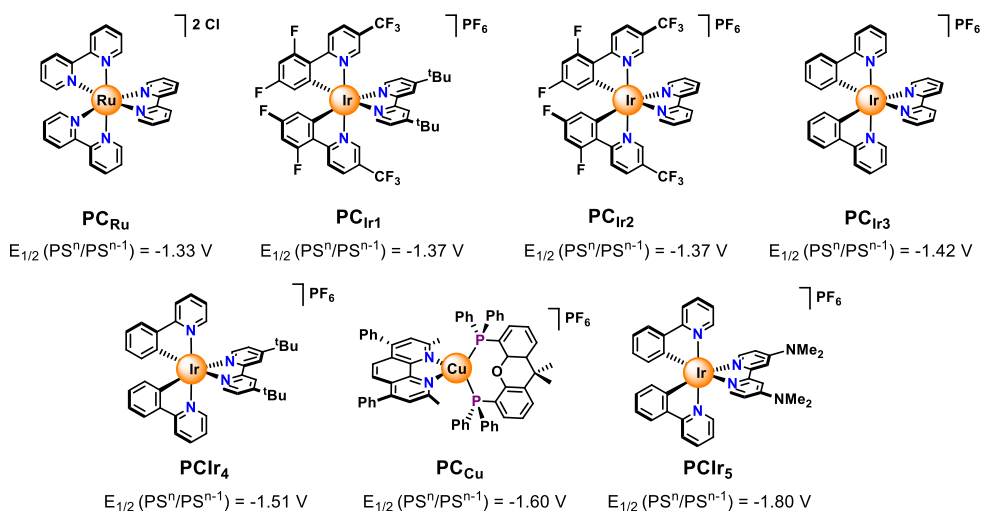


Figure IV.12 Molecular structures of the photocatalysts tested in the screening. Redox potentials in MeCN vs SCE.

Table IV.6 Photoredox catalyst screening for the cyclization of non-activated alkyl chlorides.

Entry	PC	$E_{1/2}$ (PC ⁿ /PC ⁿ⁻¹)*	Conv. (%)	Yield (%)
1	PC _{Ru} (2)	-1.33 ⁴⁹	< 5	< 5
2	PC _{Ir1} (2)	-1.37 ⁵⁰	46	37
3	PC _{Ir2} (2)	-1.37 ⁵¹	63	46
4	PC _{Ir3} (2)	-1.42 ⁵²	17	12
5	PC _{Ir4} (2)	-1.51 ⁵³	45	37
6	PC_{Cu} (2)	-1.69⁵⁴	96	83
7	PC_{Ir5} (2)	-1.80⁵⁵	93	84
8	-	-	< 5	-
9	PC _{Cu} (2) ^a	-1.69	< 5	-
10	PC _{Cu} (2) ^b	-1.69	-	-

Conditions: 10 mM concentration of substrate with 14.4 eq. of Et₃N as ED 5 mol% of ¹HCo and 2 mol% of PC under visible-light irradiation with blue LEDs (1 W, 447 nm). Conversion and yield were determined by GC using biphenyl as internal standard. *V vs SCE in MeCN. a) Reaction carried out in absence of ¹HCo. b) Reaction carried out in absence of ED.

Then, we questioned whether the photocatalytic cleavage of Csp³-Cl bonds under mild conditions could be accomplished with similar cobalt or even nickel

coordination complexes and if we could determine the key structural ligand design principles. To this end, we examined the catalytic activity of a broad family of cobalt and nickel complexes with different coordination motifs and electronic features (**Table IV.7**). Strikingly, the analogous nickel complex ($I^H Ni$) in combination with iPr_2NEt yielded the desired cyclic product in 96 % yield (entry 2). In this regard, we examined a variety of cobalt and nickel complexes bearing different coordination motifs for the reductive cyclization of **IV.3.a** under visible-light irradiation.

In general terms, among the complexes bearing a triazacyclononane scaffold, pentacoordinate cobalt complexes $I^X Co$ ($X = H, DMM, CO_2Et$) showed higher catalytic activity on the cyclization reaction of **IV.3.a** than the tetracoordinate $2^X Co$ (70-98 % yield (entries 1, 6 and 8) vs. 18-41% (entries 14 to 16), respectively) and the tricoordinate $3Co$ (36 % of yield, entry 42). Furthermore, tuning the electronic effects on the ligand had a more significant impact on the reactivity for $I^X Ni$ (varying from 52 to 96 %, entries 2, 7 and 9) than for $I^X Co$. In addition, other pentacoordinate cobalt and nickel complexes, such as $M-N4Py$ and $M-DPA$, showed moderate and good reactivity (entries 10 to 13), this last one being a good candidate for further exploration in this type of transformation (**Figure IV.13**).

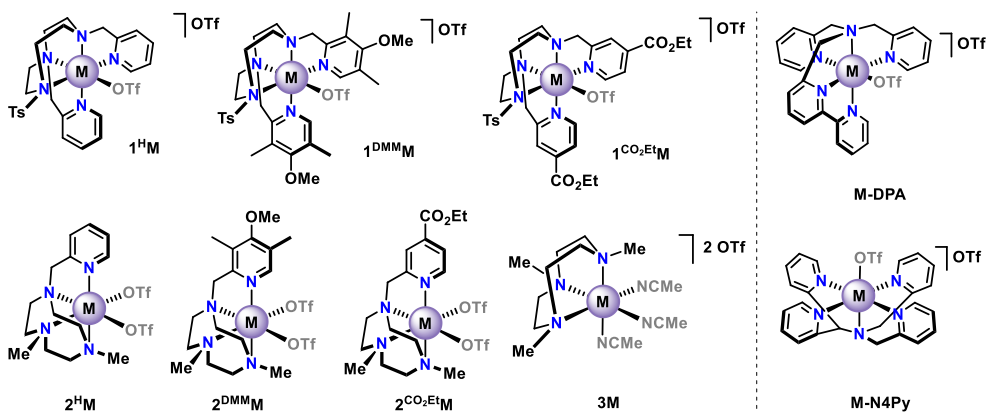


Figure IV.13 Molecular structure of triazacyclononane based catalysts ($I^X M$, $2^X M$ and $3M$), $M-DPA$ and $M-N4Py$ catalysts.

Moving to tetracoordinate complexes, complexes $M^X MCP$ (entries 17 to 24) and $M^X PDP$ (entries 25 to 31), supported by $2N_{\text{aliphatic}}2N_{\text{pyridine}}$ ligands, showed moderate reactivity (55-68%), and similar to the $Ni-TPA$ (54 %, entry 34) (**Figure IV.14**). However, the analogous cobalt complex $Co-TPA$ was not efficient for the reductive cyclization of **IV.3.a**, affording **IV.4.a** in only 16 % of yield (entry 32).

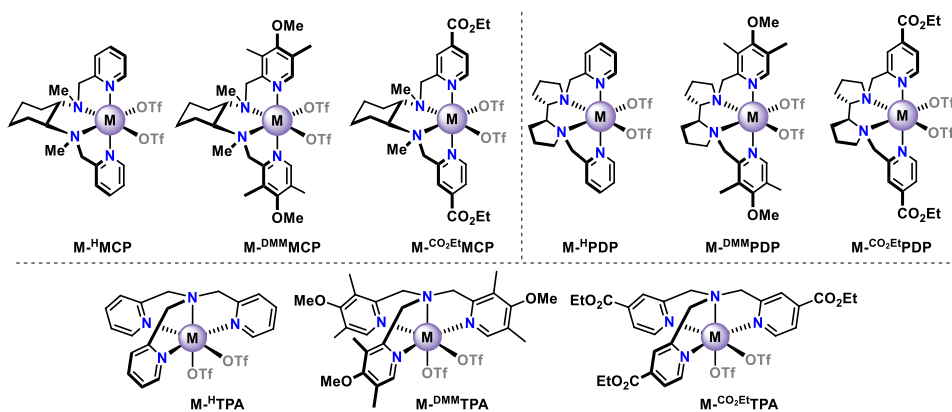


Figure IV.14 Molecular structure of $M^X MCP$, $M^X PDP$ and $M^X TPA$ catalysts. ‡ Complexes synthesis performed in collaboration with Jordi Aragon.

We also explored a variety of tetracoordinate square-planar cobalt and nickel complexes. These complexes were previously employed for the reduction of alkyl halides under chemical and electrochemical reducing conditions (**Figure IV.15**).⁵⁶⁻⁵⁹ Among complexes $M-Cyclam$ (entries 40 and 41), $M-TPP$ (entries 49 to 52) and $M-Salem$ (entries 53 and 54), only cobalt porphyrin $Co-TPP$ and $Ni-Cyclam$ afforded **IV.4.a** in remarkably good yields, 80 % and 82 % respectively. Finally, the combination of terpyridine or 4,4'-di-*tert*-butyl-2,2'-dipyridyl (*dtbbpy*) ligands with cobalt and nickel salts under optimized reaction conditions gave **IV.4.a** in low yields (<12 %, excluding $Co-Terpy$ that afforded **IV.4.a** with 42 % yield, entries 55 to 58). Commercially available Cobalt dimethylglyoxime ($Co-DMG$) afforded product **IV.4.a** with a 6% yield (entry 48) under visible-light photocatalysis, whereas natural cobalamin *Vitamin B₁₂* gave irreproducible results. Finally, only traces of the desired cyclic product were obtained by using the simple cobalt or nickel triflate salts (entries 61 and 62).

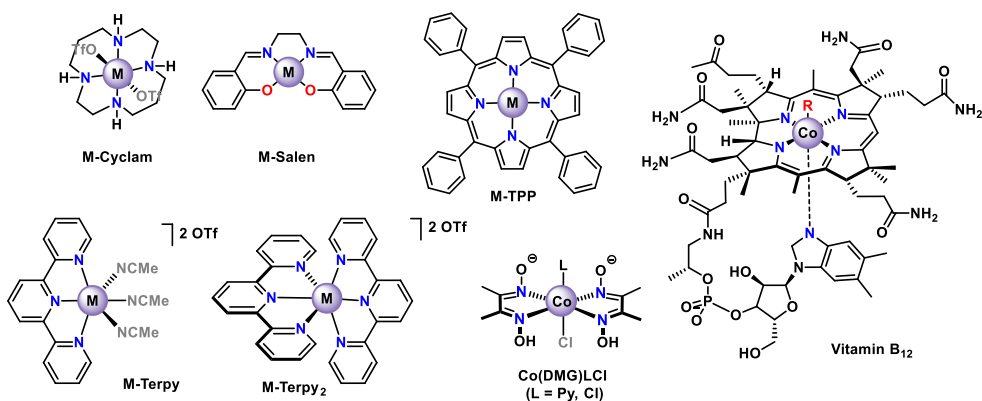
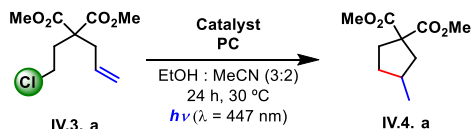


Figure IV.15 Molecular structure of *M*-Cyclam, *M*-Salen, *M*-TPP, *M*-Terpy, *M*-Terpy₂, Co(DMG)LCl (L = Py, Cl) and Vitamin B₁₂ catalysts.

This series of experiments showed that photogenerated low-valent octahedral cobalt and nickel complexes with tetra- and pentacoordinate nitrogen ligands are potential candidates to develop synthetic methodologies for the functionalization of strong Csp^3-Cl bonds under visible-light photoredox catalysis.

Table IV.7 Catalyst screening for the reductive cyclization of non-activated alkyl chlorides.



Entry	Catalyst (mol%)	PC (%)	ED (eq.)	Conv. (%) ^a	Yield (%) ^a
1	1^HCo (5)	PC _{Cu} (2)	Et ₃ N (14.4)	96	83
2	1^HNi (5)	PC _{Cu} (2)	<i>i</i> Pr ₂ NEt (11.4)	99	96
3	1 ^H Ni (5) ^b	PC _{Cu} (2)	<i>i</i> Pr ₂ NEt (11.4)	100	91
4	1 ^H Ni (5) ^c	PC _{Cu} (2)	<i>i</i> Pr ₂ NEt (11.4)	100	90
5	1 ^H Co (10)	PC _{Cu} (2)	Et ₃ N (14.4)	84	80
6	1 ^{DMM} Co (5)	PC _{Cu} (2)	Et ₃ N (14.4)	87	80
7	1 ^{DMM} Ni (5)	PC _{Cu} (2)	<i>i</i> Pr ₂ NEt (11.4)	70	52
8	1 ^{CO₂Et} Co (5)	PC _{Cu} (2)	Et ₃ N (14.4)	83	70
9	1 ^{CO₂Et} Ni (5) ^b	PC _{Cu} (2)	<i>i</i> Pr ₂ NEt (11.4)	73	63
10	Co-N4Py (5)	PC _{Cu} (2)	Et ₃ N (14.4)	43	36

Entry	Catalyst (mol%)	PC (%)	ED (eq.)	Conv. (%) ^a	Yield (%) ^a
11	Ni-N4Py (5)	PC _{Cu} (2)	<i>i</i> Pr ₂ NEt (11.4)	73	33
12	Co-DPA (5)	PC _{Cu} (2)	Et ₃ N (14.4)	97	89
13	Ni-DPA (5)	PC _{Cu} (2)	<i>i</i> Pr ₂ NEt (11.4)	96	91
14	² HCo (5)	PC _{Cu} (2)	Et ₃ N (14.4)	42	30
15	² DMMCo (5)	PC _{Cu} (2)	Et ₃ N (14.4)	22	18
16	² CO ₂ EtCo (5)	PC _{Cu} (2)	Et ₃ N (14.4)	50	41
17	Co- ^H MCP_OTf ₂ (5)	PC _{Cu} (2)	Et ₃ N (14.4)	71	68
18	Co- ^H MCP_Cl ₂ (5)	PC _{Cu} (2)	Et ₃ N (14.4)	71	64
19	Ni- ^H MCP_OTf ₂ (5) ^b	PC _{Cu} (2)	<i>i</i> Pr ₂ NEt (11.4)	90	55
20	Ni- ^H MCP_Cl ₂ (5)	PC _{Cu} (2)	<i>i</i> Pr ₂ NEt (11.4)	95	48
21	Co- ^{DMM} MCP_Cl ₂ (5)	PC _{Cu} (2)	<i>i</i> Pr ₂ NEt (11.4)	36	31
22	Ni- ^{DMM} MCP_Cl ₂ (5)	PC _{Cu} (2)	<i>i</i> Pr ₂ NEt (11.4)	100	75
23	Co- ^{CO₂Et} MCP_Cl ₂ (5)	PC _{Cu} (2)	<i>i</i> Pr ₂ NEt (11.4)	96	71
24	Ni- ^{CO₂Et} MCP_Cl ₂ (5)	PC _{Cu} (2)	<i>i</i> Pr ₂ NEt (11.4)	91	69
25	Co- ^H PDP_OTf ₂ (5)	PC _{Cu} (2)	Et ₃ N (14.4)	67	60
26	Ni- ^H PDP_OTf ₂ (5) ^b	PC _{Cu} (2)	<i>i</i> Pr ₂ NEt (11.4)	94	68
27	Ni- ^H PDP_Cl ₂ (5)	PC _{Cu} (2)	<i>i</i> Pr ₂ NEt (11.4)	96	32
28	Co- ^{DMM} PDP_OTf ₂ (5)	PC _{Cu} (2)	<i>i</i> Pr ₂ NEt (11.4)	36	31
29	Ni- ^{DMM} PDP_OTf ₂ (5)	PC _{Cu} (2)	<i>i</i> Pr ₂ NEt (11.4)	100	75
30	Co- ^{CO₂Et} PDP_OTf ₂ (5)	PC _{Cu} (2)	<i>i</i> Pr ₂ NEt (11.4)	96	71
31	Ni- ^{CO₂Et} PDP_OTf ₂ (5)	PC _{Cu} (2)	<i>i</i> Pr ₂ NEt (11.4)	91	69
32	Co- ^H TPA_OTf ₂ (5)	PC _{Cu} (2)	Et ₃ N (14.4)	15	16
33	Co- ^H TPA_Cl ₂ (5)	PC _{Cu} (2)	Et ₃ N (14.4)	13	11
34	Ni- ^H TPA_OTf ₂ (5) ^b	PC _{Cu} (2)	<i>i</i> Pr ₂ NEt (11.4)	96	54
35	Ni- ^H TPA_Cl ₂ (5)	PC _{Cu} (2)	<i>i</i> Pr ₂ NEt (11.4)	96	54
36	Co- ^{DMM} TPA_Cl ₂ (5)	PC _{Cu} (2)	<i>i</i> Pr ₂ NEt (11.4)	66	56
37	Ni- ^{DMM} TPA_Cl ₂ (5)	PC _{Cu} (2)	<i>i</i> Pr ₂ NEt (11.4)	83	66
38	Co- ^{CO₂Et} TPA_Cl ₂ (5)	PC _{Cu} (2)	<i>i</i> Pr ₂ NEt (11.4)	42	21
39	Ni- ^{CO₂Et} TPA_Cl ₂ (5)	PC _{Cu} (2)	<i>i</i> Pr ₂ NEt (11.4)	29	14

Entry	Catalyst (mol%)	PC (%)	ED (eq.)	Conv. (%) ^a	Yield (%) ^a
40	Co-Cyclam (5)	PC _{Cu} (2)	Et ₃ N (14.4)	18	10
41	Ni-Cyclam (5)	PC _{Cu} (2)	<i>i</i> Pr ₂ NEt (11.4)	100	82
42	3Co (5) ^b	PC _{Cu} (2)	Et ₃ N (14.4)	48	36
43	3Ni (5) ^b	PC _{Cu} (2)	<i>i</i> Pr ₂ NEt (11.4)	19	2
44	Co-dtbbpy (5)	PC _{Cu} (2)	Et ₃ N (14.4)	21	10
45	Co-dtbbpy (5)	PC _{Ir2} (2)	Et ₃ N (14.4)	38	13
46	Ni-dtbbpy (5)	PC _{Cu} (2)	Et ₃ N (14.4)	13	3
47	Ni-dtbbpy (5)	PC _{Ir2} (2)	Et ₃ N (14.4)	11	4
48	Co-DMG (5)	PC _{Cu} (2)	Et ₃ N (14.4)	7	6
49	Co-TPP (5)	PC _{Cu} (2)	Et ₃ N (14.4)	100	74
50	Co-TPP (5)	PC _{Cu} (2)	<i>i</i> Pr ₂ NEt (11.4)	100	80
51	Ni-TPP (5)	PC _{Cu} (2)	Et ₃ N (14.4)	13	7
52	Ni-TPP (5)	PC _{Cu} (2)	<i>i</i> Pr ₂ NEt (11.4)	30	19
53	Co-Salen (5)	PC _{Cu} (2)	Et ₃ N (14.4)	33	12
54	Ni-Salen (5)	PC _{Cu} (2)	<i>i</i> Pr ₂ NEt (11.4)	20	10
55	Co-Terpy (5) ^b	PC _{Cu} (2)	Et ₃ N (14.4)	57	42
56	Ni-Terpy (5) ^b	PC _{Cu} (2)	<i>i</i> Pr ₂ NEt (11.4)	29	12
57	Co-Terpy ₂ (5) ^d	PC _{Cu} (2)	Et ₃ N (14.4)	57	42
58	Ni-Terpy ₂ (5) ^d	PC _{Cu} (2)	<i>i</i> Pr ₂ NEt (11.4)	29	12
59	Ni-Cod ₂ (5)	PC _{Cu} (2)	<i>i</i> Pr ₂ NEt (11.4)	19	5
60	Ni-Cod ₂ (5) ^e	PC _{Cu} (2)	<i>i</i> Pr ₂ NEt (11.4)	26	13
61	Co(OTf) ₂ (MeCN) ₂ (5)	PC _{Cu} (2)	Et ₃ N (14.4)	7	5
62	Ni(OTf) ₂ (MeCN) ₂ (5)	PC _{Cu} (2)	Et ₃ N (14.4)	8	1
63	--	PC _{Cu} (2)	Et ₃ N (14.4)	10	1
64	¹ HCo (5)	--	Et ₃ N (14.4)	-	-
65	¹ HNi (5)	--	Et ₃ N (14.4)	-	-
66	¹ HCo (5)	PC _{Cu} (2)	--	-	-
67	¹ HNi (5)	PC _{Cu} (2)	--	2	2
68	¹ HNi (5) ^f	--	<i>i</i> Pr ₂ NEt (11.4)	20	14

Entry	Catalyst (mol%)	PC (%)	ED (eq.)	Conv. (%) ^a	Yield (%) ^a
69	$I^H\text{Ni}$ (5) ^g	--	<i>i</i> Pr ₂ NEt (11.4)	7	-
70	$I^H\text{Ni}$ (5) ^h	--	<i>i</i> Pr ₂ NEt (11.4)	15	-
71	$I^H\text{Ni}$ (5) ⁱ	--	<i>i</i> Pr ₂ NEt (11.4)	13	-

Conditions: 10 mM concentration of substrate under visible-light irradiation with blue LEDs (1 W, 447 nm). a) Conversion and yield were determined by GC using biphenyl as internal standard. b) Complex formed in situ by reacting equimolar amounts of ligand and the triflate metal salt. c) Reactions were carried out in presence of 500 eq. of mercury. d) Complex formed in situ by reacting two equivalents of the ligand with one equivalent of the triflate metal salt. e) Reactions were carried out with one equivalent of the ^HPy₂ta₂n ligand. f) Reactions were carried out using two equivalents of zinc as reductant in presence of light. g) Reactions were carried out using two equivalents of zinc as reductant in absence of light. h) Reactions were carried out using two equivalents of manganese as reductant in presence of light. i) Reactions were carried out using two equivalents of manganese as reductant in absence of light.

Finally, the use of zinc or manganese as reductants as an alternative to the photoredox catalyst and *ED* was attempted, but it did not yield the targeted product **IV.4.a** (entries 68 to 71). Reactivity through reduced metal nanoparticles was discarded due to the poor results obtained when *Ni(COD)*₂ was used as catalyst (in presence or absence of ligand *LI*^H under photocatalytic conditions, entries 59 and 60) and the negative result of the mercury poisoning test (entry 4). Experiments shown in **Table IV.7** indicate that 4 and 5 coordinative cobalt and nickel complexes bearing basic *N-based* ligands are remarkably active catalysts for the activation of *C*_{sp³}-*Cl* bonds.

IV.3.2. 2 Single-Point Monitoring and Selectivity Studies.

At this point, we performed single-point monitoring reactions with the best catalysts resulting from the previous catalyst screening, *I*^H*Co* and *I*^H*Ni*. From these experiments, we observed faster kinetics with nickel catalyst *I*^H*Ni* than with the analogous *I*^H*Co* (**Figure IV.16**), which is then translated in higher yields. We also observed approximately 80% yield of the cyclic product after two hours with both Ni and Co catalysts. However, in order to reach full conversion, we need to irradiate

the sample for 24 h. This is most probably because the catalyst deactivation during the reaction advance due to the formation of Cl^- .

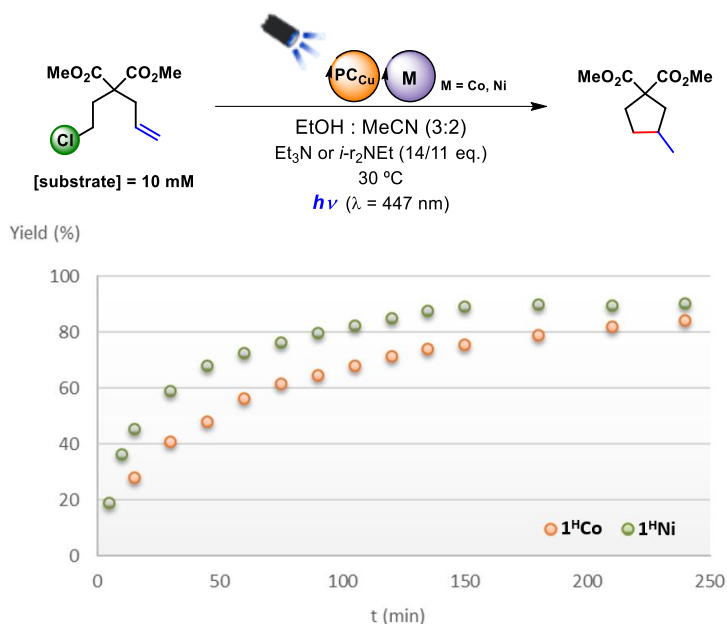


Figure IV.16 Single-point monitoring experiments of the reductive cyclization of **IV.3.a**.

Furthermore, a single-point monitoring experiment of the catalytic reduction of **IV.3.a** throughout light-dark cycles indicates that the catalytic reaction is light-mediated as the reaction does not proceed when the sample is not irradiated, and it is immediately restarted upon light exposure (**Figure IV.17**).

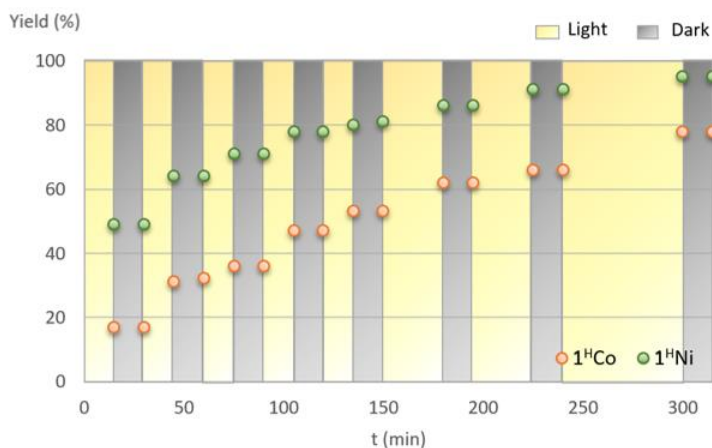


Figure IV.17 Single-point monitoring experiment throughout light-dark cycles.

Single-point monitoring experiments of competition between alkyl chlorides and bromides reveal that the activation of the alkyl chlorides starts just after the complete consumption of the alkyl bromide derivative. Under optimized conditions, full consumption of the alkyl bromide is obtained after ten minutes of reaction, point where the reaction of the alkyl chloride starts (Figure IV.18 top). For the competition experiments between alkyl bromides and chlorides, we employed methyl and ethyl malonates, respectively, in order to monitor the product formation by GC analysis. Control experiments with both methyl and ethyl bromo and chloro malonate substrates were done in order to discard kinetic issues related to the malonate scaffold (Figure IV.18 bottom), observing in both cases similar kinetics.

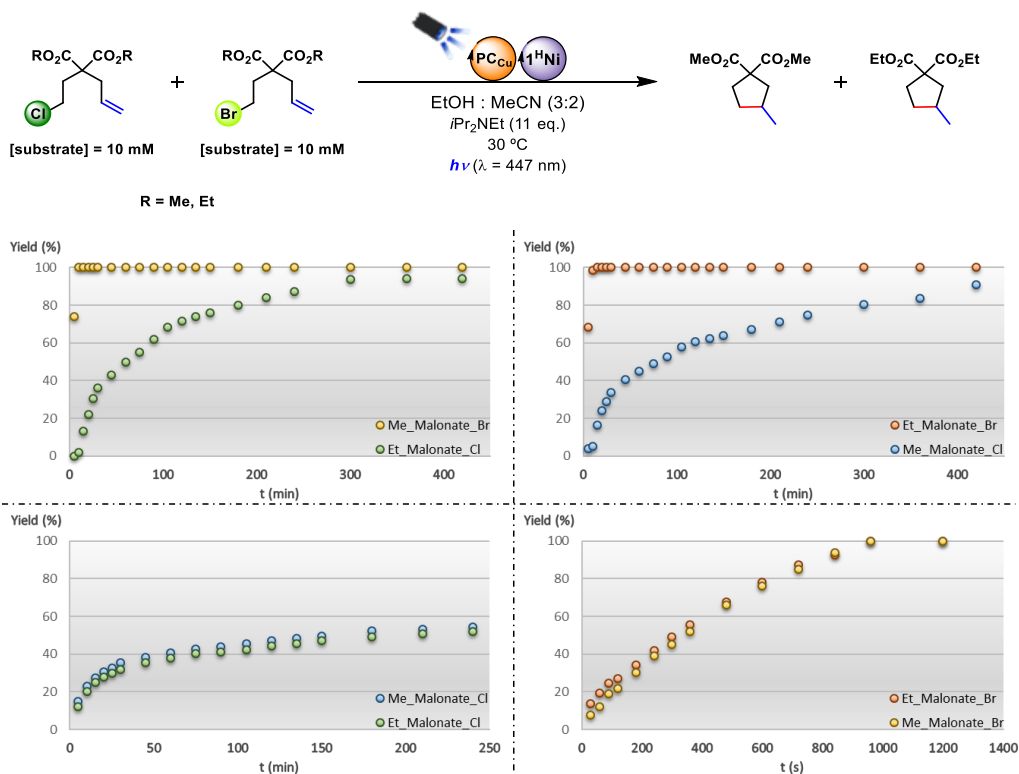


Figure IV.18 Single-point monitoring experiment of bromine/chlorine selectivity. Subsequent reaction of alkyl-chloride substrates after alkyl-bromide substrates (top) and concurrently reaction of methyl and ethyl malonate derivatives in alkyl chloride substrates (bottom left) and alkyl bromide substrates (bottom right).

IV.3.2. 3 Hydrogen formation as a Side Reaction.

Aminopyridine cobalt complexes are well-known active catalysts for hydrogen formation in neutral aqueous conditions^{60,61} due to their stability toward hydrolysis. In 2014, our group published an elegant photo- and electrocatalytic hydrogen production method by first-row transition metal complexes based on pentacoordinated triazacyclononane (*^HPy₂tacn*) ligand. Mechanistic investigations revealed the formation of a key low-valent cobalt intermediate, which is then protonated forming a transient Co^{III}-H species before the formation of the molecular hydrogen. In the case of nickel derivatives, the protonation of the postulated low-valent nickel intermediate is not favoured and, as consequence, the formation of hydrogen is not observed. We considered that hydrogen generation could be an important side reaction that competes with the *Csp³-Cl* bond cleavage step in protic solvents during the developed cyclization reaction. For that reason, monitoring of the hydrogen evolution reaction was carried out under optimized conditions. In the case of employing cobalt complex *I^HCo*, considerable amounts of hydrogen were measured with and without adding the substrate **IV.3.a** (**Figure IV.19**). The addition of substrate **IV.3.a** decreases the rate of H₂ formation since the Co complex is also catalyzing the *Csp³-Cl* bond cleavage reaction. In contrast, H₂ monitoring experiments indicate that *I^HNi* is not able to catalyze proton reduction towards H₂ formation under photocatalytic conditions. The observation that *I^HCo* catalyzes H₂ formation in contrast to *I^HNi* might help to explain the higher efficiency of nickel towards the developed reductive cyclization reactions (**Figure IV.19**).

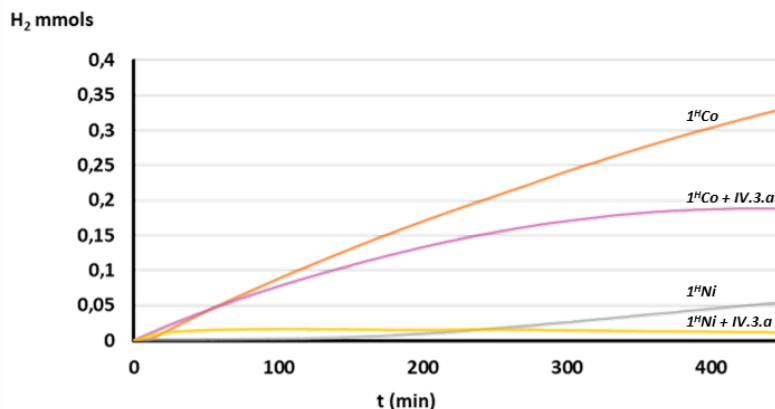


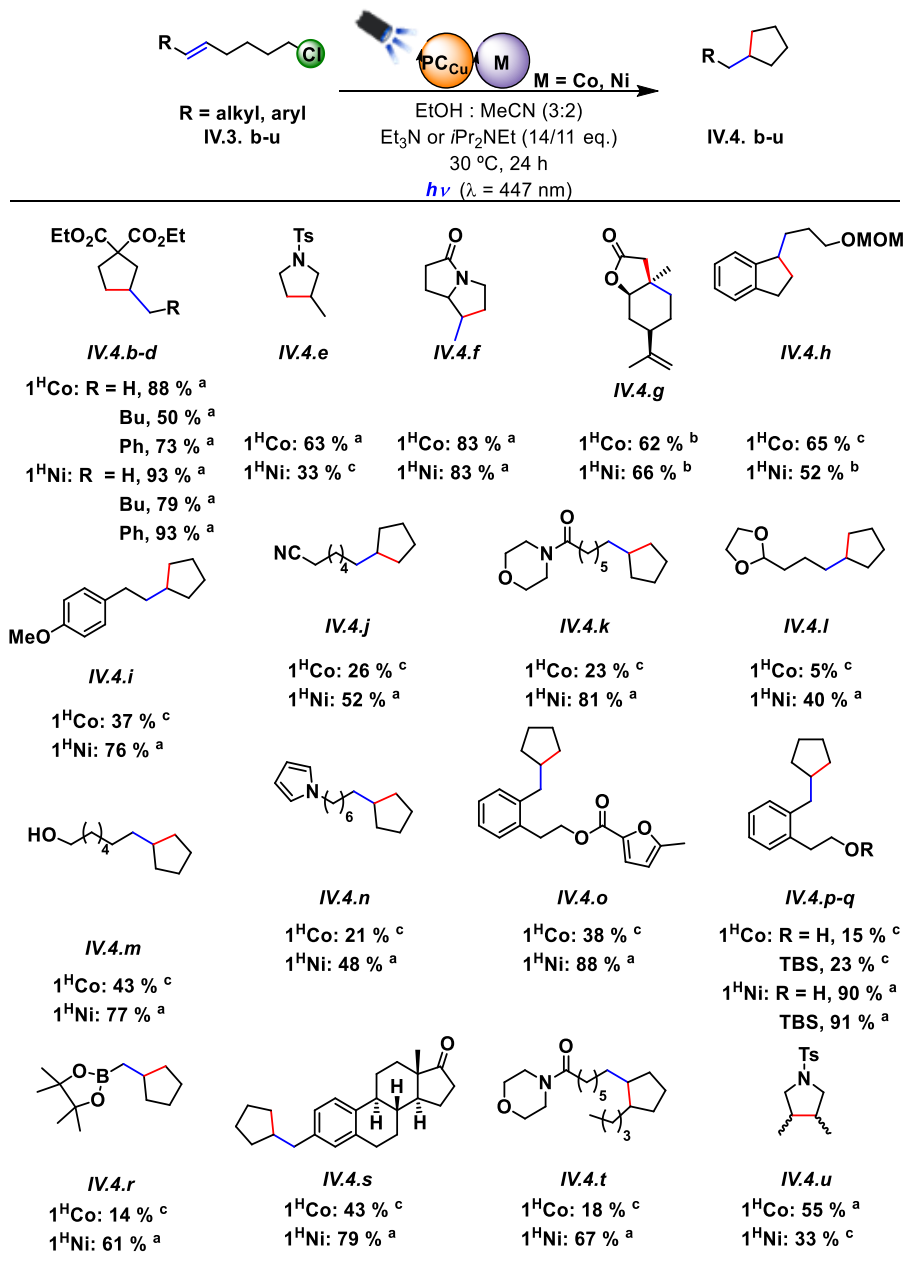
Figure IV.19 Hydrogen evolution monitoring in the optimized conditions for the cyclization reaction of substrate IV.3.a.

IV.3.2. 4 Substrate Scope.

Owing to the excellent catalytic performance of $I^H M$ ($M = \text{Co}, \text{Ni}$) complexes in combination with PC_{Cu} , we decided to further explore the synthetic potential of our photocatalytic protocol for reductive cyclization reactions. First, we investigated the dual $PC_{Cu}/I^H Co$ catalytic system and the functionalization of different diethyl malonates, bearing either a tethered terminal olefin (IV.3.b) or an internal olefin with alkyl (IV.3.c) or phenyl substituents (IV.3.d) (see Table IV.8). The desired five-membered carbocyclic products from these substrates were obtained in moderate to good yields ranging from 50% to 88%. Then, we turned our attention towards the formation of heterocycles such as pyrrolidine and [5,5] pyrrolizidinone affording the desired cycles IV.4.e and IV.4.f in 63 and 83% yield respectively. Similarly, a [5,6] (*R*)-carveol derivative IV.4.g was obtained with 62% yield (over 2 steps) by applying our dual catalytic system. Encouraged by these results, we then investigated whether this protocol allowed direct access of carbocyclic structures starting from linear alkyl chlorides. However, the low conversions and low yields were obtained with linear substrates is a limitation for the $PC_{Cu}/I^H Co$ catalytic system. This limitation could be explained as due to the simultaneous formation of H_2 as a side reaction. As it was explained in the previous section, nickel is not capable of catalyzing H_2 formation, and the whole catalyst

loading is required for enabling the Csp^3-Cl bond activation reaction. Indeed, the combination of PCu and this nickel catalyst drastically enhanced the conversion of alkyl chlorides into the five-membered cyclic product. Starting from diethyl malonate derivatives the corresponding cyclic products could be obtained in yields ranging from 79-93%, and we also obtained bicyclic structures **IV.4.f** and **IV.4.g** in 83% and 66% (over two steps) yields respectively. The superior catalytic activity of complex $I^H Ni$ is evidenced by the preparation of indane structure **IV.4.h** that is obtained in 52% isolated yield, an example where catalyst $I^H Co$ is not a competent catalyst. Remarkably, the bimetallic $PCu/I^H Ni$ catalytic system allowed the cyclization reaction of several linear hex-5-enyl chlorides with synthetically useful yields and exhibiting various degrees of complexity as well as different functional groups. The mildness of the reaction conditions enables a broad functional group tolerance, which illustrates a high degree of chemoselectivity. Interestingly, this photocatalytic protocol is compatible with alkyl chlorides bearing esters (**IV.4.b-d**, **IV.4.g**, **IV.4.o**), alkenes (**IV.4.g**), nitriles (**IV.4.j**), carbamates (**IV.4.f**, **IV.4.k**, **IV.4.t**), ketones (**IV.4.s**), a variety of common alcohol protecting groups (MOM (**IV.4.h**), TBS (**IV.4.q**) as well as free alcohols (**IV.4.m**, **IV.4.p**) and dioxolanes (**IV.4.l**). Alkylboronates (**IV.4.r**), which can be further manipulated, are also tolerated, which enhances the synthetic utility of this transformation. The compatibility of heteroaromatics is showcased by alkyl chlorides containing pyrrole (**IV.4.n**) and furan (**IV.4.o**) groups. Furthermore, substrates **IV.3.t** and **IV.3.s**, which contain a secondary alkyl chloride with a tethered alkene can also be functionalized under optimized reaction conditions yielding the corresponding cyclic products **IV.4.t** at 67% yield. Finally, **IV.4.u** could be obtained with the $PCu/I^H Co$ pair at 55% yield showing the possibility of the use of secondary alkyl chlorides also with cobalt. In contrast, *N*-tosyl pyrrolidine was formed in low yields with the pair $PCu/I^H Ni$ system (33% of yield) due to the activation of the *N-S* bond by the nucleophilic nickel catalyst.

Table IV.8 Substrate scope of the cyclization of non-activated alkyl chlorides with tethered alkenes.

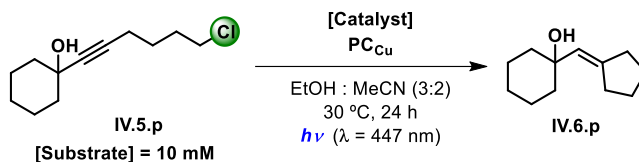


Standard conditions: substrate (10 mM), PCu (2 mol%), ^1HCo or ^1HNi catalyst (5 mol%), ED [Et_3N (14.4 eq.) or $i\text{Pr}_2\text{NEt}$ (11.4 eq.)], $\text{EtOH}:\text{MeCN}$ (3:2), visible-light irradiation with blue LEDs ($\lambda = 447 \text{ nm}$) at 30°C for 24 h. a) Isolated yield. b) Isolated yield over two steps. c) The yield was determined by GC using biphenyl as internal standard.

IV.3.3 Visible-Light Photoredox Reductive Cyclization from Non-Activated Alkyl Chlorides with Tethered Alkynes.

At this point, we decided to expand the scope of the visible-light photoredox cyclization reactions to include chloroalkynes bearing a pendant triple bond. In this case, the obtained alkene product offers the possibility for further functionalizations through a variety of reactions at the C=C bond. To begin this study, we selected substrate **IV.5.p** as model substrate due to its ease of synthesis. The optimized conditions for the previous section gave us 51 % yield for the desired cyclic product (**Table IV.9**, entry 1), a result that enhances by 10% just by doubling the amount of nickel catalyst (entry 2). The increase in the amount of PC_{Cu} , *ED* or temperature did not produce significant improvement (entries 3 to 6).

Table IV.9 Screening of the conditions for the cyclization of non-activated alkyl chlorides been tethered alkynes.



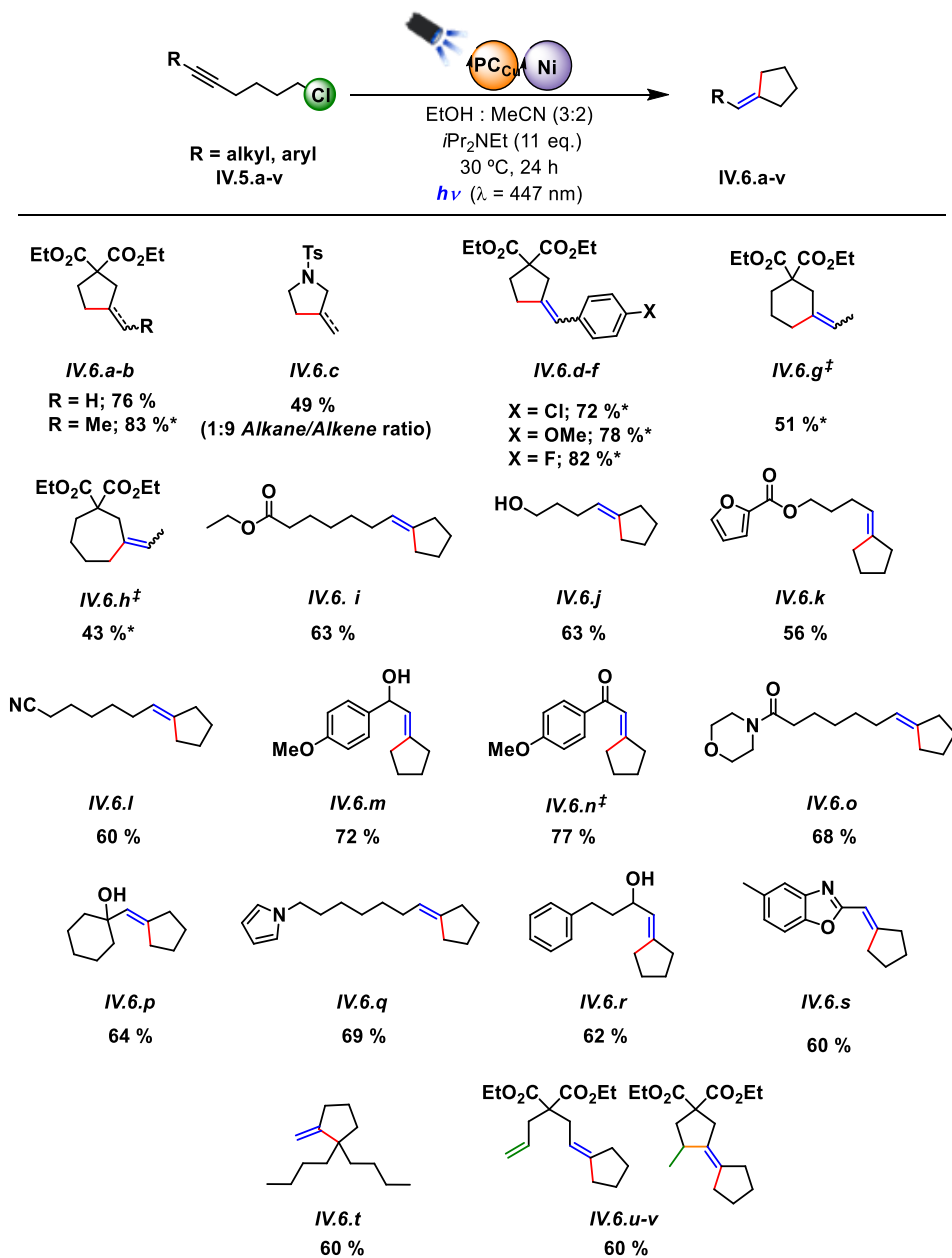
Entry	Catalyst (mol%)	PC (%)	T (°C)	ED (eq.)	Conv. (%)	Yield (%)
1	$1^H Ni$ (5)	PC_{Cu} (2)	30	<i>iPr</i> ₂ NEt (11.4)	89	51
2	$1^H Ni$ (10)	PC_{Cu} (2)	30	<i>iPr</i> ₂ NEt (11.4)	100	61
3	$1^H Ni$ (10)	PC_{Cu} (4)	30	<i>iPr</i> ₂ NEt (11.4)	100	65
4	$1^H Ni$ (10)	PC_{Cu} (4)	30	<i>iPr</i> ₂ NEt (22.8)	100	62
5	$1^H Ni$ (5)	PC_{Cu} (2)	50	<i>iPr</i> ₂ NEt (11.4)	100	65
6	$1^H Ni$ (10)	PC_{Cu} (4)	50	<i>iPr</i>₂NEt (22.8)	100	67

Conditions: 10 mM concentration of substrate under visible-light irradiation with blue LEDs (1 W, 447 nm). Conversion and yield were determined by GC using biphenyl as internal standard.

Having determined the optimal conditions, we reacted several internal and terminal alkynes with different functionalities under those conditions (**Table IV.10**). Again, *Thorpe-Ingold* effect containing substrates worked nicely for the 5-*exo-dig*

cyclization reaction for terminal **IV.6.a** (with a 1:9 ratio of the alkane to alkene products) and internal alkynes (**IV.6.b-IV.6.d-f**). Different size rings were also tested obtaining lower but synthetically useful yields for the formation of 6 and 7 membered rings (**IV.6.g, IV.6.h**). Likewise, the bimetallic $PCu/I^H Ni$ catalyst system allowed the cyclization of several linear hex-5-ynyl chlorides with remarkable yields and a broad functional group tolerance such as esters (**IV.6.i**), nitriles (**IV.6.l**), carbamates (**IV.6.o**), aromatic ketones (**IV.6.n**), alcohol protecting groups (**IV.6.k**), propargylic (**IV.6.m, IV.6.p** and **IV.6.r**), and neutral free alcohols (**IV.6.j**). Heteroaromatics as pyrrole (**IV.6.q**) and benzoxazole (**IV.6.s**) and tertiary alkyl chlorides (**IV.6.v**) are also tolerated with synthetically useful yields. Attempts towards the *5-endo-dig* cyclization were also carried out, and they gave almost full conversion towards the proto-dehalogenated product together with traces of the desired cyclic product. Radical chain sustainable substrates (**IV.5.u**) were also tested under the optimized conditions obtaining mixtures of *mono* and *bicycle* products in a ratio 2/1. The proposal of free radical intermediates during the reaction might explain the 1:1 mixture of the *E/Z* olefin products in substrates **IV.5.b, IV.5.d-h**.

Table IV.10 Substrate scope of the cyclization of non-activated alkyl chlorides with tethered alkynes.

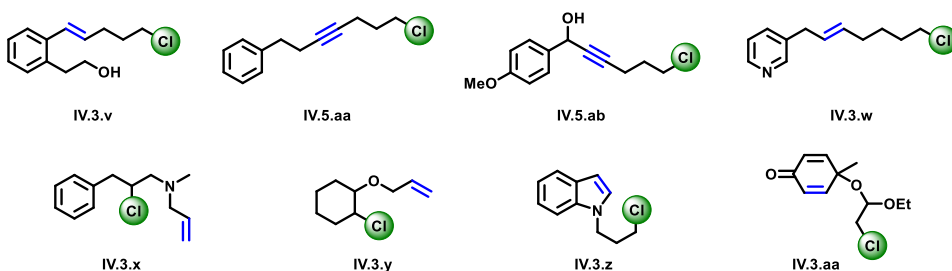


Standard conditions: substrate (10 mM), PCu (2 mol%), ¹HNi catalyst (10 mol%), 11.4 eq. of *i*Pr₂NEt as ED, EtOH:MeCN (3:2), under visible-light irradiation with blue LEDs (λ = 447 nm) at 30 °C for 24 h. All are isolated yields averages of at least 3 reactions. * 1/1 mixture of E/Z isomers. ‡ Substrates performed in collaboration with Jordi Aragon.

IV.3. 4 Unsuccessful Substrates.

Although there is broad functional group tolerance utilizing this methodology, there are some examples where the cyclization did not occur (**Table IV.11**). First, the thermodynamically disfavored *5-endo* cyclization was not observed for substrates **IV.3.v**, **IV.5.aa** and **IV.5.ab**. Instead, we obtained the proto-dehalogenated product as the main one. Additionally, the pyridine containing chloroalkane **IV.3.w** does not react under optimized conditions and was fully recovered after the reaction. We rationalize the absence of reactivity due to the strong binding affinity of pyridine ligands to the single labile coordination site in complex $I^H Ni$ presumably causing the deactivation towards the cleavage of the Csp^3-Cl bond. For the cyclization of substrate **IV.3.x**, which contains a tertiary amine, the cyclic product was observed. In this case, the presence of the tertiary allylic amine in the substrate skeleton could serve as electron donor, not being activated the Csp^3-Cl by the nickel catalyst. For the substrates **IV.3.y**, **IV.3.z** and **IV.3.aa**, decomposition of the molecules were observed after the reaction.

Table IV.11 Unsuccessful substrates for the reductive cyclization methodology.



Standard conditions: substrate (10 mM), PCu (2 mol%), $I^H Ni$ catalyst (10 mol%), 11.4 eq. of iPr_2NEt as ED, EtOH:MeCN (3:2), under visible-light irradiation with blue LEDs ($\lambda = 447$ nm) at 30 °C for 24 h.

IV.4. Conclusions.

In this chapter, we have described a dual catalyst system that promotes the intramolecular cyclization of non-activated alkyl halides ($X = \text{Cl}, \text{Br}$) with pendant alkenes or alkynes. The combination of $[\text{Cu}(\text{bathocuproine})(\text{Xantphos})](\text{PF}_6)$ (PC_{Cu}) as photocatalyst and $[\text{M}(\text{OTf})(\text{Py}_2^{\text{Tstacn}})](\text{OTf})$ as coordination cobalt or nickel catalyst ($\text{I}^{\text{H}}\text{Co}$, $\text{I}^{\text{H}}\text{Ni}$) in the presence of electron-donor (Et_3N or $i\text{Pr}_2\text{NEt}$) resulted in optimal conditions for obtaining the desired reactivity. The presence of ethanol as a protic solvent turned out to have a significant impact on obtaining high yields. A broad family of cobalt and nickel complexes were tested, identifying that tetra- and penta-coordinated cobalt and nickel complexes bearing basic *N-based* ligands are remarkably active for the activation of $\text{C}_{\text{sp}^3}\text{-Cl}$ bonds. Blank experiments together with single-point monitoring reactions under light-dark cycles revealed that the presence of all components (photocatalyst, coordination catalyst, electron-donor and light) are essential for the reaction to occur. The presence of protic solvents possibilities for H_2 -formation as a side reaction, which was confirmed when using $\text{I}^{\text{H}}\text{Co}$ but not for $\text{I}^{\text{H}}\text{Ni}$. The optimized reaction conditions for the cyclization procedure give access to a broad substrate scope with good to excellent yields for the *5-exo-trig* and *5-exo-dig* cyclization reaction of non-activated alkyl chlorides bearing tethered alkenes and alkynes.

IV.5. Experimental Section.

IV.5.1 Material and Reagents.

Reagents and solvents were used as received from the commercial supplier unless otherwise stated. Triethylamine and di-*isopropylethylamine* were distilled over potassium hydroxide and were stored under argon. For the synthesis of reagents, the solvents (Hexane, Et₂O, DCM, MeCN, DMF and toluene) were used from a SPS-400, Innovative Technology solvent purification system and stored under argon with activated 4 Å molecular sieves.

Anhydrous acetonitrile was purchased from Sigma-Aldrich® and water was purified with a Milli-Q Millipore Gradient AIS system. Water, methanol, ethanol, isopropanol, butyronitrile, isobutyronitrile and trimethylacetonitrile used for photoreactions were degassed by freeze-pump-thaw method (repeated 3 cycles) and were stored under argon.

The synthesis of air-sensitive reagents as well as the preparation of visible-light photocatalytic reactions were conducted inside a nitrogen-filled glove box (mBraun Unilab) with concentrations of O₂ and H₂O lower than 0.5 ppm and using Schlenk techniques under argon atmosphere.

IV.5.2 Instrumentation.

NMR spectra were recorded on a Bruker 300 MHz, 400 MHz or 500 MHz spectrometers at room temperature. ¹H and ¹³C NMR chemical shifts are reported in parts per million (ppm), relative to the residual solvent peak as the internal reference. Multiplicities are reported as follows: singlet (s), doublet (d), doublet of doublet (dd), triplet of doublets (td), triplet (t), broad signal (br) and multiplet (m). Deuterated solvents (CDCl₃, CD₃CN, EtOD) were stored with activated 4 Å molecular sieves, and they were degassed by freeze-pump-thaw method when it was required for photocatalytic reactions.

High resolution Mass Spectrometry (HRMS) data was collected on an HPLC-QqTOF (Maxis Impact, Bruker Daltonics) or HPLC-TOF (MicroTOF Focus, Bruker Daltonics) mass spectrometer using 1 mM solution of the analyzed compound.

Gas chromatography analysis and quantification of the starting materials and products were carried out on an Agilent 7820A gas chromatograph (HP5 capillary column, 30 m x 320 μm x 0.25 μm or Sapiens 5MS capillary column, 30 m x 250 μm x 0.25 μm) and a flame ionization detector (FID). GC-MS spectral analyses were performed on an Agilent 7890A gas chromatograph (HP5 capillary column, 30 m x 320 μm x 0.25 μm) interfaced with an Agilent 5975c MS mass spectrometer.

Gas chromatography identification gases at the headspace was analyzed with an Agilent 7820A GC System equipped with columns Washed Molecular Sieve 5A, 2m x 1/8'' OD, Mesh 60/80 SS and Porapak Q, 4m x 1/8'' OD, SS, Mesh: 80/100 SS and a Thermal Conductivity Detector. The H_2 amount obtained was calculated through the interpolation of the previous calibration using different H_2/N_2 mixtures.

IV.5.2. 1 In-house developed parallel photoreactor.

Light source: The reactions were performed using Royal-Blue ($\lambda = 447\pm 20$ nm) LUXEON Rebel ES LED, mounted on a 20 mm Square Saber - 1030 mW @ 700mA (Datasheet: <https://www.luxeonstar.com/assets/downloads/ds68.pdf>) as a light source.

Temperature Control: Reaction temperature was controlled by a high precision thermoregulation Hubber K6 cryostat. Likewise, aiming at ensuring stable irradiation, the temperature of the LEDs was controlled and set at 22 $^\circ\text{C}$.

IV.5.2.2 Parallel pressure transducer hardware.

The parallel pressure transducer device is composed of 8 differential pressure transducers (Honeywell-ASCX15DN, ± 15 psi) connected to a hardware data-acquisition system (based on an Atmega microcontroller) controlled by a home-developed software program. The differential pressure transducer Honeywell-ASCX15DN gives a 100 microseconds response with a signal-conditioned output (high-level span, 4.5 V), and contains a calibrated sensor that is temperature compensated (from 0 °C to 70 °C). The differential sensor has two sensing ports that can be used for differential pressure measurements.

The pressure calibration device was offset within ± 0.5 matm and the span adjusted *via* software with a high precision pressure transducer (PX409-030GUSB, 0.08 % of accuracy). Each of the 8 differential 4 pressure transducers (Honeywell-ASCX15DN, ± 15 psi) produce a voltage output that can be directly transformed to a pressure difference between two measuring ports. The voltage output is digitalized with a resolution of 0.25 matm from 0 to 175 matm, and 1 matm from 176 to 1000 matm using an Atmega microcontroller with an independent voltage auto-calibration. The firmware for the Atmega microcontroller and the control software were developed in-house.

Gases at the headspace were analyzed with an Agilent 7820A GC System equipped with columns Washed Molecular Sieve 5Å, 2m x 1/8'' OD, Mesh 60/80 SS and Porapak Q, 4m x 1/8'' OD, SS. Mesh: 80/100 SS and a Thermal Conductivity Detector. The quantification of the H₂ obtained was measured through the interpolation of a previous calibration using different H₂/N₂ mixtures.

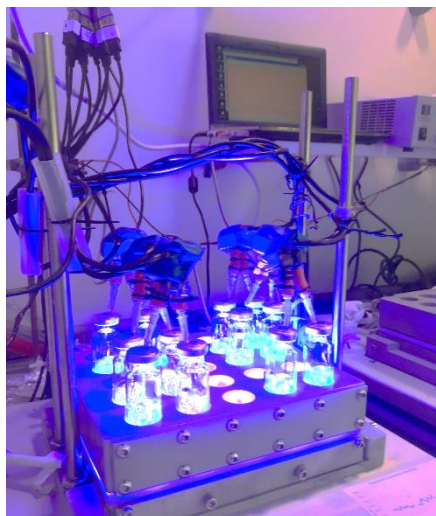


Figure IV.20 In-house developed parallel photoreactors coupled with parallel pressure transducer device.

IV.5. 3 Experimental Procedures.

General procedure for optimization screening: Inside an anaerobic box, aliquots from stock solutions of dimethyl allyl chloroethylmalonate (0.2 mL, 0.02 mmol, 1.0 eq.), $I^H M$ catalyst (M = Co or Ni, 0.1 mL, 0.001 mmol, 5 mol %), PC_{Cu} (0.1 mL, 4×10^{-4} mmol, 2 mol %) and acetonitrile (0.4 mL) were equally distributed into a vial (10 mL of headspace) that contained glass beads. The vial was sealed with a septum and removed from the anaerobic box. The degassed protic solvent was added to the vial to reach a total volume of 2 mL (total concentration of substrate 10 mM). Et_3N (40 μ L, 0.286 mmol, 14.4 eq.) or iPr_2NEt (40 μ L, 0.229 mmol, 11.4 eq.) was added to each vial, which was placed in the photoreactor at the indicated temperature (30 °C). After irradiating for 24 h with blue LEDs ($\lambda = 447$ nm), the sample was diluted with ethyl acetate (2 mL). A solution of biphenyl in ethyl acetate was added as internal standard (8.7×10^{-3} mmol in 0.25 mL). Then, the addition of 1 mL of H_2O formed a biphasic solution, and an aliquot of the organic phase was passed through a plug of $MgSO_4$ and eluted with EtOAc. The resulting solution was

analyzed by gas chromatography. The yields reported for each reaction are given as an average of at least two runs.

General procedure for single-point monitoring experiments: Inside an anaerobic box, aliquots from stock solutions of dimethyl allyl chloroethylmalonate (0.2 mL, 0.02 mmol, 1.0 eq.), complex I^HCo or I^HNi (0.1 mL, 0.002 mmol, 5 mol%), PCu (0.1 mL, 4×10^{-4} mmol, 2 mol%) and acetonitrile (0.4 mL) were equally distributed into 8 vials (10 mL of headspace) that contained glass beads. The vials were sealed with a septum and removed from the anaerobic box. Degassed ethanol was added to each vial to reach a total volume of 2 mL (total concentration of substrate 10 mM). Et_3N (40 μ L, 0.29 mmol, 14.4 eq.) or iPr_2NEt (40 μ L, 0.23 mmol, 11.4 eq.) was added to each vial, which was placed in the photoreactor at the indicated temperature (30 °C). At specific points of time (see plot), aliquots of 100 μ L were taken from the sealed vials and mixed with 29 μ L of a solution of biphenyl in EtOAc (34.8 mM) and the resulting mixture was analyzed by GC-FID. Light irradiation was switched off and on at specific points of the single-point monitoring experiment, which indicates that the reaction stops when the vial is not irradiated with visible-light.

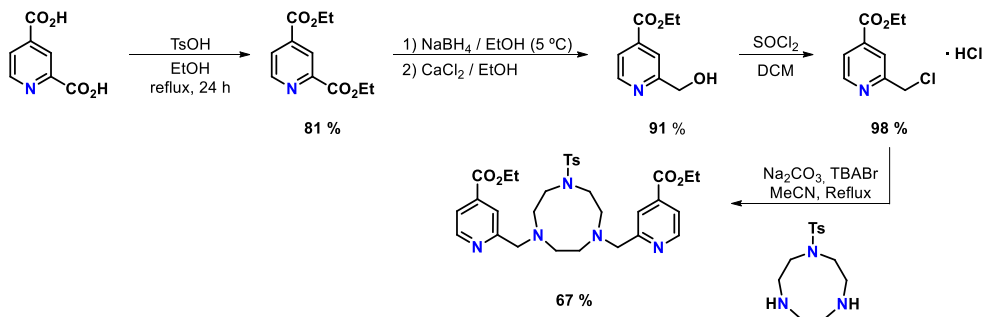
General procedure for H_2 -evolution monitoring experiments: Inside an anaerobic box, aliquots from stock solutions of dimethyl allyl chloroethylmalonate (**2a**, 1.5 mL, 0.15 mmol, 1.0 eq.), complex I^HCo or I^HNi (0.75 mL, 7.5×10^{-3} mmol, 5 mol%), photosensitizer PCu (0.75 mL, 3×10^{-3} mmol, 2 mol%) and acetonitrile (3 mL) were equally distributed into 3 vials (22 mL of headspace) that contained glass beads. The vials were sealed with a septum and removed from the anaerobic box. Degassed ethanol was added to each vial to reach a total volume of 15 mL (total concentration of substrate 10 mM). Et_3N (300 μ L, 2.16 mmol, 14.4 eq.) or iPr_2NEt (300 μ L, 1.72 mmol, 11.4 eq.) was added to each vial, which was placed in the photoreactor at 30 °C. Each reaction vial was connected to a differential pressure transducer sensor (Honeywell-ASCX15DN) with a reference vial that contains only PCu , electron donor and solvents. The reaction and reference vials were kept under

the same experimental conditions to compensate for the noise due to temperature-pressure fluctuations. The dihydrogen generated in the reaction vessels were monitored by recording the increase of pressure in the headspace, which is measured as the difference in pressure between the reaction and the reference vial. Also, blank experiments in order to monitor the dihydrogen evolution in the absence of substrate **IV.3.a** were performed at the same reaction conditions.

General procedure for reductive cyclization reactions: A solution of chloroalkane (0.6 mL, 0.06 mmol, 1.0 eq.), I^HCo or I^HNi (0.3 mL, 0.003 mmol, 5 mol%), PCu (0.3 mL, 1.2×10^{-3} mmol, 2 mol%) and acetonitrile (1.2 mL) was equally distributed into vials (10 mL of headspace) containing glass beads. The vials were sealed with a septum and removed from the glovebox. Degassed EtOH was added to each vial to reach a total volume of 6 mL (total concentration of substrate 10 mM). To these vials, Et_3N (120 μ L, 0.865 mmol, 14.4 eq.) or iPr_2NEt (120 μ L, 0.687 mmol, 11.4 eq.) was added and the vials were placed in the photoreactor at the indicated temperature (30 °C), and stirring was switched on. After irradiating the vials for 24 h with visible-light (blue LED, 447 nm), they were opened, and the content was combined in a separatory funnel. H_2O (15 mL) and Et_2O (15 mL) was added, and the organic layer was separated. The aqueous layer was extracted with Et_2O (3 x 15 mL), and the combined organic extracts were washed with brine (15 mL) and dried over $MgSO_4$. The solvent was removed under reduced pressure, and the crude material was purified via column chromatography.

IV.5. 4 Synthesis and Characterization of Metal Complexes.

Synthesis of ligand Ts^{CO2Et}Py₂tacn.



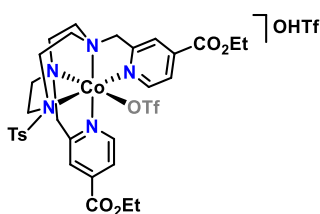
4-ethoxycarbonyl-2-chloromethylpyridine hydrochloride was synthesized following the reported procedure starting from 2,4-Pyridine dicarboxylic acid.⁶²

1,4-dimethyl-7-(4-ethoxycarbonyl-2-pyridylmethyl)-1,4,7-triazacyclononane, (Ts^{CO2Et}Py₂tacn) was synthesized following a reported procedure with slight modifications in the purification steps.⁶ Ethyl 2-(chloromethyl)isonicotinate hydrochloride (2,17 g, 9.25 mmol), *Tstacn* (1.31g, 4.63 mmol) and anhydrous acetonitrile (80 mL) were mixed in a 250 mL flask. Na₂CO₃ (2.4 g) and tetrabutylammonium bromide (TBABr, 160 mg) were added directly as solids, and the resulting mixture was heated at reflux for 22 hours under N₂. After cooling at room temperature, the resulting orange mixture was filtered, and the filter cake was washed with DCM. The combined filtrates were evaporated under reduced pressure. To the resulting residue, 2 M NaOH (15 mL) was added, and the mixture was extracted with DCM (4 x 40 mL). The combined organic layers were dried over MgSO₄, and the solvent was removed under reduced pressure. The remaining oil residue was dissolved with 5 mL of DCM, and the addition of Hexane (20 mL) caused the precipitation of a yellowish oil that was dried under reduced pressure to yield 3.8 g of a pale yellow oil (6.4 mmol, 67 %).

¹H NMR (400 MHz, CDCl₃): δ = 8.68 - 8.64 (m, 2H), 7.99 (s, 2H), 7.72 - 7.68 (m, 2H), 7.67 - 7.61 (m, 2H), 7.29 - 7.24 (m, 2H), 4.39 (q, *J* = 7.1 Hz, 4H), 3.94 (s, 4H),

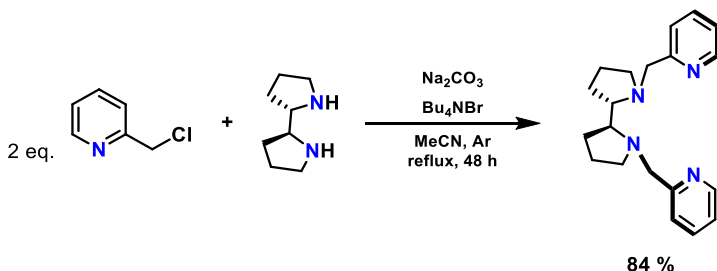
3.31 - 3.12 (m, 8H), 2.85 (s, 4H), 2.40 (s, 3H), 1.39 (t, $J = 7.1$ Hz, 6H) ppm. ^{13}C NMR (101 MHz, CDCl_3): $\delta = 165.2$ (2C), 161.1 (2C), 149.8 (2C), 143.0, 138.14 (2C), 135.8, 129.6 (2C), 127.0 (2C), 122.4 (2C), 121.2 (2C), 63.1 (br, 2C), 61.7 (2C), 55.5 (br, 4C), 50.5 (br, 2C), 21.4, 14.6 (2C) ppm. **IR** (film): 2929, 1723, 1599, 1562, 1287, 1203, 1156, 1902, 1018, 914, 763, 728, 694, 548 cm^{-1} . **MS**: m/z calcd. for $\text{C}_{31}\text{H}_{40}\text{N}_5\text{O}_6\text{S}$ $[\text{M}+\text{H}]^+$: 610,2699, found 610.2694. The spectroscopic data is in agreement with previously reported data for this compound.⁶³

Synthesis of $I^{\text{CO}_2\text{Et}}\text{Co}$.



$I^{\text{CO}_2\text{Et}}\text{Co}$ was synthesized following the analogous procedure to the described for complex $I^{\text{DMM}}\text{Co}$ obtaining 0.210 g of the desired product as a brown crystalline solid (66 %). **MS** (m/z): 817.1468 $[\text{M} - \text{OTf}]^+$. The spectroscopic data is in agreement with previously reported data for this compound.⁶³

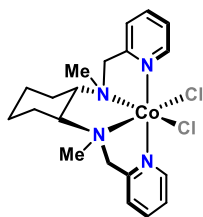
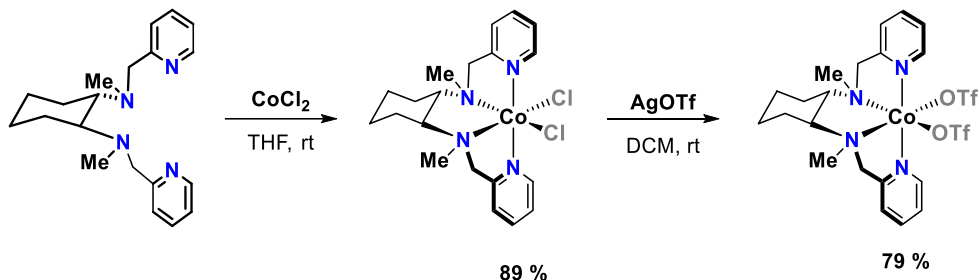
Synthesis of ((1*R*)-*N*1,*N*2-dimethyl-*N*1,*N*2-bis(pyridin-2-ylmethyl)cycloHexane-1,2-diamine (PDP).



(*S,S*)-2,2'-bipyrrolidine (0.25 g, 1.8 mmol), Na_2CO_3 (0.57g, 50.35 mmol, 3 eq.) and TBABr (0.57 g, 1.8 mmol) in MeCN (3 mL) was added to a 25 mL round bottom flask charged with a stir bar and $^{\text{H}}\text{PyCH}_2\text{Cl}\cdot\text{HCl}$ (2-chloromethyl-pyridine hydrochloride) (0.5 g, 3.9 mmol) dissolved in MeCN (6 mL). The combined mixture was stirred for 48 hours. At this point, the aqueous phase was extracted with DCM (3 x 5 mL). The organic fractions were combined, dried over MgSO_4 , and the solvent

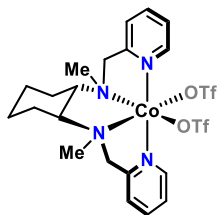
was eliminated under vacuum. The obtained brown oil that was purified by neutral alumina column (Hexane:EtOAc 80:20) and the collected fractions were removed under reduced pressure to provide 483 mg (1.78 mmol, yield 84%) of white oil.

Synthesis of Co-MCP_OTf.



Complex $[\text{Co}(\text{MCP})\text{Cl}_2]$ was synthesized following a reported procedure with slight modifications.⁶⁴ In a glovebox, a solution of MCP ligand⁶⁵ (357 mg, 1.1 mmol) in THF (1 mL) was added dropwise to a vigorously stirred suspension of CoCl_2 (130 mg, 1 mmol) in THF (1 mL). After few minutes, a purple solid precipitated. After stirring for an additional 2 hours, the solid was allowed to settle down, and the solution was filtered washed with DCM (3 x 2 mL) and dried under vacuum. This solid was dissolved in DCM, filtered through Celite[®], and the slow diffusion of diethyl ether into a solution of the complex produced a crystalline pink solid, which was dried under vacuum to give 447 mg of the title compound (0.889 mmol, 89 %).

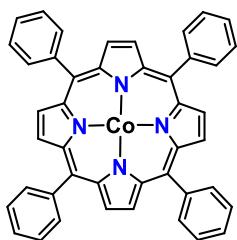
¹H NMR (400 MHz, CDCl_3): δ = 164.91, 101.2, 62.66, 50.65, 23.76, 21.23, 18.40, 8.23, 6.45, 2.14, 0.22, -16.95 ppm. **MS**: m/z calcd. for $\text{C}_{20}\text{H}_{28}\text{ClCoN}_4$ $[\text{M}-\text{Cl}]^+$: 418.1329, found 418.1321. **Anal.** Calcd. (%) for $\text{C}_{20}\text{H}_{28}\text{Cl}_2\text{CoN}_4$: C, 52.87; H, 6.21; N, 12.33. Found: C, 52.37; H, 6.04; N, 12.08. The spectroscopic data is in agreement with that reported.⁶⁴



[Co(MCP)(OTf)₂] In a glovebox, to a stirred suspension of AgOTf (0.71 g, 0.660 mmol) in DCM (1 mL) was added a solution of [Co(MCP)Cl₂] complex (0.1 g, 0.220 mmol) in DCM (1 mL) at room temperature. After stirring overnight, the solution was filtered to remove the silver salts. The resulting pale pink solution was evaporated under vacuum to give 118 mg of the title compound as a pink solid (0.173 mmol, 79 %).

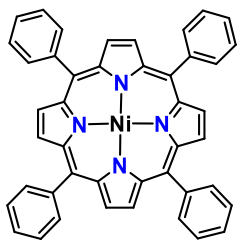
MS (m/z): 532.1161 [M - OTf]⁺. **Anal.** Calcd. (%) for C₂₂H₂₈CoF₆N₄O₆S₂: C, 38.77; H, 4.14; N, 8.22. Found: C, 38.28; H, 4.06; N, 8.05.

Synthesis of Co-TPP and Ni-TPP.



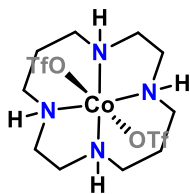
Co-TPP Compound has been synthesized according to the procedure described in the literature with slight modifications.⁶⁶ CoCl₂ (0.116 g, 0.488 mmol) dissolved in DMF (30 mL) was added to a solution of the ligand (0.3 g, 0.488 mmol) in DMF (10 mL). The resulting solution was warmed for one hour in a sealed tube at 120 °C. After cooling to room temperature, 100 mL of deionized water was added, and the resulting suspension was refrigerated overnight. The precipitate obtained was filtered, washed with deionized water and dried under vacuum at 80 °C yielded a red solid (266 mg, 0.395 mmol, 81 %).

Anal. Calcd. for C₄₄H₃₀CoN₄: C, 74.67; N, 7.91; H, 4.27 %. Found: C, 74.92; N, 7.98; H, 4.19 %. **MS** (m/z): 671.1642 [M]⁺.



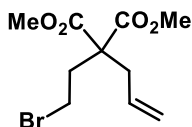
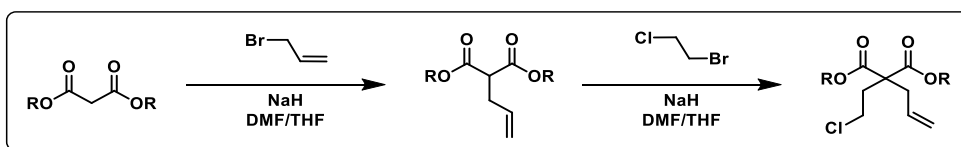
Ni-TPP was synthesized following the analogous procedure to the described for complex *Co-TPP* obtaining 0.253 g of the desired product as a purple crystalline solid (77 %). **Anal.** Calcd. for C₄₄H₃₀NiN₄: C, 74.70; N, 7.92; H, 4.56 %. Found: C, 74.82; N, 7.52; H, 4.60 %. **MS** (m/z): 670.1774 [M]⁺.

Synthesis of Co-cyclam and Ni-cyclam.



Co-cyclam was synthesized following the analogous procedure to the described for complex *Ni-cyclam* obtaining 0.496 g of the desired product as a brown crystalline solid (56 %). **Anal.** Calcd. for $C_{12}H_{24}F_6N_4CoO_6S_2$: C, 25.86; N, 10.05; H, 4.33 %. Found: C, 25.69; N, 10.10; H, 4.23 %. **MS** (m/z): 408.0 $[M - OTf]^+$.

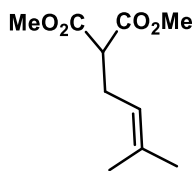
IV.5.5 Synthesis and Characterization of Substrates



Substrate (IV.1.a): A solution of dimethyl allylmalonate (500 mg, 2.90 mmol) in THF (5 mL) was added dropwise to a suspension of NaH (60% in mineral oil, 139 mg, 3.48 mmol) in THF (10 mL)

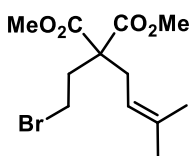
at 0 °C under Ar. The ice bath was removed, and the mixture was stirred for 60 min at ambient temperature. Then, freshly distilled 1,2-dibromoethane (0.36 mL, 3.78 mmol) was added via syringe slowly over 15 min, and the resulting mixture was stirred overnight. The reaction mixture was quenched with saturated aq. NH_4Cl . The aqueous solution was extracted with DCM, and the combined filtrates were dried over $MgSO_4$ and evaporated under reduced pressure. The crude product was purified by flash chromatography (SiO_2 , 2% EtOAc in Hexane) to give 600 mg (74%) of the title compound as light yellow oil.

1H NMR (400 MHz, $CDCl_3$): δ = 5.69 - 5.58 (m, 1H), 5.18 - 5.10 (m, 1H), 3.74 (s, 6H), 2.67 (dt, J = 7.4, 1.2 Hz, 2H), 2.48 - 2.42 ppm (m, 2H). **^{13}C NMR** (101 MHz, $CDCl_3$): δ = 170.8 (2C), 131.8, 119.9, 57.8, 52.8 (2C), 38.1, 36.4, 27.1 ppm. **IR** (film): 2953, 1729, 1640, 1434, 1208, 1162, 925, 643, 545 cm^{-1} . **MS**: m/z calcd. for $C_{10}H_{15}BrNaO_4$: 301.0046, found 301.0049.



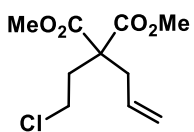
Int1: A round-bottom flask equipped with a magnetic stirring bar is charged with NaH and suspended in THF (20 mL) under argon. A solution of diimethylmalonate in 5 mL of THF is added dropwise with a dropping funnel at 0°C, and H₂ evolution proceeded. The resulting mixture is stirred for 1 h at rt. Then, a solution of 1-bromo-3-methylbutane in THF (10 mL) is added with a dropping funnel at rt, and the resulting solution is stirred overnight. Purification by column chromatography in silica gel using as eluent Hexane:EtOAc (98:2) yielded 0,957 g of a colourless oil. (63 %)

¹H NMR (300 MHz, CDCl₃): δ = 5.23 – 4.99 (m, 1H), 3.75 (d, *J* = 2.9 Hz, 6H), 3.50 – 3.18 (m, 1H), 2.61 (s, 2H), 1.70 (s, 3H), 1.64 (s, 3H) ppm.



Substrate (IV.1.b): A solution of **Int1** in 5 mL of THF is added dropwise to a suspension of NaH in THF (20 mL) under argon at 0 °C. The resulting mixture is stirred for 1h at rt. Then, a solution of 1,2-dibromoethane in THF (10mL) is added with a dropping funnel at rt and the resulting solution is stirred overnight. Purification by column chromatography in silica gel using as eluent Hexane:EtOAc (98:2) yielded 0,957 g of a colorless oil. (63 %).

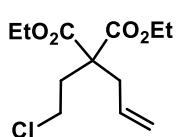
¹H NMR (400 MHz, CDCl₃): δ = 5.69 - 5.58 (m, 1H), 3.74 (s, 6H), 3.50 – 3.18 (m, 2H), 2.67 (dt, *J* = 7.4, 1.2 Hz, 2H), 2.48 - 2.42 ppm (m, 2H) 1.70 (s, 3H), 1.64 (s, 3H) ppm. **¹³C NMR** (101 MHz, CDCl₃): δ = 171.0 (2C), 133.8, 119.9, 57.8, 52.8 (2C), 38.1, 36.4, 27.1, 24.6, 18.6 ppm.



Substrate (IV.3.a): To a suspension of NaH (176 mg, 7.32 mmol, 1.1 eq.) in DMF (10 mL) was added at 0 °C a solution of dimethyl allylmalonate (1.2 g, 6.97 mmol, 1.0 eq.) in THF (5 mL). The mixture was stirred at room temperature for 30 min in which it became a clear solution. To this solution was added dropwise a solution of freshly distilled 1-bromo-2-chloroethane (1.5 g, 10.45 mmol, 1.5 eq.) in THF (2 mL). The solution was stirred

overnight at room temperature. The reaction was quenched by the addition of H₂O (15 mL) and extracted with Et₂O (3 × 15 mL). The combined organic extracts were dried over MgSO₄ and the solvent was removed under reduced pressure. The crude material was purified by flash chromatography (SiO₂, 10 % diethyl ether in Hexane) to yield 1.05 g (64 %) of the title compound as colorless oil.

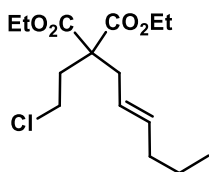
¹H NMR (400 MHz, CDCl₃): δ = 5.73 - 5.52 (m, 1H), 5.23 - 5.02 (m, 2H), 3.74 (s, 6H), 3.53 (t, *J* = 7.6 Hz, 2H), 2.68 (dt, *J* = 7.4, 1.2 Hz, 2H), 2.37 (d, *J* = 7.6 Hz, 2H) ppm. **¹³C NMR** (101 MHz, CDCl₃): δ = 170.9 (2C), 131.8, 119.9, 56.7, 52.8 (2C), 39.9, 38.0, 36.0 ppm. **IR** (film): 2955, 1730, 1435, 1208, 1172, 925, 648 cm⁻¹. **MS**: *m/z* calcd. for C₁₀H₁₅ClNaO₄ [M + Na]⁺: 257.0551, found 257.0549.



Substrate (IV.3.b): A solution of dimethyl allylmalonate (1.59 g, 7.98 mmol, 1 eq.) in THF (30 mL) was added dropwise to a suspension of NaH (286 mg, 11.91 mmol, 1.5 eq.) in THF at 0 °C.

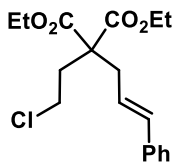
The cooling bath was removed, and the mixture was stirred for 60 min at room temperature. Freshly distilled 1-bromo-2-chloroethane (3.4 g, 23.82 mmol, 3.0 eq.) was added over 15 min, and the resulting mixture was stirred for 48 h at rt. The reaction was quenched with saturated aqueous NH₄Cl. The aqueous solution was extracted with DCM (2 × 15 mL), and the combined organic extracts were dried over MgSO₄, and the solvent was removed under reduced pressure. The crude material was purified by flash chromatography (SiO₂, 3 % ethyl acetate in Hexane) to yield 1.6 g (75 %) of the title compound as a colourless oil.

¹H NMR (400 MHz, CDCl₃): δ = 5.71 - 5.58 (m, 1H), 5.19 - 5.09 (m, 2H), 4.20 (qd, *J* = 7.1, 1.3 Hz, 4H), 3.53 (t, *J* = 7.80 Hz, 2H), 2.67 (dt, *J* = 7.4, 1.2 Hz, 2H), 2.35 (t, *J* = 8.14 Hz, 2H), 1.26 (t, *J* = 7.1 Hz, 6H) ppm. **¹³C NMR** (101 MHz, CDCl₃): δ = 170.5 (2C), 132.0, 119.8, 61.7 (2C), 56.7, 40.0, 37.9, 35.9, 14.2 (2C) ppm. **IR** (film): 2981, 1727, 1641, 1203, 1177, 923, 858 cm⁻¹. **MS**: *m/z* calcd. for C₁₂H₁₉ClNaO₄ [M + Na]⁺: 285.0864, found 285.0877.



Substrate (IV.3.c): A solution of diethyl (*E*)-2-(hex-2-en-1-yl)malonate⁶⁷ (0.69 g, 2,9 mmol, 1.0 eq.) in THF (5 mL) was added dropwise at 0 °C to a suspension of NaH (72.5 mg, 2,9 mmol, 1.1 eq.) in DMF (10 mL). The cooling bath was removed and the mixture was stirred at room temperature for 1h. The suspension was again cooled to 0 °C and 1-bromo-2-chloroethane (0.49 g, 3.4 mmol, 1.2 eq.) was added and stirring was continued overnight at room temperature. The reaction was quenched by addition of saturated aqueous NH₄Cl (10 mL). The organic layer was separated and the aqueous layer was extracted with Et₂O (3 × 10 mL). The combined organic extracts were dried over MgSO₄ and the solvent was removed under reduced pressure. The crude material was purified by flash chromatography (SiO₂, 2 % → 5 % → 10 % Et₂O in Hexane) to yield 0.48 g (55 %) of title compound as a colorless oil.

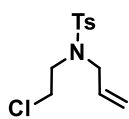
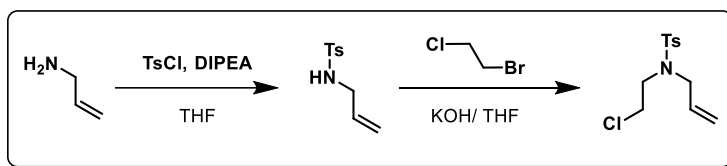
¹H NMR (400 MHz, CDCl₃): δ = 5.53 (dtt, *J* = 15.0, 6.9, 1.3 Hz, 1H), 5.23 (dtt, *J* = 15.0, 7.4, 1.4 Hz, 1H), 4.19 (qd, *J* = 7.1, 0.9 Hz, 4H), 3.56 - 3.43 (m, 2H), 2.61 (dt, *J* = 7.4, 1.1 Hz, 2H), 2.37 - 2.31 (m, 2H), 2.01 - 1.91 (m, 2H), 1.35 (q, *J* = 7.4 Hz, 2H), 1.26 (t, *J* = 7.1 Hz, 6H), 0.87 ppm (t, *J* = 7.3 Hz, 3H) ppm. **¹³C NMR** (126 MHz, CDCl₃) δ = 170.1 (2C), 136.0, 123.2, 61.6 (2C), 56.9, 40.1, 36.8, 35.9, 34.8, 22.6, 14.2 (2C), 13.7 ppm. **IR** (film): 2960, 1728, 1446, 1367, 1229, 1176, 971, 859, 731 cm⁻¹. **MS**: *m/z* calcd for C₁₅H₂₅ClNaO₄ [M + Na]⁺: 327.1334, found 327.1349.



Substrate (IV.3.d): A solution of diethyl cinnamylmalonate⁶⁸ (0.82 g, 3,0 mmol, 1.0 eq.) in THF (3 mL) was added dropwise at 0 °C to a suspension of NaH (78.1 mg, 3.3 mmol, 1.1 eq.) in DMF (12 mL). The cooling bath was removed and the mixture was stirred at room temperature for 1h. The suspension was again cooled to 0 °C and 1-bromo-2-chloroethane (0.55 g, 3.9 mmol, 1.3 eq.) was added and the mixture was stirred overnight at room temperature. After 24 h another portion of NaH (78.1 mg, 3.3 mmol, 1.1 eq.) and 1-bromo-2-chloroethane (0.55 g, 3.9 mmol, 1.3 eq.) was added since TLC revealed incomplete conversion. Stirring was continued for additional 18

h and the reaction was quenched by addition of saturated aqueous NH_4Cl (10 mL). The organic layer was separated and the aqueous layer was extracted with Et_2O (3×10 mL). The combined organic extracts were dried over MgSO_4 and the solvent was removed under reduced pressure. The crude material was purified by flash chromatography (SiO_2 , 2 % \rightarrow 5 % Et_2O in Hexane) to yield 0.48 g (78 %) of title compound as a colorless oil.

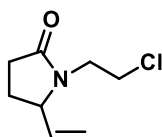
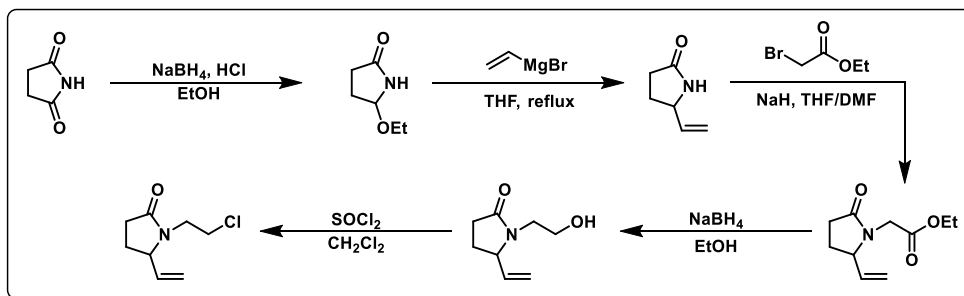
^1H NMR (500 MHz, CDCl_3): δ = 7.35 - 7.19 (m, 5H), 6.47 (dt, J = 15.7, 1.4 Hz, 1H), 6.03 (dt, J = 15.7, 7.5 Hz, 1H), 4.22 (m, 4H), 3.61 - 3.56 (m, 2H), 2.83 (dd, J = 7.6, 1.4 Hz, 2H), 2.44 - 2.38 (m, 2H), 1.27 (t, J = 7.1 Hz, 6H) ppm. **^{13}C NMR** (126 MHz, CDCl_3) δ = 170.5 (2C), 137.0, 134.6, 128.7 (2C), 127.7, 126.4 (2C), 123.4, 61.8 (2C), 57.1, 40.1, 37.4, 36.3, 14.2 (2C) ppm. **IR** (film): 2980, 1726, 1447, 1367, 1177, 1094, 967, 739, 693 cm^{-1} . **MS**: m/z calcd. for $\text{C}_{18}\text{H}_{23}\text{ClNaO}_4$ [$\text{M} + \text{Na}$] $^+$: 361.1177, found 361.1191.



Substrate (IV.3.e): Tetrabutylammonium bromide was added to a solution of N-allyl-4-methylbenzenesulfonamide,⁶⁹ potassium hydroxide, and 1-bromo-2-chloroethane in THF (30 mL). The white mixture was stirred at room temperature for 16 h, and then partitioned between ethyl ether (100 mL) and water (40 mL). The organic layer was washed with water (40 mL), brine (40 mL), dried (MgSO_4), and concentrated. The crude product was purified by flash chromatography (SiO_2 , ethyl acetate: Hexane) to afford the chloride substrate as a colorless oil. 2.39 g, 50 % yield.

^1H NMR (400 MHz, CDCl_3): δ = 7.72 - 7.69 (m, 2H), 7.34 - 7.30 (m, 2H), 5.67 (ddt, J = 16.8, 10.2, 6.5 Hz, 1H), 5.23 - 5.15 (m, 2H), 3.83 (dt, J = 6.5, 1.4 Hz, 2H), 3.62 (dd, J = 7.9, 6.9 Hz, 2H), 3.37 (dd, J = 8.0, 6.9 Hz, 2H), 2.43 (s, 3H) ppm. **^{13}C**

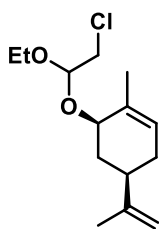
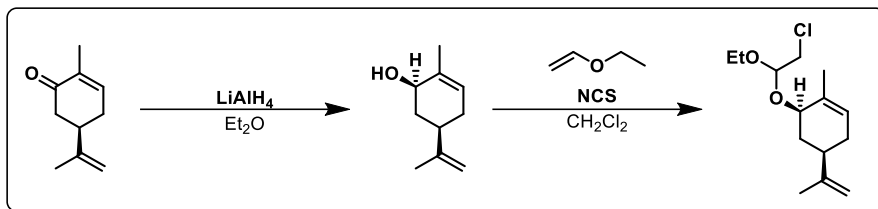
NMR (126 MHz, CDCl₃) δ = 144.1, 136.7, 133.2, 130.2 (2C), 127.6 (2C), 120.0, 52.5, 49.2, 42.1, 21.9 ppm. **MS**: m/z calcd. for C₁₂H₁₇ClNO₂S [M + H]⁺: 274.0668, found 274.0663.



Substrate (IV.3.f): Thionyl chloride (0.35 mL, 4.8 mmol, 1.5 eq.) was added dropwise to a solution of 1-(2-hydroxyethyl)-5-vinylpyrrolidin-2-one^{70,71} (0.5 g, 3.2 mmol, 1.0 eq.) in DCM (15 mL)

at 0 °C. The cooling bath was removed and the mixture was warmed to 40 °C and maintained at this temperature for 2 h. The reaction was carefully quenched by addition of saturated aqueous NaHCO₃ (10 mL) and diluted with DCM (15 mL). The organic layer was separated and the aqueous layer was extracted with DCM (2×10 mL). The combined organic extracts were dried over MgSO₄ and the solvent was removed under reduced pressure. The crude material was purified by flash chromatography (SiO₂, 80 % → 90 → 100 % Et₂O in Hexane) to yield 0.49 g (88 %) of the desired product as light yellow liquid.

¹H NMR (300 MHz, CDCl₃): δ = 5.67 (ddd, J = 17.1, 9.9, 8.5 Hz, 1H), 5.38 - 5.11 (m, 2H), 4.19 (td, J = 8.0, 5.8 Hz, 1H), 3.83 (dt, J = 14.0, 6.1 Hz, 1H), 3.72 - 3.52 (m, 2H), 3.36 - 3.17 ppm (m, 1H), 2.45 - 2.36 (m, 2H), 2.36 - 2.21 (m, 1H), 1.87 - 1.71 (m, 1H). **¹³C NMR** (75 MHz, CDCl₃) δ = 175.6, 137.6, 118.8, 62.5, 42.7, 41.4, 29.9, 25.8 ppm. **IR** (film) cm⁻¹: 2971, 1682, 1408, 1258, 929, 666, 564, 506 cm⁻¹. **MS**: m/z calcd. for C₈H₁₃ClNO [M + H]⁺: 174.0680, found 174.0680.

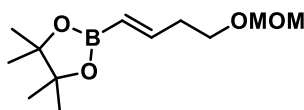
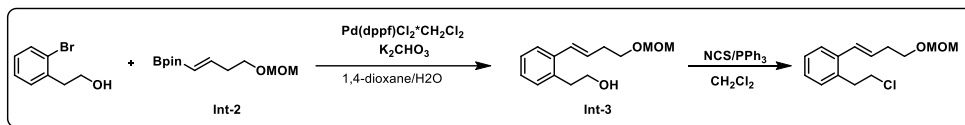


Substrate (IV.3.g): *N*-Chlorosuccinimide (0.43 g, 3.2 mmol, 1.4 eq.) was added to a solution of (*R,R*)-carveol⁷² (0.35 g, 2.3 mmol, 1.0 eq.) and ethyl vinyl ether (0.55 mL, 5.8 mmol, 2.5 eq.) in DCM (8 mL) at -45 °C. The solution was allowed to reach room temperature over the course of 2 h. Stirring was continued until no further conversion

was observed as judged by TLC. The reaction was quenched with saturated aqueous NH₄Cl (10 mL) and diluted with Et₂O (10 mL). The organic layer was separated and the aqueous phase was extracted with Et₂O (3 × 10 mL). The combined organic extracts were dried over MgSO₄ and the solvent was removed under reduced pressure. The crude material was purified by flash chromatography (SiO₂, 10 % → 20 % Et₂O in Hexane) to yield 0.25 g (42 %) as a 1:1 diastereomeric mixture of title compound and 0.16 g (47 %) of recovered starting material.

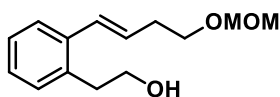
(1:1 mixture of diastereoisomers) ¹H NMR (400 MHz, CDCl₃): δ = 5.56 - 5.55 (m, 1H {isomer A}), 5.53 - 5.52, (m, 1H {isomer B}) 4.81 - 4.73 (m, 3 H, each), 4.26 (s, 1H {isomer A}), 4.13 (s, 1H {isomer B}), 3.73 - 3.61 (m, 2H, each), 3.58 - 3.47 (m, 2H, each) 2.26 - 2.16 (m, 2H, each), 2.07 - 1.88 (m, 2H, each), 1.76 - 1.73 (m, 6H, each), 1.63 - 1.43 (m, 1H, each), 1.27 - 1.22 (td, *J* = 7.0, 2.4 Hz, 3H each) ppm. ¹³C NMR (101 MHz, CDCl₃) δ = 149.0, 148.9, 134.9, 134.7, 125.4, 125.2, 109.4, 109.3, 103.0, 99.9, 78.6, 75.8, 61.6, 61.4, 44.4, 44.3, 40.9, 40.7, 36.2, 34.8, 31.0, 31.0, 20.5, 20.5, 19.6, 19.6, 15.5, 15.4 ppm. IR (film): 2971, 2918, 2885, 1112, 1035, 889, 759 cm⁻¹. MS: *m/z* calcd. for C₁₄H₂₃ClNaO₂ [M + Na]⁺: 281.1279, found 281.1283.

Substrate (IV.3.h)



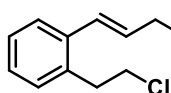
Int-2: A Schlenk flask was charged with dicyclohexylborane (55 mg, 0.31 mmol, 7 mol%) and to this flask was added pinacolborane (0.67 mL, 4.82 mmol, 1.1 eq.) and 4-(methoxy)but-1-yne (0.5 g, 4.38 mmol, 1.0 eq.) at 0 °C. The mixture was stirred for 24 h at room temperature, diluted with Hexane (25 mL) followed by bubbling air through the solution for 2 h. The organic layer was washed with H₂O (3 × 20 mL) and the solvent was removed under reduced pressure to yield 0.61 g (58 %) of title compound as a colorless oil.

¹H NMR (400 MHz, CDCl₃): δ = 6.62 (dt, *J* = 18.0, 6.4 Hz, 1H), 5.53 (dt, *J* = 18.1, 1.6 Hz, 1H), 4.62 (s, 2H), 3.62 (t, *J* = 6.7 Hz, 2H), 3.35 (s, 3H), 2.46 (qd, *J* = 6.6, 1.6 Hz, 2H), 1.26 (s, 12H) ppm. **¹³C NMR** (126 MHz, CDCl₃): δ = 150.5, 96.5, 83.2 (2C), 66.5, 55.3, 36.2, 24.9 (4C) ppm. **IR** (film): 2979, 1641, 1361, 1146 cm⁻¹. **MS**: *m/z* calcd for C₁₂H₂₃NaO₄B [M + Na]⁺: 264.1618, found 264.1611.



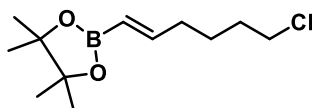
Int-3: Inside an anaerobic box, a Schlenk flask was charged with PdCl₂(dppf)·DCM (91 mg, 0.11 mmol, 0.05 eq.). The flask was removed from the glovebox and degassed 1,4-dioxane/H₂O (5:1, 18 mL), intermediate 1 (0.59 g, 2.4 mmol, 1.1 eq.), aryl bromide (0.45 g, 2.24 mmol, 1.0 eq.) and K₂CO₃ (0.93 g, 6.71 mmol, 3.0 eq.) were successively added. The mixture was stirred at 70 °C for 18 h. After reaching room temperature the reaction was quenched with saturated aqueous NH₄Cl (20 mL) and diluted with DCM (20 mL). The organic layer was separated and the aqueous layer was extracted with DCM (3 × 15 mL). The combined organic extracts were dried over MgSO₄ and the solvent was removed under reduced pressure. The crude material was purified by flash chromatography (SiO₂, 5 % → 10 % Et₂O in Hexane) to yield 0.48 g (91 %) of the title compound as a colorless oil.

¹H NMR (500 MHz, CDCl₃): δ = 7.47 - 7.40 (m, 1H), 7.22 - 7.14 (m, 3H), 6.74 (dt, *J* = 15.7, 1.6 Hz, 1H), 6.11 (dt, *J* = 15.7, 7.0 Hz, 1H), 4.65 (s, 2H), 3.85 - 3.79 (m, 2H), 3.67 (t, *J* = 6.6 Hz, 2H), 3.38 (s, 3H), 2.96 (t, *J* = 6.9 Hz, 2H), 2.54 (qd, *J* = 6.7, 1.5 Hz, 2H) ppm. **¹³C NMR** (126 MHz, CDCl₃): δ = 137.1, 135.4, 130.3, 129.4, 129.3, 127.4, 127.0, 126.4, 96.6, 67.4, 63.3, 55.4, 36.6, 33.8 ppm. **IR** (film): 2934, 2881, 1148, 1108, 1037, 966 cm⁻¹. **MS**: *m/z* calcd. for C₁₄H₂₀NaO₃ 259.1305, found 259.1303.



Substrate (IV.3.h): *N*-Chlorosuccinimide (0.37 g, 2.81 mmol, 1.4 eq.) was added at 0 °C to a solution of PPh₃ (0.74 g, 2.81 mmol, 1.4 eq.) and alcohol (0.47 g, 2.0 mmol, 1.0 eq.) in DCM (10 mL). The mixture was stirred at 0 °C for 5 h until complete consumption of starting material was observed on TLC. Hexane (10 mL) was added and the suspension was stirred for additional 10 min and then filtered. The solvent was removed under reduced pressure and the crude material was purified by flash chromatography (10 % → 20 % Et₂O in Hexane) to yield 287 mg (56 %) of title compound as a light yellow oil.

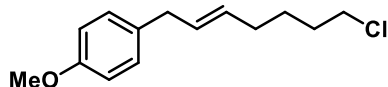
¹H NMR (400 MHz, CDCl₃): δ = 7.47 - 7.41 (m, 1H), 7.24 - 7.13 (m, 3H), 6.69 (dt, *J* = 15.7, 1.5 Hz, 1H), 6.14 (dt, *J* = 15.6, 7.0 Hz, 1H), 4.67 (s, 2H), 3.83 - 3.60 (m, 4H), 3.38 (s, 3H), 3.14 (dd, *J* = 8.5, 7.2 Hz, 2H), 2.55 (qd, *J* = 6.6, 1.5 Hz, 2H) ppm. **¹³C NMR** (101 MHz, CDCl₃): δ = 136.9, 135.0, 130.2, 130.0, 128.8, 127.5, 127.5, 126.5, 96.6, 67.3, 55.4, 44.2, 36.9, 33.9 ppm. **IR** (film): 2932, 2883, 1149, 1110, 1035, 965 cm⁻¹. **MS**: *m/z* calcd for C₁₄H₁₉ClNaO₂ [M + Na]⁺: 277.0966, found 277.0975.



Substrate (IV.3.r): A Schlenk flask was charged with dicyclohexylborane (0.274 g, 1.54 mmol, 7 mol%) and to this flask was added pinacolborane (3.35 mL, 23.10 mmol, 1.05 eq.) and 6-chlorohex-1-yne (2.67 mL, 22 mmol, 1.0 eq.) at 0 °C. The mixture was stirred for 24 h at room temperature, diluted Hexane (25 mL) followed

by bubbling air through the solution for 2 h. The organic layer was washed with H₂O (3 × 20 mL) and the solvent was removed under reduced pressure to yield 5.01 g (93 %) of title compound as a colorless oil.

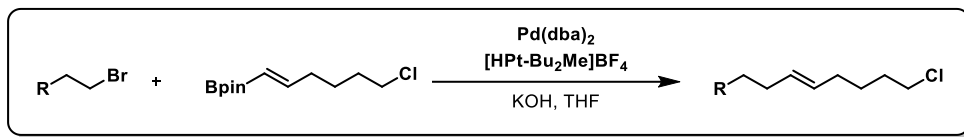
¹H NMR (400 MHz, CDCl₃): δ = 6.60 (dt, *J* = 18.0, 6.4 Hz, 1H), 5.45 (dt, *J* = 18.0, 1.7 Hz, 1H), 3.52 (t, *J* = 6.7 Hz, 2H), 2.28 - 2.08 (m, 2H), 1.89 - 1.70 (m, 2H), 1.64 - 1.51 (m, 2H), 1.26 (s, 12H) ppm. **¹³C NMR** (101 MHz, CDCl₃): δ = 153.6, 83.2 (2C), 45.0, 35.0, 32.1, 25.5, 24.9 (4C) ppm. **IR** (film): 2978, 2905, 1639, 1357, 1319, 1144, 968, 849 cm⁻¹. **MS**: *m/z* calcd for C₁₂H₂₂NaO₂BCl [M + Na]⁺: 266.1330, found 266.1325.



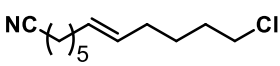
Substrate (IV.3.i): A Schlenk flask was charged with Pd(dppf)Cl₂·DCM (0.11 g, 0.13 mmol, 0.05 eq.), K₂CO₃ (1.1 g, 7.98 mmol, 3.0 eq.) benzyl bromide (0.54 g, 2.66 mmol, 1.0 eq.) and substrate **IV.3. r** (0.72 g, 2.93 mmol, 1.1 eq.) and 1,4-dioxane/H₂O (4:1, 15 mL). The mixture was stirred at 70 °C for 18 h. After cooling down to room temperature the reaction was quenched by addition of saturated aqueous NH₄Cl (10 mL) and diluted with Et₂O (20 mL). The organic layer was separated and the aqueous layer was extracted with Et₂O (3 × 20 mL). The combined organic extracts were dried over MgSO₄ and the solvent was removed under reduced pressure. The crude material was purified by flash chromatography (5 % Et₂O in Hexane) to yield 0.315 g (49 %) of title compound.

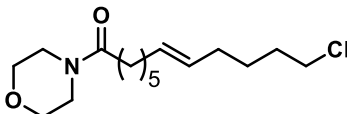
¹H NMR (500 MHz, CDCl₃): δ = 7.12 - 7.06 (m, 2H), 6.84 (d, *J* = 8.6 Hz, 2H), 5.65 - 5.52 (m, 1H), 5.52 - 5.42 (m, 1H), 3.79 (s, 3H), 3.53 (t, *J* = 6.7 Hz, 2H), 3.27 (d, *J* = 6.6 Hz, 2H), 2.23 - 1.94 (m, 2H), 1.82 - 1.73 (m, 2H), 1.53 (dt, *J* = 10.1, 7.1 Hz, 2H) ppm. **¹³C NMR** (126 MHz, CDCl₃) δ = 158.0, 133.1, 130.8, 130.1, 129.5, 113.9, 55.4, 45.1, 38.2, 32.2, 31.8, 26.8 ppm. **IR** (film): 2932, 2835, 1509, 1243, 1036 cm⁻¹. **MS**: *m/z* calcd for C₁₄H₂₀ClO [M + H]⁺: 239.1197, found 239,1195.

Substrates **IV.3. j - IV.3.n**:

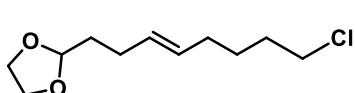


A slightly modified procedure from Nishibara and co-workers was followed for Suzuki-Miyaura Cross-Coupling reaction of (*E*)-6-chloro-1-hexen-1-ylboronic acid pinacol ester (**IV.3. r**) with alkyl bromides.⁷³ To a solution of bis(dibenzylidene)palladium (Pd(dba)₂) (5 mol%), [HPt-Bu₂Me]BF₄ (10 mol%), and substrate **IV.3. r** (1.5 eq.) in THF (3.5 mL) in a 25 mL Schlenk flask were added the corresponding alkyl bromide (1 eq.) and KOH (3 eq.) at room temperature under argon atmosphere. After stirring for 24h, the reaction mixture was quenched by addition of saturated aqueous NH₄Cl (10 mL) and diluted with DCM (20 mL). The organic layer was separated and the aqueous layer was extracted with DCM (3 × 20 mL). The combined organic extracts were dried over MgSO₄ and the solvent was removed under reduced pressure. Column chromatography in silica gel gave the corresponding cross-coupling products.

 **Substrate (IV.3.j)**: Isolated as colorless liquid in 65 % yield (236 mg, 1.1 mmol). ¹H NMR (400 MHz, CDCl₃): δ = 5.43 - 5.35 (m, 2H), 3.53 (t, *J* = 6.7 Hz, 1H), 2.33 (t, *J* = 7.1 Hz, 1H), 2.07 - 1.96 (m, 2H), 1.82 - 1.72 (m, 2H), 1.71 - 1.60 (m, 2H), 1.54 - 1.33 (m, 4H) ppm. ¹³C NMR (101 MHz, CDCl₃): δ = 130.5, 130.3, 119.9, 45.2, 32.3, 32.2, 31.9, 28.8, 28.2, 26.9, 25.4, 17.3 ppm. **IR** (film): 2930, 2856, 2244, 1457, 1457, 968, 724, 649 cm⁻¹. **MS**: *m/z* calcd for C₁₂H₂₀ClNNa [M + Na]⁺: 236.1176, found 236.1172.

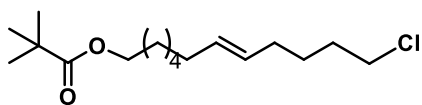
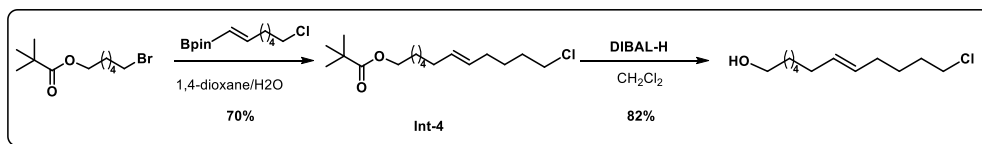
 **Substrate (IV.3.k)**: Isolated as colorless liquid in 45 % yield (560 mg, 1.85 mmol). ¹H NMR (400 MHz, CDCl₃): δ = 5.47 - 5.32 (m, 2H), 3.68 - 3.65 (m, 4H), 3.64 - 3.59 (m, 2H), 3.53 (t, *J* = 6.7 Hz, 2H), 3.48 - 3.43 (m, 2H), 2.30 (t, *J* = 7.6 Hz, 2H), 2.06 - 1.95 (m, 4H), 1.82 - 1.72 (m, 2H), 1.68 - 1.59 (m, 2H), 1.54 - 1.44 (m,

2H), 1.41 - 1.29 (m, 2H) ppm. ¹³C NMR (101 MHz, CDCl₃) δ = 171.9, 131.0, 129.8, 67.1, 66.8, 46.2, 45.2, 42.0, 33.2, 32.5, 32.2, 31.9, 29.5, 29.1, 26.9, 25.2 ppm. **IR** (film): 2923, 2853, 1641, 1441, 1429, 1228, 1115, 967, 848 cm⁻¹. **MS**: *m/z* calcd for C₁₆H₂₈ClNaO₂ [M + Na]⁺: 324.1701, found 324.1699.

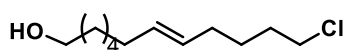


Substrate (IV.3.1): Isolated as light yellow liquid in 74 % yield (662 mg, 3 mmol). ¹H NMR (400 MHz, CDCl₃): δ = 5.53 - 5.39 (m, 2H), 4.89 (t, *J* = 4.8 Hz, 1H), 4.02 - 3.95 (m, 2H), 3.92 - 3.82 (m, 2H), 3.55 (t, *J* = 6.7 Hz, 2H), 2.20 - 2.10 (m, 2H), 2.08 - 1.98 (m, 2H), 1.84 - 1.70 (m, 4H), 1.59 - 1.46 (m, 3H) ppm. ¹³C NMR (101 MHz, CDCl₃): δ = 130.2, 130.0, 104.3, 65.0 (2C), 45.1, 33.9, 32.1, 31.8, 27.2, 26.8 ppm. **IR** (film): 2933, 2882, 1446, 1407, 1133, 1034, 967 cm⁻¹. **MS**: *m/z* calcd for C₁₁H₂₀ClO₂ [M + H]⁺: 219.1146, found 219.1152.

Substrate (IV.3.m)



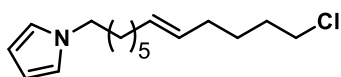
Int-4. Isolated as light yellow liquid in 70 % yield (320 mg, 1.06 mmol). ¹H NMR (400 MHz, CDCl₃): δ = 5.47 - 5.32 (m, 2H), 4.05 (t, *J* = 6.5 Hz, 2H), 3.53 (t, *J* = 6.7 Hz, 2H), 2.06 - 1.93 (m, 4H), 1.82 - 1.73 (m, 2H), 1.68 - 1.57 (m, 2H), 1.56 - 1.45 (m, 3H), 1.38 - 1.30 (m, 6H), 1.19 (s + m, 9 + 1H) ppm. ¹³C NMR (101 MHz, CDCl₃) δ = 178.8, 131.1, 129.7, 64.5, 45.1, 38.9, 32.5, 32.2, 31.9, 29.5, 28.8, 28.7, 27.3 (3C), 26.9, 25.9 ppm. **IR** (film): 2931, 1728, 1284, 1154 cm⁻¹. **MS**: *m/z* calcd for C₁₇H₃₁ClNaO₂ [M + Na]⁺: 325.1905, found 325.1901.



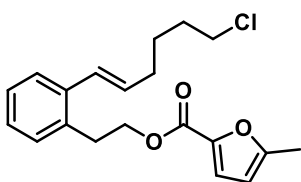
Substrate (IV.3.m): To a solution of pivalate derivate **Int-3** (0.3 g, 0.99 mmol, 1.0 eq.) in DCM (10 mL) was added at -78 °C dropwise DIBAL-H (1 M in THF, 1.98 mL, 1.98 mmol, 2.0 eq.) and the mixture was stirred at -78 °C for 30 min. The reaction was quenched

by addition of aqueous saturated Na/K tartrate (10 mL). The suspension was allowed to reach room temperature, stirred at room temperature for 30 min and then filtered through Celite[®], which was rinsed several times with DCM (30 mL). The solvent was removed under reduced pressure and the crude material was purified via flash chromatography (SiO₂, 20 % Et₂O in Hexane) to yield 177 mg (82 %) of title compound as a colorless oil.

¹H NMR (400 MHz, CDCl₃): δ = 5.46 - 5.32 (m, 2H), 3.64 (t, *J* = 6.6 Hz, 2H), 3.53 (t, *J* = 6.7 Hz, 2H), 2.05 - 1.95 (m, 4H), 1.81 - 1.73 (m, 2H), 1.60 - 1.54 (m, 2H), 1.54 - 1.46 (m, 2H), 1.39 - 1.29 (m, 7H) ppm. **¹³C NMR** (101 MHz, CDCl₃) δ = 131.2, 129.6, 63.2, 45.1, 32.9, 32.6, 32.2, 31.9, 29.6, 29.0, 26.9, 25.7 ppm. **IR** (film): 2927, 2855, 1456, 1055, 967 cm⁻¹. **MS**: *m/z* calcd. for C₁₂H₂₄ClO [M + H]⁺: 219.1510, found 219.1501.



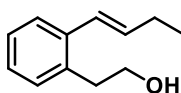
Substrate (IV.3.n): Isolated as pale yellow liquid in 66 % yield (383 mg, 1.4 mmol). **¹H NMR** (400 MHz, CDCl₃): δ = 6.55 (t, *J* = 2.1 Hz, 2H), 6.03 (t, *J* = 2.1 Hz, 2H), 5.35 - 5.22 (m, 2H), 3.76 (t, *J* = 7.2 Hz, 2H), 3.43 (t, *J* = 6.7 Hz, 2H), 1.98 - 1.82 (m, 4H), 1.74 - 1.59 (m, 4H), 1.45 - 1.35 (m, 2H), 1.28 - 1.12 (m, 6H) ppm. **¹³C NMR** (101 MHz, CDCl₃) δ = 131.1, 129.7, 120.6, 107.9, 49.7, 45.2, 32.6, 32.2, 31.9, 31.7, 29.5, 28.8, 26.9, 26.8 ppm. **IR** (film): 2978, 2931, 2857, 1638, 1358, 1318, 1144, 968, 849, 717, 640 cm⁻¹. **MS**: *m/z* calcd. for C₁₆H₂₇ClN: [M + H]⁺: 268.1827, found 268.1838.



Substrate (IV.3.o): *N,N'*-Dicyclohexylcarbodiimide (145 mg, 0.7 mmol, 1.2 eq.) and DMAP (21 mg, 0.17 mmol, 0.3 eq.) were added to a solution of alcohol **IV.3.p** (140 mg, 0.58 mmol, 1.0 eq.) and 5-methylfuran-2-carboxylic acid (89 mg, 0.7 mmol, 1.2 eq.) in DCM (5 mL). The mixture was stirred overnight and the reaction was quenched by addition of saturated aqueous NH₄Cl (10 mL). The organic layer was separated and the aqueous layer was extracted with Et₂O (3 × 10 mL). The combined organic extracts

were dried over MgSO_4 and the solvent was removed under reduced pressure. The crude material was purified by flash chromatography (5 % \rightarrow 10 % Et_2O in Hexane) to yield 160 mg (79 %) of title compound as colorless oil.

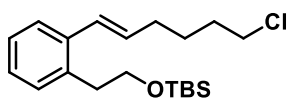
^1H NMR (400 MHz, CDCl_3): δ = 7.47 - 7.42 (m, 1H), 7.24 - 7.17 (m, 3H), 7.06 (d, J = 3.4 Hz, 1H), 6.74 (d, J = 15.6 Hz, 1H), 6.15 - 6.04 (m, 2H), 4.42 (dd, J = 8.0, 7.2 Hz, 2H), 3.57 (t, J = 6.6 Hz, 2H), 3.11 (t, J = 7.6 Hz, 2H), 2.39 (s, 3H), 2.29 (qd, J = 7.2, 1.5 Hz, 2H), 1.85 (dq, J = 8.7, 6.5 Hz, 2H), 1.69 - 1.60 (m, 2H) ppm. **^{13}C NMR** (101 MHz, CDCl_3): δ = 158.9, 157.4, 143.2, 137.3, 134.3, 132.7, 130.3, 127.8, 127.3, 127.2, 126.2, 119.6, 108.5, 64.7, 45.1, 32.8, 32.6, 32.2, 26.7, 14.1 ppm. **IR** (film): 1712, 1530, 1297, 1208, 1182 cm^{-1} . **MS**: m/z calcd. for $\text{C}_{20}\text{H}_{23}\text{ClNaO}_3$ [$\text{M} + \text{Na}$] $^+$: 369.1228, found 369.1236.



Substrate (IV.3.p): A Schlenk flask was charged with $\text{Pd}(\text{dppf})\text{Cl}_2 \cdot \text{DCM}$ (0.1 g, 0.122 mmol, 0.1 eq.), NaOH (0.245 g, 6.12 mmol, 2.0 eq.) aryl bromide (0.615 g, 3.06 mmol, 1.0 eq.) and substrate **IV.3. r** (0.86 g, 3.52 mmol, 1.15 eq.) and 1,4-dioxane/ H_2O (4:1, 15 mL). The mixture was stirred at 70 $^\circ\text{C}$ for 18 h. After reaching room temperature the reaction was quenched by addition of saturated aqueous NH_4Cl (10 mL) and diluted with Et_2O (20 mL). The organic layer was separated and the aqueous layer was extracted with Et_2O (3×20 mL). The combined organic extracts were dried over MgSO_4 and the solvent was removed under reduced pressure. The crude material was purified by flash chromatography (5 % Et_2O in Hexane) to yield 0.68 g (93 %) of title compound.

^1H NMR (400 MHz, CDCl_3): δ = 7.50 - 7.42 (m, 1H), 7.27 - 7.16 (m, 3H), 6.69 (dt, J = 15.6 Hz, 1H), 6.10 (dt, J = 15.6, 7.0 Hz, 1H), 3.85 (t, J = 6.8 Hz, 2H), 3.60 (t, J = 6.6 Hz, 2H), 2.98 (t, J = 6.8 Hz, 2H), 2.30 (qd, J = 7.2, 1.5 Hz, 2H), 1.94 - 1.82 (m, 2H), 1.71 - 1.62 (m, 2H) ppm. **^{13}C NMR** (101 MHz, CDCl_3): δ = 137.2, 135.2, 132.5, 130.3, 128.0, 127.3, 127.0, 126.4, 63.3, 45.0, 36.6, 32.6, 32.2, 26.7 ppm. **IR**

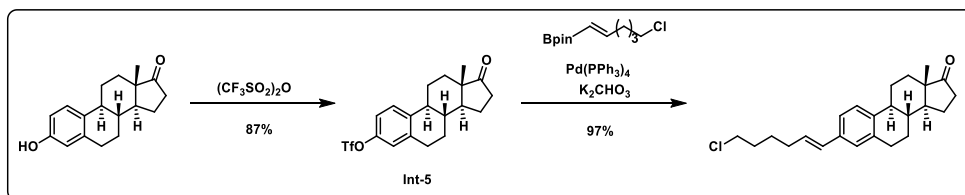
(film): 3321, 2933, 1447, 1041 cm^{-1} . **MS**: m/z calcd. for $\text{C}_{14}\text{H}_{19}\text{ClNaO}$ [$\text{M} + \text{Na}$] $^{+}$: 261.1017, found 261.1025.

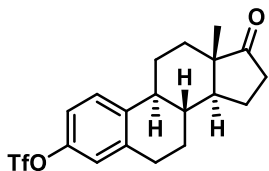


Substrate (IV.3.q): A Schlenk flask was charged with $\text{PdCl}_2(\text{dppf}) \cdot \text{DCM}$ (0.11 g, 0.13 mmol, 5 mol%). The flask was removed from the anaerobic box and degassed 1,4-dioxane/ H_2O (5:1, 24 mL), substrate **IV.3. r** (0.716 g, 2.93 mmol, 1.1 eq.), aryl bromide⁷⁴ (0.84 g, 2.66 mmol, 1.0 eq.) and K_2CO_3 (1.1 g, 7.98 mmol, 3.0 eq.) were added. The reaction mixture was stirred for 6 h at 70 °C. After reaching room temperature the reaction was quenched with saturated aqueous NH_4Cl (20 mL) and diluted with Et_2O (20 mL). The organic layer was separated and the aqueous layer was extracted with Et_2O (3×15 mL). The combined organic layers were dried over MgSO_4 and the solvent was removed under reduced pressure. The crude material was purified by flash chromatography (SiO_2 , 5 % Et_2O in Hexane) to yield 0.47 g (50 %) of the title compound as a colorless oil.

^1H NMR (400 MHz, CDCl_3): δ = 7.44 - 7.38 (m, 1H), 7.21 - 7.11 (m, 3H), 6.68 (dt, J = 15.6, 1.6 Hz, 1H), 6.06 (dt, J = 15.6, 7.0 Hz, 1H), 3.75 (t, J = 7.9 Hz, 2H), 3.57 (t, J = 6.7 Hz, 2H), 2.90 (t, J = 7.5 Hz, 2H), 2.27 (qd, J = 7.2, 1.5 Hz, 2H), 1.95 - 1.78 (m, 2H), 1.71 - 1.59 (m, 2H), 0.88 (s, 9H), -0.01 (s, 6H) ppm. **^{13}C NMR** (101 MHz, CDCl_3): δ = 137.1, 135.8, 132.0, 130.6, 128.3, 127.1, 126.7, 126.0, 64.0, 45.0, 37.1, 32.6, 32.2, 26.8, 26.1 (3C), 18.5, -5.3 (2C) ppm. **IR** (film): 2928, 2856, 1461, 1252, 1089, 834 cm^{-1} . **MS**: m/z calcd for $\text{C}_{20}\text{H}_{33}\text{ClNaOSi}$ [$\text{M} + \text{Na}$] $^{+}$: 375.1881, found 375.1900.

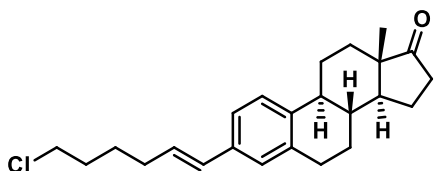
Substrate (IV.3.s)





Int-5: Triflic anhydride (0.36 mL, 2.17 mmol, 1.15 eq.) was added at 0°C to a Schlenk flask containing estrone (0.5 g, 1.85 mmol, 1.0 eq.) and NEt₃ (0.52 mL, 3.7 mmol) in DCM (15 mL). The mixture was stirred at 0°C for 1 h before the reaction was quenched by addition of saturated aqueous NaHCO₃ (20 mL). The organic layer was separated and the aqueous layer was extracted with DCM (3×10 mL). The combined organic extracts were dried over MgSO₄ and the solvent was removed under reduced pressure. The crude material was purified by flash chromatography (SiO₂, 10 % → 20 % → 30 % Et₂O in Hexane) to yield 0.65 g (87 %) of title compound as an off-white solid. Spectral data is in agreement with previously reported data for this compound.⁷⁵

¹H NMR (400 MHz, CDCl₃): δ = 7.34 (dd, *J* = 8.7, 1.1 Hz, 1H), 7.07 – 6.96 (m, 2H), 2.98 - 2.88 (m, 2H), 2.57 - 2.48 (m, 1H), 2.46 - 2.37 (m, 1H), 2.30 (td, *J* = 10.6, 4.3 Hz, 1H), 2.22 - 1.95 (m, 4H), 1.70 - 1.39 (m, 6H), 0.92 (s, 3H) ppm. ¹³C NMR (101 MHz, CDCl₃): δ = 220.6, 147.7, 140.4, 139.4, 127.3, 121.4, 118.4 (2C), 50.5, 48.0, 44.2, 37.9, 35.9, 31.6, 29.5, 26.2, 25.8, 21.7, 13.9 ppm.

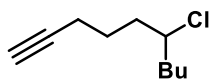
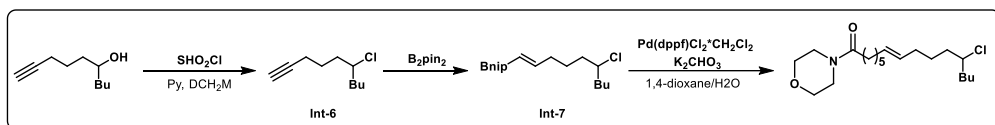


Substrate (IV.3.s): K₂CO₃ (103 mg, 0.75 mmol, 3.0 eq.) was added to a solution of Pd(PPh₃)₄ (29 mg, 0.025 mmol, 10 mol%), estrone derivate **Int-5** (100 mg, 0.25 mmol, 1.0 eq.) and substrate **IV.3. r** (73 mg, 0.3 mmol, 1.2 eq.) in 1,4-dioxane/H₂O (4:1, 3.5 mL). The mixture was heated for 18 h at 100 °C in a sealed flask. The reaction was allowed to reach room temperature and the solvent was removed under reduced pressure. The crude material was directly purified by flash chromatography (10 % → 20 % Et₂O in Hexane) to yield 89 mg (97 %) of title compound as a white solid.

¹H NMR (400 MHz, CDCl₃): δ = 7.23 (d, *J* = 8.1 Hz, 1H), 7.14 (dd, *J* = 8.2, 1.9 Hz, 1H), 7.08 (s, 1H), 6.34 (d, *J* = 15.8 Hz, 1H), 6.15 (dt, *J* = 15.7, 6.9 Hz, 1H), 3.56 (t, *J* = 6.7 Hz, 2H), 2.90 (dd, *J* = 9.1, 4.2 Hz, 2H), 2.51 (dd, *J* = 19.0, 8.7 Hz, 1H), 2.46 - 2.38 (m, 1H), 2.33 – 2.20 (m, 3H), 2.15 (dt, *J* = 18.8, 8.9 Hz, 1H), 2.09 - 1.99 (m,

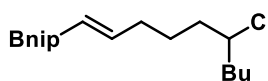
2H), 1.98 - 1.94 (m, 1H), 1.83 (dt, $J = 14.5, 6.8$ Hz, 2H), 1.68 - 1.58 (m, 4H), 1.56 - 1.48 (m, 3H), 1.48 - 1.39 (m, 1H), 0.91 (s, 3H) ppm. $^{13}\text{C NMR}$ (101 MHz, CDCl_3): $\delta = 221.0, 138.8, 136.6, 135.4, 130.2, 129.6, 126.7, 125.6, 123.5, 50.6, 48.1, 45.1, 44.5, 38.3, 36.0, 32.3, 32.2, 31.7, 29.5, 26.7, 26.7, 25.9, 21.7, 14.0$ ppm. **IR** (film): 2931, 2860, 1739, 966 cm^{-1} . **MS**: m/z calcd for $\text{C}_{24}\text{H}_{31}\text{ClNaO}$ [$\text{M} + \text{Na}$] $^+$: 393.1956, found 393.1956.

Substrate (IV.3.t)



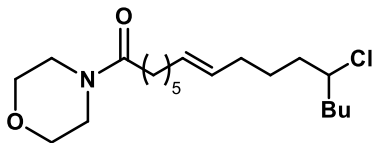
Int-6: Over a solution of dec-9-yn-5-ol⁷⁶ (1.4 g, 9.08 mmol) and pyridine (0.1 mL, 1.24 mmol) in DCM (10 mL) is added dropwise a solution of thionyl chloride (6.6 mL, 90 mmol) in DCM (10 mL) at 0 °C. Then, the reaction mixture was allowed to warm up to room temperature and it is stirred overnight. The crude was diluted with DCM (30 mL) and the residual thionyl chloride was quenched by adding slowly ice/water into the flask. The organic layer was separated and the aqueous layer was extracted with DCM (3 × 20 mL). The combined organic extracts were dried over MgSO_4 and the solvent was removed under reduced pressure. The crude material was purified by flash chromatography (5 % EtOAc in Hexane) to yield 0.66 g (42 %) of title compound.

$^1\text{H NMR}$ (400 MHz, CDCl_3): $\delta = 3.96\text{-}3.86$ (m, 1H), 2.23 (td, $J = 6.8, 2.7$ Hz, 2H), 1.96 (t, $J = 2.7$ Hz, 1 H), 1.95-1.60 (m, 6H), 1.59-1.30 (m, 4H), 0.92 (t, $J = 7.2$ Hz, 3H) ppm. $^{13}\text{C NMR}$ (101 MHz, CDCl_3): $\delta = 84.0, 68.9, 63.6, 38.5, 37.5, 28.8, 25.5, 22.4, 18.1, 14.1$ ppm. **MS**: m/z calcd for $\text{C}_{10}\text{H}_{17}$ [$\text{M} - \text{Cl}$] $^+$: 137.1325, found 137.1321.



Int-7: Following the procedure above described for substrate **IV.3.r** with intermediate **Int-6** gave intermediate **Int-7**: as a white solid that was used without further purification.

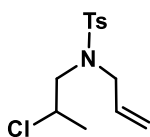
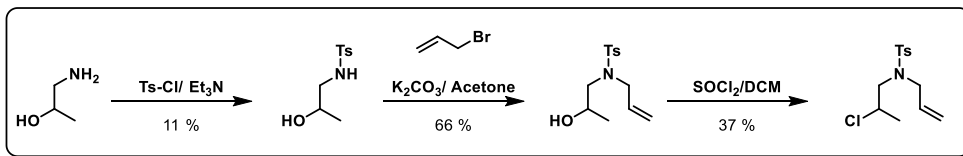
¹H NMR (400 MHz, CDCl₃): δ = 6.61 (dt, *J* = 18.0, 6.4 Hz, 1H), 5.45 (dt, *J* = 17.9, 1.6 Hz, 1H), 3.93-3.83 (m, 1H), 2.24-2.11 (m, 2H), 1.80-1.63 (m, 6H), 1.60-1.44 (m, 2H), 1.44-1.19 (m, 14H), 0.91 (t, *J* = 7.2 Hz, 3H) ppm.



Substrate (IV.3.t): Isolated as colorless liquid in 73 % yield (261 mg, 0.7 mmol) following the analogous procedure to **IV.3.k**.

¹H NMR (400 MHz, CDCl₃): δ = 5.46-4.30 (m, 2H), 3.95-3.82 (m, 1H), 3.71-3.64 (m, 4H), 3.63-3.57 (m, 2H), 3.49-3.41 (m, 2H), 2.30 (t, *J* = 8.0 Hz, 2H), 2.08-1.92 (m, 4H), 1.78-1.24 (m, 16H), 0.91 (t, *J* = 7.2 Hz, 3H) ppm. **¹³C NMR** (101 MHz, CDCl₃): δ = 172.0, 130.9, 130.0, 67.1, 66.8, 64.3, 46.2, 42.0, 38.4, 38.1, 33.2, 32.5, 32.2, 29.5, 29.1, 28.8, 26.5, 25.2, 22.4, 14.1 ppm. **IR** (film): 3452, 2961, 2921, 2855, 1638, 1429, 1271, 1235, 1113, 1068, 1028, 913, 847, 701, 571 cm⁻¹. **MS**: *m/z* calcd for C₂₀H₃₆ClNNaO₂ [M + Na]⁺: 380.2332, found 380.2327.

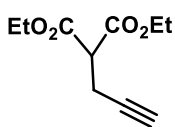
Substrate (IV.3. u):



Thionyl chloride (2,5 mL) was added dropwise (exothermic reaction) to a stirred solution of the alcohol derivative (150 mg) in CHCl₃, (10 ml)⁷⁷. The solution is refluxed for 1.5h. TLC to monitor the reaction. There are five spots in the TLC with less polarity than the starting alcohol. The crude is poured into water with ice and neutralized with NaHCO₃ and extracted with DCM. The organic phase is dried over MgSO₄ and the solvent removed under reduced pressure. Purification by column chromatography in silica gel using as eluent Hexane: EtOAc (80:20). 60 mg isolated.

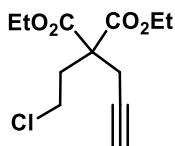
¹H NMR (400 MHz, CDCl₃): δ = 7.71 (d, *J* = 8.3 Hz, 2H), 7.35 – 7.28 (m, 2H), 5.59 (ddt, *J* = 17.4, 9.9, 6.6 Hz, 1H), 5.22 – 5.14 (m, 2H), 4.24 (q, *J* = 6.8 Hz, 1H), 3.91 – 3.81 (m, 2H), 3.36 (ddd, *J* = 14.6, 7.2, 0.6 Hz, 1H), 3.24 (dd, *J* = 14.6, 6.8 Hz, 1H),

2.43 (s, 3H), 1.53 (d, $J = 6.6$ Hz, 3H) ppm. ^{13}C NMR (101 MHz, CDCl_3): $\delta = 143.6$, 136.4, 132.7, 129.8 (2C), 127.3 (2C), 119.8, 55.5, 54.6, 52.5, 22.5, 21.5 ppm. IR (film): 2928, 1597, 1447, 1340, 1157, 1069. 991, 933, 866, 757, 662, 549 cm^{-1} . MS: m/z calcd for $\text{C}_{13}\text{H}_{18}\text{ClNaO}_2\text{S}$ $[\text{M} + \text{Na}]^+$: 310.0644, found 310.0639.



Int-8: Diethyl malonate (25.9 g; 161 mmol) was added dropwise to an ice-cold suspension of sodium hydride (6.46 g, 60 wt % in mineral oil, 161 mmol) in dry THF. The reaction mixture was allowed to stir for 2 h at room temperature. To this solution propargyl bromide (8 g; 53.8 mmol) were added dropwise at 0 °C and the solution was allowed to warm to room temperature with continuous stirring 24 h. The solvent was removed under reduce pressure. The reaction was quenched by addition of 50 mL of water, extracted with EtOAc (3 x 15mL). The combined organic layer were the concentrated in reduced pressure. The required product was purified by fractional distillation in vifreux column at 80 °C (1.6×10^{-1} mbar), yielding 9.75 g (91 %) of the desired product as a colorless oil.

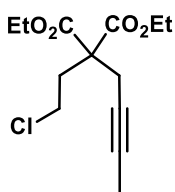
^1H NMR (400 MHz, CDCl_3): $\delta = 4.23$ (q, $J = 7.1$, 0.8 Hz, 4H), 3.64 – 3.42 (m, 1H), 2.78 (ddd, $J = 7.7$, 2.7, 0.6 Hz, 2H), 2.01 (d, $J = 0.7$ Hz, 1H), 1.28 (td, $J = 7.1$, 0.7 Hz, 6H) ppm. ^{13}C NMR (101 MHz, CDCl_3): $\delta = 167.9$ (2C), 78.0, 70.4, 61.8 (2C), 51.2, 22.5, 18.1, 14.0 (2C) ppm.



Substrate (IV.5.a): To a suspension of NaH (0.1 g, 4.47 mmol) in DMF (5 mL) was added at 0 °C a solution of diethyl 2-(prop-2-yn-1-yl)malonate (**Int-8**) (3.7 mmol, 1 g) in DMF (3 mL). The mixture was stirred at rt for 30 min in which it became a clear solution. To this solution was added dropwise a solution of 1-bromo-2-chloroethane (7.46 mmol, 1.07 g) in DMF (3 mL). The mixture was stirring at room temperature overnight. Then, the reaction was quenched by addition of 15 mL of water and extracted with diethyl ether (3*15 mL). The combined organic extracts were dried over MgSO_4 , the solvent was removed under reduce pressure and the crude Material was purified by flash column

chromatography (Hexane 95:5 EtOAc) yielding 0.644 g of the desired product as a colorless oil (66 % of yield).

¹H NMR (400 MHz, CDCl₃): δ = 4.24 (qd, *J* = 7.1, 3.2 Hz, 4H), 3.84 – 3.44 (m, 2H), 2.88 (d, *J* = 2.7 Hz, 2H), 2.77 – 2.49 (m, 2H), 2.06 (t, *J* = 2.7 Hz, 1H), 1.28 (t, *J* = 7.1 Hz, 6H) ppm. **¹³C NMR** (101 MHz, CDCl₃): δ = 169.4, 78.2, 72.0, 62.0, 55.8, 39.8, 35.3, 23.4, 14.0 ppm. **IR** (film): 2981, 2937, 1730, 1446, 1327, 1300, 1264, 1230, 1195, 1179, 1066, 1030, 859, 751, 526 cm⁻¹. **MS**: *m/z* calcd. for C₁₂H₁₇ClNaO₄ [M + Na]⁺: 283.0713, found 283.0708.

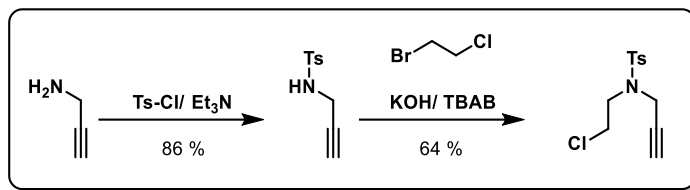


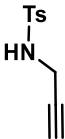
Substrate (IV.5.b): To a suspension of NaH (0.09 g, 3.61 mmol) in DMF (5 mL) was added at rt a solution of diethyl 2-(3-(4-methoxyphenyl)prop-2-yn-1-yl)malonate (3.3 mmol, 1 g) in DMF (3 mL). The mixture was stirred at rt for 30 min in which it became a clear solution. To this solution was added dropwise a solution of

1-bromo-2-chloroethane (6.6 mmol, 0.9 g) in THF (3 mL). The mixture was stirring at room temperature overnight. Then, the reaction was quenched by addition of 15 mL of water and extracted with diethyl ether (3 x 15 mL). The combined organic extracts were dried over MgSO₄, the solvent was removed under reduce pressure. The crude material was directly purified by flash chromatography (5 % Et₂O in Hexane) to yield 569 mg (60 %) of title compound as a colorless oil.

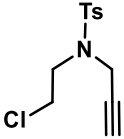
¹H NMR (400 MHz, CDCl₃): δ = 4.20 (qd, *J* = 7.1, 2.9 Hz, 4H), 3.60 – 3.51 (m, 2H), 2.78 (q, *J* = 2.6 Hz, 2H), 2.58 – 2.47 (m, 2H), 1.75 (t, *J* = 2.6 Hz, 3H), 1.25 (t, *J* = 7.1 Hz, 6H) ppm. **¹³C NMR** (101 MHz, CDCl₃): δ = 169.9 (2C), 79.5, 72.9, 61.9 (2C), 56.3, 40.1, 35.6, 23.8, 14.1 (2C), 3.6 ppm. **IR** (film): 2981, 2937, 1730, 1446, 1327, 1300, 1264, 1230, 1195, 1179, 1066, 1030, 859, 751, 526 cm⁻¹. **MS**: *m/z* calcd. for C₁₃H₁₉ClNaO₄ [M + Na]⁺: 297.0870, found 297.0864.

Substrate (IV.5. c)



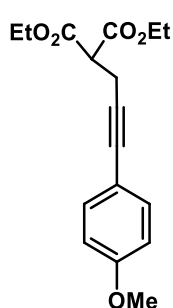
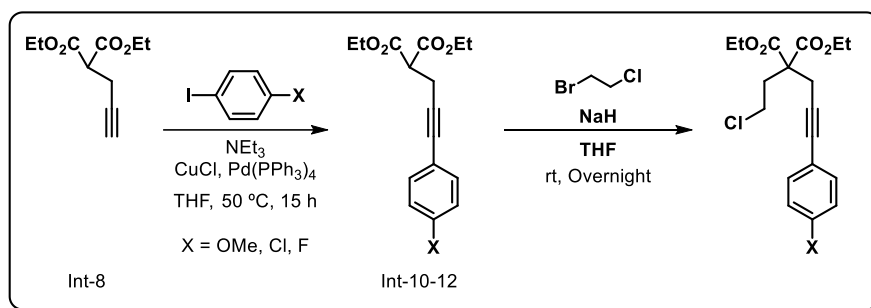
 **Int-9:** To a solution of propargylamine (1,7 mL, 25 mmol) in THF (50 mL) was added iPr₂NEt (4.8 mL, 27,5 mmol) and *p*-Toluenesulfonyl chloride (5.24g, 27,5 mmol). The mixture was stirred overnight at room temperature. The reaction was quenched by addition of NH₄Cl (30 mL). The organic layer was separated and the aq. layer was extracted with DCM (3 x 20 mL). The combined organic extracts were dried over MgSO₄ and the solvent was removed under reduced pressure. The crude Material was purified by flash chromatography (SiO₂, 40% → 50% → 60% Et₂O in Hexane) to yield 4.48 g (86%) of the desired product as a white powder.

¹H NMR (400 MHz, CDCl₃): δ = 7.80 (d, *J* = 8.3 Hz, 2H), 7.33 (dd, *J* = 8.0, 0.8 Hz, 2H), 4.97 (d, *J* = 6.0 Hz, 1H), 3.83 (dd, *J* = 6.0, 2.5 Hz, 2H), 2.44 (s, 3H), 2.12 (s, 1H) ppm. **¹³C NMR** (101 MHz, CDCl₃): δ = 143.8, 136.5, 129.7 (2C), 127.4 (2C), 78.0, 73.0, 32.8, 21.6 ppm.

 **Substrate (IV.3.c):** N-Ts propargylamine (1.0 g, 4.78 mmol, 1.0 eq.) was added to a suspension of KOH (0.4 g, 7.17 mmol, 1.5 eq.) and TBABr (0.15 g, 0.47 mmol, 10 mol%) in acetone (15 mL) and the mixture was stirred for 30 min at ambient temperature. 1-Bromo-2-chloroethane (0.59 mL, 7.17 mmol, 1.5 eq.) was added and the mixture was stirred at ambient temperature overnight. The reaction was quenched by addition of sat. aq. NH₄Cl (10 mL) and diluted with EtOAc (20 mL). The org. layer was separated and the aq. layer was extracted with EtOAc (3 x 15 mL). The combined org. extracts were dried over MgSO₄ and the solvent was removed under reduced pressure. The crude material was purified by column chromatography (SiO₂, 10% → 20% → 30% EtOAc in Hexane) to yield 0.71 g (55%) of the title compound as a colorless solid.

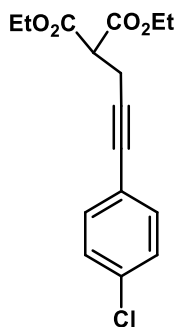
¹H NMR (400 MHz, CDCl₃): δ = 7.74 (d, *J* = 8.3 Hz, 2H), 7.31 (d, *J* = 8.3 Hz, 2H), 4.19 (d, *J* = 2.5 Hz, 2H), 3.70 (dd, *J* = 7.2, 6.6 Hz, 2H), 3.50 (dd, *J* = 7.3, 6.7 Hz, 2H), 2.43 (s, 3H) ppm. **¹³C NMR** (101 MHz, CDCl₃): δ = 144.0, 135.5, 129.7 (2C), 127.7 (2C), 76.7, 74.1, 48.3, 41.8, 38.2, 21.6 ppm. **MS**: *m/z* calcd. for C₁₂H₁₄ClNO₂S [M]⁺: 271.7, found 272.1.

Substrates **IV.5.d - IV.5.f**:



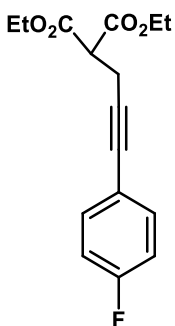
Int-10: Diethyl 2-(prop-2-yn-1-yl)malonate (2.0 g; 10.09 mmol) and 1-iodo-4-methoxybenzene (2.66 g; 11.37 mmol) were added to a stirring solution of Pd(PPh₃)₄ (0.583 g; 0.504 mmol), CuI (0.288 g; 1.513 mmol) and Et₃N (1.021 g; 10.09 mmol) in THF (20 mL). The mixture was heated for 15 h at 50 °C. The reaction was quenched by addition of 15 mL of water, extracted with Et₂O (3 x 15mL). The crude material was purified by flash chromatography (10 % of EtOAc in Hexane) to yield 1.46 g (48 %) of title compound as a pale yellow oil.

¹H NMR (400 MHz, CDCl₃): δ = 7.32 – 7.27 (m, 2H), 6.86 – 6.69 (m, 2H), 4.24 (qd, *J* = 7.1, 0.9 Hz, 4H), 3.79 (s, 3H), 3.63 (t, *J* = 7.8 Hz, 1H), 2.98 (d, *J* = 7.8 Hz, 2H), 1.28 (t, *J* = 7.1 Hz, 6H) ppm. **¹³C NMR** (126 MHz, CDCl₃): δ = 168.1 (2C), 159.3, 133.0 (2C), 115.4, 113.8 (2C), 83.9, 82.2, 61.7 (2C), 55.3, 51.6, 19.5, 14.1 (2C) ppm. **IR** (film): 2981, 1731, 1606, 1509, 1464, 1369, 1290, 1244, 1172, 1030, 832, 539 cm⁻¹.



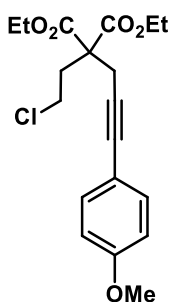
Int-11: Diethyl 2-(prop-2-yn-1-yl)malonate (0.650 g; 3.28 mmol) and 1-chloro-4-iodobenzene (0.860 g; 3.61 mmol) were added to a stirring solution of Pd(PPh₃)₄ (0.094 g; 0.492 mmol), CuI (0.094 g; 0.492 mmol) and Et₃N (0.332 g; 3.28 mmol) in THF (10 mL). The mixture was heated for 15 h at 50 °C. The reaction was quenched by addition of 15 mL of water, extracted with Et₂O (3 x 15mL). The crude material was purified by flash chromatography (10 % of EtOAc in Hexane) to yield 605 mg (78 %) of title compound as a pale yellow oil.

¹H NMR (300 MHz, CDCl₃): δ = 7.59 – 7.14 (m, 4H), 4.42 – 4.09 (m, 4H), 3.65 (t, *J* = 7.7 Hz, 1H), 3.01 (dd, *J* = 7.7, 1.3 Hz, 2H), 1.30 (t, *J* = 7.1 Hz, 6H) ppm. **¹³C NMR** (101 MHz, CDCl₃): δ = 168.0 (2C), 133.0, 132.8 (2C), 128.5 (2C), 121.7, 86.6, 81.4, 61.8 (2C), 51.4, 19.41, 14.1 (2C) ppm. **IR** (film): 2982, 1731, 1489, 1639, 1231, 1153, 1059, 1032, 1015, 828, 526 cm⁻¹. **MS:** *m/z* calcd. for C₁₆H₁₇ClNaO₄ [M + Na]⁺: 331.0713, found 331.0708.



Int-12: Diethyl 2-(prop-2-yn-1-yl)malonate (0.50 g; 2.52 mmol) and 1-fluoro-4-iodobenzene (0.618 g; 2.77 mmol) were added to a stirring solution of Pd(PPh₃)₄ (0.146 g; 0.126 mmol), CuI (0.037 g; 0.376 mmol) and Et₃N (0.255 g; 2.52 mmol) in THF (10 mL). The mixture was heated for 15 h at 50 °C. The reaction was quenched by addition of 15 mL of water, extracted with Et₂O (3 x 15mL). The crude material was purified by flash chromatography (10 % of EtOAc in Hexane) to yield 632 mg (86 %) of title compound as a pale yellow oil.

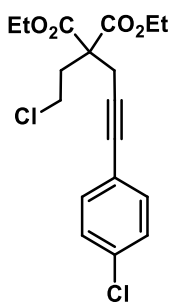
¹H NMR (300 MHz, CDCl₃): δ = 7.34 (dd, *J* = 8.9, 5.4 Hz, 2H), 6.96 (t, *J* = 8.8 Hz, 2H), 4.24 (qd, *J* = 7.1, 0.6 Hz, 4H), 3.63 (t, *J* = 7.7 Hz, 1H), 2.98 (d, *J* = 7.7 Hz, 2H), 1.28 (t, *J* = 7.1 Hz, 6H) ppm. **¹³C NMR** (126 MHz, CDCl₃): δ = 168.0, 163.5, 161.1, 133.5, 133.40, 119.3, 119.3 (2C), 115.5, 115.3, 85.1, 81.4, 61.8, 51.4, 19.4, 14.1 ppm. **IR** (film): 2982, 1731, 1601, 1507, 1335, 1221, 1154, 1032, 837, 532 cm⁻¹. **MS:** *m/z* calcd. for C₁₆H₁₇FNaO₄ [M + Na]⁺: 315.1009, found 315.1003.



Substrate (IV.5.d): To a suspension of NaH (0.06 g, 2.30 mmol) in DMF (5 mL) was added at rt a solution of diethyl 2-(3-(4-methoxyphenyl)prop-2-yn-1-yl)malonate (2.3 mmol, 0.7 g) in DMF (3 mL). The mixture was stirred at rt for 30 min in which it became a clear solution. To this solution was added dropwise a solution of 1-bromo-2-chloroethane (4.6 mmol, 0.67 g) in DMF (3 mL). The mixture was stirring at room temperature overnight. Then, the

reaction was quenched by addition of 15 mL of water and extracted with Et₂O (3 x 15 mL). The combined organic extracts were dried over MgSO₄, the solvent was removed under reduce pressure and the crude material was purified by column chromatography (5 % of Et₂O in Hexane) to yield 533 mg (63 %) of title compound as a white solid.

¹H NMR (400 MHz, CDCl₃): δ = 7.29 (d, *J* = 8.8 Hz, 2H), 6.81 (d, *J* = 8.8 Hz, 2H), 4.24 (qd, *J* = 7.1, 5.6 Hz, 4H), 3.80 (s, 3H), 3.68 – 3.60 (m, 2H), 3.05 (s, 2H), 2.61 (m, 7.2 Hz, 2H), 1.27 (t, *J* = 7.1 Hz, 6H) ppm. **¹³C NMR** (126 MHz, CDCl₃): δ = 169.7, 159.5, 133.0, 115.1, 113.9, 83.8, 82.0, 61.9, 56.3, 55.38, 40.0, 35.7, 24.4, 14.0 ppm. **IR** (film): 2980, 2937, 2906, 2838, 1730, 1606, 1509, 0444, 1289, 1245, 1173, 1030, 832, 537 cm⁻¹. **MS:** *m/z* calcd. for C₂₄H₃₁ClNaO [M + Na]⁺: 389.1132, found 389.1126.

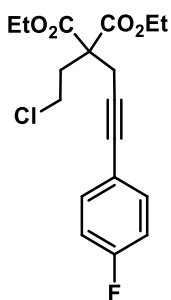


Substrate (IV.5.e): To a suspension of NaH (0.09 g, 3.61 mmol) in DMF (5 mL) was added at rt a solution of diethyl 2-(3-(4-chlorophenyl)prop-2-yn-1-yl)malonate (3.3 mmol, 1 g) in DMF (3 mL). The mixture was stirred at rt for 30 min in which it became a clear solution. To this solution was added dropwise a solution of 1-bromo-2-chloroethane (6.6 mmol, 0.9 g) in DMF (3 mL). The mixture was stirring at room temperature overnight. Then, the

reaction was quenched by addition of 15 mL of water and extracted with Et₂O (3 x 15 mL). The combined organic extracts were dried over MgSO₄, the solvent was removed under reduce pressure and the crude material was purified by column

chromatography (5 % of Et₂O in Hexane) to yield 543 mg (77 %) of title compound as a white solid.

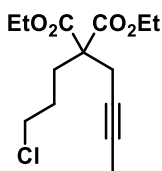
¹H NMR (400 MHz, CDCl₃): δ = 7.34 – 7.25 (m, 4H), 4.33 – 4.20 (m, 4H), 3.68 – 3.62 (m, 2H), 3.09 (s, 2H), 2.66 – 2.59 (m, 2H), 1.30 (t, *J* = 7.1 Hz, 6H) ppm. **¹³C NMR** (101 MHz, CDCl₃): δ = 169.5, 134.2, 132.8, 128.6, 121.4, 84.8, 82.9, 62.0, 56.2, 39.9, 35.6, 24.48, 14.0 ppm. **IR** (film): 2980, 2935, 2873, 1730, 1489, 1367, 1327, 1299, 1264, 1230, 1193, 1179, 1088, 1067, 1015, 828, 526 cm⁻¹. **MS**: *m/z* calcd. for C₁₈H₂₀Cl₂NaO₄ [M + Na]⁺: 393.0636, found 393.0631.



Substrate (IV.5.f): To a suspension of NaH (0.05 g, 2.05 mmol) in DMF (5 mL) was added at rt a solution of diethyl 2-(3-(4-fluorophenyl)prop-2-yn-1-yl)malonate (1.7 mmol, 0.5 g) in DMF (3 mL). The mixture was stirred at rt for 30 min in which it became a clear solution. To this solution was added dropwise a solution of 1-bromo-2-chloroethane (3.4 mmol, 0.5 g) in DMF (3 mL). The mixture was stirring at room temperature overnight. Then, the

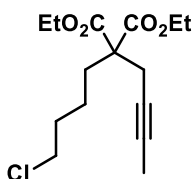
reaction was quenched by addition of 15 mL of water and extracted with Et₂O (3 x 15 mL). The combined organic extracts were dried over MgSO₄, the solvent was removed under reduce pressure and the crude material was purified by column chromatography (5 % of Et₂O in Hexane) to yield to yield 237 mg (40 %) of title compound as a white solid.

¹H NMR (400 MHz, CDCl₃): δ = 7.33 (dd, *J* = 8.8, 5.3 Hz, 2H), 6.97 (t, *J* = 8.7 Hz, 2H), 4.24 (qd, *J* = 7.1, 5.0 Hz, 4H), 3.74 – 3.54 (m, 2H), 3.06 (s, 2H), 2.68 – 2.53 (m, 2H), 1.27 (t, *J* = 7.1 Hz, 6H) ppm. **¹³C NMR** (101 MHz, CDCl₃): δ = 169.5 (2C), 163.6, 161.2, 133.5 (2C), 119.0 (2C), 115.4, 83.4, 82.9, 62.0 (2C), 56.2, 39.9, 35.6, 24.3, 14.0 (2C) ppm. **IR** (film): 2981, 1730, 1601, 1507, 1220, 1179, 1067, 1015, 836, 653, 531 cm⁻¹. **MS**: *m/z* calcd. for C₁₈H₂₀ClFNaO₄ [M + Na]⁺: 377.0932, found 377.0926.



Substrate (IV.3.g): To a suspension of NaH (0.09 g, 3.77 mmol) in DMF (5 mL) was added at rt a solution of diethyl 2-(but-2-yn-1-yl)malonate (0.4 g, 1.885 mmol) in DMF (3 mL). The mixture was stirred at rt for 30 min in which it became a clear solution. To this solution was added dropwise a solution of 1-bromo-3-chloropropane (0.899 g, 5.65 mmol) in DMF (3 mL). The mixture was stirring at room temperature overnight. Then, the reaction was quenched by addition of 15 mL of water and extracted with diethyl ether (3 x 15 mL). The combined organic extracts were dried over MgSO₄, the solvent was removed under reduce pressure and the crude material was purified by column chromatography (Hexane 95:5 EtOAc) obtaining 0,222 g of a colorless oil (41%).

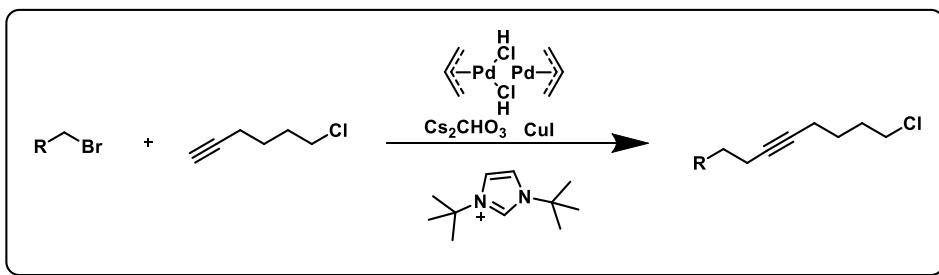
¹H NMR (300 MHz, CDCl₃): δ = 4.35 – 3.87 (m, 4H), 3.56 (t, J = 6.6 Hz, 2H), 2.91 (d, J = 2.5 Hz, 2H), 2.77 (d, J = 2.6 Hz, 2H), 2.15 (s, 3H), 1.77 (td, J = 2.6 Hz, 2H), 1.27 (td, J = 7.1 Hz, 6H) ppm. **¹³C NMR** (126 MHz, CDCl₃): δ = 170.41 (2C), 79.09, 73.76, 61.79 (2C), 57.36, 45.07, 36.80, 30.01, 23.28, 14.43 (2C), 3.45 ppm. **MS**: m/z calcd. for C₁₄H₂₁ClNaO₄ [M + Na]⁺: 311.1021, found 311.1035.



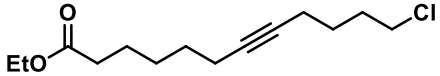
Substrate (IV.3.h): To a suspension of NaH (0.045 g, 1.885 mmol) in DMF (5 mL) was added at rt a solution of dimethyl 2-propargylmalonate (0.2 g, 0.942 mmol) in DMF (3 mL). The mixture was stirred at rt for 30 min in which it became a clear solution. To this solution was added dropwise a solution of 1-bromo-4-chlorobutane (0.490 g, 2.83 mmol) in DMF (3 mL). The mixture was stirring at room temperature overnight. Then, the reaction was quenched by addition of 15 mL of water and extracted with diethyl ether (3 x 15 mL). The combined organic extracts were dried over MgSO₄, the solvent was removed under reduce pressure and the crude material was purified by column chromatography (Hexane 95:5 EtOAc) obtaining 0,120 g of a colorless oil (42%).

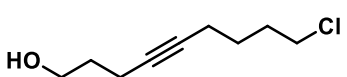
¹H NMR (400 MHz, CDCl₃): δ = 4.20 (q, *J* = 7.1 Hz, 4H), 3.54 (t, *J* = 6.6 Hz, 2H), 2.76 (d, *J* = 2.6 Hz, 2H), 2.03 (s, 3H), 1.87 – 1.77 (m, 2H), 1.74 (t, *J* = 2.6 Hz, 2H), 1.40 – 1.29 (m, 2H), 1.25 (t, *J* = 7.1 Hz, 6H) ppm. **¹³C NMR** (126 MHz, CDCl₃): δ = 170.21 (2C), 78.88, 73.56, 61.59 (2C), 57.16, 44.86, 36.60, 27.85, 23.08, 14.23 (2C), 3.68 ppm. **MS**: *m/z* calcd. for C₁₅H₂₃ClNaO₄ [M + Na]⁺: 325.1177, found 325.1176.

Substrates **IV.3.i - IV.3.n**:

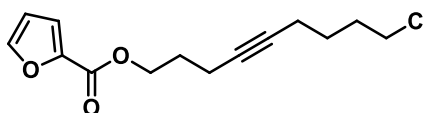
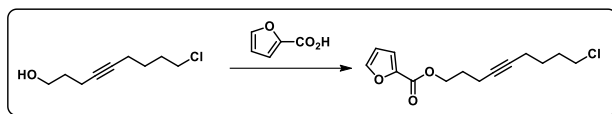


To a mixture of allyl palladium chloride, copper iodide, cesium carbonate and imidazolium salt in DMF/Et₂O, was added dropwise the 6-chlorohex-1-yne. After 10 minutes under stirrer conditions, bromoalkyl compound was added and the mixture is heated at 45 °C for 24 h.

 **Substrate (IV.3.i)**: Isolated as yellow oil in 48 % yield (536 mg, 4.48 mmol). **¹H NMR** (400 MHz, CDCl₃): δ = 4.18 – 4.09 (m, 2H), 3.57 (t, *J* = 6.6 Hz, 2H), 2.32 (td, *J* = 7.5, 6.0 Hz, 2H), 2.18 (dt, *J* = 18.4, 7.0, 2.4 Hz, 4H), 1.99 – 1.83 (m, 2H), 1.71 – 1.58 (m, 4H), 1.56 – 1.37 (m, 2H), 1.27 (td, *J* = 7.1, 1.2 Hz, 3H) ppm. **¹³C NMR** (101 MHz, CDCl₃): δ = 173.7, 80.6, 79.4, 60.2, 44.6, 34.3, 31.6, 28.7, 28.3, 26.2, 24.5, 18.6, 18.0, 14.3 ppm. **MS**: *m/z* calcd. for C₁₄H₂₃ClNaO₂ [M + Na]⁺: 281.1284, found 281.1282.

 **Substrate (IV.3.j)**: Isolated as colorless oil in 74 % yield (2.60 g, 14.9 mmol). **¹H NMR** (400 MHz, CDCl₃): δ = 3.77 (t, *J* = 6.1 Hz, 2H), 3.58 (t, *J* = 6.6 Hz, 2H), 2.29 (ddt, *J* = 6.9, 4.8,

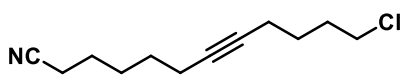
2.4 Hz, 2H), 2.21 (ddt, $J = 6.9, 4.8, 2.4$ Hz, 2H), 1.96 – 1.84 (m, 2H), 1.75 (tt, $J = 6.9, 6.1$ Hz, 2H), 1.71 – 1.57 (m, 2H) ppm. $^{13}\text{C NMR}$ (101 MHz, CDCl_3): $\delta = 82.4, 79.9, 61.3, 43.3, 31.1, 30.8, 26.0, 18.3, 14.6$ ppm. **MS**: m/z calcd. for $\text{C}_9\text{H}_{15}\text{ClO}$ $[\text{M}]^+$: 174.7, found 174.6.



Substrate (IV.3.k): An oven-dried 100 mL 2-neck flask under argon was charged with furan-2-carboxylic acid (1.68 g, 15.0 mmol,

1.0 eq.), 4-dimethylaminopyridine (0.046 g, 0.375 mmol, 0.025 eq.), hex-5-en-1-ol (4.51 g, 5.4 mL, 45 mmol, 3.0 eq.), and DCM (18 mL). The resultant solution was cooled to 0 °C and dicyclohexycarbodiimide (3.09 g, 15 mmol, 3.0 eq.) was added. The reaction mixture was stirred for 5 min and then the ice bath was removed. After stirring for 20 h at room temperature, the reaction mixture was filtered through a pad of celite, using additional DCM to wash the cake. The resultant solution was washed with 2.0M HCl (25 mL), Sat. NaHCO_3 (25 mL), dried over Na_2SO_4 and concentrated. Purification by flash column chromatography (Hexane:EtOAc, 80:20) afforded the desired product in 81 % of yield

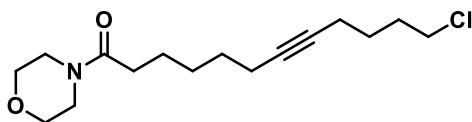
$^1\text{H NMR}$ (400 MHz, CDCl_3): $\delta = 7.59$ (dd, $J = 1.8, 0.9$ Hz, 1H), 7.18 (dd, $J = 3.5, 0.9$ Hz, 1H), 6.56 – 6.42 (m, 1H), 4.40 (t, $J = 6.4$ Hz, 2H), 3.57 (t, $J = 6.5$ Hz, 2H), 2.39 – 2.26 (m, 2H), 2.24 – 2.13 (m, 2H), 1.97 – 1.80 (m, 4H), 1.68 – 1.61 (m, 2H) ppm. $^{13}\text{C NMR}$ (101 MHz, CDCl_3): $\delta = 158.7, 146.3, 144.7, 117.9, 111.8, 80.3, 79.2, 63.7, 44.6, 31.6, 28.2, 26.1, 18.0, 15.5$ ppm. **MS**: m/z calcd. for $\text{C}_{14}\text{H}_{17}\text{ClNaO}_3$ $[\text{M} + \text{Na}]^+$: 291.0764, found 291.0758.



Substrate (IV.3.1): Isolated as colorless oil in 65 % yield (480 mg, 2.26 mmol). $^1\text{H NMR}$ (500

MHz, CDCl_3): $\delta = 3.56$ (t, $J = 6.6$ Hz, 2H), 2.35 (t, $J = 7.1$ Hz, 2H), 2.22 – 2.16 (m,

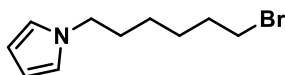
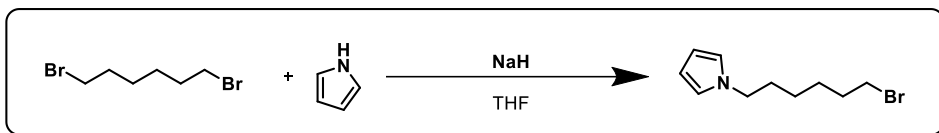
4H), 1.92 – 1.84 (m, 2H), 1.68 (dd, $J = 7.9, 6.4$ Hz, 2H), 1.65 – 1.59 (m, 2H), 1.59 – 1.49 (m, 2H) ppm. ^{13}C NMR (101 MHz, CDCl_3): $\delta = 119.8, 80.2, 80.0, 44.8, 31.8, 28.3, 28.0, 26.3, 25.1, 18.6, 18.2, 17.3$ ppm. **MS**: m/z calcd. for $\text{C}_{12}\text{H}_{18}\text{ClN}$ [M] $^+$: 211.7, found 211.7.



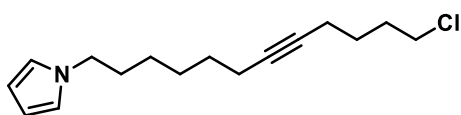
Substrate (IV.3.m): Isolated as colorless oil in 65 % yield (560 mg, 2.88 mmol).

^1H NMR (400 MHz, CDCl_3): $\delta = 3.72 - 3.66$ (m, 4H), 3.66 – 3.61 (m, 2H), 3.59 (t, $J = 6.6$ Hz, 2H), 3.48 (t, $J = 4.9$ Hz, 2H), 2.37 – 2.29 (m, 2H), 2.20 (dtt, $J = 11.6, 7.0, 2.4$ Hz, 3H), 1.96 – 1.86 (m, 2H), 1.73 – 1.61 (m, 4H), 1.57 – 1.40 (m, 2H) ppm. ^{13}C NMR (101 MHz, CDCl_3): $\delta = 171.6, 80.7, 79.4, 67.0, 66.7, 46.0, 44.7, 41.9, 33.0, 31.6, 28.8, 28.7, 26.2, 24.8, 18.6, 18.1$ ppm.

Substrate (IV.3.q):

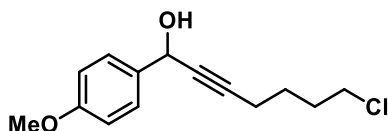


Int-13: In a 100 mL two-necked round bottom flask, sodium hydride was added to 30 mL of dry THF. At 0°C , a solution of pyrrole was added drop wise and the mixture was stirred for 1 h in an inert atmosphere of argon. Afterwards, a solution of dibromoalkane in 50 mL of dry THF was added dropwise. The mixture was stirred for overnight at room temperature. Water were introduced and the solution was stirred for 30 min. After that, the product was extracted with diethyl ether (3 x 30 mL) and the organic phase dried over MgSO_4 . Then the solvent was removed under reduced pressure. The spectroscopic data is in agreement with previously reported data for this compound.⁷⁸



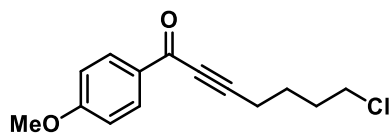
Substrate (IV.3.q): Isolated as colorless oil in 68 % yield (0.785 g, 2.9 mmol). ^1H NMR (400 MHz, CDCl_3): $\delta = 6.84 - 6.24$

(m, 2H), 6.17 (d, $J = 1.2$ Hz, 2H), 3.90 (t, $J = 7.1$, Hz, 2H), 3.67 – 3.44 (m, 2H), 2.23 (tdd, $J = 5.6, 3.5, 1.8$ Hz, 2H), 2.17 (ddt, $J = 6.9, 4.1, 1.5$ Hz, 2H), 1.98 – 1.87 (m, 2H), 1.81 (td, $J = 7.0, 2.6$ Hz, 2H), 1.72 – 1.62 (m, 2H), 1.54 – 1.39 (m, 4H), 1.34 (tt, $J = 8.4, 4.5$ Hz, 2H) ppm. $^{13}\text{C NMR}$ (101 MHz, CDCl_3): $\delta = 120.5, 107.8, 80.7, 79.4, 49.5, 44.6, 31.6, 31.5, 28.9, 28.4, 26.3, 26.2, 18.6, 18.1$ ppm. **MS**: m/z calcd. for $\text{C}_{16}\text{H}_{25}\text{ClN}$ $[\text{M} + \text{H}]^+$: 266.1676, found 266.1670.



Substrate (IV.3.m): In a Schlenk, the terminal alkyne (0.856 g, 7.34 mmol) is deprotonated with BuLi (4.6 mL, 7.34 mmol, 1.6 M in THF) at -78 °C in THF and then warmed up to rt for 30 mins. Then, the p-anisaldehyde (1 g, 7.34 mmol) is added and the mixture is stirred overnight at rt. The crude is extracted with $\text{DCM}:\text{H}_2\text{O}$ and the organic phase is dried over MgSO_4 and the solvent removed under reduced pressure. Purification with column chromatography in SiO_2 using Hexane:EtOAc (90:10) as eluent yielding 1.34 g of the desired product (73 % yield).

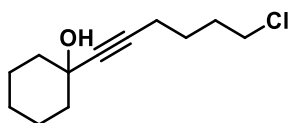
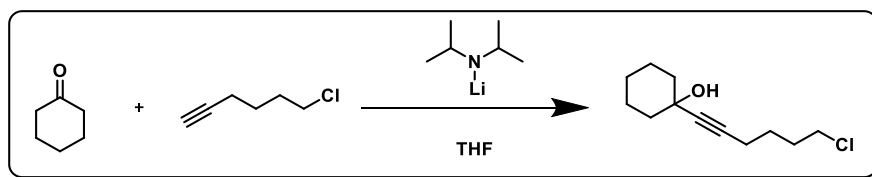
$^1\text{H NMR}$ (400 MHz, CDCl_3): $\delta = 7.64 - 7.36$ (m, 2H), 6.93 (d, $J = 8.8$ Hz, 2H), 5.59 – 5.23 (m, 1H), 3.84 (s, 3H), 3.59 (t, $J = 6.5$ Hz, 2H), 2.36 (td, $J = 7.0, 2.0$ Hz, 2H), 2.01 – 1.83 (m, 2H), 1.77 – 1.64 (m, 2H) ppm. $^{13}\text{C NMR}$ (101 MHz, CDCl_3): $\delta = 159.6, 133.5, 128.0$ (2C), 113.9 (2C), 86.4, 80.8, 64.4, 55.3, 44.5, 31.6, 25.3, 18.2 ppm. **MS**: m/z calcd. for $\text{C}_{14}\text{H}_{17}\text{ClNaO}_2$ $[\text{M} + \text{Na}]^+$: 275.0803, found 275.0809.



Substrate (IV.3.n): 7-chloro-1-(4-methoxyphenyl)hept-2-yn-1-ol (0.500 g, 1.978 mmol) was added to a suspension of MnO_2 (1.720 g, 19.78 mmol) in DCM (15 mL) at 0 °C, and the resulting mixture was stirred for 2 h at 0 °C. After filtered through Celite/ MgSO_4 , the solvent was removed under vacuum. The residue was passed through a pad of silica gel with Et_2O to afford the desired product as a colorless oil (0.490 g, 99% yield).

¹H NMR (300 MHz, CDCl₃): δ = 8.36 – 7.90 (m, 2H), 7.09 – 6.82 (m, 2H), 3.91 (s, 3H), 3.63 (t, 2H), 2.57 (t, 2H), 1.99 (d, 2H), 1.95 – 1.80 (m, 2H) ppm. **¹³C NMR** (101 MHz, CDCl₃) δ 176.7, 164.3, 131.9 (2C), 130.2 (2C), 113.7, 94.4, 80.0, 55.5, 44.2, 31.5, 25.1, 18.5 ppm. **MS**: *m/z* calcd. for C₁₄H₁₅ClNaO₂ [M + Na]⁺: 273.0653, found 273.0656.

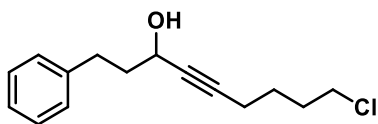
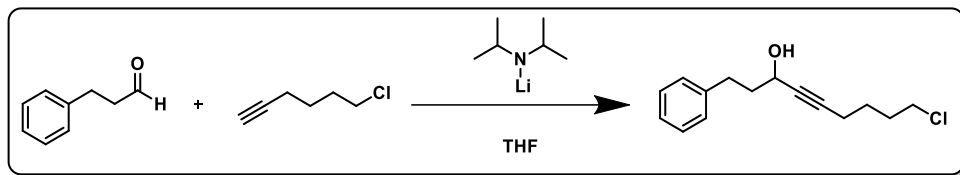
Substrate (IV.3.p):



Substrate (IV.3.p): In a Schlenk, LDA (1M in THF) was added dropwise (4.59 ml, 7.34 mmol) to a solution of the 6-cyclohexanone (0.856 g, 7.34 mmol) in THF (10 ml) at -78°C, then the reaction mixture was warmed up to rt for 30 mins. Then, 4-methoxybenzaldehyde (1 g, 7.34 mmol) was added and the mixture was stirred overnight at rt. The crude was extracted with DCM water and organic phase is dried over MgSO₄ and the solvent removed under reduced pressure. The crude was purified by flash chromatography by silica Hexane/EtOAc (90:10), obtaining 0.7 g (78%) of a colorless oil.

¹H NMR (400 MHz, CDCl₃): δ = 3.57 (t, *J* = 6.5 Hz, 2H), 2.27 (t, *J* = 7.0 Hz, 2H), 2.00 – 1.78 (m, 5H), 1.75 – 1.63 (m, 4H), 1.60 – 1.48 (m, 5H), 1.35 – 1.11 (m, 2H) ppm. **¹³C NMR** (101 MHz, CDCl₃): δ = 84.6, 83.7, 68.8, 44.5, 40.2 (2C), 31.6, 25.9, 25.2 (2C), 23.4, 18.0 ppm. **MS**: *m/z* calcd. for C₁₂H₁₉ClO [M + Na]⁺: 214.1, found 214.1.

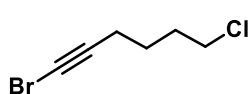
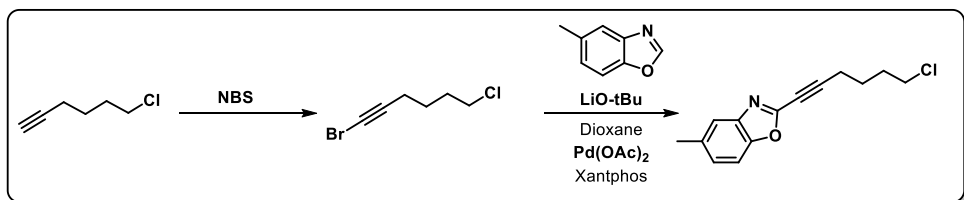
Substrate (IV.3.r):



Substrate (IV.3.r): The alkyne is added dropwise to a suspension of LDA (1 M in THF) at -78°C . After 10 minutes, the mixture is warmed to rt, and is left there during 30 minutes. The ketone is dissolved in THF, and the mixture is cooled at 0°C and the deprotonated alkyne is added dropwise into the ketone solution. The reaction mixture is left under stirring conditions overnight. The reaction crude is then extracted 3 times with $\text{DCM}:\text{H}_2\text{O}$ and the organic phase was dried over MgSO_4 . The residue was purified by flash-column chromatography affording 1.34 g of the desired product as yellow oil (72 % of yield).

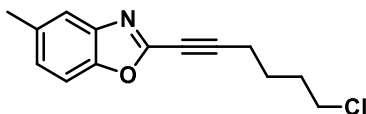
$^1\text{H NMR}$ (500 MHz, CDCl_3): $\delta = 7.30$ (td, $J = 7.4, 1.4$ Hz, 2H), 7.24 – 7.17 (m, 3H), 4.37 (tt, $J = 6.5, 2.0$ Hz, 1H), 3.57 (t, $J = 6.5$ Hz, 2H), 2.79 (t, $J = 7.9$ Hz, 2H), 2.29 (td, $J = 7.0, 2.0$ Hz, 2H), 2.07 – 1.94 (m, 2H), 1.94 – 1.86 (m, 2H), 1.73 – 1.64 (m, 2H) ppm. **$^{13}\text{C NMR}$** (101 MHz, CDCl_3): $\delta = 141.8, 128.9, 128.8, 126.3, 85.3, 82.1, 62.4, 44.9, 30.0, 31.9, 31.9, 26.2, 18.4$ ppm. **MS:** m/z calcd. for $\text{C}_{15}\text{H}_{20}\text{ClO}$ [$\text{M} + \text{Na}$] $^+$: 251.1203, found 251.1254.

Substrate (IV.3.s):



Int-14: General procedure: Heptyne (4.8 g, 50 mmol, 1 eq) in acetone (250 mL) was mixed in a 1 L round bottom flask and then added NBS (9.8 g, 55.5 mmol) and AgNO_3 (0.85 g, 5 mmol) at room temperature with magnetic stirring for 4 hours. Then the reaction mixture was diluted

with Hexanes (500 mL) and white crystals formed were filtered. The filtrate was collected and evaporated under reduced pressure to afford (8.26 g, 47.5 mmol) 95percent 1-bromohept-1-yne as colorless oil. The following compound was used with no further purification. Spectral data is in agreement with previously reported data for this compound.⁷⁹

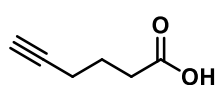
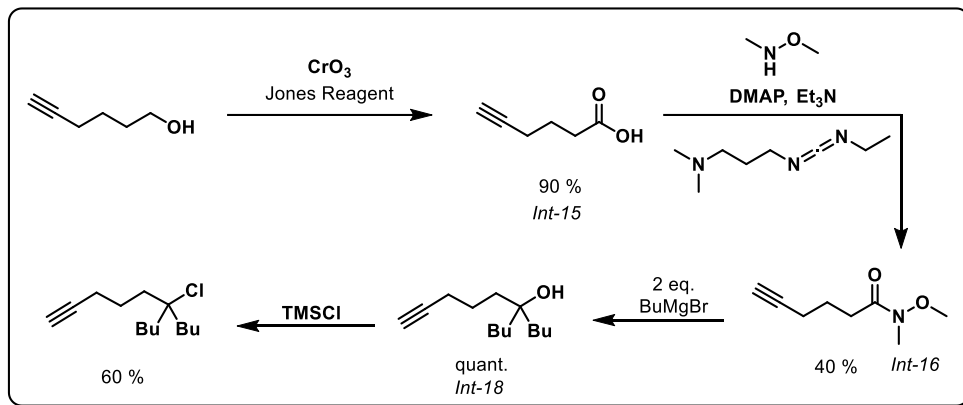


Substrate (IV.3.s): To an oven dried Schlenk tube were added azole (0.6 mmol), Pd(OAc)₂ (2.5 mol %), Xantphos (2.8 mol %) and LiOtBu (1 mmol).

The tube was then purged with argon and addition of 1-bromoalkyne (0.5 mmol) to the reaction vessel was followed by the addition of anhydrous 1,4-dioxane (3 mL). The reaction mixture was stirred in a pre-heated oil bath at 100 °C for an indicated time, and then cooled to ambient temperature, filtered through a pad of Celite washing with DCM (3 x 10 mL). The solvents were removed under reduced pressure and the crude product was purified by flash chromatography on silica gel (Hexane/EtOAc) to give the desired product.

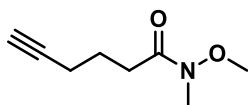
¹H NMR (400 MHz, CDCl₃): δ = 7.53 – 7.49 (m, 1H), 7.38 (d, *J* = 8.3 Hz, 1H), 7.21 (ddd, *J* = 8.4, 1.7, 0.7 Hz, H), 3.62 (t, *J* = 6.4 Hz, 2H), 2.59 (t, *J* = 6.9 Hz, 2H), 2.48 (d, *J* = 0.7 Hz, 3H), 2.11 – 1.95 (m, 2H), 1.92 – 1.81 (m, 2H) ppm. ¹³C NMR (101 MHz, CDCl₃): δ = 148.4, 147.6, 141.0, 134.8, 127.3, 120.1, 109.8, 94.9, 70.2, 44.2, 31.4, 25.0, 21.4, 18.7 ppm. **MS:** *m/z* calcd. for C₁₄H₁₅ClNO [M + H]⁺: 236.1176, found 248.1.

Substrate (IV.3.t):



Int-15: The procedure used was a modification of that reported by Gilman.⁶⁷ To 5-hexyn-1-ol (9.816 g, 100 mmol) in acetone (1000 mL) at 0 °C was added Jones' reagent drop by drop with vigorous stirring until the mixture remained slightly orange. Slow addition was necessary to keep the blue precipitate which was formed from forming a gum, thus stopping the stirrer. The ice bath was removed, and more oxidizing reagent was added to maintain the orange color. After 1 h at room temperature, isopropyl alcohol was added to decompose the excess Jones' reagent. The mixture was filtered through Celite, and the salts were washed several times with acetone. Removal of the solvent by rotary evaporation produced a blue oil (contaminated with chromium salts), which was redissolved in ether, extracted with water, and dried over MgSO_4 . Evaporation of the ether gave an oil, distillation of which through a Kugelrohr apparatus yielded a colorless oil (3.46 g, 64 % yield).

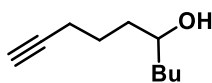
$^1\text{H NMR}$ (400 MHz, CDCl_3): δ = 2.54 (t, J = 7.4 Hz, 2H), 2.31 (td, J = 6.9, 2.7 Hz, 2H), 2.00 (t, J = 2.6 Hz, 1H), 1.87 (p, J = 7.2 Hz, 2H) ppm. $^{13}\text{C NMR}$ (101 MHz, CDCl_3): δ = 179.4, 82.8, 71.2, 30.9, 26.3, 20.9 ppm.



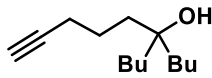
Int-16: To a mixture of the corresponding carboxylic acid (10.0 mmol), N,O-dimethylhydroxylamine hydrochloride (1.268 g, 13.0 mmol) and DMAP (0.122 g, 1.0 mmol) in DCM (50.0 mL) at 0 °C were added NEt_3 (1.8 mL, 13.3 mmol) and EDC (2.492 g,

13.0 mmol) successively. The reaction mixture was stirred at 0 °C for 1 h, then allowed to warm to room temperature and stirred overnight. The reaction was diluted with EtOAc (100 mL). The organic layer was washed with 1 N HCl (3 × 10 mL), aqueous saturated NaHCO₃ (3 × 10 mL), and brine (20 mL). The combined organic layers were dried over anhydrous Na₂SO₄, filtered, and concentrated under reduced pressure. The residue was purified by flash chromatography on silica gel (EtOAc/Hexane = 1:3).

¹H NMR (400 MHz, CDCl₃): δ = 3.71 (s, 3H), 3.19 (s, 3H), 2.58 (t, *J* = 7.4 Hz, 2H), 2.29 (td, *J* = 6.9, 2.7 Hz, 2H), 1.97 (t, *J* = 2.7 Hz, 1H), 1.88 (dt, *J* = 7.7, 6.9 Hz, 2H) ppm. ¹³C NMR (101 MHz, CDCl₃): δ = 171.1, 83.8, 68.8, 61.0, 23.2, 21.0, 18.0, 14.2 ppm.

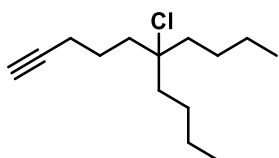


Int-17: A solution of 2-chloro-*N*-methoxy-*N*-methylacetamide (10.00 g, 72.7 mmol) in 300 mL of dry THF at 0°C was treated with 46 mL of hexylmagnesium bromide (2.0 M in diethyl ether). The mixture was allowed to slowly warm to room temperature and stir for 3 hours before being quenched with a 5% HCl solution. The reaction mixture was diluted with diethyl ether (300 mL) and the organic layer was washed once with saturated sodium bicarbonate (200 mL) and two times with brine (200 mL each). The organic layer was dried over MgSO₄ and concentrated under vacuum to give 10.86 g (92%) of the title compound, a yellow. It was obtained the monoalkylated product clean enough for the next step without purification.



Int-18: A solution of 205 mL ethynylmagnesium bromide (0.5M in THF) at 0°C was treated with a solution of 1-chloro-2-octanone (9.83g, 60.4 mmol) in 30 mL of dry THF.⁸⁰ The combined solution was stirred at 0°C for 22 hours before being diluted with Hexanes (300 mL) and quenched with saturated ammonium chloride. The organic layer was washed three times with brine (200 mL), dried over MgSO₄, and concentrated under vacuum to give 10.70g (94%) of the title compound, a dark orange oil that was used without further purification.

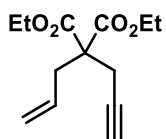
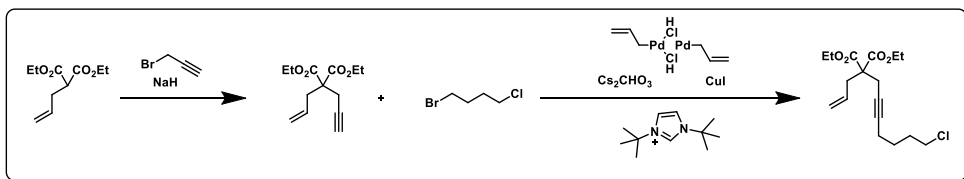
¹H NMR (400 MHz, CDCl₃): δ = 2.22 (tdd, *J* = 4.0, 2.6, 1.5 Hz, 2H), 1.97 (t, *J* = 2.6 Hz, 1H), 1.93 – 1.78 (m, 2H), 1.58 – 1.50 (m, 4H), 1.48 – 1.38 (m, 4H), 1.35 – 1.27 (m, 4H), 1.22 (m, 2H), 0.97 – 0.85 (m, 6H) ppm.



Substrate (IV.3.t): General procedure: A mixture of alcohol (0.5 mmol) in the case of solids, which had been powdered for 1-2 min and halosilanes (0.55 mmol) was transferred to a 4 mL screw-capped vial, and stirred at rt or heated at 70-75 °C for 0.5 h-24 h. The progress of the reaction mixture was monitored by TLC. Upon completion of the reaction, the crude reaction mixture was cooled down to the room temperature and volatile product (TMS)₂O was removed by evaporation at 30-35°C under reduced pressure. Finally, the pure final product was obtained after column chromatography on dried silica (80:20) yielding 120 mg of the desired product as colorless oil (60%).

¹H NMR (400 MHz, CDCl₃): δ = 2.24 (td, *J* = 6.9, 2.6 Hz, 2H), 1.99 (t, *J* = 2.7 Hz, 1H), 1.91 – 1.84 (m, 2H), 1.80 – 1.73 (m, 2H), 1.73 – 1.62 (m, 2H), 1.43 – 1.29 (m, 6H), 0.99 – 0.89 (m, 6H) ppm. **¹³C NMR** (101 MHz, CDCl₃): δ = 84.1, 78.2, 68.6, 41.0 (2C), 40.4, 26.4 (2C), 23.4, 22.9 (2C), 18.6, 14.02 (2C) ppm. **MS:** *m/z* calcd. for C₁₄H₂₅ [M - Cl]⁺: 193.1962, found 193.1951.

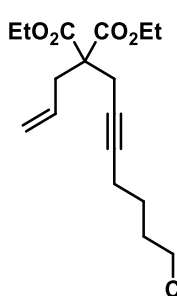
Substrate (IV.3.u):



Int-19: To a suspension of NaH (0.10 g, 4.18 mmol, 1.2 eq.) in THF (3 mL) was added at rt a solution of diethyl- 2-allyl-malonate (0.3g, 1.49 mmol, 1.0 eq.) in THF (1 mL). The mixture was stirred at rt for 40 min in which it became a nearly clear solution. To this solution was added dropwise a solution of 1-bromo-2-chloroethane (1.0 g, 6.96 mmol, 2.0 eq.) in DMF

(3 mL). The mixture was stirring at room temperature overnight. The reaction was quenched by addition of 15 mL of water and extracted with diethyl ether (3 x 15 mL). The combined organic extracts were dried over MgSO₄, the solvent was removed under reduce pressure and the crude material was purified by column chromatography yielding 0.28g (78 %) of the desired product as a colorless oil.

¹H NMR (300 MHz, CDCl₃): δ = 5.63 (ddt, *J* = 17.4, 10.1, 7.5 Hz, 1H), 5.27 – 5.09 (m, 2H), 4.21 (q, *J* = 7.1 Hz, 4H), 2.88 – 2.72 (m, 4H), 2.01 (t, *J* = 2.7 Hz, 1H), 1.25 (t, *J* = 7.1 Hz, 6H) ppm. ¹³C NMR (101 MHz, CDCl₃): δ = 169.7 (2C), 131.7, 119.8, 78.9, 71.4, 61.7 (2C), 56.6, 36.4, 22.6, 14.1 (2C) ppm.

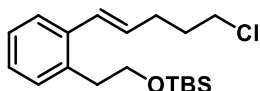
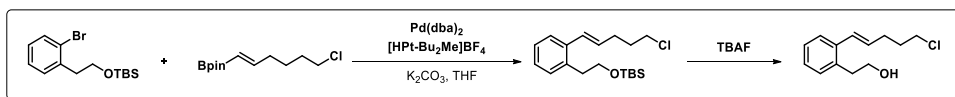


Substrate (IV.3.u): Isolated as colorless oil in 76 % yield (0.314 mg, 1.259 mmol).

¹H NMR (400 MHz, CDCl₃): δ = 5.82 – 5.49 (m, 1H), 5.41 – 4.95 (m, 2H), 4.21 (q, *J* = 7.1 Hz, 4H), 3.57 (t, *J* = 6.6 Hz, 2H), 3.12 – 2.67 (m, 4H), 2.33 – 2.05 (m, 2H), 2.02 – 1.80 (m, 2H), 1.77 – 1.59 (m, 2H), 1.27 (t, *J* = 7.1 Hz, 6H) ppm. ¹³C NMR (101 MHz,

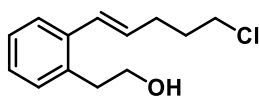
CDCl₃): δ = 170.0, 132.0, 119.5, 82.6, 75.2, 61.5, 57.0, 44.6, 36.5, 31.4, 29.7, 26.0, 22.9, 17.9, 14.1 ppm. **MS:** *m/z* calcd. for C₁₇H₂₆ClO₄ [M + Na]⁺: 329.1514, found 329.1520.

Substrate (IV.3.v):



In a Schlenk tube with rubber septum the hydroboration product (1.0 eq.) was dissolved in 1,4-dioxane/H₂O (5:1, 24 mL). K₂CO₃(3.0 eq.), aryl bromide (1.0–1.4 eq.) and PdCl₂(dppf)DCM(0.05 eq.) were added and the mixture was stirred for 6 h at 70°C.⁸¹ After cooling to room temperature the reaction mixture was quenched with sat. aq. NH₄Cl (15 mL) and extracted with Et₂O (2 x 20 mL). Combined organic layers were dried over MgSO₄

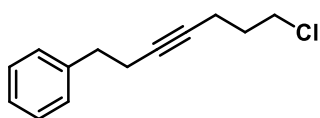
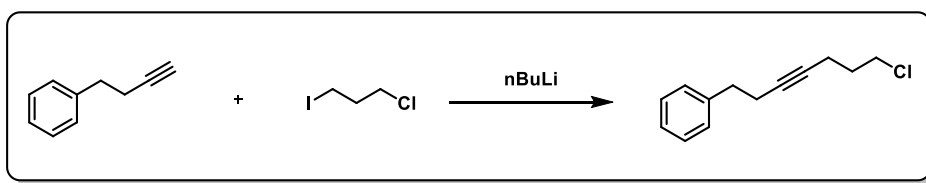
and concentrated in vacuum. Purification by column chromatography delivered: 120 mg fairly clean (impurity 6% by NMR) and 620 mg of mixed fraction. The spectroscopic data is in agreement with previously reported data for this compound.⁸²



Substrate (IV.3.v): To a solution of TBS-ether in THF (1 mL) was added TBAF (1 M in THF, 1.3 eq.) at 0 °C. The mixture was stirred until complete conversion of starting material was observed by TLC. The reaction was quenched with sat. aq. NH₄Cl (5 mL) and diluted with Et₂O (5 mL). The organic layer was separated and the aq. layer was extracted with Et₂O (3 x 5 mL). The combined org. extracts were dried over MgSO₄ and the solvent was removed under reduced pressure. Crude material was purified by column chromatography (20% → 30% → 40% → 50% Et₂O in Hexane).

¹H NMR (400 MHz, CDCl₃): δ = 7.47 – 7.40 (m, 1H), 7.21 – 7.11 (m, 3H), 6.72 (d, *J* = 15.6 Hz, 1H), 6.05 (dt, *J* = 15.6, 7.1 Hz, 2H), 3.94 – 3.73 (m, 2H), 3.60 (t, *J* = 6.5 Hz, 2H), 2.96 (t, *J* = 6.8 Hz, 2H), 2.41 (qd, *J* = 7.2, 1.5 Hz, 2H), 1.96 (dq, *J* = 8.0, 6.6 Hz, 2H) ppm. **¹³C NMR** (126 MHz, CDCl₃): δ = 135.2, 133.0, 130.9, 130.3, 128.7, 127.3, 126.9, 126.3, 63.2, 44.3, 36.5, 32.1, 30.3 ppm. **MS:** *m/z* calcd. for C₁₃H₁₇ClO [M]⁺: 224.1, found 224.1.

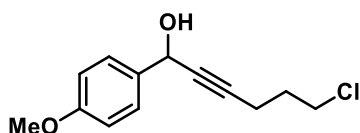
Substrate (IV.5.aa):



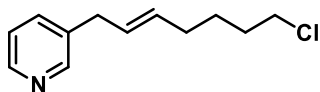
Substrate (IV.5.aa): To a stirred solution of the terminal alkyne (1.0 eq) in dry THF (0.3 M) under Ar at -78 °C, n-BuLi (2.5 M, 1.03 eq.) was slowly added by syringe (After the addition of the BuLi solution, the solution change to yellow).⁸³ The reaction mixture was stirred for 30 min and then warmed up to room temperature. Then, 1,4-diiodobutane (1.5 eq.) was added and the mixture was

refluxed until total consumption of the alkyne. The reaction was then cooled down to room temperature, diluted with diethyl ether, washed with water (2 x 10 mL), sodium thiosulfate (aq. 10%) and brine (2 x 10 mL). The organic layer was dried over anhydrous MgSO₄, filtered, and concentrated under vacuum. The residue was purified by silica gel flash chromatography (Hexane 99:1 EtOAc) to deliver the corresponding alkyl chloride. (623 mg, 57 % yield).

¹H NMR (400 MHz, CDCl₃): δ = 7.35 – 7.27 (m, 2H), 7.25 – 7.20 (m, 3H), 3.58 (t, *J* = 6.4 Hz, 2H), 2.81 (t, *J* = 7.5 Hz, 2H), 2.46 (tt, *J* = 7.4, 2.4 Hz, 2H), 2.33 (tt, *J* = 6.7, 2.4 Hz, 2H), 1.90 (p, *J* = 6.5 Hz, 2H) ppm. ¹³C NMR (101 MHz, CDCl₃): δ = 140.8, 128.5, 128.5, 128.3, 128.3, 126.2, 80.0, 79.0, 43.8, 35.4, 31.7, 20.9, 16.2 ppm. MS: *m/z* calcd. for C₁₃H₁₅Cl [M]⁺: 206.1, found 205.9.



Substrate (IV.5.ab): In a Schlenk, 1.6 M BuLi was added dropwise (4.59 ml, 7.34 mmol) to a solution of the 5-chloropent-1-yne (0.769 g, 7.34 mmol) in THF (10 ml) at -78°C, then the reaction mixture was warmed up to rt for 30 mins. Then, 4-methoxybenzaldehyde (1 g, 7.34 mmol) was added and the mixture was stirred overnight at rt. The crude was extracted with DCM water and organic phase is dried over MgSO₄ and the solvent removed under reduced pressure. The crude was purified by flash chromatography by silica Hexane/acetate (90:10). ¹H NMR (500 MHz, CDCl₃): δ = 7.49 – 7.34 (m, 2H), 6.94 – 6.82 (m, 2H), 5.39 (d, *J* = 5.9 Hz 1H), 3.80 (s, 3H), 3.64 (t, *J* = 6.3 Hz 2H), 2.47 (td, *J* = 6.8 Hz 2H), 2.04 – 1.90 (m, 2H) ppm. ¹³C NMR (126 MHz, CDCl₃): δ = 160.0, 133.7, 128.3 (2C), 114.3 (2C), 85.6, 81.5, 64.7, 55.7, 44.0, 31.6, 16.6 ppm. MS: *m/z* calcd. for C₁₃H₁₅ClNaO₂ [M + Na]⁺: 261.0653, found 261.0655.

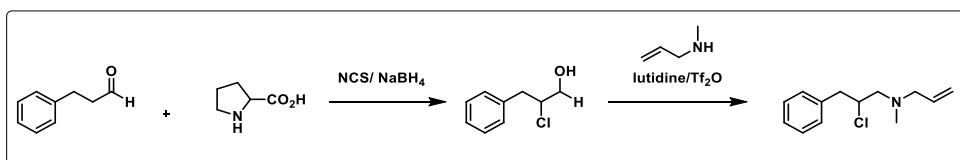


Substrate (IV.3.w): 3-Bromomethyl pyridine hydrobromide (0.37 g, 1.46 mmol, 1.0 eq.) was added to a Schlenk flask containing, Na₂CO₃ (0.74 g, 7.02 mmol, 4.8 eq.), Pd(PPh₃)₄ (0.15

g, 0,13 mmol, 9 mol%) and (*E*)-6-chloro-1-hexen-1-ylboronic acid pinacol ester (0.36 g, 1,46 mmol, 1.0 eq.) in 1,4-dioxane/H₂O (4:1, 5 mL). The mixture was stirred for 18 h at 80 °C. After reaching room temperature the reaction was quenched by addition of saturated aqueous NH₄Cl (10 mL) and diluted with Et₂O (10 mL). The organic layer was separated and the aqueous layer was extracted with Et₂O (3 × 10 mL). The combined organic extracts were washed with saturated aqueous NaCl (2 × 10 mL) and dried over MgSO₄. The solvent was removed under reduced pressure and the crude material was purified by flash chromatography (SiO₂, 10 % Et₂O → 20 % Et₂O) to yield 130 mg (42 %) of title compound as yellow oil which darkens on standing.

¹H NMR (400 MHz, CDCl₃): δ = 8.44 (dd, *J* = 5.1, 1.9 Hz, 2H), 7.52 - 7.43 (m, 1H), 7.21 (ddd, *J* = 7.8, 4.8, 0.9 Hz, 1H), 5.62 - 5.44 (m, 2H), 3.53 (t, *J* = 6.7 Hz, 2H), 3.33 (d, *J* = 5.8 Hz, 2H), 2.12 - 2.02 (m, 2H), 1.83 - 1.72 (m, 3H) ppm. ¹³C NMR (101 MHz, CDCl₃) δ = 150.1, 147.6, 136.2, 136.1, 132.3, 128.4, 123.4, 45.0, 36.2, 32.1, 31.8, 26.6 ppm. IR (film): 2937, 1478, 1422, 970 cm⁻¹. MS: *m/z* calcd. for C₁₂H₁₇ClN [M + H]⁺: 210.1044, found 210.1047.

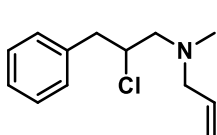
Substrate (IV.3.x):



Int-21: Suspended 3-phenylpropanal (1.5 g, 11.18 mmol) in anhydrous DCM (30 mL) and cooled to 0 °C. DL-proline (257 mg, 2.23 mmol) was added followed by *N*-chlorosuccinimide (1.94 g, 14.53 mmol). Once complete, methanol (31.0 mL) was added at 0 °C followed by slow addition of sodium borohydride (2.15 g, 55.9 mmol). Continued stirring for 30 minutes before water was added and the solution was extracted with DCM. After drying over sodium sulfate, filtering, and concentrating, the crude

material was purified by column chromatography (10% ethyl acetate in Hexanes) to yield chloro-alcohol 0.96 g, (50%).

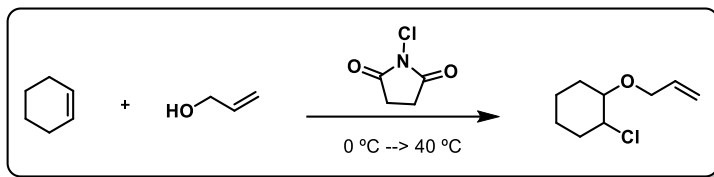
¹H NMR (400 MHz, CDCl₃): δ = 7.39 – 7.19 (m, 5H), 3.89 – 3.78 (m, 1H), 3.72 (dt, *J* = 12.2, 6.2 Hz, 1H), 3.17 (dd, *J* = 14.1, 7.0 Hz, 1H), 3.09 (dd, *J* = 14.1, 7.4 Hz, 1H) ppm. **¹³C NMR** (101 MHz, CDCl₃) δ = 137.1, 129.3 (2C), 128.6 (2C), 127.0, 65.9, 64.9, 40.7 ppm.

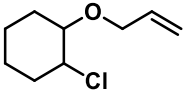


Substrate (IV.3.x): 2-chloro-4-phenylpropan-1-ol (0.92 g, 5.39 mmol) was dissolved in DCM (20 mL) and to this 2,6-lutidine (5 mL, 43.1 mmol) was added. This solution was cooled to -78 °C before triflic anhydride (1.2 mL, 7.01 mmol) was added dropwise. The solution stirred for 30 minutes *N*-methylprop-2-en-1-amine (1.8 mL, 19.41 mmol) in DCM (2.0 mL) was added to the solution dropwise. The solution was allowed to reach ambient temperature overnight. The reaction was quenched by addition of sat. aq. NH₄Cl (15 mL) and the org. layer was separated. The aq. layer was extracted with DCM (3 x 10 mL) and the combined org. extracts were dried over MgSO₄. The solvent was removed under reduced pressure and the crude material was purified by column chromatography to yield 0.76g of title compound.⁸⁴

¹H NMR (400 MHz, CDCl₃): δ = 7.39 – 7.21 (m, 5H), 5.88 (ddt, *J* = 16.8, 10.2, 6.5 Hz, 1H), 5.30 – 5.09 (m, 2H), 4.33 – 4.07 (m, 1H), 3.29 (dd, *J* = 14.3, 4.5 Hz, 1H), 3.10 (dq, *J* = 6.6, 1.3 Hz, 2H), 2.92 (dd, *J* = 14.3, 8.5 Hz, 1H), 2.81 – 2.58 (m, 2H), 2.55 (s, 3H) ppm. **¹³C NMR** (101 MHz, CDCl₃) δ = 137.9, 135.1, 131.78, 129.4 (2C), 128.3 (2C), 126.7, 63.0, 61.2, 60.8, 42.7, 42.4 ppm.

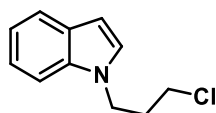
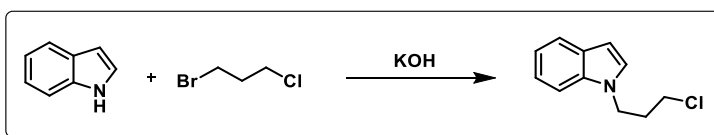
Substrate (IV.3.y):



 *Substrate (IV.3.y)*: A vigorously stirred suspension of NCS (2.6 g, 20 mmol) in ice chilled allyl alcohol (8 mL) was treated with cyclohexene (2 mL, 20 mmol) as previously described. The reaction mixture was stirred at 0°C for 1 h, then warmed to 40 °C. After being stirred overnight, the mixture was poured onto crushed ice and extracted with diethyl ether. Silica gel chromatography (Hexane 95: 5 EtOAc) of the crude residue furnished the desired chloride as a colorless oil (0.236g, 56 %).

¹H NMR (500 MHz, CDCl₃): δ = 6.05 – 5.82 (m, 1H), 5.29 (dd, *J* = 17.2, 1.7 Hz, 1H), 5.16 (dd, *J* = 10.3, 1.6 Hz, 1H), 4.18 – 4.07 (m, 2H), 3.85 (ddd, *J* = 9.7, 8.0, 4.3 Hz, 1H), 3.48 – 3.12 (m, 1H), 2.50 – 2.11 (m, 1H), 2.08 (ddd, *J* = 9.2, 4.4, 1.7 Hz, 1H), 1.82 – 1.60 (m, 3H), 1.50 – 1.12 (m, 3H) ppm. **¹³C NMR** (126 MHz, CDCl₃): δ = 135.2, 116.8, 81.0, 70.9, 62.7, 34.6, 30.4, 24.2, 23.1 ppm. **MS**: *m/z* calcd. for C₉H₁₅ClO [M + Na]⁺: 174.6, found 174.0.

Substrate (IV.3.z):

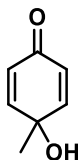
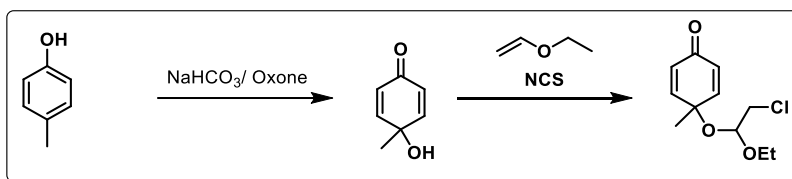


Substrate (IV.3.z): Potassium Hydroxide (1,24g, 22,2 mmol) was added to a solution of indole (2g, 17,07 mmol) in DMSO (10 mL). The suspension was sonicated for 10 min before 1-bromo-chloropropane (5,38g, 34.1 mmol) was added. The reaction was stirred overnight at rt. The reaction was quenched by addition of H₂O (20 mL) and diluted with Et₂O (30 mL). The organic layer was separated and the aq. layer was extracted with Et₂O (2 x 20 mL). The combined organic extracts were dried over MgSO₄ and

the solvent was removed under reduced pressure. Column chromatography: Hexane -> 1% Et₂O in Hexane yielded 2.15 g of product (65 %).

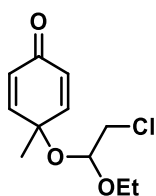
¹H NMR (400 MHz, CDCl₃): δ = 7.65 (dd, *J* = 7.9, 1.0 Hz, 1H), 7.41 – 7.34 (m, 1H), 7.29 – 7.19 (m, 1H), 7.16 – 7.08 (m, 2H), 6.52 (dd, *J* = 3.2, 0.9 Hz, 1H), 4.35 (t, *J* = 6.4 Hz, 2H), 3.46 (t, *J* = 6.0 Hz, 2H), 2.38 – 2.13 (m, 2H) ppm. ¹³C NMR (101 MHz, CDCl₃): δ = 135.8, 128.7, 128.0, 121.7, 121.1, 119.5, 109.2, 101.5, 42.9, 41.9, 32.6 ppm.

Substrate (IV.3.aa):



Int-22: *p*-Cresol (1,10g, 10,2 mmol) was dissolved in a mixture of H₂O (140 mL) and CH₃CN (42 mL). To this solution was added a fine powdered mixture of NaHCO₃ (20,51g, 244 mmol) and Oxone (25,01g, 81 mmol) in one portion. Immediately after addition the flask was capped with a septum connected to a balloon to trap the produced oxygen. The mixture was stirred overnight and the reaction was quenched by addition sat. aq. Na₂S₂O₃ (50 mL). The mixture was diluted by Et₂O and the organic layer was separated. The aq. layer was extracted with Et₂O (3 x 30 mL) and the combined organic extracts were dried over MgSO₄. The solvent was removed under reduced pressure and the obtained crude material was purified by column chromatography (SiO₂, 40% -> 50% -> 60% Et₂O in Hexane) to obtain 460 mg of an off-white solid.

¹H NMR (400 MHz, CDCl₃): δ = 6.88 (d, *J* = 10.1 Hz, 2H), 6.13 (d, *J* = 10.1 Hz, 2H), 1.48 (d, *J* = 0.7 Hz, 3H) ppm. ¹³C NMR (101 MHz, CDCl₃) δ = 185.2, 151.8 (2C), 127.3 (2C), 65.8, 15.3 ppm.

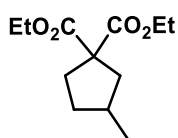


Substrate (IV.3.aa): NCS (0,68g, 5, 16 mmol) was added to a mixture of ethyl vinyl ether (0, 37 mL, 3, 87 mmol) and cyclohexadienone (0, 32g, 2, 58 mmol) in DCM (3 mL) at -25 °C. The mixture was allowed to reach ambient temperature over the course of 2 h. The mixture was further stirred for 24 h at ambient temperature at which point no further conversion was observed according to TLC. The reaction was quenched by addition of sat. aq. Na₂S₂O₃ (10 mL) and diluted with Et₂O (10 mL). The organic layer was separated and the aq. phase was extracted with Et₂O (3 x 10 mL). The combined organic extracts were washed with H₂O (2 x 10 mL) and dried over MgSO₄. The solvent was removed under reduced pressure and the crude material was purified by column chromatography (SiO₂, 20% ->30% ->40% Et₂O in Hexane) to obtain 0.21g (35%) of desired product as a colorless oil and recovering 90 mg of the starting compound.

¹H NMR (400 MHz, CDCl₃): δ = 7.00 (dd, *J* = 10.2, 3.1 Hz, 1H), 6.81 (dd, *J* = 10.2, 3.1 Hz, 1H), 6.32 (dd, *J* = 10.2, 2.0 Hz, 1H), 6.20 (dd, *J* = 10.2, 2.0 Hz, 1H), 4.42 (dd, *J* = 6.2, 4.5 Hz, 1H), 3.81 – 3.24 (m, 4H), 1.50 (s, 3H), 1.16 (t, *J* = 7.0 Hz, 3H) ppm. **¹³C NMR** (101 MHz, CDCl₃): δ = 183.4, 152.1, 150.2, 130.3, 127.5, 99.6, 72.8, 62.9, 44.3, 26.4, 15.1 ppm.

IV.5. 6 Synthesis and Characterization of Products.

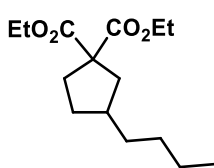
Reductive cyclization from non-activated alkyl chlorides with tethered alkenes.



Product (IV.4.b): Cyclization according to general procedure: scale 0.3 mmol, flash chromatography (SiO₂, 100 % Hexane) yielded 64 mg (93 %) of the title compound as a colorless liquid.

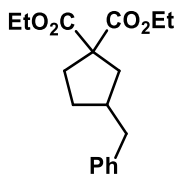
¹H NMR (400 MHz, CDCl₃): δ = 4.19 (q, *J* = 7.1 Hz, 4H), 2.51 - 2.41 (m, 1H), 2.33 (ddd, *J* = 13.6, 8.5, 3.8 Hz, 1H), 2.21 - 2.12 (m, 1H), 2.10 - 2.01 (m, 1H), 1.91 – 1.80 (m, 1H), 1.72 - 1.60 (m, 1H), 1.25 (t, *J* = 7.1 Hz, 6H), 1.03 (d, *J* = 6.6 Hz, 3H) ppm. **¹³C NMR** (101 MHz, CDCl₃) δ = 172.8 (2C), 61.2 (2C), 60.5, 42.5, 34.5, 34.2, 34.0,

29.7, 19.6, 14.0 (2C) ppm. **IR** (film): 2955, 2928, 2871, 1728, 1446, 1252, 1158, 859 cm^{-1} . **MS** (ESI-pos): m/z 229.1 $[\text{M} + \text{H}^+]$. The spectroscopic characterization is in agreement with the literature reported.³⁰



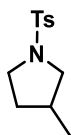
Product (IV.4.c): Cyclization according to general procedure: scale 0.3 mmol, flash chromatography (SiO_2 , 0 % \rightarrow 2 % Et_2O in Hexane) yielded 79 mg (79 %) of the title compound as a light yellow liquid.

^1H NMR (400 MHz, CDCl_3): δ = 4.19 (qd, J = 7.1, 1.6 Hz, 4H), 2.50 - 2.43 (m, 1H), 2.31 (ddd, J = 13.5, 8.5, 3.6 Hz, 1H), 2.14 (ddd, J = 13.5, 9.4, 7.3 Hz, 1H), 2.01 - 1.83 (m, 2H), 1.70 (dd, J = 13.3, 9.9 Hz, 1H), 1.60 (s, 1H), 1.29 - 1.21 (m, 9H), 0.96 - 0.85 (m, 3H) ppm. **^{13}C NMR** (101 MHz, CDCl_3) δ = 172.8 (2C), 61.2 (2C), 60.0, 40.8, 39.8, 35.0, 33.8, 32.2, 30.7, 22.8, 14.1, 14.0 (2C) ppm. **IR** (film): 2957, 2927, 1728, 1465, 1446, 1253, 1175, 1157, 860 cm^{-1} . **MS**: m/z calcd. for $\text{C}_{13}\text{H}_{29}\text{NaO}_4$ $[\text{M} + \text{Na}]^+$: 293.1729, found 293.1723.



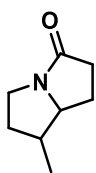
Product (IV.4.d): Cyclization according to general procedure: scale 0.2 mmol, flash chromatography (SiO_2 , 0 % \rightarrow 5 % Et_2O in Hexane) yielded 73 mg (93 %) of the title compound as a light yellow liquid.

^1H NMR (400 MHz, CDCl_3): δ = 7.38 - 7.25 (m, 2H), 7.24 - 7.14 (m, 3H), 4.19 (dq, J = 11.5, 7.0 Hz, 4H), 2.67 (qd, J = 13.5, 7.4 Hz, 2H), 2.48 - 2.38 (m, 1H), 2.38 - 2.25 (m, 2H), 2.23 - 2.10 (m, 1H), 1.85 (dd, J = 13.3, 9.6 Hz, 2H), 1.47 - 1.32 (m, 1H), 1.25 (dt, J = 10.0, 7.5 Hz, 6H) ppm. **^{13}C NMR** (101 MHz, CDCl_3) δ = 172.7, 172.7, 141.2, 128.7, 128.3, 125.8, 61.3, 61.3, 60.0, 41.5, 41.3, 40.4, 33.7, 32.0, 14.0 (2C) ppm. **IR** (film): 3027, 2981, 2937, 1726, 1603, 1496, 1453, 1366, 1248, 1207, 1176, 1097, 1029, 860, 745, 700 cm^{-1} . **MS**: m/z calcd. for $\text{C}_{18}\text{H}_{24}\text{NaO}_4$ $[\text{M} + \text{Na}]^+$: 327.1572, found 327.1567.



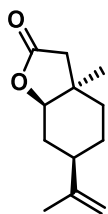
Product (IV.4.e): Cyclization according to general procedure: Scale 0.24 mmol, flash chromatography (SiO₂, 90 % Et₂O → 100 % in Hexane) yielded 59 mg (63 %) of title compound as an orange/brown liquid, which darkens rapidly on standing.

¹H NMR (400 MHz, CDCl₃): δ = 7.70 (d, J = 8.2 Hz, 2H), 7.33 – 7.25 (m, 2H), 3.41 (dd, J = 9.7, 7.1 Hz, 1H), 3.33 (ddd, J = 9.8, 8.2, 4.2 Hz, 1H), 3.25 – 3.16 (m, 1H), 2.73 (dd, J = 9.7, 7.8 Hz, 1H), 2.42 (s, 3H), 2.10 (ddt, J = 13.6, 8.2, 6.8 Hz, 1H), 1.88 (ddd, J = 13.9, 7.2, 3.5 Hz, 1H), 1.39 – 1.30 (m, 1H), 0.90 (d, J = 6.7, 0.6 Hz, 3H) ppm. **¹³C NMR** (101 MHz, CDCl₃) δ = 143.3, 134.0, 129.6, 127.5, 54.8, 47.6, 33.3, 33.2, 21.5, 17.6 ppm. **IR** (film): 2960, 2923, 2878, 2852, 1720, 1598, 1456, 1334, 1157, 1088, 1038, 814, 800, 659, 590, 544 cm⁻¹. **MS**: m/z calcd. for C₁₂H₁₇NO₂S [M]⁺: 239.1, found 239.1.



Product (IV.4.f): Cyclization according to general procedure: scale 0.24 mmol, flash chromatography (SiO₂, 90 % Et₂O → 100 % in Hexane, then 10 % MeOH in Et₂O) yielded 27.7 mg (83 %) of title compound as an orange/brown liquid, which darkens rapidly on standing.

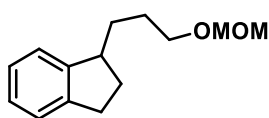
¹H NMR (400 MHz, CDCl₃): δ = 3.60 - 3.28 (m, 2H), 3.15 (ddt, J = 11.5, 9.5, 1.8 Hz, 1H), 2.72 (ddd, J = 16.7, 10.7, 9.4, 1.3 Hz, 1H), 2.44 (ddd, J = 16.7, 9.7, 2.3 Hz, 1H), 2.36 – 2.19 (m, 2H), 1.78 - 1.56 (m, 3H), 1.04 ppm (d, J = 6.2 Hz, 3H) ppm. **¹³C NMR** (101 MHz, CDCl₃) δ = 174.8, 68.3, 41.1, 40.7, 35.7, 35.0, 25.3, 15.4 ppm. **IR** (film): 3458, 2957, 2930, 2872, 1679, 1562, 1409, 1250 cm⁻¹. **MS**: m/z calcd. for C₈H₁₄NO [M + H]⁺: 140.1070, found 140.1071.



Product (IV.4.g): Cyclization according to general procedure: scale 0.24 mmol yielded 41 mg (66 % over 2 steps) of the title compound a light yellow liquid. The reaction crude containing a mixture of diastereoisomeric hemiacetals was dissolved in acetone (4 mL), cooled to 0 °C and Jones reagent (2 M CrO₃ in aqueous H₂SO₄, 0.26 mL, 0.53 mmol, 2.2 eq.) was added dropwise. The mixture was stirred for 90 min at 0 °C. After

complete conversion of starting material as judged by TLC the reaction was diluted with Et₂O (10 mL) and carefully quenched by addition of 2-propanol (1 mL). Saturated aqueous NaHCO₃ (10 mL) was added and the organic layer was separated. The aqueous layer was extracted with Et₂O (3 x 10 mL) and the combined organic extracts were dried over MgSO₄. The solvent was removed under reduced pressure and the crude material was purified by column chromatography (SiO₂, 5 % → 10 % → 20 % Et₂O in Hexane).

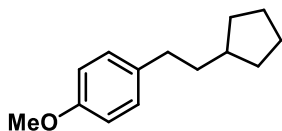
¹H NMR (400 MHz, CDCl₃): δ = 4.78 - 4.65 (m, 2H), 4.17 (dd, *J* = 10.6, 6.4 Hz, 1H), 2.64 (dd, *J* = 17.0, 0.9 Hz, 1H), 2.21 (ddt, *J* = 13.3, 6.4, 2.6 Hz, 1H), 2.00 (d, *J* = 17.0 Hz, 1H), 1.93 - 1.82 (m, 2H), 1.73 (t, *J* = 1.1 Hz, 3H), 1.52 - 1.40 (m, 1H), 1.37 - 1.21 (m, 1H), 1.18 (d, *J* = 0.8 Hz, 3H), 0.90 - 0.82 ppm (m, 2H) ppm. **¹³C NMR** (101 MHz, CDCl₃) δ = 176.8, 148.1, 109.6, 85.2, 41.5, 38.5, 38.1, 35.3, 33.6, 28.5, 26.9, 21.0 ppm. **IR** (film): 2931, 2858, 1774, 1456, 1158, 979, 886 cm⁻¹. **MS**: *m/z* calcd. for C₁₂H₁₈NaO₂ [M + Na]⁺: 217.1199, found 217.1199.



Product (IV.4.h): Cyclization according to general procedure: Scale 0.24 mmol, flash chromatography (SiO₂, 5 % → 10 % Et₂O in Hexane) yielded 27.3 mg (52 %) of

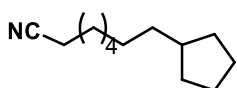
title compound as a light yellow oil.

¹H NMR (400 MHz, CDCl₃): δ = 7.25 - 7.19 (m, 2H), 7.19 - 7.14 (m, 2H), 4.65 (s, 2H), 3.59 (t, *J* = 6.6 Hz, 2H), 3.38 (s, 3H), 3.14 (m, 1H), 2.94 (ddd, *J* = 15.1, 8.5, 4.8 Hz, 1H), 2.86 (m, 1H), 2.31 (dtd, *J* = 12.6, 7.9, 4.8 Hz, 1H), 2.04 - 1.90 (m, 1H), 1.85 - 1.65 (m, 3H), 1.55 - 1.43 (m, 1H) ppm. **¹³C NMR** (101 MHz, CDCl₃) δ = 147.5, 144.1, 126.4, 126.1, 124.5, 123.7, 96.6, 68.1, 55.2, 44.7, 32.2, 31.7, 31.5, 28.0 ppm. **IR** (film): 2930, 1146, 1109, 1041, 918 cm⁻¹. **MS**: *m/z* calcd. for C₁₄H₂₀NaO₂ [M + Na]⁺: 243.1356, found 243.1350.



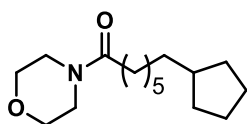
Product (IV.4.i): Cyclization according to general procedure: scale 0.3 mmol, flash chromatography (SiO₂, 5 % → 10 % Et₂O in Hexane) yielded 46 mg (76 %) of the title compound as a light liquid yellow oil.

¹H NMR (400 MHz, CDCl₃): δ = 7.13 - 7.07 (m, 2H), 6.86 - 6.79 (m, 2H), 3.79 (s, 3H), 2.86 - 2.45 (m, 2H), 1.95 - 1.73 (m, 3H), 1.64 - 1.48 (m, 6H), 1.20 - 1.06 (m, 2H) ppm. **¹³C NMR** (101 MHz, CDCl₃): δ = 157.7, 135.1, 129.3 (2C), 113.8 (2C), 55.4, 39.7, 38.5, 34.3, 32.8 (2C), 25.4 (2C) ppm. **IR** (film): 2946, 1511, 1246, 1039 cm⁻¹. **MS**: *m/z* calcd. for C₁₄H₂₁O [M + H]⁺: 205.1587, found 205.1585.



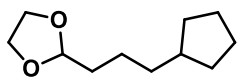
Product (IV.4.j): Cyclization according to general procedure: scale 0.24 mmol, flash chromatography (SiO₂, 5 % → 10 % → 20 % Et₂O in Hexane) yielded 22.3 mg (52 %) of title compound as a light yellow oil.

¹H NMR (400 MHz, CDCl₃): δ = 2.33 (t, *J* = 7.1 Hz, 2H), 1.79 - 1.68 (m, 3H), 1.68 - 1.61 (m, 2H), 1.61 - 1.53 (m, 2H), 1.53 - 1.39 (m, 4H), 1.37 - 1.25 (m, 6H), 1.11 - 0.99 (m, 2H) ppm. **¹³C NMR** (126 MHz, CDCl₃): δ = 120.0, 40.2, 36.2, 32.8 (2C), 29.2, 28.8, 28.6, 25.5, 25.3 (2C), 17.3 ppm. **IR** (film): 2927, 2857, 1818, 1452, 1064 cm⁻¹. **MS**: *m/z* calcd. for C₁₂H₂₂N 180.1747, found 180.1750.



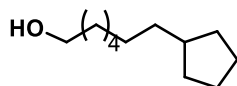
Product (IV.4.k): Cyclization according to general procedure: scale 0.24 mmol, flash chromatography (SiO₂, 5 % → 10 % → 20 % Et₂O in Hexane) yielded 52.2 mg (81 %) of title compound as a light liquid yellow oil.

¹H NMR (400 MHz, CDCl₃): δ = 3.70 - 3.64 (m, 4H), 3.61 (d, *J* = 4.9 Hz, 2H), 3.46 (t, *J* = 4.8 Hz, 2H), 2.30 (t, *J* = 7.6 Hz, 2H), 1.76 - 1.69 (m, 2H), 1.67 - 1.55 (m, 6H), 1.54 - 1.46 (m, 2H), 1.37 - 1.25 (m, 7H), 1.10 - 1.00 (m, 2H) ppm. **¹³C NMR** (101 MHz, CDCl₃): δ = 172.1, 67.1, 66.8, 46.2, 42.0, 40.3, 36.3, 33.3, 32.8 (2C), 29.8, 29.6, 28.8, 25.4, 25.3 (2C) ppm. **IR** (film): 2922, 2853, 1649, 1430, 1116 cm⁻¹. **MS**: *m/z* calcd. for C₁₆H₂₉NNaO₂ [M + Na]⁺: 290.2091, found 290.2093.



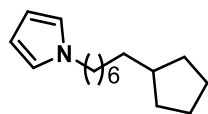
Product (IV.4.l): Cyclization according to general procedure: 0.3 mmol, flash chromatography (SiO₂, 5 % of Et₂O in Hexane) yielded 22 mg (40 % + 36 % of the starting material) of title compound as a light yellow oil.

¹H NMR (400 MHz, CDCl₃): δ = 4.84 (t, *J* = 4.8 Hz, 1H), 4.19 - 3.92 (m, 2H), 3.90 - 3.81 (m, 2H), 1.83 - 1.69 (m, 3H), 1.69 - 1.61 (m, 2H), 1.61 - 1.54 (m, 2H), 1.53 - 1.46 (m, 2H), 1.46 - 1.38 (m, 2H), 1.37 - 1.29 (m, 2H), 1.13 - 1.01 (m, 2H) ppm. **¹³C NMR** (101 MHz, CDCl₃) δ = 104.7, 64.8, 40.1, 36.1, 34.2, 32.6, 25.2, 23.3 ppm. **IR** (film): 2945, 2864, 1737, 1454, 1409, 1260, 1130, 1033, 943, 805 cm⁻¹. **MS**: *m/z* calcd. for C₁₁H₂₁O₂ [M + H]⁺: 185.1, found 185.2.



Product (IV.4.m): Cyclization according to general procedure: scale 0.3 mmol, flash chromatography (SiO₂, 5 % → 10 % → 20 % Et₂O in Hexane) yielded 42.5 mg (77 %) of title compound as a light yellow oil.

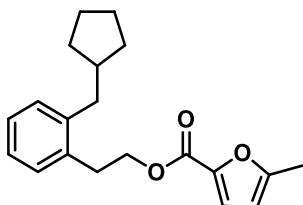
¹H NMR (400 MHz, CDCl₃): δ = 3.64 (t, *J* = 6.6 Hz, 2H), 1.79 - 1.66 (m, 3H), 1.62 - 1.44 (m, 6H), 1.31 (d, *J* = 20.7 Hz, 11H), 1.12 - 1.00 (m, 2H) ppm. **¹³C NMR** (101 MHz, CDCl₃): δ = 63.2, 40.3, 36.4, 33.0, 32.9 (2C), 30.0, 29.6, 28.8, 25.9, 25.3 (2C) ppm. **IR** (film): 2922, 2854, 1453, 1057 cm⁻¹. **IR** (film): 2922, 2854, 1453, 1057 cm⁻¹. **MS**: *m/z* calcd. For C₁₂H₂₅O [M + H]⁺: 185.1905, found 185.1888.



Product (IV.4.n): Cyclization according to general procedure: 0.24 mmol, flash chromatography (SiO₂, 5 % of Et₂O in Hexane) yielded 27 mg (48 %) of title compound as a yellow oil.

¹H NMR (400 MHz, CDCl₃): δ = 6.65 (t, *J* = 2.1 Hz, 2H), 6.14 (t, *J* = 2.1 Hz, 2H), 3.86 (t, *J* = 7.2 Hz, 2H), 1.82 - 1.68 (m, 5H), 1.64 - 1.53 (m, 2H), 1.50 (dq, *J* = 7.2, 2.9, 2.5 Hz, 2H), 1.32 - 1.22 (m, 10H), 1.11 - 1.00 (m, 2H) ppm. **¹³C NMR** (101 MHz, CDCl₃) δ = 120.6, 107.9, 49.8, 40.3, 36.3, 32.9, 31.7, 29.9, 29.4, 28.8, 26.9, 25.3 ppm. **IR** (film): 3114, 2922, 2853, 1705, 1499, 1451, 1356, 1281, 1088, 1062,

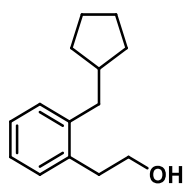
967, 717, 616 cm^{-1} . **MS:** m/z calcd. for $\text{C}_{16}\text{H}_{28}\text{N}$ $[\text{M} + \text{H}]^+$: 234.2222, found 234,2216.



Product (IV.4.o): Cyclization according to general procedure: 0.04 mmol. Aqueous work up including several washings with saturated aqueous NaCl (3 x 10 mL), drying over MgSO_4 and removal of the solvent under reduced pressure yielded 11 mg (88 %) of title

compound as a light liquid yellow oil.

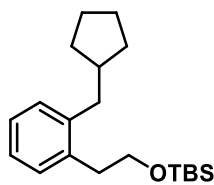
$^1\text{H NMR}$ (400 MHz, CDCl_3): δ = 7.23 - 7.12 (m, 4H), 7.08 (dd, J = 3.4, 0.6 Hz, 1H), 6.12 (dt, J = 3.4, 1.0 Hz, 1H), 4.45 (dd, J = 8.0, 7.2 Hz, 2H), 3.08 (t, J = 7.6 Hz, 2H), 2.70 (d, J = 7.4 Hz, 2H), 2.39 (s, 3H), 2.09 (dtd, J = 14.6, 7.2, 1.4 Hz, 1H), 1.78 - 1.69 (m, 2H), 1.69 - 1.59 (m, 2H), 1.56 - 1.47 (m, 2H), 1.28 - 1.18 (m, 2H) **$^{13}\text{C NMR}$** (101 MHz, CDCl_3): δ = 158.9, 157.3, 143.2, 140.8, 135.3, 130.1, 129.9, 126.7, 126.1, 119.5, 108.5, 65.1, 41.5, 38.6, 32.8 (2C), 32.1, 25.0 (2C), 14.1. **IR** (film): cm^{-1} 2949, 2860, 1718, 1530, 1298, 1134, 755. **MS:** m/z calcd. for $\text{C}_{20}\text{H}_{24}\text{NaO}_3$ $[\text{M} + \text{Na}]^+$: 335.1618, found 335.1616.



Product (IV.4.p): Cyclization according to general procedure: 0.24 mmol. Aqueous work up including several washings with saturated aqueous NaCl (4 x 10 mL), drying over MgSO_4 and

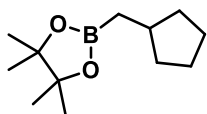
removal of the solvent under reduced pressure yielded 44 mg (90 %) of title compound as a light liquid yellow oil.

$^1\text{H NMR}$ (400 MHz, CDCl_3): δ = 7.20 - 7.13 (m, 4H), 3.85 (t, J = 7.0 Hz, 2H), 2.93 (t, J = 7.0 Hz, 2H), 2.66 (d, J = 7.4 Hz, 2H), 2.12 - 2.04 (m, 1H), 1.75 - 1.68 (m, 2H), 1.68 - 1.62 (m, 2H), 1.56 - 1.49 (m, 3H), 1.28 - 1.17 (m, 2H) ppm. **$^{13}\text{C NMR}$** (101 MHz, CDCl_3): δ = 140.8, 136.0, 130.2, 129.8, 126.5, 126.1, 63.5, 41.5, 38.7, 35.9, 32.8 (2C), 25.0 (2C) ppm. **IR** (film): 2948, 2867, 1450, 1043, 750 cm^{-1} . **MS:** m/z calcd. for $\text{C}_{14}\text{H}_{19}$ $[\text{M} - \text{H}_2\text{O}]$: 187.1481, found 187.1481.



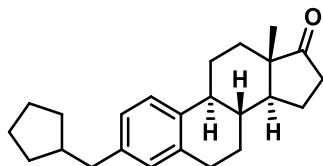
Product (IV.4.q): Cyclization according to general procedure: 0.24 mmol. Aqueous work up including several washings with saturated aqueous NaCl (4 x 10 mL), drying over MgSO₄ and removal of the solvent under reduced pressure yielded 70 mg (91 %) of title compound as a light liquid yellow oil.

¹H NMR (400 MHz, CDCl₃): δ = 7.18 - 7.04 (m, 4H), 3.77 (t, *J* = 7.6 Hz, 2H), 2.88 (t, *J* = 7.6 Hz, 2H), 2.65 (d, *J* = 7.4 Hz, 2H), 2.08 (p, *J* = 7.7 Hz, 1H), 1.76 - 1.68 (m, 2H), 1.68 - 1.62 (m, 2H), 1.54 - 1.49 (m, 2H), 1.27 - 1.19 (m, 2H), 0.89 (s, 9H), 0.02 (s, 6H) ppm. **¹³C NMR** (101 MHz, CDCl₃): δ = 140.6, 136.7, 130.1, 129.8, 126.2, 125.8, 64.5, 41.5, 38.8, 36.4, 32.8 (2C), 26.1 (3C), 25.0 (2C), 18.5, -5.2 (2C) ppm. **IR** (film): 2952, 2858, 1471, 1254, 1093 cm⁻¹. **MS:** *m/z* calcd. for C₂₀H₃₄NaOSi [M + Na]⁺: 341.2277 found 341.2273.



Product (IV.4.r): Cyclization according to general procedure: 0.3 mmol. Aqueous work up including several washings with saturated aqueous NaCl (3 x 10 mL) and filtration through a short pad of Celite[®] yielded 37.8 mg (61 %) of title compound as a yellow/brownish oil. Spectral data is in agreement with previously reported data for this compound.⁸⁵

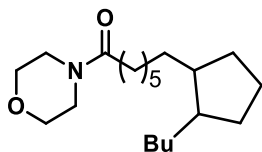
¹H NMR (400 MHz, CDCl₃): δ = 1.99 - 1.91 (m, 1H), 1.82 - 1.73 (m, 2H), 1.65 - 1.56 (m, 2H), 1.49 (ddq, *J* = 7.5, 4.6, 2.3, 1.8 Hz, 2H), 1.23 (s, 12H), 1.10 - 1.02 (m, 2H), 0.83 (d, *J* = 7.5 Hz, 2H) ppm. **¹³C NMR** (126 MHz, CDCl₃): δ = 82.9 (2C), 36.2, 35.2 (2C), 25.2 (2C), 24.9 (4C) ppm.



Product (IV.4.s): Cyclization according to general procedure: scale 0.06 mmol, flash chromatography (SiO₂, 5 % → 10 % Et₂O in Hexane) yielded 15.9 mg (79 %) of title compound as a white solid, which darkens at room temperature.

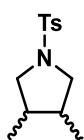
¹H NMR (400 MHz, CDCl₃): δ = 7.21 - 7.17 (m, 1H), 6.97 (dd, *J* = 7.9, 1.9 Hz, 1H), 6.91 (s, 1H), 2.93 - 2.85 (m, 2H), 2.55 (d, *J* = 7.3 Hz, 2H), 2.53 - 2.46 (m, 1H), 2.45 - 2.39 (m, 1H), 2.34 - 2.25 (m, 1H), 2.21 - 2.11 (m, 1H), 2.10 - 1.93 (m, 4H), 1.77 -

1.67 (m, 2H), 1.67 - 1.59 (m, 4H), 1.58 - 1.46 (m, 6H), 1.24 - 1.15 (m, 2H), 0.91 (s, 3H) ppm. $^{13}\text{C NMR}$ (101 MHz, CDCl_3): $\delta = 221.0, 140.0, 137.0, 136.2, 129.5, 126.4, 125.2, 50.7, 48.1, 44.5, 42.0, 41.7, 38.4, 36.0, 32.7, 31.8, 29.6, 26.8, 25.9, 25.1, 21.7, 19.5, 14.0, 1.1$ ppm. **IR** (film): 2928, 2864, 1741, 1453 cm^{-1} . **MS**: m/z calcd. for $\text{C}_{24}\text{H}_{32}\text{NaO}$ $[\text{M} + \text{Na}]^+$: 359.2345, found 359.2337.



Product (IV.4.t): Cyclization according to general procedure: 0.11 mmol, flash chromatography (SiO_2 , 10 % \rightarrow 20 % Et_2O in Hexane) yielded 23.1 mg (67 %) of title compound as a light brown oil.

$^1\text{H NMR}$ (500 MHz, CDCl_3) $\delta = 3.69$ (dd, $J = 5.7, 4.0$ Hz, 4H), 3.64 (d, $J = 5.2$ Hz, 2H), 3.49 (t, $J = 4.8$ Hz, 2H), 2.35 - 2.31 (m, 2H), 1.84 - 1.73 (m, 2H), 1.71 - 1.60 (m, 4H), 1.56 - 1.47 (m, 1H), 1.37 - 1.26 (m, 14H), 1.24 - 1.20 (m, 1H), 1.07 (td, $J = 7.3, 5.6, 2.7$ Hz, 2H), 0.93 - 0.86 (m, 3H). $^{13}\text{C NMR}$ (126 MHz, CDCl_3) δ 171.9 {mayor and minor}, 67.0 {mayor}, 66.7 {mayor}, 46.1 {mayor}, 46.0 {mayor}, 42.6 {mayor and minor}, 41.8 {mayor}, 35.3 {minor}, 35.0 {minor}, 33.2 {mayor}, 32.3 {mayor}, 30.9 {mayor}, 30.8 {minor}, 30.2 {mayor and minor}, 29.9 {mayor}, 29.8 {minor}, 29.6 {mayor}, 29.5 {minor}, 29.3 {mayor}, 29.0 {mayor}, 28.5 {mayor}, 28.4 {minor}, 25.3 {mayor and minor}, 25.3 {minor}, 23.9 {minor}, 23.1 {mayor}, 23.1 {minor}, 22.5 {mayor}, 14.2 {mayor}. **IR** (film): 2958, 2924, 2854, 1720, 1643, 1458, 1361, 1258, 1175, 1084, 1010, 791, 682, 661, 570 cm^{-1} . **MS**: m/z calcd. for $\text{C}_{20}\text{H}_{38}\text{NO}_2$ $[\text{M} + \text{H}]^+$: 324.2903 found 324.2897.

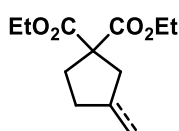


Product (IV.4.u): Cyclization according to general procedure: 0.11 mmol, flash chromatography (SiO_2 , 5 % Et_2O in Hexane) yielded 42 mg (55 %) of title compound as a light brown oil as a 4 to 1 mixture of *anti/syn* respectively.

$^1\text{H NMR}$ (400 MHz, CDCl_3) $\delta = 7.73 - 7.68$ (m, 2H), 7.30 (dq, $J = 7.8, 0.7$ Hz, 2H), 3.50 (dd, $J = 9.8, 6.9$ Hz, 1H, minor), 3.40 - 3.33 (m, 2H, mayor), 2.97 - 2.91 (m, 2H, mayor), 2.78 (t, $J = 9.4$ Hz, 1H, minor), 2.42 (d, $J = 1.5$ Hz, 4H, mayor and

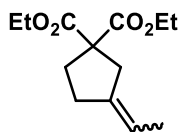
minor), 2.16 – 2.05 (m, 2H, mayor), 1.72 – 1.50 (m, 1H, minor), 0.92 – 0.88 (m, 2H, minor), 0.78 – 0.72 (m, 6H, mayor). ^{13}C NMR (101 MHz, CDCl_3) δ = 143.3, 134.3, 129.7, 129.6, 127.5, 127.5, 55.1 (2C) {minor}, 53.96 (2C) {mayor}, 40.6 (2C) {minor}, 36.3 (2C) {mayor}, 21.6 {mayor and minor}, 15.7 (2C) {minor}, 12.9 (2C) {mayor}. **IR** (film): 2964, 2255, 1598, 1454, 1340, 1155, 1094, 1017, 908, 808, 729, 665, 585, 548 cm^{-1} . **MS**: m/z calcd. for $\text{C}_{13}\text{H}_{19}\text{NO}_2\text{S}$ [M]: 253.1 found 253.1.

Reductive cyclization from non-activated alkyl chlorides with tethered alkynes.



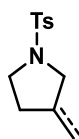
Product (IV.6.a): Cyclization according to general procedure **A**: scale 0.36 mmol, flash chromatography (SiO_2 , 2 % Et_2O in Hexane) yielded 42 mg (76 %) of title compound as a colorless oil as a mixture of alkane and alkene in a 1 to 9 ratio analyzed by GC.

^1H NMR (300 MHz, CDCl_3): δ = 5.74 – 5.56 (m, 1H), 5.19 – 5.11 (m, 1H), 4.25 – 4.13 (m, 4H), 2.69 (d, J = 7.4 Hz, 2H), 2.49 – 2.38 (m, 2H), 2.29 (d, J = 7.5 Hz, 2H), 1.31 – 1.23 (m, 6H) ppm. ^{13}C NMR (101 MHz, CDCl_3): δ = 171.7 (2C), 131.8, 119.6, 61.40(2C), 60.2, 37.8, 33.7, 31.2, 14.0 (2C) ppm. **MS**: m/z calcd. for $\text{C}_{12}\text{H}_{18}\text{O}_4$ [M] $^+$: 226.1, found 226.1.



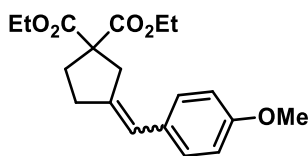
Product (IV.6.b): Cyclization according to general procedure: scale 0.36 mmol, flash chromatography (SiO_2 , 2 % Et_2O in Hexane) yielded 70 mg (83 %) of title compound as a colorless oil as a mixture of E/Z isomers (1:1).

^1H NMR (300 MHz, CDCl_3): δ = 5.35 (dq, J = 6.7, 2.2 Hz, 1H), 4.78 - 3.75 (m, 4H), 3.17 - 2.69 (m, 2H), 2.56 - 1.96 (m, 4H), 1.72 - 1.38 (m, 3H), 1.25 (t, J = 7.1 Hz, 6H) ppm. ^{13}C NMR (101 MHz, CDCl_3): δ = 172.0, 139.3, 139.1, 116.4, 116.2, 61.4, 61.3, 60.1, 59.9, 41.0, 36.6, 33.6, 33.4, 31.6, 27.0, 14.7, 14.6, 14.0 ppm. **IR** (film): 2980, 2931, 2900, 2838, 1726, 1607, 1510, 1443, 1366, 1245, 1157, 1034, 833, 530 cm^{-1} . **MS**: m/z calcd. for $\text{C}_{13}\text{H}_{20}\text{NaO}_4$ [M + Na] $^+$: 263.1259, found 263.1254.



Product (IV.6.c): Cyclization according to general procedure: scale 0.36 mmol, flash chromatography (SiO₂, 2 % Et₂O in Hexane) yielded 70 mg (49 %) of title compound as a colorless oil as a mixture of alkane/alkene isomers (1:9).

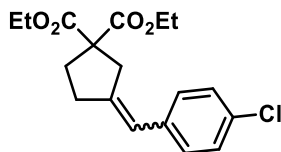
¹H NMR (400 MHz, CDCl₃): δ = 7.75 – 7.70 (m, 2H) {minor and mayor}, 7.36 – 7.31 (m, 2H) {minor and mayor}, 4.93 (dt, J = 7.2, 2.2 Hz, 2H) {minor}, 3.79 (tt, J = 2.3, 1.4 Hz, 2H) {minor}, 3.44 (dd, J = 9.7, 7.2 Hz, 1H) {mayor}, 3.36 (ddd, J = 9.8, 8.2, 4.2 Hz, 1H) {mayor}, 3.30 (t, J = 7.1 Hz, 2H) {minor}, 3.23 (ddd, J = 9.8, 8.2, 7.3 Hz, 1H) {mayor}, 2.76 (dd, J = 9.7, 7.8 Hz, 1H) {mayor}, 2.49 (ttd, J = 7.1, 2.2, 1.1 Hz, 2H) {minor}, 2.45 (d, J = 0.8 Hz, 3H) {minor and mayor}, 2.20 – 2.06 (m, 1H) {mayor}, 1.92 (dtd, J = 13.9, 7.0, 4.1 Hz, 1H) {mayor}, 1.36 (dq, J = 12.3, 8.3 Hz, 1H) {mayor}, 0.93 (d, J = 6.7 Hz, 3H) {mayor} ppm. **¹³C NMR** (101 MHz, CDCl₃): δ = 144.1 {mayor}, 143.7 {minor}, 143.2, 134.0 {mayor and minor}, 132.7 {minor}, 129.7 (2C) {minor}, 129.6 (2C) {mayor}, 127.8 (2C) {minor}, 127.5 (2C) {mayor}, 107.4 {minor}, 54.8 {mayor}, 51.9 {minor}, 48.1 {minor}, 47.6 {mayor}, 33.3 {mayor}, 33.2 {mayor}, 31.8 {minor}, 21.5 {minor}, 21.5 {mayor}, 17.6 {mayor} ppm. **IR** (film): 2962, 2878, 1597, 1455, 1335, 1157, 1089, 1038, 985, 814, 765, 658, 587, 544, 492 cm⁻¹. **MS**: m/z calcd. for C₁₂H₁₇NO₂S [M₁] and C₁₂H₁₅NO₂S [M₂]: 239.1 and 237.1, found 239.1 and 237.0.



Product (IV.6.d): Cyclization according to general procedure: scale 0.3 mmol, flash chromatography (SiO₂, 2 % Et₂O in Hexane) yielded 78 mg (78 %) of title compound as a colorless oil as a mixture of E/Z isomers (1:1).

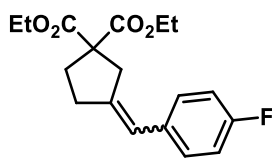
¹H NMR (400 MHz, CDCl₃): δ = 7.21 (dd, J = 8.9, 7.3 Hz, 2H), 6.86 (dd, J = 8.7, 6.0 Hz, 2H), 6.33 – 6.27 (m, 1H), 4.24 – 4.14 (m, 4H), 3.80 (d, J = 2.6 Hz, 3H), 3.21 – 3.15 (m, 1H), 3.11 (d, J = 1.6 Hz, 1H), 2.67 (t, J = 7.6 Hz, 1H), 2.61 (td, J = 7.5, 1.7 Hz, 1H), 2.36 (t, J = 7.5 Hz, 1H), 2.26 (t, J = 7.5 Hz, 1H), 1.24 (td, J = 7.1, 5.9

Hz, 6H) ppm. ^{13}C NMR (101 MHz, CDCl_3): $\delta = 171.6, 157.9, 139.5, 130.9, 129.3, 129.2, 121.8, 113.7, 61.4, 61.0, 59.2, 55.3, 43.0, 38.4, 34.4, 33.9, 32.9, 31.6, 29.5, 22.7, 14.1$ ppm. IR (film): 2980, 2937, 2907, 2838, 1726, 1607, 1510, 1443, 1245, 1157, 1034, 833, 530 cm^{-1} . MS: m/z calcd. for $\text{C}_{19}\text{H}_{24}\text{NaO}_5$ $[\text{M} + \text{Na}]^+$: 355.1521, found 355.1516.



Product (IV.6.e): Cyclization according to general procedure: scale 0.24 mmol, flash chromatography (SiO_2 , 2 % Et_2O in Hexane) yielded 65 mg (72 %) of title compound as a yellow oil as a mixture of E/Z isomers (1:1).

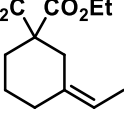
^1H NMR (500 MHz, CDCl_3): $\delta = 7.63 - 7.29$ (m, 2H), 7.21 (t, $J = 8.7$ Hz, 2H), 6.33 (dt, $J = 9.2, 2.4$ Hz, 1H), 4.62 - 4.08 (m, 4H), 3.39 - 3.13 (m, 2H), 2.84 - 2.57 (m, 24H), 2.40 (t, $J = 7.6$ Hz, 1H), 2.30 (t, $J = 7.5$ Hz, 1H), 1.27 (dt, $J = 8.2, 7.1$ Hz, 6H) ppm. ^{13}C NMR (126 MHz, CDCl_3): $\delta = 171.6, 171.5, 142.7, 142.6, 136.5, 136.4, 131.8, 131.7, 129.3, 129.3, 128.4, 128.4, 121.5, 121.4, 61.6, 61.5, 60.9, 59.1, 43.0, 38.5, 34.2, 33.9, 32.7, 29.7, 14.0, 14.0$ ppm. MS: m/z calcd. for $\text{C}_{18}\text{H}_{21}\text{ClNaO}_4$ $[\text{M} + \text{Na}]^+$: 359.1026, found 359.1021.

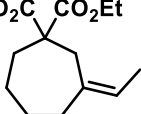


Product (IV.6.f): Cyclization according to general procedure: scale 0.3 mmol, flash chromatography (SiO_2 , 2 % Et_2O in Hexane) yielded 85 mg (82 %) of title compound as a pale-yellow oil as a mixture of E/Z isomers (1:1).

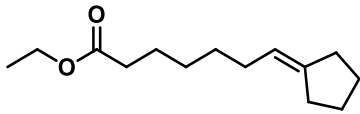
^1H NMR (400 MHz, CDCl_3): $\delta = 7.44 - 7.14$ (m, 2H), 6.99 (td, $J = 8.7, 6.1$ Hz, 2H), 6.35 - 6.28 (m, 1H), 4.24 - 4.14 (m, 4H), 3.17 - 3.09 (m, 2H), 2.68 - 2.58 (m, 2H), 2.37 (t, $J = 7.5$ Hz, 1H), 2.27 (t, $J = 7.5$ Hz, 1H), 1.24 (dt, $J = 7.1$ Hz, 6H) ppm. ^{13}C NMR (101 MHz, CDCl_3): $\delta = 171.6, 171.5, 162.4, 162.4, 159.9, 141.4, 141.4, 141.4, 141.4, 134.2, 134.1, 129.6, 129.6, 129.5, 129.5, 121.4, 121.4, 115.2, 115.2, 115.0, 114.9, 61.6, 61.5, 60.9, 59.1, 42.9, 38.4, 34.2, 33.8, 32.8, 29.5, 14.1, 14.0$ ppm. IR

(film): 2980, 2937, 2873, 1727, 1602, 1508, 1446, 1272, 1245, 1221, 1157, 1065, 862, 522 cm^{-1} . **MS:** m/z calcd. for $\text{C}_{18}\text{H}_{21}\text{FNaO}_4$ [$\text{M} + \text{Na}$] $^+$: 343.1322, found 343.1316.

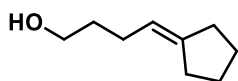
 **Product (IV.6.g):** Cyclization according to general procedure: scale 0.36 mmol, flash chromatography (SiO_2 , in Hexane) yielded 24 mg (51 %) of title compound as a colorless oil. **$^1\text{H NMR}$** (400 MHz, CDCl_3): δ = 5.67 – 5.55 (m, 1H), 5.17 – 5.06 (m, 2H), 4.17 (q, J = 7.1 Hz, 4H), 2.76 (dd, J = 7.5, 1.1 Hz, 2H), 2.71 (d, J = 2.6 Hz, 1H), 1.73 (t, J = 2.5 Hz, 3H), 1.22 (t, J = 7.1 Hz, 6H) ppm. **$^{13}\text{C NMR}$** (101 MHz, CDCl_3): δ = 170.4 (2C), 132.5, 119.8, 79.1, 73.8, 61.8 (2C), 57.4, 36.8, 23.3, 14.4 (2C), 14.4 ppm. **MS:** m/z calcd. for $\text{C}_{14}\text{H}_{22}\text{O}_4$ [$\text{M} + \text{Na}$] $^+$: 254.2, found 254.2.

 **Product (IV.6.h):** Cyclization according to general procedure: scale 0.36 mmol, flash chromatography (SiO_2 , in Hexane) yielded 15 mg (43 %) of title compound as a colorless oil.

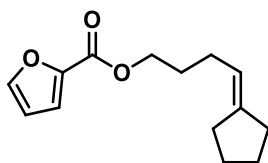
$^1\text{H NMR}$ (400 MHz, CDCl_3): δ = 5.63 (dd, J = 6.4, 3.2 Hz, 1H), 5.29 (qd, J = 7.1, 6.3 Hz, 2H), 4.20 (q, J = 7.1 Hz, 4H), 2.76 (q, J = 2.5 Hz, 4H), 2.06 – 1.93 (m, 2H), 1.75 (t, J = 2.6 Hz, 3H), 1.67 (dd, J = 7.1, 3.2 Hz, 2H), 1.29 – 1.20 (m, 6H) ppm. **$^{13}\text{C NMR}$** (101 MHz, CDCl_3): δ = 170.9 (2C), 134.3, 112.0, 79.1, 73.8, 61.8 (2C), 57.4, 43.2, 36.8, 23.3, 14.4 (2C), 14.4 ppm. **MS:** m/z calcd. for $\text{C}_{14}\text{H}_{24}\text{O}_4$ [$\text{M} + \text{Na}$] $^+$: 268.3, found 268.1.

 **Product (IV.6.i):** Cyclization according to general procedure: scale 0.36 mmol, flash chromatography (SiO_2 , 2 % Et_2O in Hexane) yielded 42 mg (63 %) of title compound as a brown oil. **$^1\text{H NMR}$** (400 MHz, CDCl_3): δ = 5.21 (tt, J = 4.8, 2.4 Hz, 1H), 4.12 (q, J = 7.2 Hz, 2H), 2.31 – 2.24 (q, J = 7.8 Hz, 2H), 2.23 – 2.11 (m, 2H), 2.00 – 1.93 (m, 2H), 1.70 – 1.49 (m, 6H), 1.38 – 1.29 (m, 4H), 1.24 (t, J = 7.1 Hz, 3H) ppm. **$^{13}\text{C NMR}$** (101 MHz, CDCl_3): δ = 168.4, 138.0, 123.6, 55.0, 28.9,

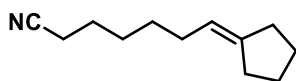
28.3, 24.6, 23.8, 23.2, 20.1, 10.0, 19.2, 18.9, 8.9 ppm. **MS:** m/z calcd. for $C_{14}H_{25}O_2$ $[M + H]^+$: 225.1855, found 343.1846.



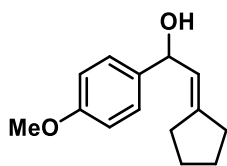
Product (IV.6.j): Cyclization according to general procedure: scale 0.36 mmol, flash chromatography (SiO_2 , 2 % Et_2O in Hexane) yielded 34 mg (63 %) of title compound as a yellowish oil. **1H NMR** (300 MHz, $CDCl_3$): δ = 5.27 (tt, J = 4.9, 2.4 Hz, 1H), 3.67 (t, J = 6.5 Hz, 2H), 2.29 – 2.13 (m, 4H), 2.08 (qt, J = 7.3, 1.5 Hz, 2H), 1.75 – 1.56 (m, 6H) ppm. **^{13}C NMR** (101 MHz, $CDCl_3$): δ = 144.0, 119.3, 62.9, 33.6, 32.6, 28.6, 26.4, 26.3, 26.0 ppm. **MS:** m/z calcd. for $C_9H_{17}O$ $[M + H]^+$: 141.2, found 141.2.



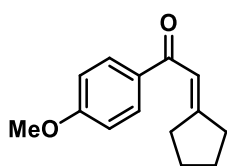
Product (IV.6.k): Cyclization according to general procedure: scale 0.36 mmol, flash chromatography (SiO_2 , 2 % Et_2O in Hexane) yielded 50 mg (56%) of title compound as a yellow oil. **1H NMR** (400 MHz, $CDCl_3$): δ = 7.57 (dd, J = 1.7, 0.9 Hz, 1H), 7.16 (dd, J = 3.5, 0.9 Hz, 1H), 6.50 (dd, J = 3.5, 1.7 Hz, 1H), 5.24 (ddt, J = 7.1, 4.8, 2.4 Hz, 1H), 4.30 (t, J = 6.7 Hz, 2H), 2.33 – 2.05 (m, 6H), 1.83 – 1.75 (m, 2H), 1.68 – 1.57 (m, 4H). ppm. **^{13}C NMR** (101 MHz, $CDCl_3$): δ = 158.8, 146.2, 144.9, 144.5, 118.5, 117.6, 111.8, 64.6, 33.6, 28.6, 28.6, 26.4, 26.3, 25.9 ppm. **MS:** m/z calcd. for $C_{18}H_{21}FNaO_4$ $[M + H]^+$: 235.1334, found 235.0962.



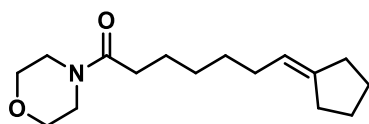
Product (IV.6.l): Cyclization according to general procedure: scale 0.36 mmol, flash chromatography (SiO_2 , 2 % Et_2O in Hexane) yielded 37 mg (60 %) of title compound as a colorless oil. **1H NMR** (400 MHz, $CDCl_3$): δ = 5.23 (tp, J = 7.0, 2.3 Hz, 1H), 2.35 (t, J = 7.2 Hz, 4H), 2.23 (tt, J = 6.8, 1.6 Hz, 2H), 2.17 (dddt, J = 8.4, 4.0, 2.7, 1.4 Hz, 2H), 2.03 – 1.96 (m, 2H), 1.78 – 1.65 (m, 6H), 1.65 – 1.58 (m, 4H) ppm. **^{13}C NMR** (101 MHz, $CDCl_3$): δ = 143.7, 119.8, 119.4, 33.6, 29.2, 28.8, 28.6, 28.3, 26.4, 26.3, 25.4, 17.1 ppm. **MS:** m/z calcd. for $C_{12}H_{19}FN$ $[M]^+$: 177.3, found 177.2.



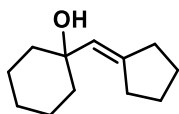
Product (IV.6.m): Cyclization according to general procedure: scale 0.36 mmol, flash chromatography (SiO₂, 5 % Et₂O in Hexane) yielded 39 mg (72 %) of title compound as a colorless oil as a mixture of E/Z isomers (1:1). **¹H NMR** (400 MHz, CDCl₃): δ = 7.35 – 7.29 (m, 2H), 6.82 – 6.78 (m, 2H), 5.57 (t, *J* = 7.4 Hz, 1H), 5.12 (tt, *J* = 7.2, 1.2 Hz, 1H), 3.13 (s, *J* = 5.9, 2.7 Hz, 3H), 2.02 (m, *J* = 2.7 Hz, 2H), 1.16 – 1.09 (m, 6H) ppm. **¹³C NMR** (101 MHz, CDCl₃): δ = 170.4, 135.2, 133.8, 133.1, 128.8, 128.7, 128.7, 128.3, 78.3, 59.8, 23.55, 18.34, 13.93, 13.82 ppm. **MS:** *m/z* calcd. for C₁₄H₁₉O₂ [M + H]⁺: 219.1385, found 219.1376.



Product (IV.6.n): Cyclization according to general procedure: scale 0.36 mmol, flash chromatography (SiO₂, 10 % Et₂O in Hexane) yielded 65 mg (77 %) of title compound as a yellow oil. **¹H NMR** (400 MHz, CDCl₃): δ = 7.94 (d, *J* = 8.9 Hz, 2H), 7.24 – 7.19 (m, 2H), 6.93 (d, *J* = 8.2 Hz, 1H), 3.86 (d, *J* = 1.3 Hz, 3H), 1.54 (m, 4H), 1.24 (m, 4H) ppm. **¹³C NMR** (101 MHz, CDCl₃): δ = 207.6, 171.2, 162.3, 134.1, 131.0, 130.4, 113.82, 113.7, 113.5, 55.5, 47.4, 29.7, 29.4, 19.3 ppm. **MS:** *m/z* calcd. for C₁₄H₁₇O₂ [M + H]⁺: 217.1229, found 217.1237.

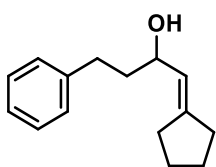


Product (IV.6.o): Cyclization according to general procedure: scale 0.36 mmol, flash chromatography (SiO₂, 5 % Et₂O in Hexane) yielded 38 mg (68 %) of title compound as a colorless oil. **¹H NMR** (400 MHz, CDCl₃): δ = 5.22 (tt, *J* = 4.8, 2.4 Hz, 1H), 3.66 (dd, *J* = 5.8, 3.9 Hz, 4H), 3.62 (d, *J* = 5.1 Hz, 2H), 3.47 (d, *J* = 4.9 Hz, 2H), 2.34 – 2.27 (m, 2H), 2.21 (ddt, *J* = 6.9, 5.2, 1.6 Hz, 4H), 2.15 (m, 2H), 1.96 (m, 2H), 1.73 – 1.50 (m, 6H), 1.38 – 1.32 (m, 2H) ppm. **¹³C NMR** (101 MHz, CDCl₃): δ = 177.9, 144.0, 119.3, 62.9 (2C), 33.6 (2C), 33.6, 32.6, 29.7, 28.6 (2C), 26.4, 26.3 (2C), 26.0. ppm. **MS:** *m/z* calcd. for C₁₆H₂₇NO₂ [M]⁺: 265.3970, found 265.1983.



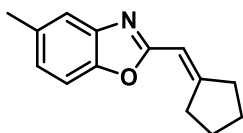
Product (IV.6.p): Cyclization according to general procedure: scale 0.36 mmol, flash chromatography (SiO₂, 5 to 10 % Et₂O in Hexane) yielded 33 mg (64 %) of title compound as a brown oil.

¹H NMR (400 MHz, CDCl₃): δ = 5.46 – 5.37 (m, 1H), 2.46 (ddt, J = 7.3, 6.0, 1.3 Hz, 2H), 2.36 – 2.26 (m, 2H), 1.75 – 1.54 (m, 10H), 1.53 – 1.37 (m, 4H) ppm. **¹³C NMR** (101 MHz, CDCl₃): δ = 144.4, 126.9, 72.2, 38.7 (2C), 35.6, 29.3, 27.3, 25.6 (2C), 25.5, 22.5 (2C) ppm. **MS:** m/z calcd. for C₁₂H₂₀O [M -OH]⁺: 181.1592, found 181.1220.



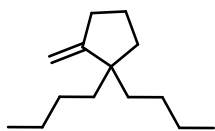
Product (IV.6.r): Cyclization according to general procedure: scale 0.36 mmol, flash chromatography (SiO₂, 10 % Et₂O in Hexane) yielded 32 mg (62 %) of title compound as a yellowish oil. **¹H NMR** (400 MHz, CDCl₃): δ = 7.32 – 7.26 (m, 3H), 7.23

– 7.18 (m, 2H), 3.67 (tt, J = 8.4, 4.3 Hz, 1H), 2.85 – 2.76 (m, 1H), 2.68 (ddd, J = 13.8, 9.8, 6.7 Hz, 2H), 2.04 (q, J = 7.2, 6.8 Hz, 2H), 1.97 – 1.87 (m, 2H), 1.84 – 1.72 (m, 2H), 1.66 – 1.43 (m, 4H) ppm. **¹³C NMR** (101 MHz, CDCl₃): δ = 132.5, 131.2, 128.9, 128.4 (2C), 126.3, 125.8, 125.3, 68.8, 52.1, 46.2, 30.6, 29.7, 24.5, 23.6 ppm. **MS:** m/z calcd. for C₁₅H₂₀O [M]⁺: 216.3, found 216.2.

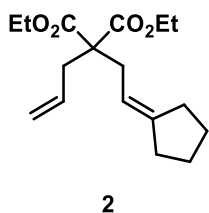


Product (IV.6.s): Cyclization according to general procedure: scale 0.36 mmol, flash chromatography (SiO₂, 10 % Et₂O in Hexane) yielded 64 mg (63 %) of title compound as a yellowish oil.

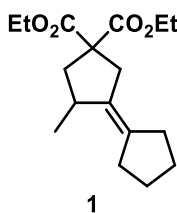
¹H NMR (400 MHz, CDCl₃): δ = 7.49 – 7.43 (m, 1H), 7.34 (d, J = 8.2 Hz, 1H), 7.08 (t, J = 7.2 Hz, 1H), 6.40 (t, J = 2.3 Hz, 1H), 2.99 – 2.85 (m, 2H), 2.59 (d, J = 2.0 Hz, 2H), 2.45 (s, 3H), 2.06 – 1.79 (m, 2H), 1.80 – 1.70 (m, 2H) ppm. **¹³C NMR** (101 MHz, CDCl₃): δ = 162.2, 125.3, 119.5, 109.5, 107.6, 36.3, 33.1, 23.9, 21.4 ppm. **MS:** m/z calcd. for C₁₄H₁₆NO [M + H]⁺: 214.2, found 214.1.



Product (IV.6.t): Cyclization according to general procedure: scale 0.36 mmol, flash chromatography (SiO₂, in pure pentane) yielded 23.3 mg (46 %) of title compound as a colorless oil. **¹H NMR** (400 MHz, CDCl₃): δ = 5.19 – 5.04 (m, 2H), 2.56 (dt, *J* = 15.7, 7.9 Hz, 2H), 1.99 (m, 2H), 1.58 (m, 10H), 1.29 (q, *J* = 12.0 Hz, 4H), 0.91 (m, 6H) ppm. **¹³C NMR** (101 MHz, CDCl₃): δ = 157.5, 124.9, 36.6, 33.4, 31.9, 29.8, 29.7, 23.3, 23.2, 22.9, 22.5, 14.2, 14.1, 13.9 ppm. **MS:** *m/z* calcd. for C₁₄H₂₆ [M]⁺: 193.1, found 193.1.



:



Product (IV.6.u-v): Cyclization according to general procedure: scale 0.36 mmol, flash chromatography (SiO₂, 2 % Et₂O in Hexane) yielded 54 mg (60 %) of title compound as a colorless oil as a mixture of products a and b in 2 to 1 ratio. **¹H NMR** (400 MHz, CDCl₃): δ = 5.70 – 5.56 (m, 1H), 5.21 – 5.07 (m, 3H), 4.25 – 4.12 (m, 8H), 3.55 (t, *J* = 6.6 Hz, 2H), 3.48 (q, *J* = 7.0 Hz, 4H), 2.79 – 2.72 (m, 4H), 2.53 – 2.23 (m, 2H), 2.24 – 2.12 (m, 4H), 2.10 – 2.06 (m, 1H), 1.94 – 1.81 (m, 4H), 1.62 (qd, *J* = 7.2, 5.8, 2.7 Hz, 4H), 1.27 – 1.21 (m, 12H), 1.20 (d, *J* = 7.0 Hz, 3H). **¹³C NMR** (101 MHz, CDCl₃): δ = 167.0(4C), 142.5, 141.2, 132.0, 132.0, 123.3, 119.5, 82.5, 75.1, 65.2, 61.9, 61.7, 61.7, 61.5, 57.0, 44.5, 36.4, 31.4 (2C), 29.7, 26.0 (2C), 22.9 (2C), 17.9 (2C), 15.2, 14.1 (2C), 14.0 (2C) ppm. **MS:** *m/z* calcd. for C₁₇H₂₆O₄ [M + Na]⁺: 294.2, found 294.1

IV.6. References

- (1) Buckingham, J.: *Dictionary of Natural Products*; Taylor & Francis, 1993.
- (2) Koch, M. A.; Schuffenhauer, A.; Scheck, M.; Wetzl, S.; Casaulta, M.; Odermatt, A.; Ertl, P.; Waldmann, H. Charting Biologically Relevant Chemical Space: A Structural Classification of Natural Products (Sconp). *Proc. Natl. Acad. Sci. U. S. A.* **2005**, *102*, 17272, doi: 10.1073/pnas.0503647102.
- (3) Bon, R. S.; Waldmann, H. Bioactivity-Guided Navigation of Chemical Space. *Acc. Chem. Res.* **2010**, *43*, 1103, doi: 10.1021/ar100014h.
- (4) Vollhardt, K. P. C.; Schore, N. E.: *Organic Chemistry*; W. H. Freeman, 2010.
- (5) McMurry, J. E.: *Fundamentals of Organic Chemistry*; Cengage Learning, 2010.
- (6) Thebtaranonth, C.; Thebtaranonth, Y. Developments in Cyclisation Reactions. *Tetrahedron* **1990**, *46*, 1385, doi: 10.1016/S0040-4020(01)81956-6.
- (7) Giese, B. K., B.; Göbel, T.; Dickhaut, J.; Thoma, G.; Kulicke, K. J.; Trach, F: Radical Cyclization Reactions. In *Organic Reactions*, 2004; pp 301.
- (8) Bar, G.; Parsons, A. F. Stereoselective Radical Reactions. *Chem. Soc. Rev.* **2003**, *32*, 251, doi: 10.1039/b111414j.
- (9) Spellmeyer, D. C.; Houk, K. N. Force-Field Model for Intramolecular Radical Additions. *J. Org. Chem.* **1987**, *52*, 959, doi: 10.1021/jo00382a001.
- (10) Beckwith, A. L. J.; Schiesser, C. H. Regio- and Stereo-Selectivity of Alkenyl Radical Ring Closure: A Theoretical Study. *Tetrahedron* **1985**, *41*, 3925, doi: 10.1016/S0040-4020(01)97174-1.
- (11) Jasperse, C. P.; Curran, D. P.; Fevig, T. L. Radical Reactions in Natural Product Synthesis. *Chem. Rev.* **1991**, *91*, 1237, doi: 10.1021/cr00006a006.
- (12) Stork, G.; Baine, N. H. Cyclization of Vinyl Radicals: A Versatile Method for the Construction of Five- and Six-Membered Rings. *J. Am. Chem. Soc.* **1982**, *104*, 2321, doi: 10.1021/ja00372a042.
- (13) Boger, D. L.; Mathvink, R. J. Acyl Radicals: Functionalized Free Radicals for Intramolecular Cyclization Reactions. *J. Org. Chem.* **1988**, *53*, 3377, doi: 10.1021/jo00249a053.
- (14) Ziegler, F. E.; Metcalf, C. A.; Schulte, G. Confirmation by Total Synthesis of the Revised Structure of Sporol: An Application of Cyclic Thionocarbonate-Initiated Radical Cyclization. *Tetrahedron Lett.* **1992**, *33*, 3117, doi: 10.1016/S0040-4039(00)79828-5.
- (15) Ardisson, J.; Férézou, J. P.; Julia, M.; Lenglet, L.; Pancrazi, A. Stereocontrolled Synthesis of the Spiroketal Unit of 22,23-Dihydroavermectin B_{1b}. *Tetrahedron Lett.* **1987**, *28*, 1997, doi: 10.1016/S0040-4039(00)96029-5.
- (16) Danishefsky, S. J.; Panek, J. S. Total Synthesis of (+,-)-3-Demethoxyerythratidinone: Demonstration of a Radical Cyclization Route to a Site Specific Enol Derivative. *J. Am. Chem. Soc.* **1987**, *109*, 917, doi: 10.1021/ja00237a057.
- (17) Clive, D. L. J.; Joussef, A. C. Synthesis of (+,-)-Frullanolide: An Application of Radical Closure. *J. Org. Chem.* **1990**, *55*, 1096, doi: 10.1021/jo00290a053.
- (18) Becking, L.; Schäfer, H. J. Pyrrolidines by Intramolecular Addition of Kolbe Radicals Generated from β -Allylaminoalkanoates. *Tetrahedron Lett.* **1988**, *29*, 2797, doi: 10.1016/0040-4039(88)85212-2.

- (19) Corey, E. J.; Kang, M. C. A New and General Synthesis of Polycyclic γ -Lactones by Double Annulation. *J. Am. Chem. Soc.* **1984**, *106*, 5384, doi: 10.1021/ja00330a076.
- (20) Kates, S. A.; Dombroski, M. A.; Snider, B. B. Manganese(III)-Based Oxidative Free-Radical Cyclization of Unsaturated β -Keto Esters, 1,3-Diketones, and Malonate Diesters. *J. Org. Chem.* **1990**, *55*, 2427, doi: 10.1021/jo00295a035.
- (21) Nugent, W. A.; RajanBabu, T. V. Transition-Metal-Centered Radicals in Organic Synthesis. Titanium(III)-Induced Cyclization of Epoxy Olefins. *J. Am. Chem. Soc.* **1988**, *110*, 8561, doi: 10.1021/ja00233a051.
- (22) Mattay, J.; Banning, A.; Bischof, E. W.; Heidbreder, A.; Runsink, J. Photoreactions of Enones with Amines – Cyclization of Unsaturated Enones and Reductive Ring Opening by Photoinduced Electron Transfer (Pet). *Chem. Ber.* **1992**, *125*, 2119, doi: 10.1002/cber.19921250921.
- (23) Hutchinson, J. H.; Pattenden, G.; Myers, P. L. Tandem Radical Cyclisation - Intramolecular Mukaiyama Aldolisation Approach to Forskolin. *Tetrahedron Lett.* **1987**, *28*, 1313, doi: 10.1016/S0040-4039(00)95357-7.
- (24) RajanBabu, T. V.; Nugent, W. A. Intermolecular Addition of Epoxides to Activated Olefins: A New Reaction. *J. Am. Chem. Soc.* **1989**, *111*, 4525, doi: 10.1021/ja00194a073.
- (25) Edmonds, D. J.; Johnston, D.; Procter, D. J. Samarium(II)-Iodide-Mediated Cyclizations in Natural Product Synthesis. *Chem. Rev.* **2004**, *104*, 3371, doi: 10.1021/cr030017a.
- (26) Curran, D. P.; Fevig, T. L.; Totleben, M. J. Sequential Radical Cyclization/Organometallic Addition. On the Mechanism of the Samarium(II) Mediated Barbier Reaction in the Presence of Hexamethylphosphoric Triamide. *Synlett* **1990**, *1990*, 773, doi: 10.1055/s-1990-21248.
- (27) Molander, G. A.; Harris, C. R. Sequenced Reactions with Samarium(II) Iodide. Tandem Intramolecular Nucleophilic Acyl Substitution/Intramolecular Barbier Cyclizations. *J. Am. Chem. Soc.* **1995**, *117*, 3705, doi: 10.1021/ja00118a007.
- (28) Tucker, J. W.; Nguyen, J. D.; Narayanam, J. M. R.; Krabbe, S. W.; Stephenson, C. R. J. Tin-Free Radical Cyclization Reactions Initiated by Visible-Light Photoredox Catalysis. *Chem. Commun.* **2010**, *46*, 4985, doi: 10.1039/c0cc00981d.
- (29) Kim, H.; Lee, C. Visible-Light-Induced Photocatalytic Reductive Transformations of Organohalides. *Angew. Chem. Int. Ed.* **2012**, *51*, 12303, doi: 10.1002/anie.201203599.
- (30) Revol, G.; McCallum, T.; Morin, M.; Gagosz, F.; Barriault, L. Photoredox Transformations with Dimeric Gold Complexes. *Angew. Chem. Int. Ed.* **2013**, *52*, 13342, doi: 10.1002/anie.201306727.
- (31) Chow, P.-K.; Cheng, G.; Tong, G. S. M.; To, W.-P.; Kwong, W.-L.; Low, K.-H.; Kwok, C.-C.; Ma, C.; Che, C.-M. Luminescent Pincer Platinum(II) Complexes with Emission Quantum Yields up to Almost Unity: Photophysics, Photoreductive C–C Bond Formation, and Materials Applications. *Angew. Chem. Int. Ed.* **2015**, *54*, 2084, doi: 10.1002/anie.201408940.
- (32) Börjesson, M.; Moragas, T.; Martin, R. Ni-Catalyzed Carboxylation of Unactivated Alkyl Chlorides with CO_2 . *J. Am. Chem. Soc.* **2016**, *138*, 7504, doi: 10.1021/jacs.6b04088.

- (33) Vechorkin, O.; Barmaz, D.; Proust, V.; Hu, X. Ni-Catalyzed Sonogashira Coupling of Nonactivated Alkyl Halides: Orthogonal Functionalization of Alkyl Iodides, Bromides, and Chlorides. *J. Am. Chem. Soc.* **2009**, *131*, 12078, doi: 10.1021/ja906040t.
- (34) Alonso, F.; Beletskaya, I. P.; Yus, M. Metal-Mediated Reductive Hydrodehalogenation of Organic Halides. *Chem. Rev.* **2002**, *102*, 4009, doi: 10.1021/cr0102967.
- (35) Ghosh, I.; Ghosh, T.; Bardagi, J. I.; König, B. Reduction of Aryl Halides by Consecutive Visible-Light-Induced Electron Transfer Processes. *Science* **2014**, *346*, 725, doi: 10.1126/science.1258232.
- (36) Meyer, A. U.; Slanina, T.; Heckel, A.; König, B. Lanthanide Ions Coupled with Photoinduced Electron Transfer Generate Strong Reduction Potentials from Visible-Light. *Chem. Eur. J.* **2017**, *23*, 7900, doi: 10.1002/chem.201701665.
- (37) Le, C.; Chen, T. Q.; Liang, T.; Zhang, P.; MacMillan, D. W. C. A Radical Approach to the Copper Oxidative Addition Problem: Trifluoromethylation of Bromoarenes. *Science* **2018**, *360*, 1010, doi: 10.1126/science.aat4133.
- (38) Johnston, C. P.; Smith, R. T.; Allmendinger, S.; MacMillan, D. W. C. Metallaphotoredox-Catalysed sp^3 - sp^3 Cross-Coupling of Carboxylic Acids with Alkyl Halides. *Nature* **2016**, *536*, 322, doi: 10.1038/nature19056.
- (39) Shimomaki, K.; Murata, K.; Martin, R.; Iwasawa, N. Visible-Light-Driven Carboxylation of Aryl Halides by the Combined Use of Palladium and Photoredox Catalysts. *J. Am. Chem. Soc.* **2017**, *139*, 9467, doi: 10.1021/jacs.7b04838.
- (40) Boyington, A. J.; Seath, C. P.; Zearfoss, A. M.; Xu, Z.; Jui, N. T. Catalytic Strategy for Regioselective Arylethylamine Synthesis. *J. Am. Chem. Soc.* **2019**, *141*, 4147, doi: 10.1021/jacs.9b01077.
- (41) Schweitzer-Chaput, B.; Horwitz, M. A.; de Pedro Beato, E.; Melchiorre, P. Photochemical Generation of Radicals from Alkyl Electrophiles Using a Nucleophilic Organic Catalyst. *Nat. Chem.* **2019**, *11*, 129, doi: 10.1038/s41557-018-0173-x.
- (42) Yao, B.; Wang, D.-X.; Huang, Z.-T.; Wang, M.-X. Room-Temperature Aerobic Formation of a Stable Aryl-Cu^{III} Complex and Its Reactions with Nucleophiles: Highly Efficient and Diverse Arene C-H Functionalizations of Azacalix[1]Arene[3]Pyridine. *Chem. Commun.* **2009**, 2899, doi: 10.1039/b902946j.
- (43) Yao, B.; Wang, Z.-L.; Zhang, H.; Wang, D.-X.; Zhao, L.; Wang, M.-X. Cu(ClO₄)₂-Mediated Arene C-H Bond Halogenations of Azacalixaromatics Using Alkali Metal Halides as Halogen Sources. *J. Org. Chem.* **2012**, *77*, 3336, doi: 10.1021/jo300152u.
- (44) Do, H.-Q.; Bachman, S.; Bissember, A. C.; Peters, J. C.; Fu, G. C. Photoinduced, Copper-Catalyzed Alkylation of Amides with Unactivated Secondary Alkyl Halides at Room Temperature. *J. Am. Chem. Soc.* **2014**, *136*, 2162, doi: 10.1021/ja4126609.
- (45) Creutz, S. E.; Lotito, K. J.; Fu, G. C.; Peters, J. C. Photoinduced Ullmann C-N Coupling: Demonstrating the Viability of a Radical Pathway. *Science* **2012**, *338*, 647, doi: 10.1126/science.1226458.
- (46) Beesley, R. M.; Ingold, C. K.; Thorpe, J. F. CXIX. The Formation and Stability of Spiro-Compounds. Part I. Spiro-Compounds from Cyclohexane. *J. Chem. Soc., Trans.* **1915**, *107*, 1080, doi: 10.1039/ct9150701080.
- (47) Yorimitsu, H.; Shinokubo, H.; Oshima, K. Synthetic Radical Reactions in Aqueous Media. *Synlett* **2002**, *2002*, 0674, doi: 10.1055/s-2002-25328.

- (48) Schmallegger, M.; Gescheidt, G. Benzil/Triethylamine: A Photo-Reducing System for Cu^{2+} . *Monatsh. Chem.* **2018**, *149*, 499, doi: 10.1007/s00706-017-2085-7.
- (49) Tokel-Takvoryan, N. E.; Hemingway, R. E.; Bard, A. J. Electrogenerated Chemiluminescence. XIII. Electrochemical and Electrogenerated Chemiluminescence Studies of Ruthenium Chelates. *J. Am. Chem. Soc.* **1973**, *95*, 6582, doi: 10.1021/ja00801a011.
- (50) Lowry, M. S.; Goldsmith, J. I.; Slinker, J. D.; Rohl, R.; Pascal, R. A.; Malliaras, G. G.; Bernhard, S. Single-Layer Electroluminescent Devices and Photoinduced Hydrogen Production from an Ionic Iridium(III) Complex. *Chem. Mater.* **2005**, *17*, 5712, doi: 10.1021/cm051312+.
- (51) Goldsmith, J. I.; Hudson, W. R.; Lowry, M. S.; Anderson, T. H.; Bernhard, S. Discovery and High-Throughput Screening of Heteroleptic Iridium Complexes for Photoinduced Hydrogen Production. *J. Am. Chem. Soc.* **2005**, *127*, 7502, doi: 10.1021/ja0427101.
- (52) Slinker, J. D.; Gorodetsky, A. A.; Lowry, M. S.; Wang, J.; Parker, S.; Rohl, R.; Bernhard, S.; Malliaras, G. G. Efficient Yellow Electroluminescence from a Single Layer of a Cyclometalated Iridium Complex. *J. Am. Chem. Soc.* **2004**, *126*, 2763, doi: 10.1021/ja0345221.
- (53) Koike, T.; Akita, M. Visible-Light Radical Reaction Designed by Ru- and Ir-Based Photoredox Catalysis. *Inorg. Chem. Front.* **2014**, *1*, 562, doi: 10.1039/c4qi00053f.
- (54) Claros, M.; Ungeheuer, F.; Franco, F.; Martin-Diaconescu, V.; Casitas, A.; Lloret-Fillol, J. Reductive Cyclization of Unactivated Alkyl Chlorides with Tethered Alkenes under Visible-Light Photoredox Catalysis. *Angew. Chem.* **2019**, *131*, 4923, doi: 10.1002/ange.201812702.
- (55) Nazeeruddin, M. K.; Wegh, R. T.; Zhou, Z.; Klein, C.; Wang, Q.; De Angelis, F.; Fantacci, S.; Grätzel, M. Efficient Green-Blue-Light-Emitting Cationic Iridium Complex for Light-Emitting Electrochemical Cells. *Inorg. Chem.* **2006**, *45*, 9245, doi: 10.1021/ic060495e.
- (56) Lexa, D.; Savéant, J. M.; Soufflet, J. P. Chemical Catalysis of the Electrochemical Reduction of Alkyl Halides: Comparison between Cobalt-Tetraphenyl Porphin and Vitamin B₁₂ Derivatives. *J. Electroanal. Chem. Interf. Electrochem.* **1979**, *100*, 159, doi: 10.1016/S0022-0728(79)80158-8.
- (57) Stolzenberg, A. M.; Stershic, M. T. Reactions of the Nickel(I) Octaethylisobacteriochlorin Anion with Alkyl Halides. *J. Am. Chem. Soc.* **1988**, *110*, 5397, doi: 10.1021/ja00224a026.
- (58) Alleman, K. S.; Peters, D. G. Catalytic Reduction of Iodoethane by Cobalt(I) Salen Electrogenerated at Vitreous Carbon Cathodes. *J. Electroanal. Chem.* **1998**, *451*, 121, doi: 10.1016/S0022-0728(98)00087-4.
- (59) Gosden, C.; Healy, K. P.; Pletcher, D. Reaction of Electrogenerated Square-Planar Nickel(I) Complexes with Alkyl Halides. *J. Chem. Soc., Dalton Trans.* **1978**, 972, doi: 10.1039/dt9780000972.
- (60) Artero, V.; Chavarot-Kerlidou, M.; Fontecave, M. Splitting Water with Cobalt. *Angew. Chem. Int. Ed.* **2011**, *50*, 7238, doi: 10.1002/anie.201007987.
- (61) Queyriaux, N.; Jane, R. T.; Massin, J.; Artero, V.; Chavarot-Kerlidou, M. Recent Developments in Hydrogen Evolving Molecular Cobalt(II)-Polypyridyl Catalysts. *Coord. Chem. Rev.* **2015**, *304-305*, 3, doi: 10.1016/j.ccr.2015.03.014.

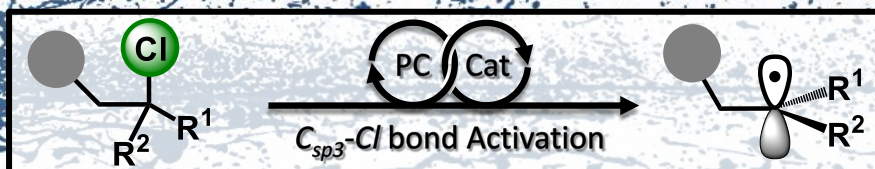
- (62) Prat, I.; Company, A.; Corona, T.; Parella, T.; Ribas, X.; Costas, M. Assessing the Impact of Electronic and Steric Tuning of the Ligand in the Spin State and Catalytic Oxidation Ability of the Fe^{II}(Pytacn) Family of Complexes. *Inorg. Chem.* **2013**, *52*, 9229, doi: 10.1021/ic4004033.
- (63) Call, A.; Lloret-Fillol, J. Enhancement and Control of the Selectivity in Light-Driven Ketone Versus Water Reduction Using Aminopyridine Cobalt Complexes. *Chem. Commun.* **2018**, *54*, 9643, doi: 10.1039/c8cc04239j.
- (64) Kooistra, T. M.; Hekking, Koen, F. W.; Knijnenburg, Q.; de Bruin, B.; Budzelaar, Peter, H. M.; de Gelder, R.; Smits, Jan, M. M.; Gal, Anton, W. Cobalt Chloride Complexes of N3 and N4 Donor Ligands. *Eur. J. Inorg. Chem.* **2003**, *2003*, 648, doi: 10.1002/ejic.200390090.
- (65) Maity, N. C.; Kumar Bera, P.; Ghosh, D.; Abdi, S. H. R.; Kureshy, R. I.; Khan, N.-u. H.; Bajaj, H. C.; Suresh, E. Manganese Complexes with Non-Porphyrin N4 Ligands as Recyclable Catalyst for the Asymmetric Epoxidation of Olefins. *Catal. Sci. Technol.* **2014**, *4*, 208, doi: 10.1039/c3cy00528c.
- (66) Lin, X.; Zhao, S.; Chen, Y.; Fu, L.; Zhu, R.; Liu, Z. Nitrogen-Doped Carbon Cobalt Grafted on Graphitic Carbon Nitride Catalysts with Enhanced Catalytic Performance for Ethylbenzene Oxidation. *J. Mol. Catal. A: Chem.* **2016**, *420*, 11, doi: 10.1016/j.molcata.2016.04.004.
- (67) Takeuchi, R.; Kashio, M. Iridium Complex-Catalyzed Allylic Alkylation of Allylic Esters and Allylic Alcohols: Unique Regio- and Stereoselectivity. *J. Am. Chem. Soc.* **1998**, *120*, 8647, doi: 10.1021/ja981560p.
- (68) Yip, K.-T.; Zhu, N.-Y.; Yang, D. Palladium-Catalyzed Highly Diastereoselective Oxidative Cascade Cyclization Reactions. *Org. Lett.* **2009**, *11*, 1911, doi: 10.1021/ol900355h.
- (69) Tracz, A.; Matczak, M.; Urbaniak, K.; Skowerski, K. Nitro-Grela-Type Complexes Containing Iodides – Robust and Selective Catalysts for Olefin Metathesis under Challenging Conditions. *Beilstein J. Org. Chem.* **2015**, *11*, 1823, doi: 10.3762/bjoc.11.198.
- (70) Toja, E.; Gorini, C.; Zirotti, C.; Barzaghi, F.; Galliani, G. Amnesia-Reversal Activity of a Series of 5-Alkoxy-1-Arylsulfonyl-2-Pyrrolidinones. *Eur. J. Med. Chem.* **1991**, *26*, 403, doi: 10.1016/0223-5234(91)90101-R.
- (71) Keusenkothen, P. F.; Smith, M. B. Asymmetric Radical Cyclization with Pyroglutamate: Synthesis of 7-Substituted Pyrrolizidinones. *J. Chem. Soc., Perkin Trans. 1* **1994**, 2485, doi: 10.1039/p19940002485.
- (72) Elamparuthi, E.; Fellay, C.; Neuburger, M.; Gademann, K. Total Synthesis of Cyrneine A. *Angew. Chem. Int. Ed.* **2012**, *51*, 4071, doi: 10.1002/anie.201200515.
- (73) Nishihara, Y.; Okada, Y.; Jiao, J.; Suetsugu, M.; Lan, M.-T.; Kinoshita, M.; Iwasaki, M.; Takagi, K. Highly Regio- and Stereoselective Synthesis of Multialkylated Olefins through Carbozirconation of Alkynylboronates and Sequential Negishi and Suzuki–Miyaura Coupling Reactions. *Angew. Chem. Int. Ed.* **2011**, *50*, 8660, doi: 10.1002/anie.201103601.
- (74) Feldman, K. S.; Bruendl, M. M.; Schildknecht, K.; Bohnstedt, A. C. Inter- and Intramolecular Addition/Cyclizations of Sulfonamide Anions with Alkynyliodonium Triflates. Synthesis of Dihydropyrrole, Pyrrole, Indole, and Tosylenamide Heterocycles. *J. Org. Chem.* **1996**, *61*, 5440, doi: 10.1021/jo9605814.

- (75) van der Born, D.; Sewing, C.; Herscheid, J. D. M.; Windhorst, A. D.; Orru, R. V. A.; Vugts, D. J. A Universal Procedure for the [¹⁸F]Trifluoromethylation of Aryl Iodides and Aryl Boronic Acids with Highly Improved Specific Activity. *Angew. Chem. Int. Ed.* **2014**, *53*, 11046, doi: 10.1002/anie.201406221.
- (76) Rizk, T.; Bilodeau, E. J.-F.; Beauchemin, A. M. Synthesis of Pyridines and Pyrazines Using an Intramolecular Hydroamination-Based Reaction Sequence. *Angew. Chem. Int. Ed.* **2009**, *48*, 8325, doi: 10.1002/anie.200903922.
- (77) Achini, R. Synthesis of Phenyl- and Benzyl-Substituted Pyrrolidines and of a Piperidine by Intramolecular C-Alkylation. Synthons for Tricyclic Skeletons. *Helv. Chim. Acta* **1981**, *64*, 2203, doi: 10.1002/hlca.19810640727.
- (78) Karsten, S.; Ameen, M. A.; Källäne, S. I.; Nan, A.; Turcu, R.; Liebscher, J. A Versatile Method of Tethering Biomolecules to Pyrrole Precursors for Functionalized Magnetic Polypyrrole Core-Shell Nanoparticles. *Synthesis* **2010**, *2010*, 3021, doi: 10.1055/s-0029-1218846.
- (79) Molander, G. A.; Fumagalli, T. Palladium(0)-Catalyzed Suzuki–Miyaura Cross-Coupling Reactions of Potassium Aryl- and Heteroaryltrifluoroborates with Alkenyl Bromides. *J. Org. Chem.* **2006**, *71*, 5743, doi: 10.1021/jo0608366.
- (80) Jahnke, A. A.; Djukic, B.; McCormick, T. M.; Buchaca Domingo, E.; Hellmann, C.; Lee, Y.; Seferos, D. S. Poly(3-Alkyltellurophene)S Are Solution-Processable Polyheterocycles. *J. Am. Chem. Soc.* **2013**, *135*, 951, doi: 10.1021/ja309404j.
- (81) Hellenbrand, T.; Höfner, G.; Wein, T.; Wanner, K. T. Synthesis of 4-Substituted Nipecotic Acid Derivatives and Their Evaluation as Potential Gaba Uptake Inhibitors. *Biorg. Med. Chem.* **2016**, *24*, 2072, doi: 10.1016/j.bmc.2016.03.038.
- (82) Wang, Y.-M.; Bruno, N. C.; Placeres, Á. L.; Zhu, S.; Buchwald, S. L. Enantioselective Synthesis of Carbo- and Heterocycles through a CuH-Catalyzed Hydroalkylation Approach. *J. Am. Chem. Soc.* **2015**, *137*, 10524, doi: 10.1021/jacs.5b07061.
- (83) Shen, Y.; Cornella, J.; Juliá-Hernández, F.; Martín, R. Visible-Light-Promoted Atom Transfer Radical Cyclization of Unactivated Alkyl Iodides. *ACS Catal.* **2017**, *7*, 409, doi: 10.1021/acscatal.6b03205.
- (84) Berry, C. B.; Bubser, M.; Jones, C. K.; Hayes, J. P.; Wepy, J. A.; Locuson, C. W.; Daniels, J. S.; Lindsley, C. W.; Hopkins, C. R. Discovery and Characterization of MI398, a Potent and Selective Antagonist of the D4 Receptor with in Vivo Activity. *ACS Medicinal Chemistry Letters* **2014**, *5*, 1060, doi: 10.1021/ml500267c.
- (85) Kubota, K.; Yamamoto, E.; Ito, H. Copper(I)-Catalyzed Borylative Exo-Cyclization of Alkenyl Halides Containing Unactivated Double Bond. *J. Am. Chem. Soc.* **2013**, *135*, 2635, doi: 10.1021/ja3104582.

UNIVERSITAT ROVIRA I VIRGILI
DEVELOPMENT OF VISIBLE LIGHT PHOTOREDOX METHODOLOGIES TOWARDS THE ACTIVATION
OF CARBON-HALOGEN BONDS
Miguel Claros Casielles

UNIVERSITAT ROVIRA I VIRGILI
DEVELOPMENT OF VISIBLE LIGHT PHOTOREDOX METHODOLOGIES TOWARDS THE ACTIVATION
OF CARBON-HALOGEN BONDS
Miguel Claros Casielles

Chapter V



Mechanistic Understanding of Visible-Light Activation of C-Cl

UNIVERSITAT ROVIRA I VIRGILI
DEVELOPMENT OF VISIBLE LIGHT PHOTOREDOX METHODOLOGIES TOWARDS THE ACTIVATION
OF CARBON-HALOGEN BONDS
Miguel Claros Casielles

V.1.	Contents	
V.2.	State-of-the-art	277
V.2. 1	Two-Electron Redox Mechanism	278
V.2. 2	Single-Electron Mechanism	281
V.2. 3	Photoredox coupled mechanism	285
V.3.	Results and Discussion	293
V.3. 1	Detection of Carbon-Centered Radical Intermediates	293
V3. 2	Detection of the Ni-Active Species	298
V.3. 3	Exploring the Reaction between Ni-Active Compound and Alkyl- Chlorides	304
V.3. 4	DPA-based System	310
V.3. 5	Mechanistic Proposal	317
V.4.	Conclusions	319
V.5.	Experimental Section	321
V.5. 1	Material and Reagents	321
V.5. 2	Instrumentation	321
V.5. 3	Synthesis of Metal Complexes	323
V.5. 4	Characterization of Products	324
V.6.	References of the Chapter	329

Figure V.1 Comparison of the properties of Ni and Pd: more accessible oxidation states for nickel and palladium (top), different modes of reactivity (bottom-left) energetic barriers for β -hydride elimination for both metals (bottom-right) Free-energy values calculated for $M(PPh_3)_2$ complexes.	277
Figure V.2 Common mechanisms of two-electron Ni^0/Ni^{II} -catalyzed cross-coupling reactions.....	278
Figure V.3 Ni^I-Ni^{III} cycle in Buchwald-Hartwig amination of aryl bromides mediated by NHC- Ni^I complexes.....	279
Figure V.4 Nevado's mechanistic proposal for the reductive dicarbofunctionalization of non-activated olefins.	280
Figure V.5 Initial step in the MCR-catalyzed methane formation.	281
Figure V.6 Single-electron pathways involving Ni^0 , Ni^I , Ni^{II} , Ni^{III} and organic radicals.	282
Figure V.7 Nickel-catalyzed Negishi reaction.....	283
Figure V.8 Nickel-catalyzed Kumada cross-coupling reaction by radical rebounding mechanism.....	283
Figure V.9 (Xantphos) Ni^I -mediated alkyl bromide activation.	284
Figure V.10 Radical clock and stoichiometric experiments for the reductive coupling of alkyl acids developed by Gong and co-workers.....	285
Figure V.11 Dual photoredox-nickel-catalyzed $C-C$ bond forming reaction through oxidative radical generation.	287
Figure V.12 MacMillan's photoredox-nickel coupled functionalization of $C-H$ bonds mediated by amine radical cation.	288
Figure V.13 Doyle's proposed mechanism for the nickel-catalyzed $C-H$ functionalization by chlorine radical hydrogen abstraction.	289

Figure V.14 Molander’s C–H functionalization by energy-transfer mechanism through iridium photocatalyst and nickel complexes.....	290
Figure V.15 Cross-electrophile coupling mediated by silyl radicals.....	291
Figure V.16 Dowd-Beckwith ring expansion reaction mechanism.....	304
Figure V.17 ¹ H NMR spectrum in CDCl ₃ (top) and ² H NMR spectrum in CHCl ₃ (bottom) of deuterated (<i>E</i>)-1-(hex-2-en-1-yl)-4-methoxybenzene.....	294
Figure V.18 Isotopic-labeling experiments for the reductive cyclization reaction of substrate IV.3.p.....	295
Figure V.19 ¹ H NMR spectrum in CDCl ₃ (top) and ² H NMR spectrum in CHCl ₃ (bottom) of protonated IV.4.p.....	295
Figure V.20 ¹ H NMR spectrum in CDCl ₃ (top) and ² H NMR spectrum in CHCl ₃ (bottom) of deuterated [d]-IV.4.p.....	296
Figure V.21 Isotopic-labeling experiments for the reductive cyclization reaction of substrate IV.3.t.....	296
Figure V.22 ¹ H NMR spectrum in CDCl ₃ (top) and ² H NMR spectrum in CHCl ₃ (bottom) of protonated IV.4.t.....	296
Figure V.23 ¹ H NMR spectrum in CDCl ₃ (top) and ² H NMR spectrum in CHCl ₃ (bottom) of deuterated [d]-IV.4.t.....	297
Figure V.24 Calculate BDE for IV.4.t and the energy balance of HAT reaction with CH ₃ CH ₂ OD.....	297
Figure V.25 Calculate BDE for IV.4.p and the energy balance of HAT reaction with CH ₃ CH ₂ OD.....	298
Figure V.26 UV-Vis of ^I HNi (50 μM) in a solution of PC _{Cu} (20 μM) in CH ₃ CN with 11.4 mM DIPEA (left). CVs of ^I HNi (0.5 mM) in 0.1 M TBAH/CH ₃ CN electrolyte at 0.1 V s ⁻¹ . E _{1/2} (Ni ^{III}) = -1.46 V vs. Fc/Fc ⁺ (right).....	299

Figure V.27 UV-Vis SEC of $I^H Ni$ (4 mM) in 0.2 M TBAH/CH₃CN electrolyte. 300

Figure V.28 UV-Vis SEC of $I^H Ni$ (4 mM) in 0.2 M TBAH/CH₃CN electrolyte in the presence of 20 equivalents of substrate *IV.3.i* (80 mM). 300

Figure V.29 UV-Vis SEC of $I^H Ni$ (4 mM) in 0.2 M TBAH/CH₃CN electrolyte in the presence of 20 equivalents of substrate *IV.3.a* (80 mM). 301

Figure V.30 CVs of $I^H Ni$ (0.5 mM) in 0.1 M TBAH/CH₃CN:EtOH (2:3) electrolyte at 0.1 V s⁻¹ in the absence and upon the addition of substrate *IV.3.a*. 301

Figure V.31 UV-Vis SEC of $I^H Ni$ (4 mM) in 0.2 M TBAH/CH₃CN:EtOH (2:3) electrolyte. 302

Figure V.32 UV-Vis SEC of $I^H Ni$ (4 mM) in 0.2 M TBAH/CH₃CN:EtOH (2:3) electrolyte in the presence of 20 equivalents of substrate *IV.3.i* (80 mM). 302

Figure V.33 UV-Vis SEC of $I^H Ni$ (4 mM) in 0.2 M TBAH/ CH₃CN:EtOH (2:3) electrolyte) in the presence of 20 equivalents of substrate *IV.3.a* (80 mM) without (left) and with 114.5 mM DIPEA (right)..... 303

Figure V.34 EPR spectra and simulations of reaction mixture with substrate (left), reaction mixture and $I^H Ni$ complex (bottom left), reaction mixture and $I^H Ni$ complex with substrate *IV.3.i* (bottom right). 304

Figure V.35 UV-Vis of $I^H Ni$ (50 μM) in a solution of PCu (20 μM) in CH₃CN:EtOH (2:3) with 11.4 mM DIPEA. 20 equivalents of substrate *IV.3.a* (1 mM) were added after 218 s of monitoring. 305

Figure V.36 Absorbance monitored at 536 nm of an irradiated (447 nm) solution containing PCu (20 μM) in CH₃CN:EtOH (2:3) with DIPEA (11.4 mM) after the addition of $I^H Ni$ (50 μM) (40 s from irradiation started). and 20 eq. of *IV.3.a*.... 306

Figure V.37 Thermodynamics of the coordination of CH₃CN and Cl⁻ to $[Ni^I(Ts^H Py_2 tacn)]^+$ 307

Figure V.38 CVs of $I^H Ni$ (0.5 mM) in 0.1 M TBAH/CH ₃ CN electrolyte at 0.1 V s ⁻¹ in the absence and presence of TBACl.....	307
Figure V.39 Comparison between DFT(uB3LYP/6-31g**/uB3LYP/6-311+g**) calculated free energy barriers for the reaction of [Ni ^I (Ts ^H Py ₂ tacn)] (II) with the model substrates (3-chloropropyl)benzene as an oxidative S _N 2-type reaction (green profile) or concerted halogen atom abstraction (red).	308
Figure V.40 B3LYP-D ₃ /6-311+G** spin densities of intermediates I ₃ _{NiIII-C...Cl-} (left) and I ₃ _{NiII-Cl...R·} (right).	309
Figure V.41 Summary of the DFT data.	309
Figure V. 42 UV-Vis spectra of UV-Vis of <i>Ni-DPA</i> (50 μM) in a solution of <i>PC_{Cu}</i> (20 μM) in CH ₃ CN with 11.4 mM.	310
Figure V.43 UV-Vis SEC of <i>Ni-DPA</i> (4 mM) in 0.2 M TBAH/CH ₃ CN electrolyte.	311
Figure V.44 Cyclic voltammograms of [Ni ^{II} (DPA-bpy)(OTf)]OTf (1mM) in 0.2 M TBAH/CH ₃ CN electrolyte at 0.1 V s ⁻¹	311
Figure V.45 EPR spectra and simulations of <i>Ni-DPA</i> (orange), the mixture of <i>Ni-DPA</i> and <i>PC_{Cu}</i> before (yellow) and after irradiation (purple).	312
Figure V.46 General scheme for the <i>Ni^I-DPA</i> promote activation of <i>Csp³-Cl</i> bonds.	312
Figure V.47 UV-Vis of <i>Ni-DPA</i> (50 μM), <i>PC_{Cu}</i> (20 μM) and DIPEA (11.4 mM) in CH ₃ CN (top-left), SEC of <i>Ni-DPA</i> (4 mM) in a 0.2 M TBAH/CH ₃ CN electrolyte (top-right) and UV-VIS of <i>Ni-DPA</i> (4 mM) in presence of NaBH ₄ (3 eq.) (bottom-left).	313
Figure V.48 X-Ray structure of <i>Ni^{II}-DPA_{BH₄}</i> obtained during the chemical reduction of <i>Ni^I-DPA</i> with NaBH ₄	314

Figure V.49 X-Ray structure of Ni^{II} -DPA_ NH_2Et obtained during the chemical reduction of Ni^{II} -DPA with $NaBH_4$	314
Figure V.50 Proposed reactivity of Ni^I and Alkyl-chlorides.	315
Figure V.51 Paramagnetic 1H -NMR spectrum of the product obtained by reaction of the Ni^I intermediate formed photochemically and the substrate (top) and the Ni^{II} -DPA_ Cl chemically synthesized (bottom).....	316
Figure V.52 X-Ray structure of Ni^{II} -DPA_ Cl obtained after reaction of Ni^I -DPA with (3-chloropropyl)benzene.	316
Figure V.53 CVs of $I^H Ni$ (0.5 mM) in 0.1 M TBAH/ CH_3CN electrolyte at $0.1 V s^{-1}$ in the absence (black) and presence (red) of 20 eq. of substrate (3-chloropropyl)benzene (left) and CVs of Ni -DPA (0.5 mM) in 0.1 M TBAH/ CH_3CN electrolyte at $0.1 V s^{-1}$ in the absence (black) and presence (red) of 20 eq. of substrate IV.3.a (right).....	317
Figure V.54 Proposed catalytic cycle for the visible-light reductive cyclization of non-activated alkyl chlorides with tethered alkenes.....	318
Figure V.55 Setup for UV-Vis measurement with <i>on-line</i> irradiation.	322

V.2. State-of-the-art

Nickel catalyzed $C-C$ and $C-Het$ bond forming reactions have appeared as an earth-abundant alternative to palladium, which has been used in pharmaceutical synthetic procedures since 1950's and currently provides more than 40% of metal-catalyzed $C-C$ bond-forming reactions.¹⁻³ Nickel exhibits distinctive properties compared to palladium. It is known that the majority of palladium-catalyzed reactions are based on two-electron processes (Pd^0/Pd^{II}).⁴⁻⁶ However, the more easily accessible Ni^I and Ni^{III} oxidation states allow nickel-catalysis to access to different modes of reactivity and radical mechanisms. The more confined electron cloud of nickel compared with its second and third row counterparts is translated into a higher spin pairing energy for nickel *i.e.* less covalent interactions and, therefore, more stable open-shell electronic configurations.⁷ Nickel backdonates significant electron density to π -acceptors such as olefins producing strong σ -donor/ π -acceptor bonds. Consequently, β -hydride elimination in nickel complexes tends to be slower than in equivalent palladium complexes due to the slower $M-C$ bond rotation prior to the β -hydride elimination (**Figure V.1**, bottom-right).⁸⁻¹¹

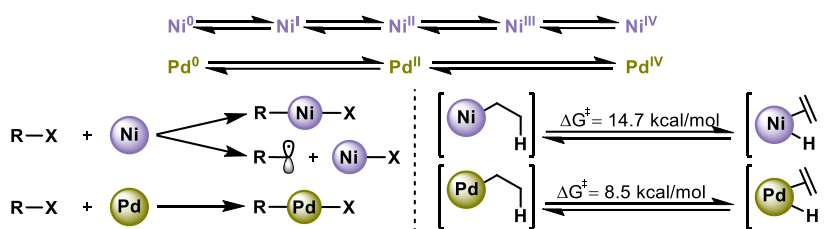


Figure V.1 Comparison of the properties of Ni and Pd: more accessible oxidation states for nickel and palladium (top), different modes of reactivity (bottom-left) energetic barriers for β -hydride elimination for both metals (bottom-right). Free-energy values calculated for $M(PPh_3)_2$ complexes.⁸

Due to the nickel's easy accessibility to its oxidation states, the reactivity of nickel complexes against electrophiles may follow either i) a classic two-electron oxidative addition (section V.2. 1) or ii) a single electron process producing radicals as intermediates (section V.2. 2). In addition, both scenarios can be seen in a photoredox-triggered mechanism (section V.2. 3) where the typically active catalyst is formed by reaction with the photoactive molecule. A detailed introduction to the

state of the art and implications of the three mentioned mechanisms is described in the following sections.

V.2.1 Two-Electron Redox Mechanism

Nickel complexes can engage in two electron catalytic cycles, *via* reaction intermediates $\text{Ni}^0/\text{Ni}^{\text{II}}$ or $\text{Ni}^{\text{I}}/\text{Ni}^{\text{III}}$. For example, the nickel-catalyzed cross-coupling reactions with Csp^2 electrophiles are mainly proposed to occur by a two-electron mechanism *via* $\text{Ni}^0/\text{Ni}^{\text{II}}$ intermediates.¹² The main steps of the catalytic cycle are the oxidative addition of aryl halides to Ni^0 , followed by transmetalation and subsequent reductive elimination (**Figure V.2**, top). Ni^0 species are highly reducing and facilitate the oxidative addition reaction with a wide range of typically inert electrophiles such as aryl chlorides,¹³ aryl ethers,¹⁴ sulfamates,¹⁵ alkyl and aryl fluorides,¹⁶ epoxides,¹⁷ aziridines,¹⁸ amides¹⁹ and nitriles.²⁰ Moreover, an S_N2 oxidative addition pathway was also proposed for the stereospecific Kumada coupling, when catalyzed by Ni-NHC or Ni-bisphosphine ligands. As a result, the nucleophilic attack of Ni-Alkyl intermediate to the benzyl/allyl ether promote an inversion of configuration at the benzylic position (**Figure V.2**, bottom).

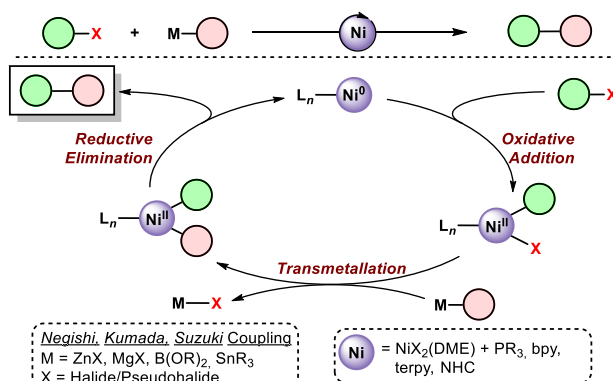


Figure V.2 Common mechanisms of two-electron $\text{Ni}^0/\text{Ni}^{\text{II}}$ -catalyzed cross-coupling reactions.

A number of two-electron redox processes are also mediated by Ni^I/Ni^{III} intermediates. Matsubara and co-workers demonstrated the feasibility of a Ni^I oxidative addition.²¹ They isolated the catalytically competent (iPr)Ni^I(NPh₂) intermediate for the *Buchwald-Hartwig* amination of aryl halides and studied their oxidative addition with Ni^I compounds to generate the Ni^{III} intermediates (**Figure V.3**). The reductive elimination from Ni^{III} complexes was also characterized in the context of C–C⁵ and C–Hal²² bond forming reactions.

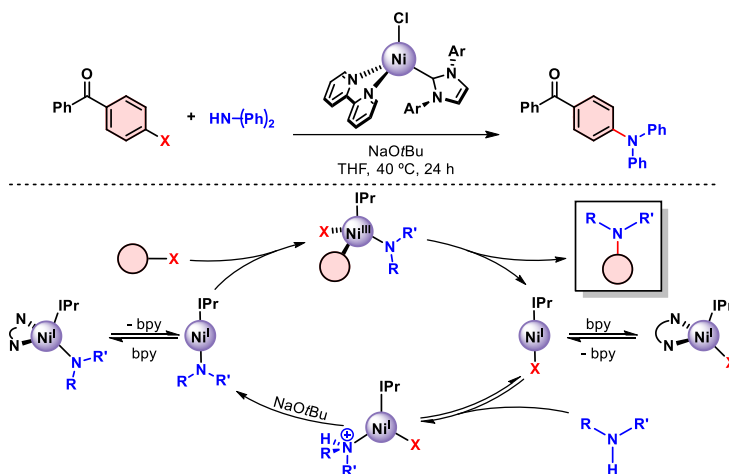


Figure V.3 Ni^I-Ni^{III} cycle in *Buchwald-Hartwig* amination of aryl bromides mediated by NHC-Ni^I complexes. IPr = 1,3-bis(2,6-diisopropylphenyl)imidazol-2-ylidene.

Very recently, Nevado and co-workers also proposed a complex mechanism involving a two-electron Ni^I/Ni^{III} mechanism with Ni^I/Ni^{II}/Ni^{III} steps for the reductive dicarbofunctionalization of non-activated alkenes.²³ In the proposed mechanism, an oxidative addition of the aryl halides followed by a two-electron-reduction yields a Ni^I-Aryl intermediate that undergoes a *Halogen Atom Abstraction* (*HAA*) releasing a carbon-centered radical. After the addition of the carbon-centered radical onto the olefin, a new carbon-centered radical species is formed which undergoes fast recombination to give a Ni^{III}-Alkyl intermediate prior to a reductive elimination to yield the coupling product and the initial Ni^I compound (**Figure V.4**).

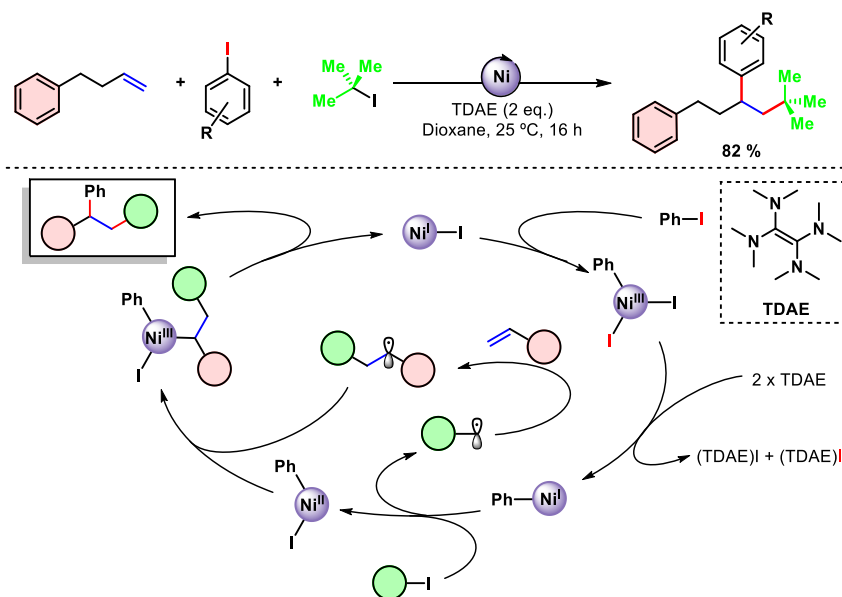


Figure V.4 Nevado's mechanistic proposal for the reductive dicarbofunctionalization of non-activated olefins.

Ni^I oxidation state has been found to be a key intermediate in the biological methane formation catalyzed by *Methyl-Coenzyme Reductase (MCR)* F₄₃₀. Based on *ESR*, *MCD* and theoretical calculations, two plausible mechanisms have been proposed for how methane is biologically generated. Both mechanisms suggest a nucleophilic attack of a Ni^I intermediate to the substrate (**Figure V.5**). In mechanism I showed in **Figure V.5** proposed by Thauer and co-workers in 1997 a nucleophilic attack of the Ni^I intermediate at the methyl group of CH₃SCoM generates a Ni^{III}-CH₃ intermediate prior to methane formation (**Figure V.5**, left).²⁴ On the other hand, a few years later, Pelmenchikov and Siegbahn proposed that the attack occurs at the thioester-S moiety to give a covalent Ni^{II}-SCoM.^{25,26} In this manner, two scenarios can take place: *i*) a *Nucleophilic Attack and Heterolytic Cleavage* forming a formally anionic methyl group (**Figure V.5**, mechanism II_a) or a *ii*) *Metal-Ion promoted Homolytic Cleavage* releasing a methyl radical (**Figure V.5**, mechanism II_b).

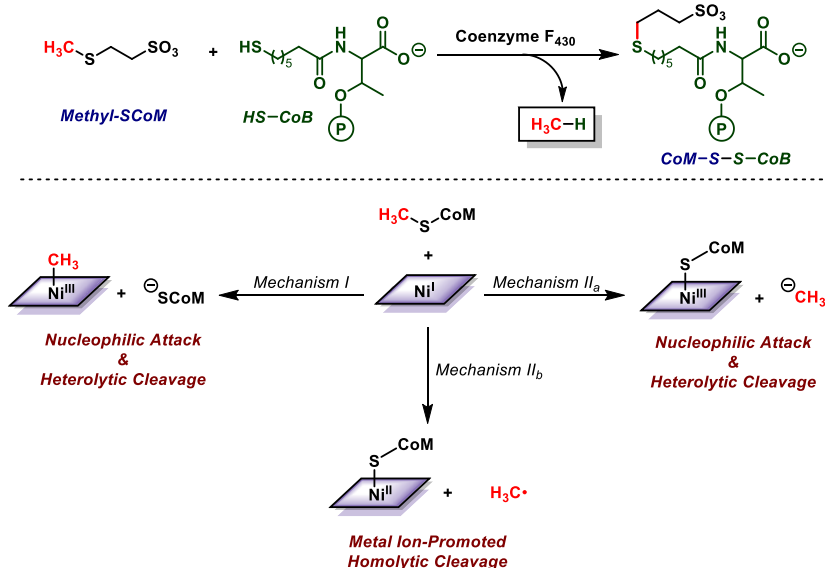


Figure V.5 Initial step in the MCR-catalyzed methane formation.

Transient kinetic, spectroscopic and computational studies performed by Ragsdale and co-workers have demonstrated the formation of Ni^{III}-SCoM ruling out the methyl-Ni^{III} intermediate.²⁷ Additional computational studies have suggested that the inaccessibility of the nucleophilic attack and heterolytic cleavage pathway is due to the positive reduction potential of the Ni^{III}-SCoM intermediate.

V.2.2 Single-Electron Mechanism

The easily accessible redox chemistry of nickel opens up different possible catalytic cycles than involve one electron processes. In those catalytic cycles we can suggest two main mechanisms. As such, a system dependent sequence of electrophile and nucleophile activation may lead to a i) *Radical rebound pathway* in which the Ni^I intermediate reacts with the nucleophile as first reaction step (**Figure V.6**, left) and a ii) *Radical chain pathway* where Ni^I initiates the formation of a radical from the electrophile prior to transmetalation with the nucleophile (**Figure V.6**, right). Both mechanisms have a common halogen atom abstraction forming a Ni^I-halide

intermediate. *N*-containing chelating ligands such as *N*-heterocyclic carbene (NHC), bipyridine or terpyridine ligands usually promote this reactivity.

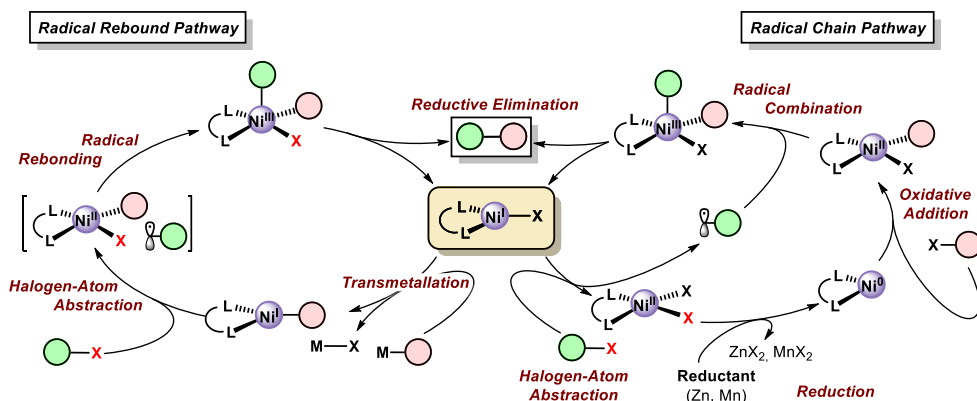


Figure V.6 Single-electron pathways involving Ni^0 , Ni^{I} , Ni^{II} , Ni^{III} and organic radicals.

Radical Rebound Pathway

Radical rebound pathway initiates with a transmetalation between Ni^{I} -halide and the nucleophile, step that forms a Ni^{I} nucleophile intermediate. Subsequently, a HAA to the electrophile yields the couple of Ni^{II} nucleophile halide/radical that collapses in a rebounding mechanism forming a Ni^{III} intermediate. Then, reductive elimination regenerates the starting Ni^{I} -halide intermediate and the coupling product.

Along these lines, Vicic and co-workers reported a nickel-catalyzed alkyl-alkyl Negishi procedure where the initial $\text{Ni}^{\text{I}}(\text{Terpy})\text{I}$ reacts through a transmetalation step with an alkyl- ZnBr .²⁸ This reaction gives $\text{Ni}^{\text{I}}(\text{Terpy})\text{R}$ as intermediate which reacts with the electrophile to get the nickel/radical couple. Radical combination yields the Ni^{III} -Alkyl intermediate that then will undergo the reductive elimination to release the final coupling product (Figure V.7).

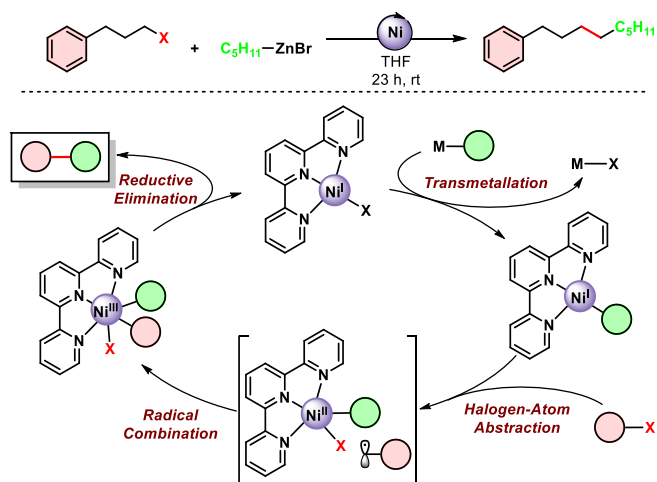


Figure V.7 Nickel-catalyzed Negishi reaction.

Independently, Hu and co-workers, reported a Kumada coupling reaction catalyzed by a $[Ni(N_2N)]$ pincer catalyst with an analogous mechanism (Figure V.8).²⁹ In this example, the transmetalation of Ni^{II} with $RMgCl$ gives $Ni^{II}-R$ intermediate that undergo a HAA of alkyl bromides. Afterwards, the free carbon-centered radical is trapped by the $Ni^{II}-R$, forming the $R-Ni^{III}-Alkyl$ compound prior the reductive elimination, which releases the final coupled product and enters the Ni^I complex. The comproportionation of Ni^I with Ni^{III} regenerates Ni^{II} starting compound.

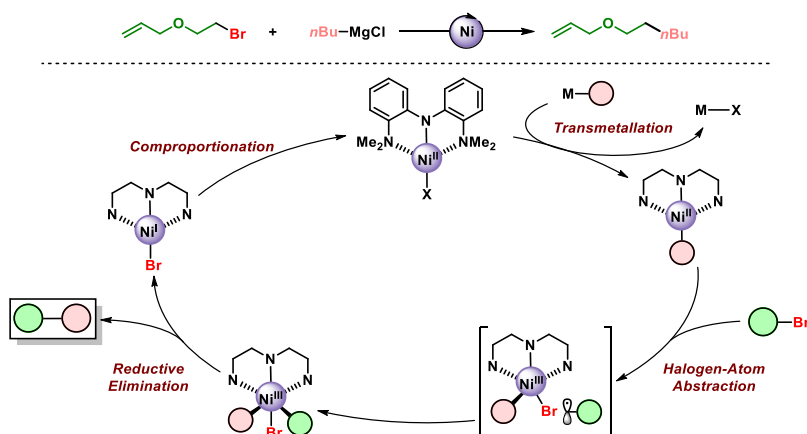


Figure V.8 Nickel-catalyzed Kumada cross-coupling reaction by radical rebounding mechanism.

Radical Chain Pathway

Secondary alkyl electrophiles are often activated *via* radical chain mechanism due to the possibility for secondary radicals to survive. This concept has been explored for the stereoconvergent reactions of propargylic carbonates, α -haloketones, boronate nucleophiles in the synthesis of chiral alcohols and carbamates³⁰ and α -silyl bromides in the synthesis of chiral alkyl silanes containing heterocycles and polar functional groups.³¹ The radical chain process involves the combination of a metal intermediate with an alkyl radical that is diffused to the bulk solution after halide abstraction from alkyl halides. Mechanistic investigations performed by Diao and co-workers for the activation of alkyl halides by (*t*Bu-Xantphos)Ni^I-Ar complexes showed the formation of carbon-centered radicals from activation by Ni^I species (**Figure V.9**). Kinetic studies on the steric, electronic and solvent effects revealed the *Concerted Halogen-Atom Abstraction (CHAA)* as the most likely mechanism as opposed to other possible pathways, such as oxidative addition, outer-sphere electron transfer, and inner-sphere electron transfer mechanisms.³²

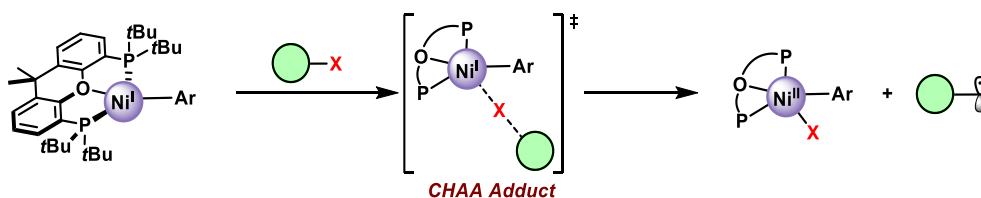


Figure V.9 (*t*Bu-Xantphos)Ni^I-mediated alkyl bromide activation.

The slower rate of primary alkyl bromides relative to secondary (1.4 vs 6.0 *10³ M⁻¹s⁻¹ for *n*propyl- and *i*propyl bromide respectively) let them to discard the oxidative addition path. Furthermore, the steric effect of the aryl groups on Ni catalyst and the correlation of ΔG^\ddagger with ΔG^0 (according to Marcus theory) provides evidences against the outer-sphere electron transfer mechanism. Additionally, polar solvents such as DME or acetone, gave them slower rates than non-polar solvents

(pentane or benzene) discarding reaction mechanisms going through ionic intermediates as outer- or inner-sphere electron transfer.

Ni-catalyzed reductive coupling of alkyl halides and alkyl acids was reported by Gong and co-workers.³³ In that work, a competition between double oxidative addition and a radical chain mechanism was proposed for the acylation event (see **Figure V.6** for comparison of both mechanisms). Stoichiometric experiments together with radical clock reactions, provide support for the radical chain process vs the double oxidative addition pathway (**Figure V.10**).

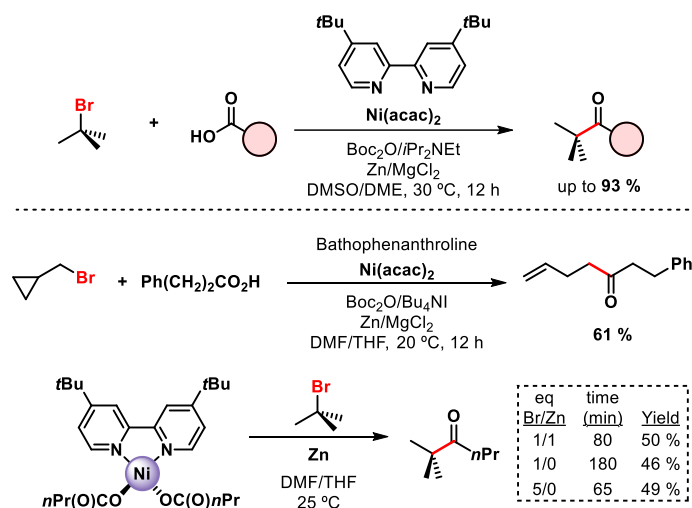


Figure V.10 Radical clock and stoichiometric experiments for the reductive coupling of alkyl acids developed by Gong and co-workers.

V.2.3 Photoredox coupled mechanism

Over the last decade, photoredox catalysis is competing with the traditional thermal catalysis and the newly branded electrocatalysis for the development of C–C and C–Het cross coupling reactions initiated by the formation of radicals. As we saw in previous chapters, oxidative and reductive quenching of light-excited photoredox catalysts by electron acceptors or electron donors, have broadened the scope of radical precursors to include trifluoroborate salts, carboxylates, silicates, and dihydropyridines. Despite the prolific success of photoredox-nickel dual catalysis from the works of Molander, Nishibayashi, Fensterbank, Doyle and MacMillan

among others, a detailed mechanistic understanding of these processes remains elusive. Usually, in merged photoredox-nickel systems, the mechanism is divided in two main parts; a photoredox cycle, mediated by the photoredox catalyst (*PC*), and the bond-formation cycle, mediated by the nickel catalyst. The photoredox mechanism is only relatively well-understood for few examples, such as ruthenium bipyridyl complexes under idealized conditions (see *Chapter I* for more details).³⁴ Even more problematic is the role of the nickel complex in the catalytic cycle which remains in the proposal stage of investigation. A clear need for detailed kinetics studies, isolation of catalytic relevant intermediates and subsequent stoichiometric studies are essential to progress in the field.

Mainly, all current mechanistic proposals rely on the same pathway type. Upon light excitation of the photocatalyst, the formed excited state can oxidize the corresponding electrophile (carboxylic acid, potassium organoborate, alkylsilicate or alkyl dihydropyridine) to yield the carbon-centered radical. Subsequently, Ni⁰ complex undergoes an oxidative addition reaction with the aryl halide forming a Ni^{II}-aryl compound which can subsequently trap the free radical species resulting in the formation of Aryl-Ni^{III}-Alkyl complex. Rapid reductive elimination releases the desired *Csp*³-*Csp*² coupled product and gives a Ni^I-X intermediate. The *SET* reaction between the Ni^I-X and the reduced photocatalyst subsequently closes both cycles. This dual nickel-photoredox mechanism for C–C bond-forming protocol has not been unambiguously established yet and alternative Ni⁰-Ni^I-Ni^{III}-Ni^I cycles have also been proposed.³⁵

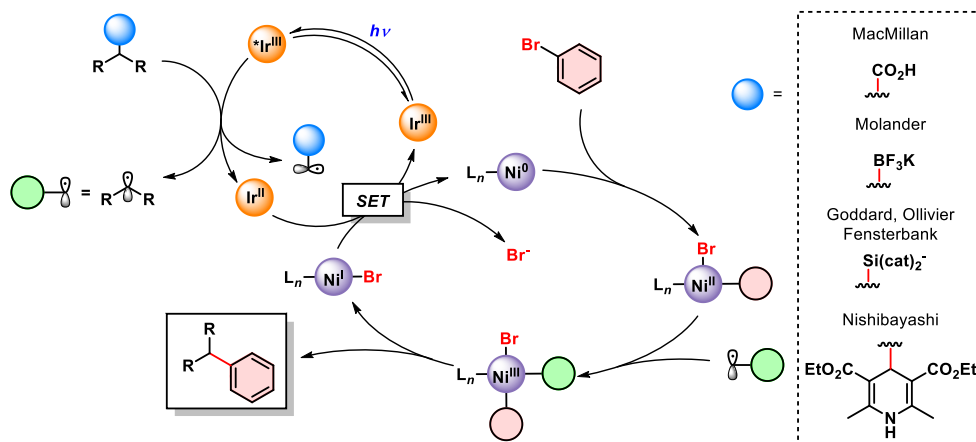


Figure V.11 Dual photoredox-nickel-catalyzed C–C bond forming reaction through oxidative radical generation.

This metallaphotoredox strategy has been successfully applied to a wide range of coupling protocols including the activation of native functional groups via CO₂-extrusion and the synthesis of aromatic and aliphatic ketones.³⁶

Recent studies described the challenging cross-coupling reactions of non-activated C–H-bonds through *Hydrogen Atom Transfer (HAT)* photoredox catalysis. MacMillan and co-workers found in 2016 that nucleophilic tertiary amines such as *quinuclidine* or *DABCO* can engage in a *SET* to the *PC* forming a *N-center* radical cation that can selectively abstract hydric protons to yield carbon-centered radicals (**Figure V.12**).³⁷ Subsequently, the Ni–Aryl complex is formed after an oxidative addition pathway with the corresponding aryl bromide from the reduced Ni⁰ intermediate. Radical trapping from Ni^{II} complex yield the Ni^{III} organometallic complex than subsequently releases the final cross-coupling product regenerating the initial Ni^I compound.

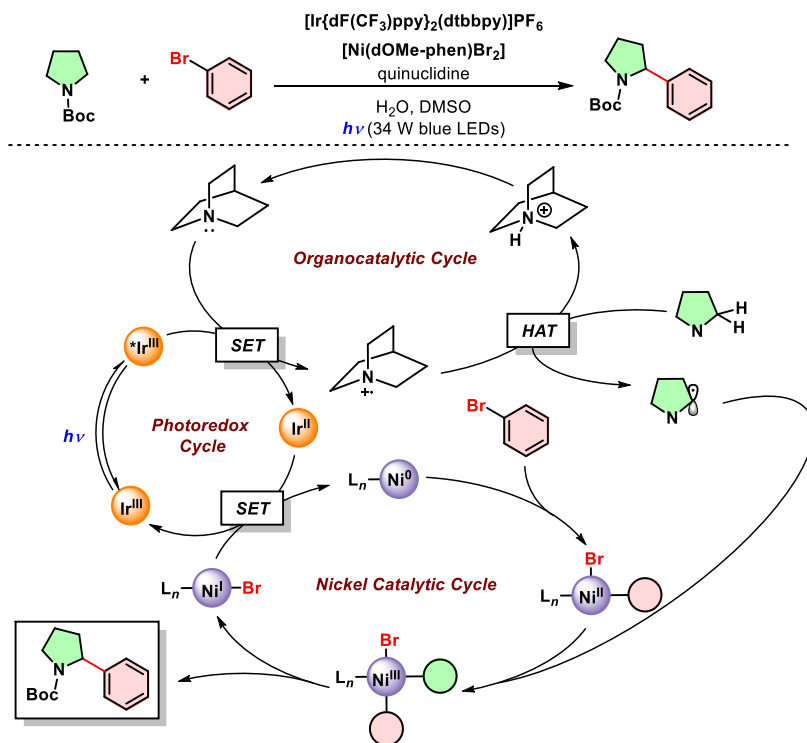


Figure V.12 MacMillan's photoredox-nickel coupled functionalization of C–H bonds mediated by amine radical cation.

In addition to amine radical cations, halogen radicals can also be used as *HAT* reagents as Doyle's group showed for the C–H arylation reaction with aryl chlorides (Figure V.13).³⁸ They proposed that the generation of chlorine radicals by a *two-photon procedure*, mechanism in which the second photon produces the photolysis of $\text{Ni}^{\text{III}}\text{-Cl}$ intermediate forming a Ni^{II} intermediate and the free chlorine radical which engage in a rapid *HAA* yielding a *carbon-centered* radical. Rebound of the resulting radical to the Ni^{II} intermediate produces a Ni^{III} organometallic compound that undergoes a reductive elimination path generating the final $Csp^3\text{-H}$ cross-coupling product.

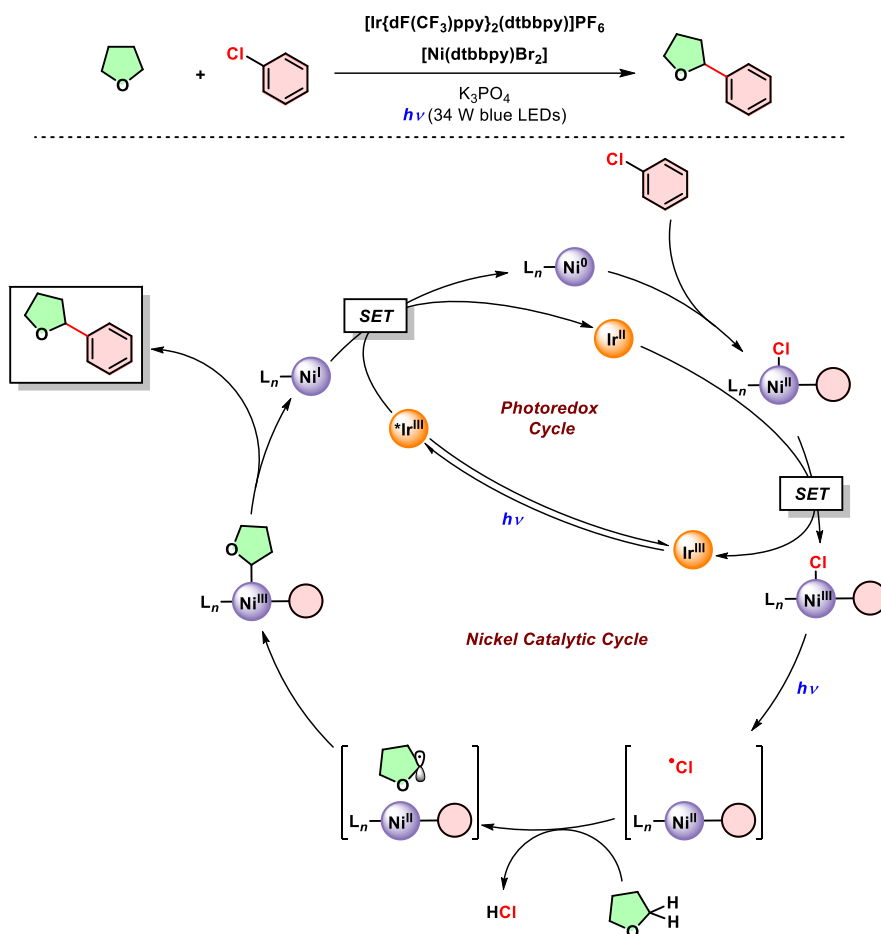


Figure V.13 Doyle's proposed mechanism for the nickel-catalyzed C–H functionalization by chlorine radical hydrogen abstraction.

A similar procedure was also used by Molander's group for the α -oxy and benzylic arylation. In this case, the authors proposed that the extrusion of the bromine radical occurs from an excited Ni^{II} -aryl bromide complex generated through an energy transfer with iridium photocatalyst (**Figure V.14**).³⁹

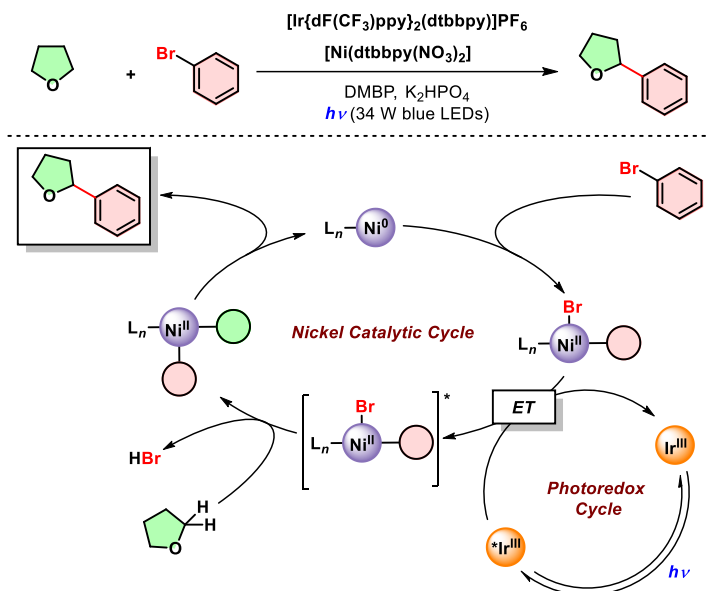


Figure V.14 Molander's C-H functionalization by energy-transfer mechanism through iridium photocatalyst and nickel complexes.

Almost at the same time, MacMillan and co-workers showed another elegant protocol for the selective activation of aryl and alkyl bromides by the combination of nickel catalyst and photoredox-generated silyl radicals. As shown in **Figure V.15**, Ni^0 undergoes preferentially oxidative addition with an aryl-bromide yielding Ni^{II} -aryl species that can trap alkyl radicals generated for the reaction of silyl radicals and alkyl bromides. A reductive elimination from Ni^{III} organometallic intermediate and subsequently *SET* to the reduced Ir^{II} close the photoredox and the nickel catalytic cycles.

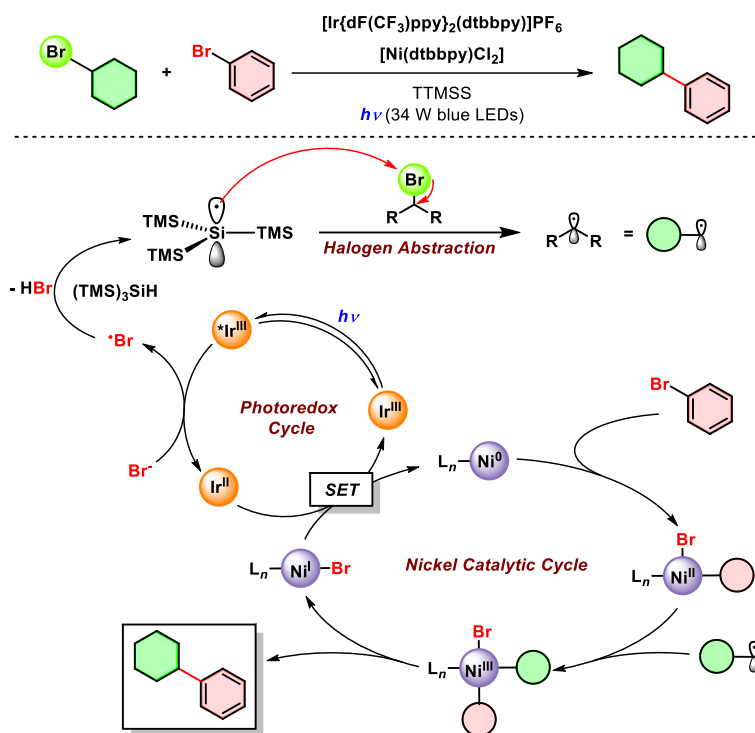


Figure V.15 Cross-electrophile coupling mediated by silyl radicals.

In almost all of these cases, the presence of bidentate (bipyridine, phenanthroline or diimine) or tridentate (terpyridine) ligands in the nickel environment allow the reaction to proceed through an oxidative addition mechanism due to the presence of labile ligands (halide or coordinative solvent molecules) that complete the first coordination sphere of the nickel. The presence of multidentate ligands, such as tetra or pentadentate, is thought to block this type of mechanistic pathway. Nevertheless, metal complexes bearing multi-chelating ligands may open up new avenues for the generation of carbon-centered radicals catalyzed by photoredox/nickel dual catalysis as we propose in this thesis.

V.3. Results and Discussion

The reductive hydro-dehalogenation and the reductive cyclization reactions of non-activated alkyl chlorides described in *Chapters III* and *IV* respectively, are proposed to proceed through carbon-centered radicals generated by the reaction of *in-situ* photogenerated low-valent Co and Ni intermediate with the corresponding alkyl halide (bromide and chloride). The main goal of this chapter is to shed some light into the mechanism of the light-driven radical formation from non-activated Csp^3 –Cl bonds.

V.3.1 Detection of Carbon-Centered Radical Intermediates

Throughout this doctoral dissertation, the formation of carbon-centered radicals was proposed to be part of the mechanism of the dual photoredox catalyzed activation of *Carbon-Halogen* bonds. This proposal stems by the preferentially formation of *5-exo-trig* cyclic products and the extremely importance of the presence of protic solvents in the activation of Csp^3 –Cl bonds.

One of the more established procedures to easily confirm the presence of free radical species is the called “Dowd-Beckwith ring expansion reaction”.^{40,41} This method is based on the studies than separately made both authors in 1987, when they discovered that after the addition of tri-*n*-butyltin hydride to 1-bromomethyl-2-oxocyclopentanone a 6-membered ring was formed (**Figure V.16**, top). They attributed the result to the formation of a free radical intermediate yielded by the homolytic dehalogenation reaction with tri-*n*-butyltin. This free radical intermediate will then attack to the carbonyl group in the key step of the rearrangement. Submitting chloromethyl β -keto ester (**V.1.a**) to our photocatalytic conditions we could isolate the corresponding one-carbon ring expanded product **V.2.a** in 49 % yield, which strongly supports the generation of alkyl radicals during the reaction (**Figure V.16**, bottom).

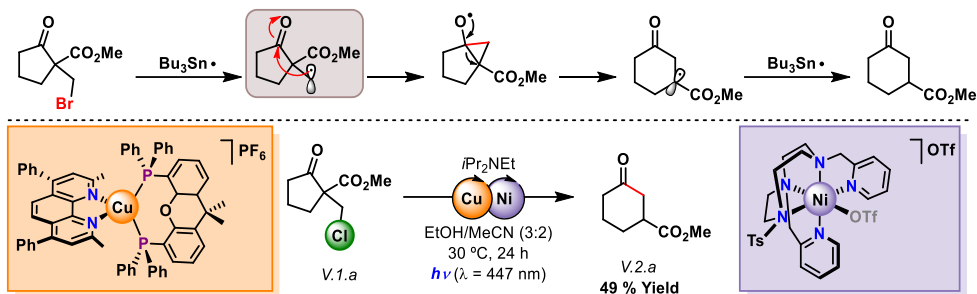


Figure V.16 Dold-Beckwith ring expansion reaction mechanism.

To gain further mechanistic insights, deuterium labeling experiments were performed for dehalogenation and cyclization reductive procedures. In the first case (hydro-dechlorination reaction), we reacted (*E*)-1-(6-chlorohex-2-en-1-yl)-4-methoxybenzene under the standard photoredox conditions using deuterated ethanol as protic solvent and normal acetonitrile as aprotic co-solvent. After standard aqueous work-up we were able to isolate (*E*)-1-(hex-2-en-1-yl-6-d)-4-methoxybenzene in a 51% yield (only 62% of conversion was observed after 24 h) with a deuterium insertion of 62% (Figure V.17).

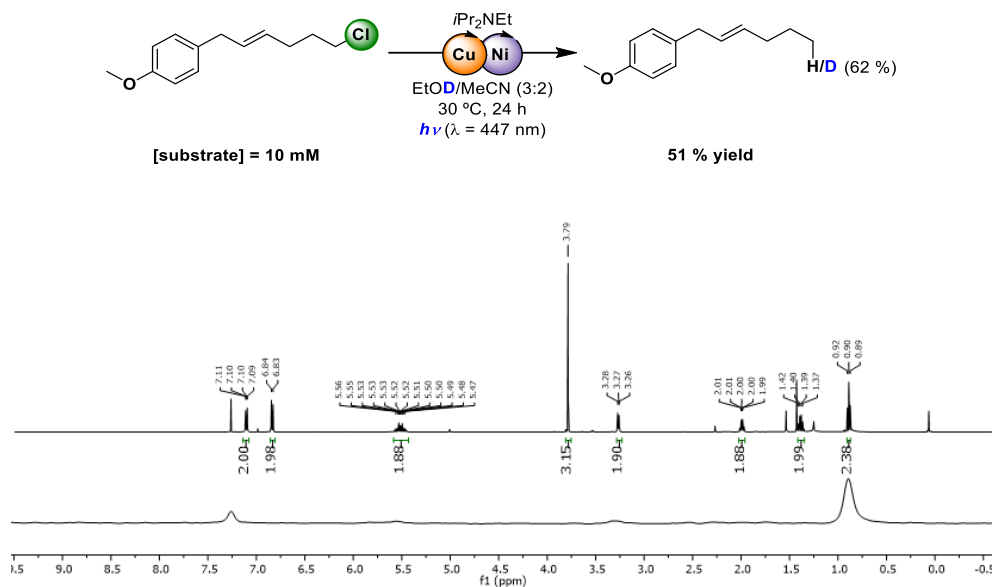


Figure V.17 ^1H NMR spectrum in CDCl_3 (top) and ^2H NMR spectrum in CHCl_3 (bottom) of deuterated (*E*)-1-(hex-2-en-1-yl)-4-methoxybenzene. The signal at 0.9 ppm, correspond to the deuterium inserted into the final product.

Deuterium experiments were also performed for the reductive cyclization reaction with deuterated solvents: ethanol and acetonitrile. For these studies we selected as model substrate one of the more reactive substrates tested in the scope: the (*E*)-2-(2-(6-chlorohex-1-en-1-yl)phenyl)ethan-1-ol. When the photocatalytic cyclization of **IV.3.p** was performed in non-deuterated ethanol and deuterated acetonitrile (EtOH:CD₃CN) no insertion of deuterium was detected in the 5-membered cyclic product (**IV.4.p**) (**Figure V.18**, left). However, when the solvent mixture was the opposite (deuterated ethanol (EtOD) and normal acetonitrile (CH₃CN)) complete incorporation of the deuterium atom was observed at *Cl* position (**Figure V.18**, right).

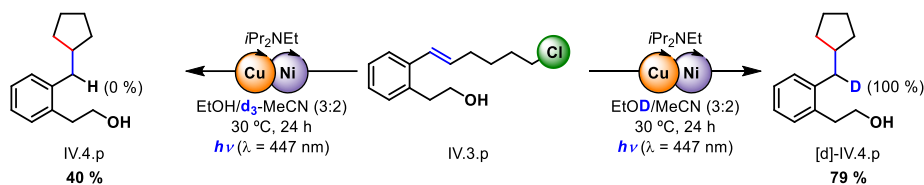


Figure V.18 Isotopic-labeling experiments for the reductive cyclization reaction of substrate **IV.3.p**.

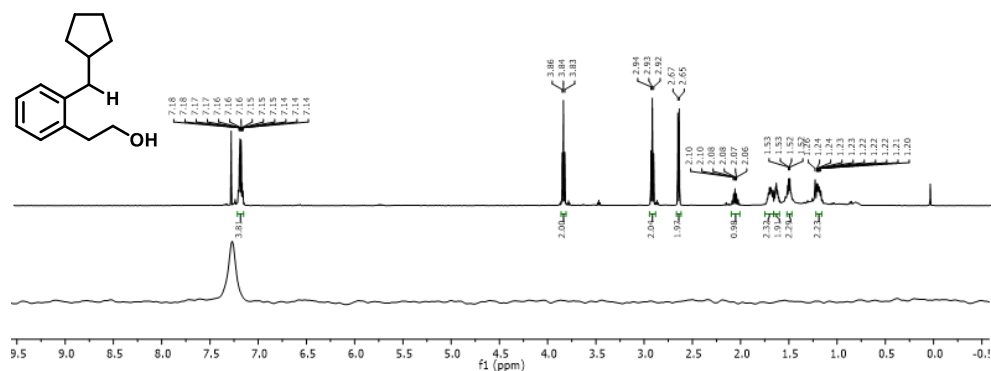


Figure V.19 ¹H NMR spectrum in CDCl₃ (top) and ²H NMR spectrum in CHCl₃ (bottom) of protonated **IV.4.p**.

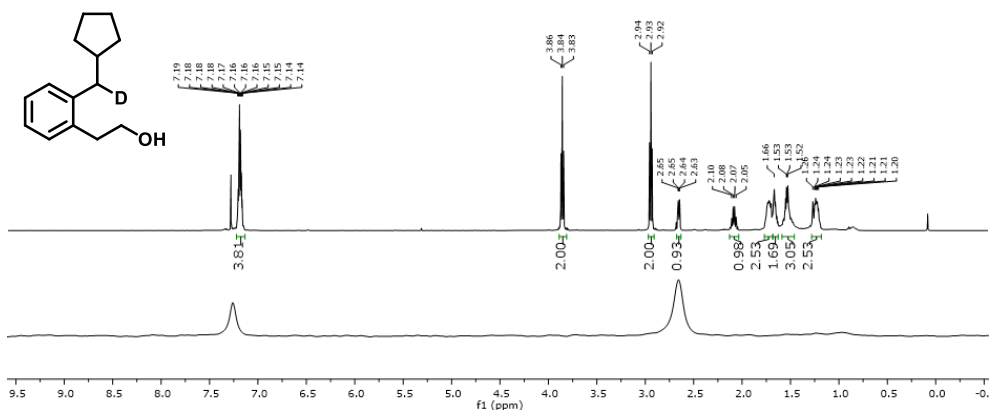


Figure V.20 ^1H NMR spectrum in CDCl_3 (top) and ^2H NMR spectrum in CHCl_3 (bottom) of deuterated $[\text{d}]\text{-IV.4.p}$. The signal at 2.6 ppm corresponds to the deuterium inserted into the final product.

In contrast, when substrate (*E*)-12-chloro-1-morpholinododec-7-en-1-one (**IV.3.t**) was treated to the same reaction conditions, less than 10% of deuterium insertion was observed in α -position to the cyclopentyl while insertion around 66% was found in α -position to the carbonyl due to the enolic equilibrium.

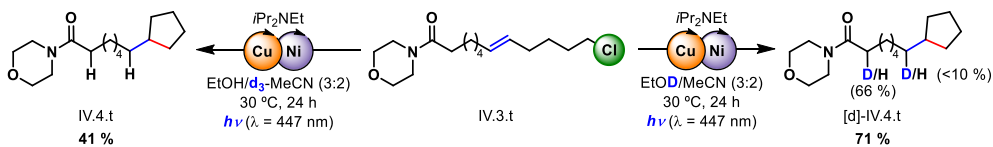


Figure V.21 Isotopic-labeling experiments for the reductive cyclization reaction of substrate **IV.3.t**.

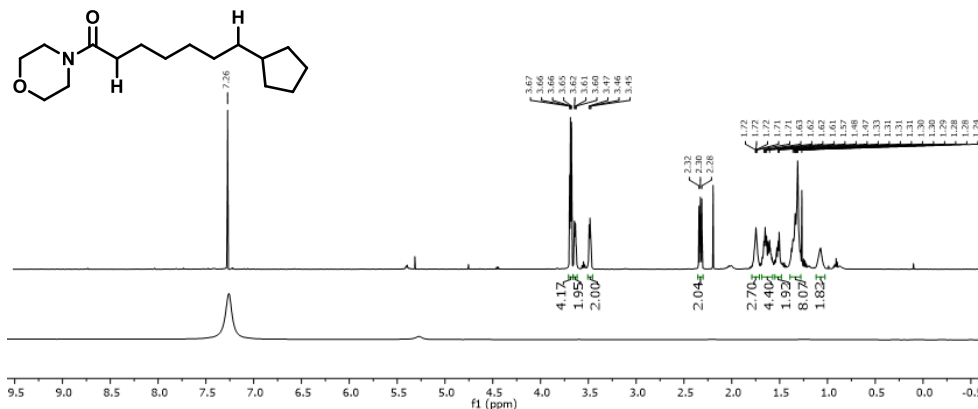


Figure V.22 ^1H NMR spectrum in CDCl_3 (top) and ^2H NMR spectrum in CHCl_3 (bottom) of protonated **IV.4.t**.

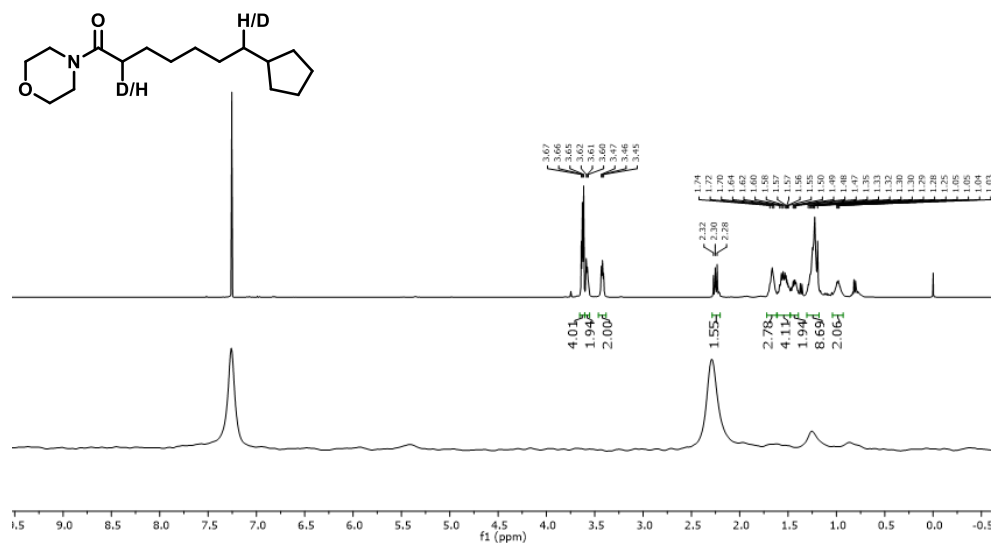


Figure V.23 ^1H NMR spectrum in CDCl_3 (top) and ^2H NMR spectrum in CHCl_3 (bottom) of deuterated $[d]\text{-IV.4.t}$. The signal at 2.3 and 1.3 ppm correspond to the deuterium inserted into the final product.

These results are in concordance with the formation of the benzylic radical for substrate **IV.3.p** which, under the reaction conditions, is reduced to the corresponding radical anion ($E_{1/2} = -1.6$ V vs SCE calculated by DFT), followed by protonation by the [D]-ethanol. On the other hand, the radical cyclization of substrate **IV.3.t** generates a highly reactive alkyl radical intermediate that engage a HAA from the solvent ([D]-ethanol, $\text{BDE}(\text{CH}_3\text{CH}_2\text{OD})\text{-BDE}(\text{IV.4.t}) = -3.1$ kcal·mol $^{-1}$, **Figure V.24**).

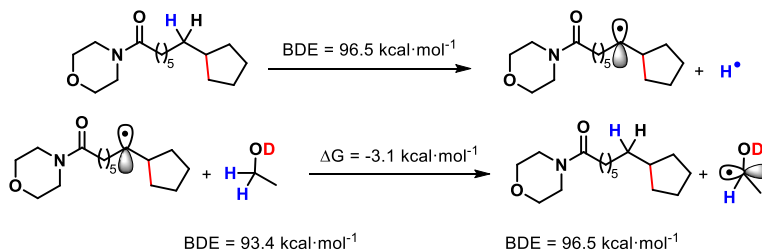


Figure V.24 Calculate BDE for **IV.4.t** and the energy balance of HAT reaction with $\text{CH}_3\text{CH}_2\text{OD}$. Energies do not include correction by concentration, which should favor the products. The energy value for the HAT reaction from $\text{CH}_3\text{CH}_2\text{OD}$ to **IV.3.t** benzyl radical (-3.1 kcal·mol $^{-1}$) is clearly thermodynamically favored. ‡ DFTs performed by Prof. Julio Lloret.

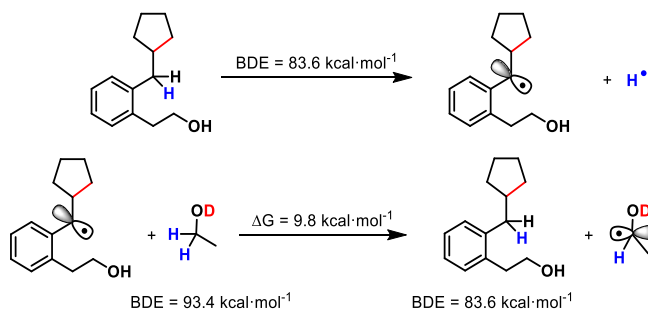


Figure V.25 Calculate BDE for IV.4.p and the energy balance of HAT reaction with $\text{CH}_3\text{CH}_2\text{OD}$. Energies do not include correction by concentration, which should favor the products. The energy value for the HAT reaction from $\text{CH}_3\text{CH}_2\text{OD}$ to IV.3.p benzyl radical ($9.8 \text{ kcal}\cdot\text{mol}^{-1}$) is thermodynamically unfavorable. ‡ DFTs performed by Prof. Julio Lloret.

The combination of both, *Dowd-Beckwith* ring expansion reaction and deuterium labelling experiments, highly support the formation of free radical intermediates in the activation of the $\text{Csp}^3\text{-Cl}$ bond under the photoredox/nickel dual catalytic system.

V3. 2 Detection of the Ni-Active Species

The mechanistic pathways for the activation of the $\text{Csp}^3\text{-Halogen}$ bonds as well as the cleavage of the M-C bond at coenzyme B_{12} derivatives have been widely studied in related model compounds⁴² and in macrocyclic nickel complexes.⁴³⁻⁴⁶ In these studies, the proposal of low-valent Co and Ni intermediates that undergo nucleophilic attack into the $\text{Csp}^3\text{-Halogen}$ bonds is common, although without conclusive experimental probes. Previous work from our group on the photocatalytic hydrogenation of ketones suggested the formation of Co^I intermediates by a *SET* pathway from reduced PCu^{n-1} ($E = -1.60 \text{ V vs SCE}$ against -1.10 V vs SCE for the reduction of $\text{Co}^{II/I}$).⁴⁷ Relying on this previous work we envisioned the postulated low-valent metal intermediate generated under photocatalytic conditions could be the responsible for the activation of the inert $\text{Csp}^3\text{-Cl}$ bond. For that, a combination of spectro- and electrochemical techniques were used to detect and characterize the low-valent metal complex focusing the studies in the use of nickel as metal center.

UV-Vis Spectroelectrochemistry

Upon visible-light irradiation, a long-lived excited PCu^* is formed which is then reductively quenched by tertiary alkylamines yielding the reduced PCu^{n-1} intermediate. This strong reductant formed is then able to reduce Ni^{II} to Ni^I ($E(1^H Ni^{II/I}) = -1.07$ V vs SCE). But it is not so reductant to reduced alkyl chlorides (see Table IV.8 entry 66 where no reaction was observed for the cyclization of non-activated alkyl chlorides with the copper photocatalyst alone). Accordingly, reduced copper PCu^{n-1} promotes a SET reaction with the initial $1^H Ni^{II}$ complex to theoretically form a low-valent Ni^I intermediate.

To prove this hypothesis, we monitored the evolution of the $1^H Ni^{II}$ complex in presence and absence of PCu , electron-donor and substrate. The UV-Vis monitoring of $1^H Ni^{II}$ in the presence of PCu and iPr_2NEt with *on-line* continuous irradiation (LED λ_{max} 447 nm) showed the generation of an intense bands with a λ_{max} at 535 and 361 nm (Figure V.26, left). The appearance of the same broad bands was also observed under spectroelectrochemical conditions, when the applied reduction potential arrives to -1.5 V vs Fc/Fc⁺, assigned to the $Ni^{III/II}$ reduction wave (Figure V.27, right). In agreement with cyclic voltammetry (CV) data, the $Ni^{III/II}$ transition is reversible, recovering the initial spectrum of $1^H Ni^{II}$ upon reoxidation by switching the potential after the $Ni^{III/II}$ wave (Figure V.27).

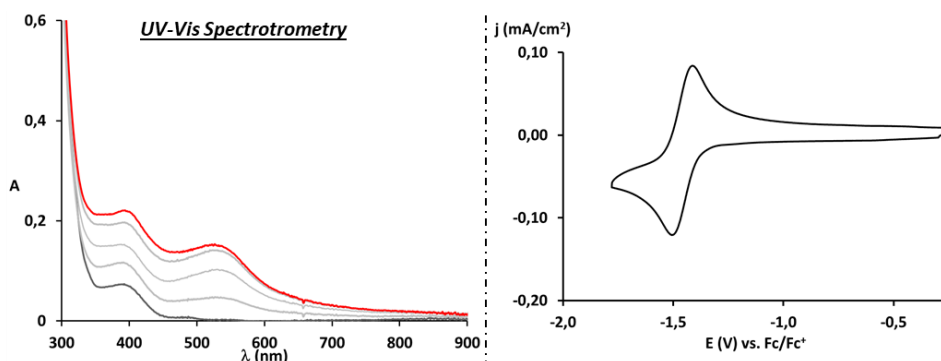


Figure V.26 UV-Vis of $1^H Ni$ (50 μM) in a solution of PCu (20 μM) in CH_3CN with 11.4 mM DIPEA (left). CVs of $1^H Ni$ (0.5 mM) in 0.1 M TBAH/ CH_3CN electrolyte at 0.1 $V s^{-1}$. $E_{1/2}(Ni^{III/II}) = -1.46$ V vs. Fc/Fc⁺ (right).

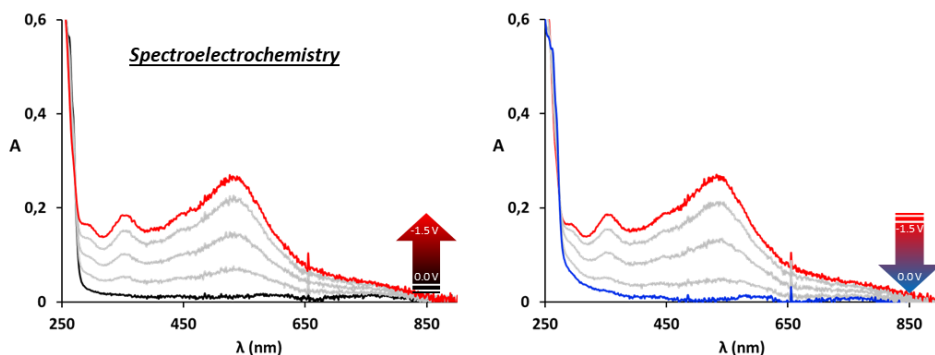


Figure V.27 UV-Vis SEC of $I^H Ni$ (4 mM) in 0.2 M TBAH/ CH_3CN electrolyte. The applied potential is slowly increased from the open circuit voltage (black) to the value corresponding to the Ni^{III} wave (ca. -1.5 V vs. Fc/Fc $^+$, red) and finally back to zero again (blue) (bottom). The intermediate spectra are depicted in grey.

The evidence of Ni^I formation was also observed, in the UV-Vis monitoring experiment under irradiation, during reduction of $I^H Ni^{(II)}$ in the presence of 20 equivalents of the substrate **IV.3.i**, as indicated by the growth of characteristic bands at λ_{max} of 535 and 361 nm (**Figure V.28**, left). However, the strong absorption at 278 nm of **IV.3.i** slowly decreases in the course of reduction (**Figure V.28**), suggesting a slow reaction between the Ni^I species and **IV.3.i**. Interestingly, SEC of $I^H Ni$ in the presence of the more reactive substrate **IV.3.a** shows that a smaller amount of unreacted Ni^I is accumulated during reduction, whereas new intense bands at λ_{max} = 290 and 359 nm appear in the final spectrum (**Figure V.29**).

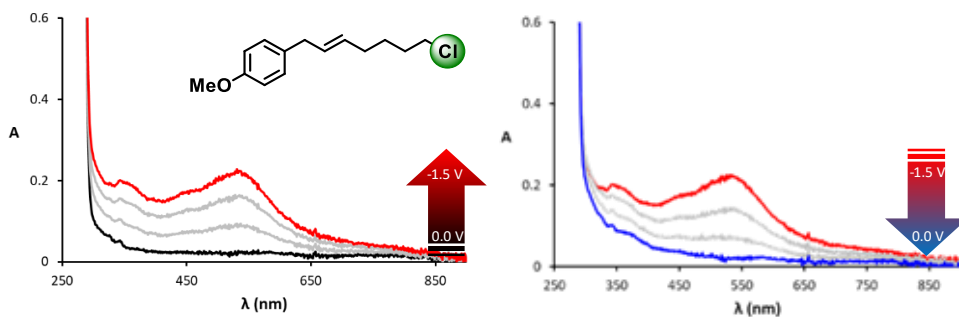


Figure V.28 UV-Vis SEC of $I^H Ni$ (4 mM) in 0.2 M TBAH/ CH_3CN electrolyte in the presence of 20 equivalents of substrate **IV.3.i** (80 mM).

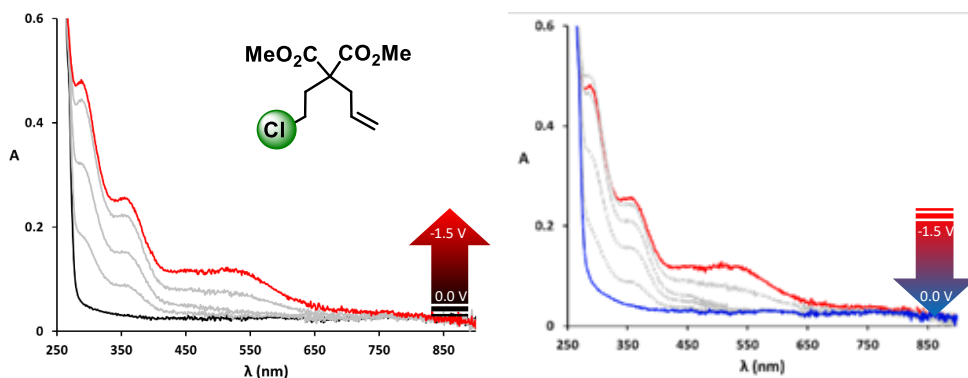


Figure V.29 UV-Vis SEC of 1^{H}Ni (4 mM) in 0.2 M TBAH/ CH_3CN electrolyte in the presence of 20 equivalents of substrate **IV.3.a** (80 mM). The applied potential is slowly increased from the open circuit voltage (black) to the value corresponding to the Ni^{III} wave (ca. -1.5 V vs. Fc/Fc^+ , red) and finally back to zero again (blue). The intermediate spectra are depicted in grey.

The differences observed in SEC between substrates **IV.3.i** and **IV.3.a** suggest the formation of an adduct derived from reaction of the electrogenerated Ni^{I} species and the alkyl chloride, considering that potential species derived from substrates should not be colored. The spectral changes observed during the backward scan may also be consistent with the presence of a mixture of species in solution. Such as, in **Figure V.30**, it can be seen how the Ni^{III} wave tends to lose reversibility by increasing the amount of added organic substrate, whereas a new anodic oxidation appears at -0.66 V vs. Fc/Fc^+ (-0.28 V vs. SCE) and progressively increases.

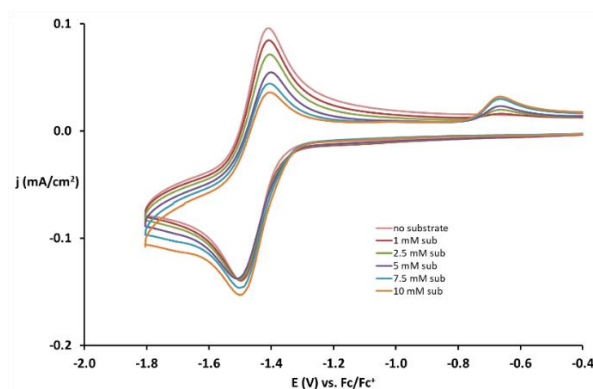


Figure V.30 CVs of 1^{H}Ni (0.5 mM) in 0.1 M TBAH/ $\text{CH}_3\text{CN}:\text{EtOH}$ (2:3) electrolyte at 0.1 V s^{-1} in the absence of substrate (pink) and upon the addition of 2 (magenta), 5 (green), 10 (violet), 15 (cyan) and 20 (orange) eq. of substrate **IV.3.a**.

SEC experiments on $I^H Ni$ in the 0.2 M TBAH/CH₃CN:EtOH (2:3) electrolyte showed analogous results to the ones obtained in pure CH₃CN, showing the reversible formation of a Ni^I species in the absence of substrate (**Figure V.31**).

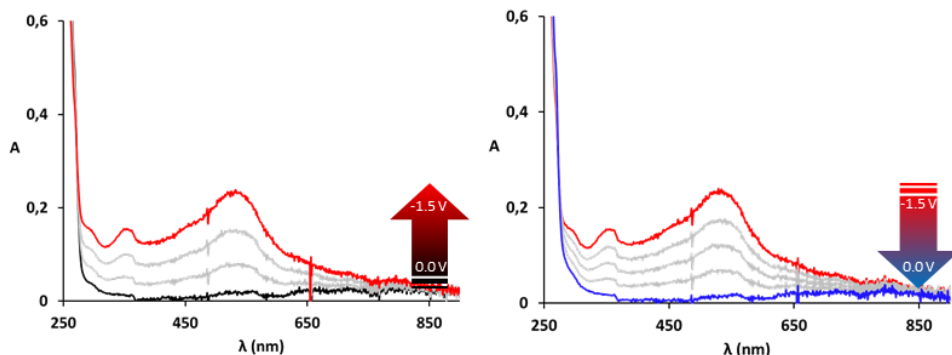


Figure V.31 UV-Vis SEC of $I^H Ni$ (4 mM) in 0.2 M TBAH/CH₃CN:EtOH (2:3) electrolyte. The applied potential is slowly increased from the open circuit voltage (black) to the value corresponding to the Ni^{II} wave (ca. -1.5 V vs. Fc/Fc⁺, red) and finally back to zero again (blue). The intermediate spectra are depicted in grey.

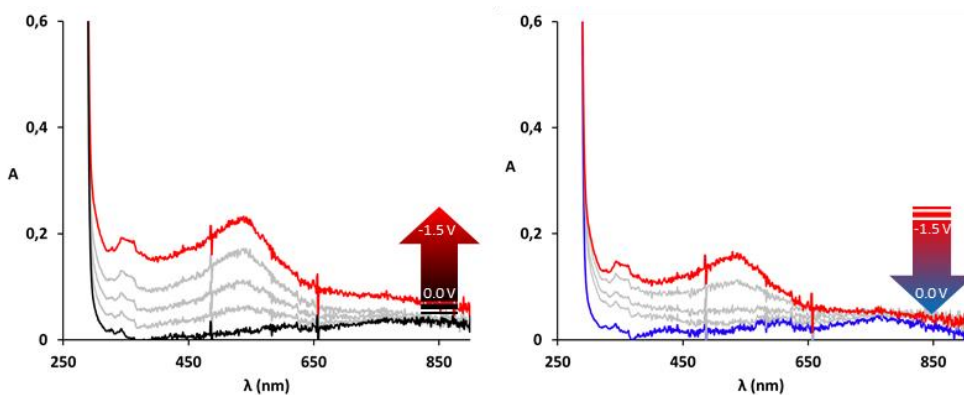


Figure V.32 UV-Vis SEC of $I^H Ni$ (4 mM) in 0.2 M TBAH/CH₃CN:EtOH (2:3) electrolyte in the presence of 20 equivalents of substrate **IV.3.i** (80 mM). The applied potential is slowly increased from the open circuit voltage (black) to the value corresponding to the Ni^{II} wave.

Conversely, the enhanced reactivity of the electrogenerated Ni^I species with the substrate **IV.3.a** is indicated by the lack of free Ni^I in the final spectrum and the appearance of new bands at $\lambda_{max} = 290$ and 359 nm (**Figure V.33**, left). Analogous results were obtained repeating the experiment by using the solvent mixture employed under catalytic conditions (**Figure V.33**, right).

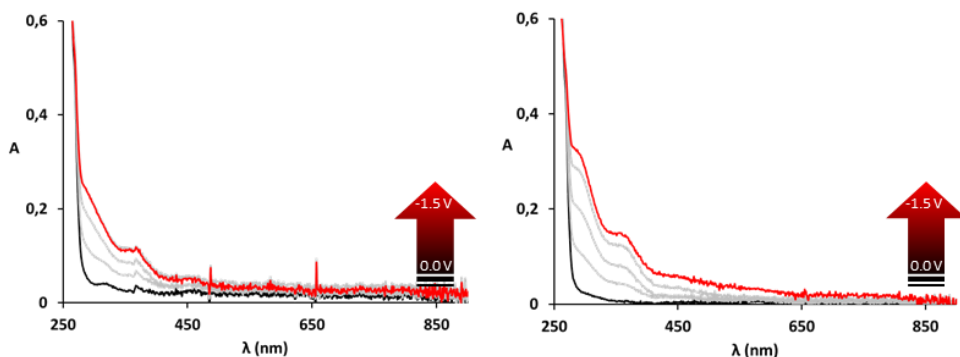


Figure V.33 UV-Vis SEC of $I^H Ni$ (4 mM) in 0.2 M TBAH/ $CH_3CN:EtOH$ (2:3) electrolyte in the presence of 20 equivalents of substrate **IV.3.a** (80 mM) without (left) and with 114.5 mM DIPEA (right). The applied potential is slowly increased from the open circuit voltage (black) to the value corresponding to the Ni^{III} wave (ca. -1.5 V vs. Fc/Fc^+ , red) and finally back to zero again (blue).

Electronic Paramagnetic Resonance Studies

Due to the paramagnetic nature of the Ni^I intermediate proposed in this study, *Electronic Paramagnetic Resonance (EPR)* experiments were performed to identify the nature of the reactive nickel species. Control experiments before irradiation as well as irradiation of the reaction mixture with substrate in the absence of Ni complex did not yield any *EPR* signal (**Figure V.34**, top). However, upon irradiation of samples containing the $I^H Ni$ comparable *EPR* signals were observed both in the absence (**Figure V.34**, bottom-left) and presence of substrate (**Figure V.34**, bottom-right) with an almost axial symmetry consistent with a pseudo-octahedral coordination environment having the unpaired electron predominantly localized in the $d_{x^2-y^2}$ orbital. Spectra simulations yield g -values centered at 2.06, 2.08 and 2.29 which together with the purple color of the solution and formation of an absorption band at 535 nm is consistent with the presence of Ni^I species as previously reported.⁴⁸

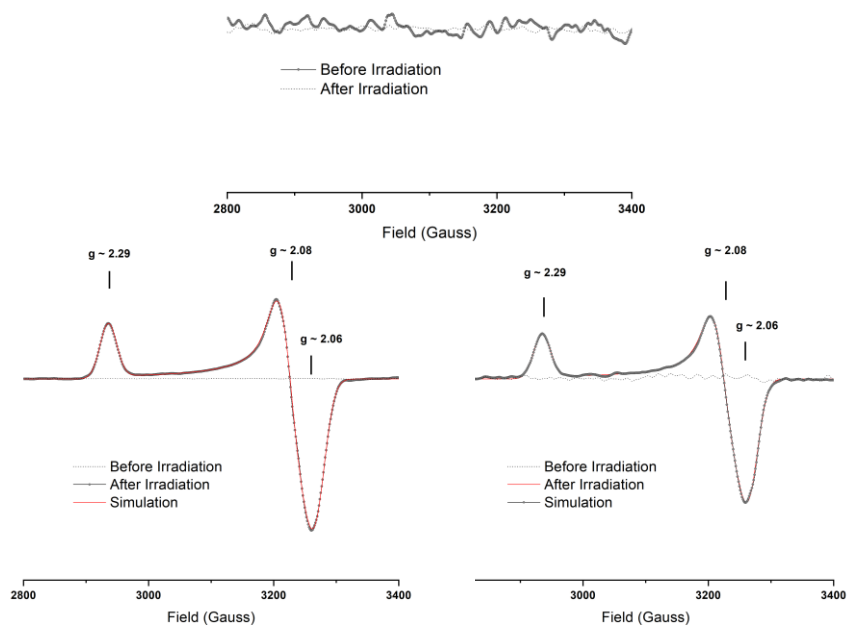


Figure V.34 EPR spectra and simulations of reaction mixture with substrate (top), reaction mixture and $I^H Ni$ complex (bottom left), reaction mixture and $I^H Ni$ complex with substrate IV.3.i (bottom right).

This evidence strongly suggests that, upon visible-light irradiation of $I^H Ni$ in the presence of PCu and iPr_2NEt as ED , a Ni^I intermediate is formed, which presents an intense absorption band at 535 nm. The combination of spectrochemical and electrochemical techniques allowed us to elucidate the nature of the intermediate formed, which yielded an EPR signal with an almost axial symmetry consistent with a pseudo-octahedral coordination environment for the nickel center.

V.3.3 Exploring the Reaction between Ni-Active Compound and Alkyl-Chlorides.

The transient Ni^I formed upon reaction of the Ni^{II} catalyst precursor with the reduced PCu is proposed to be the active species for the activation of the Csp^3-Cl bond. To demonstrate that, UV-Vis spectrochemical techniques in combination with theoretical calculations have been applied to understand how the reaction takes

place. First, spectrochemical techniques were used to detect the reaction between the Ni^I and the substrate. Then, DFT calculations have been used to elucidate the plausible steps in the reaction mechanism.

Reaction Monitoring by UV-Vis Spectrochemical Techniques

Monitoring the formation of Ni^I intermediate with *on-line* irradiations (LED, Royal blue, 447 nm.) by the reaction of PCu in the presence of iPr_2NEt as *ED*, the formation of a band at 535 nm was observed. When the formation of Ni^I was complete, 20 equivalents of substrate were added with the simultaneous cessation of irradiation (Figure V.35). At that point, a drastic decay of the signal was observed which was attributed to the reaction of the *in-situ* formed Ni^I intermediate and the substrate. A control experiment was performed by addition of an aliquot of solvent containing oxygen (same volume as the added in the case of the substrate) resulting in a less abrupt signal decrease than in the presence of the substrate (Figure V.36).

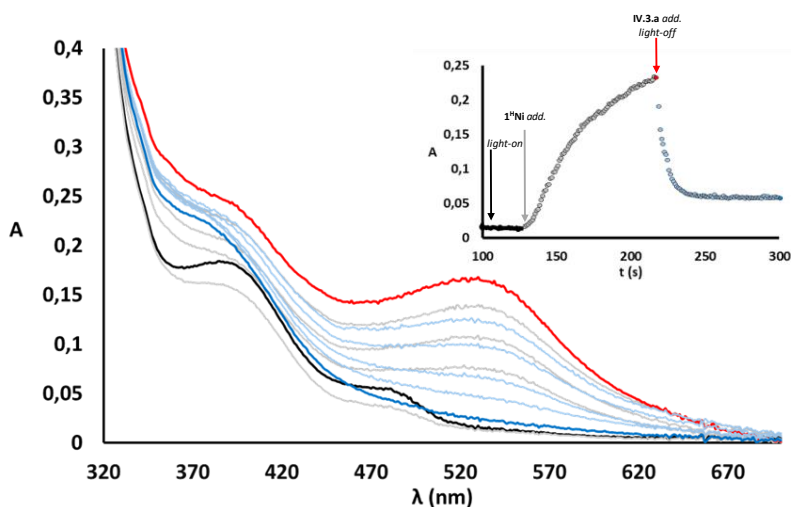


Figure V.35 UV-Vis of $1^H Ni$ ($50 \mu M$) in a solution of PCu ($20 \mu M$) in $CH_3CN:EtOH$ (2:3) with 11.4 mM DIPEA. 20 equivalents of substrate **IV.3.a** ($1 mM$) were added after 218 s of monitoring. The starting and final spectra are described by black and red curves, respectively, whereas the intermediate spectra are depicted in grey. Blue lines correspond to the spectra after the addition of the substrate, and the dark-blue line is the final spectra. Absorbance monitored at 536 nm.

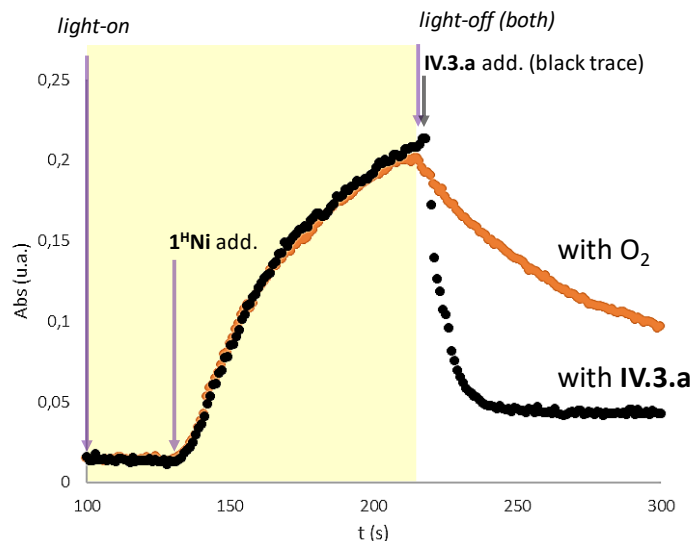


Figure V.36 Absorbance monitored at 536 nm of an irradiated (447 nm) solution containing PCu ($20 \mu\text{M}$) in $\text{CH}_3\text{CN}:\text{EtOH}$ (2:3) with DIPEA (11.4 mM) after the addition of 1^{H}Ni ($50 \mu\text{M}$) (40 s from irradiation started). After the addition of 1^{H}Ni the UV-Vis features corresponding to the $1^{\text{H}}\text{Ni}^{\text{I}}$ complex progressively increase. After 80 s from the 1^{H}Ni the light is switch off. At this point the addition of 20 eq. of IV.3.a (1 mM) triggers a rapid drop of the $1^{\text{H}}\text{Ni}^{\text{I}}$ band. In comparison, in the absence of substrate IV.3.a the decay in the dark of the $1^{\text{H}}\text{Ni}^{\text{I}}$ complex is significantly slower (orange trace).

The faster kinetic decay of the absorption signal yielded by the photogenerated Ni^{I} intermediate upon addition of the substrate *versus* addition of oxygen it is clear evidence of the reaction of the Ni^{I} intermediate with the substrate.

Theoretical Calculations for the Reaction of Ni^{I} Intermediate and Alkyl Chloride

In order to determine the feasibility of the Ni^{I} species based on the $\text{TsPy}_2^{\text{H}}\text{tacn}$ ligand to activate $\text{Csp}^3\text{-Cl}$, the reaction of the low-valent intermediate Ni^{I} (d^9 , $S = 1/2$), formed by single electron reduction starting from the 1^{H}Ni complex, with a model substrate ((3-chloropropyl)benzene) has been subjected to theoretical calculations. First, we examined the thermodynamics of both the Cl^- and CH_3CN coordination to the pentacoordinate $[\text{Ni}^{\text{I}}(\text{Ts}^{\text{H}}\text{Py}_2\text{tacn})]^+$ species (**II**) (Figure V.37). Although both coordination possibilities are endergonic, experimental cyclic voltammetry experiments are in agreement with the coordination of Cl^- to the Ni^{I} metal center (Figure V.38).

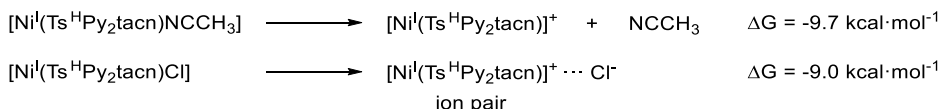


Figure V.37 Thermodynamics of the coordination of CH_3CN and Cl^- to $[\text{Ni}^{\text{I}}(\text{Ts}^{\text{H}}\text{Py}_2\text{tacn})]^+$.

Upon the addition of increasing aliquots of *TBACl* to a solution of $\text{I}^{\text{H}}\text{Ni}$, the Ni^{III} reduction peak progressively disappears, giving rise to a new peak at $E_p = -1.89$ V vs. $\text{Fc}^{+/0}$ (-1.51 V vs. SCE) which describes the $[\text{Ni}^{\text{II}}(\text{Ts}^{\text{H}}\text{Py}_2\text{tacn})\text{Cl}]^+ / [\text{Ni}^{\text{I}}(\text{Ts}^{\text{H}}\text{Py}_2\text{tacn})\text{Cl}]$ event. The irreversibility of the latter suggests a fast Cl^- dissociation after reduction, which is also consistent with the anodic peak at -1.41 V vs. $\text{Fc}^{+/0}$ upon the backward scan representing the $[\text{Ni}^{\text{I}}(\text{Ts}^{\text{H}}\text{Py}_2\text{tacn})(\text{S})]^+$ reoxidation. In line with this interpretation, the $\text{Ni}^{\text{I}/0}$ process occurring at a more cathodic potential remains almost unchanged after the addition of *TBACl.*

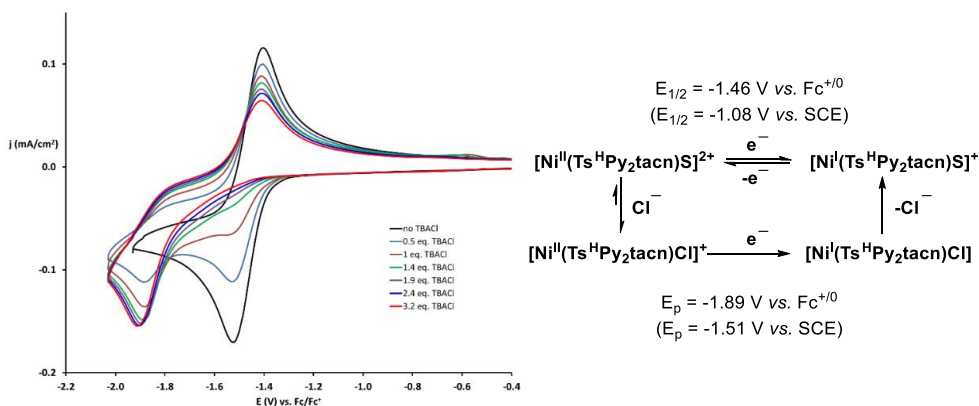


Figure V.38 CVs of $\text{I}^{\text{H}}\text{Ni}$ (0.5 mM) in $0.1 \text{ M TBAH}/\text{CH}_3\text{CN}$ electrolyte at 0.1 V s^{-1} in the absence (black) and upon the addition of 0.5 eq. (0.25 mM , cyan), 1 eq. (0.49 mM , brown), 1.4 eq. (0.73 mM , green), 1.9 eq. (1.0 mM , violet), 2.4 eq. (1.2 mM , blue) and 3.2 eq. (1.6 mM , red) of *TBACl*.

Therefore, we started to model the reaction from the pentacoordinate $[\text{Ni}^{\text{I}}(\text{Ts}^{\text{H}}\text{Py}_2\text{tacn})]^+$ species (**II**). Along the reaction pathway of **II** with (3-chloropropyl)benzene we found two different mechanisms. The lowest in energy ($\Delta G^\ddagger = 12.9 \text{ kcal}\cdot\text{mol}^{-1}$) can be described as an oxidative $\text{S}_{\text{N}}2$ -type attack of the Ni^{I} center to the aliphatic carbon center bearing the chlorine atom to give an organometallic $\text{Ni}^{\text{III}} \text{ S} = 3/2$ species (**I3**_{NiIII-C} ... Cl^-) and chloride anion (**Figure V.39**,

green energy profile). At the transition state the $Ni-C(1) - Cl$ angle is 151° and the carbon center has a close sp^2 -hybridation. The second mechanism ($\Delta G^\ddagger = 19.3$ kcal·mol $^{-1}$) can be described as a concerted halogen atom abstraction (**Figure V.39**, red energy profile) leading to the formation of $[Ni^{II}(Ts^H Py_2 tacn)Cl]$ ($I^H Ni-Cl$) complex and the free radical. Both mechanisms are accessible at room temperature. Nevertheless, for this substrate the formation of $I_{3Ni^{III}-C} \cdots Cl^-$ is favored by 6.4 kcal·mol $^{-1}$. The next step is the reaction of $I_{3Ni^{III}-C} \cdots Cl^-$. A direct $C-Ni$ homolytic cleavage of $[Ni^{III}(Ts^H Py_2 tacn)(CH_2)_3 Ph]^{2+}$ is slightly endergonic (1.7 kcal·mol $^{-1}$), and just considering acetonitrile coordination is virtually isoenergetic (-0.5 kcal·mol $^{-1}$). Further reduction of the formed organic radical ($Ph(CH_2)_3^\bullet$) and $[Ni^{II}(Ts^H Py_2 tacn)(CH_2)_3 Ph]^+$ act as an expected driving force, regenerating the Ni^I catalytically active species.

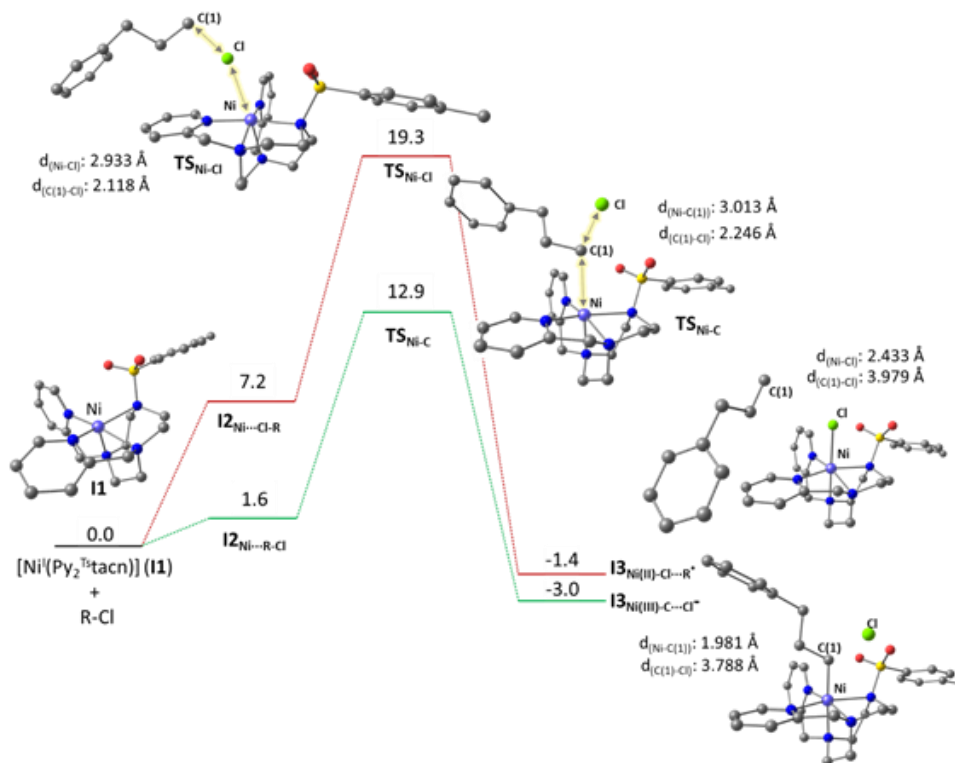


Figure V.39 Comparison between DFT(uB3LYP/6-31g**/uB3LYP/6-311+g**) calculated free energy barriers for the reaction of $[Ni^I(Ts^H Py_2 tacn)]$ (II) with the model substrate (3-chloropropyl)benzene as an oxidative S_N2 -type reaction (green profile) or concerted halogen atom abstraction (red). Energies are given in kcal·mol $^{-1}$. ‡ DFTs performed by Prof. Julio Lloret.

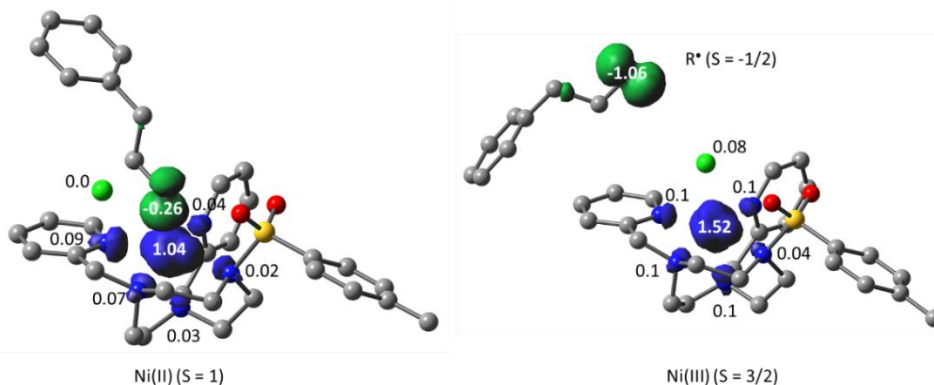


Figure V.40 B3LYP-D3/6-311+G** spin densities of intermediates $I3_{NiII-C...Cl-}$ (left) and $I3_{NiII-Cl...R^*}$ (right). Hydrogen atoms have been omitted for clarity. Isosurfaces calculated at values of 0.01. Alpha and beta spin density is represented by the green and blue colors. Relevant spin densities are represented in the figure. ‡ DFTs performed by Prof. Julio Lloret.

On the other hand, one can expect that the reduction of the formed organometallic $[Ni^{III}(Ts^H Py_2 tacn)(CH_2)_3 Ph]^+$ species is quickly reduced to $[Ni^{II}(Ts^H Py_2 tacn)(CH_2)_3 Ph]^+$ ($E_{theo} = -0.12$ V vs NHE, -0.36 vs SCE) in the reaction medium, which also leads to a significant thermodynamic stabilization (considering the experimental redox potential of the PCu of -1.45 V vs NHE (-1.69 V vs SCE) the driving force is -30.7 kcal·mol⁻¹. Now, the C–Ni homolytic cleavage in $[Ni^{II}(Ts^H Py_2 tacn)(CH_2)_3 Ph]^+$ is endergonic, but still thermodynamically accessible at room temperature (22.1 kcal·mol⁻¹), which leads to the formation of Ni^I species, regenerating the Ni^I catalytically active species (Figure V.41).

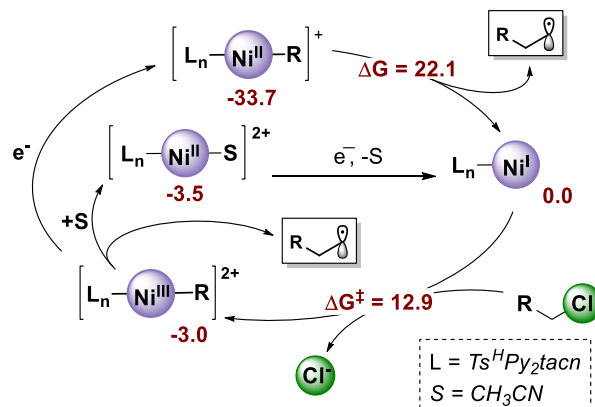


Figure V.41 Summary of the DFT data. Values represent thermodynamic energies respect $[Ni^I(Ts^H Py_2 tacn)]^+$ and are given in kcal·mol⁻¹. ‡ DFTs performed by Prof. Julio Lloret.

V.3.4 DPA-based System

In order to clarify the reaction mechanism for the activation of Csp^3-Cl bonds, the reactivity between $Ts^H Py_2 tacn$ based ($I^H Ni$) and bipyridinyl-dipyridine based catalyst ($Ni-DPA$) was compared due to the similitudes in the reactivity found in the screening of the optimized conditions (**Table IV.7**).

With the idea in mind that both pentacoordinate nickel complexes catalyze the Csp^3-Cl activation reaction in an analogous manner, similar UV-Vis and spectrochemical experiments were performed to characterize the Ni^I intermediate. In this case, UV-Vis monitoring with *on-line* continuous irradiation (LED λ_{max} 447 nm) shows the generation of two bands; one intense band with a λ_{max} at 535 nm and other broader at 910 nm which can be attributed to the bipyridine ligand. Both bands grow in the presence of PCu and iPr_2NEt as *ED* (**Figure V.43**)

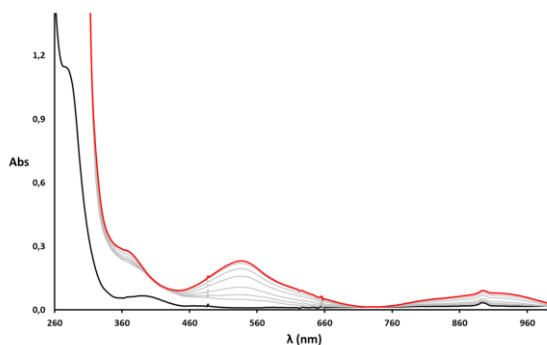


Figure V. 42 UV-Vis spectra of UV-Vis of $Ni-DPA$ ($50 \mu M$) in a solution of PCu ($20 \mu M$) in CH_3CN with $11.4 mM$. The starting and final spectra are described by black and red curves, respectively.

SEC experiments on $Ni-DPA$ in the $0.2 M$ TBAH/ CH_3CN electrolyte showed similar behavior by applying a reduction potential close to the Ni^{III} wave. In agreement with *CV* data, the Ni^{III} transition is reversible, recovering the initial spectrum of Ni^I-DPA upon reoxidation by switching the potential after the Ni^{III} wave (**Figure V.43**).

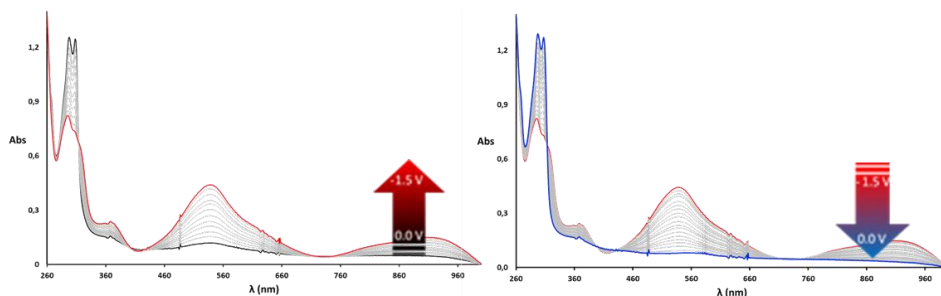


Figure V.43 UV-Vis SEC of Ni-DPA (4 mM) in 0.2 M TBAH/CH₃CN electrolyte. The applied potential is slowly increased from the open circuit voltage (black) to the value corresponding to the Ni^{II/I} wave (ca. -1.5 V vs. Fc/Fc⁺, red) and finally back to zero again (blue). The intermediate spectra are depicted in grey

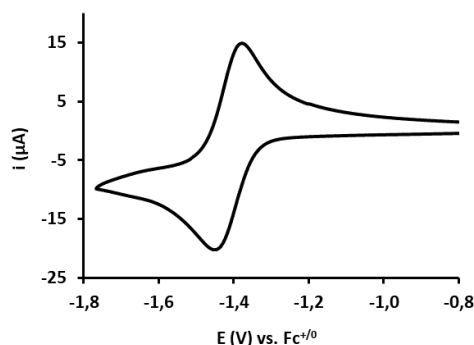


Figure V.44 Cyclic voltammograms of [Ni^{II}(DPA-bpy)(OTf)]OTf (1mM) in 0.2 M TBAH/CH₃CN electrolyte at 0.1 V s⁻¹.

Control EPR experiments of Ni-DPA complex and a mixture of Ni-DPA/PC_{Cu} were also performed before and after irradiation with any signal observed. Nonetheless upon irradiation at 467 nm an EPR signal corresponding to an anisotropic rhombic symmetry was observed (Figure V.45). Spectra simulations yield *g*-values centered at 2.07, 2.16 and 2.24. In this case, chemically generated Ni^I complex was also tested observing the same shape of signal than the one obtained by reaction with the copper photocatalyst upon visible-light irradiation.

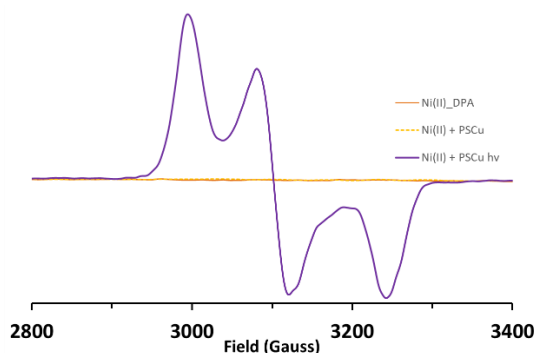


Figure V.45 EPR spectra and simulations of Ni-DPA (orange), the mixture of Ni-DPA and PCu before (yellow) and after irradiation (purple).

In order to explore the reactivity of the proposed Ni^I intermediate in the activation of Csp^3-Cl bonds, Ni^I-DPA was produced by reaction of the initial $Ni^{II}-DPA$ with $NaBH_4$. Upon slow addition of a solution of the Ni^{II} complex over $NaBH_4$ suspension in dry acetonitrile at $-35\text{ }^\circ\text{C}$ a slight-pink solution was observed. After warming the mixture to room temperature, a dark purple solution was obtained which after filtration over dry Celite® at $-35\text{ }^\circ\text{C}$ and evaporation of the solvent, yielded a new complex with equivalent UV-Vis and EPR features as the intermediate generated after the photochemical reaction (**Figure V.46**).

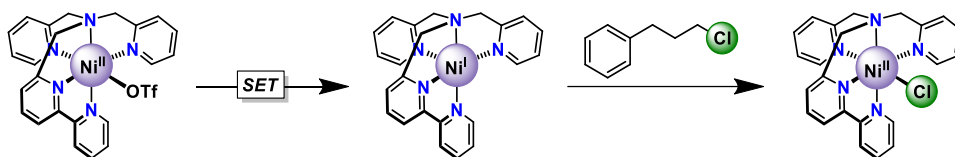


Figure V.46 General scheme for the Ni^I-DPA promote activation of Csp^3-Cl bonds.

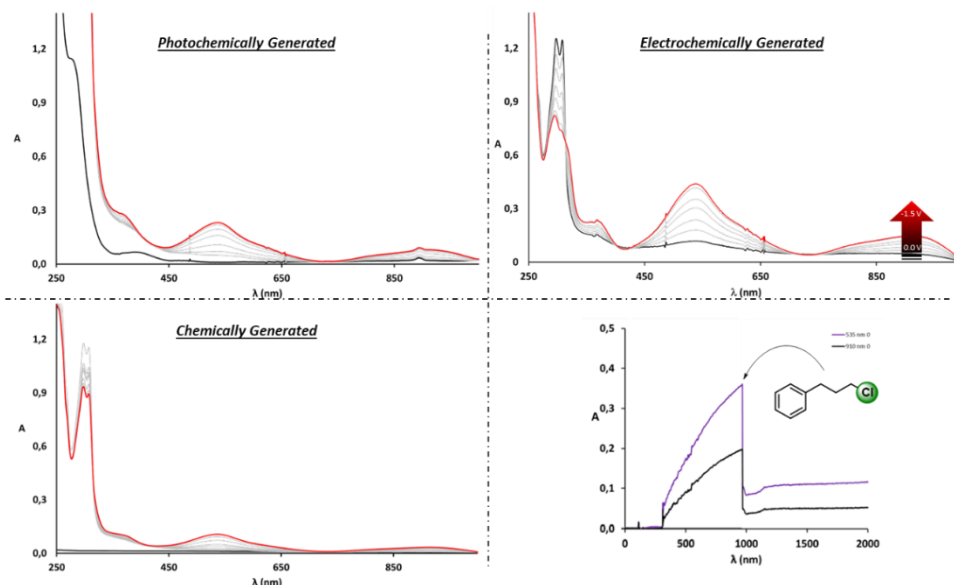


Figure V.47 UV-Vis of Ni-DPA (50 μ M), PC_{Cu} (20 μ M) and DIPEA (11.4 mM) in CH₃CN (top-left), SEC of Ni-DPA (4 mM) in a 0.2 M TBAH/CH₃CN electrolyte (top-right) and UV-VIS of Ni-DPA (4 mM) in presence of NaBH₄ (3 eq.) (bottom-left). The intermediate spectra are depicted in grey. Absorbance monitored at 537 and 910 nm of an irradiated (447 nm) solution containing PC_{Cu} (20 μ M) in CH₃CN with DIPEA (11.4 mM) after the addition of Ni-DPA (50 μ M) (180 s from irradiation started). After the addition of Ni-DPA the UV-Vis features corresponding to the Ni^I-DPA complex progressively increase. After 660 s from the Ni-DPA the light is switch off. At this point the addition of 20 eq. of (3-chloropropyl) benzene (1 mM) triggers a rapid drop of the Ni^I-DPA bands (bottom-right).

The similarities observed over the UV-Vis spectra shown in **Figure V.47** taken together with the EPR results lead us to suggest that the intermediate formed upon chemical, electrochemical or photochemical reduction is the same paramagnetic Ni^I complex. As it was previously described, the chemical reduction of Ni^{II}-DPA with NaBH₄ has been carried out at low temperature (-35 °C). This temperature was chosen to avoid over-reductions (at room temperature, a black precipitate is formed). These over-reductions could explain the presence of less quantity of the desired Ni^I-DPA and, therefore, lower absorbance (**Figure V.47**, bottom-left).

Under the same reaction conditions, different attempts for the isolation of the Ni^I desired intermediate yielded the formation of the Ni^{II}-DPA-BH₄ and Ni^{II}-DPA-NH₂Et complexes, which we were able to isolate in form of single crystals for

X-Ray analysis. $\text{Ni}^{\text{II}}\text{-BH}_4$ adducts are known as intermediates in the NaBH_4 reduction of metal salts,⁴⁹ where the sequence proposed is the one shown in **Figure V.48**.

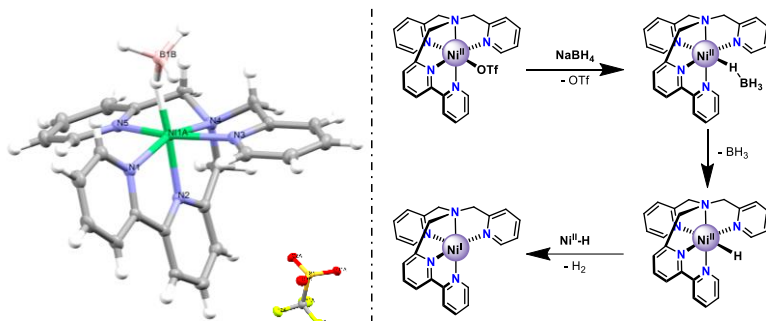


Figure V.48 X-Ray structure of $\text{Ni}^{\text{II}}\text{-DPA_BH}_4$ obtained during the chemical reduction of $\text{Ni}^{\text{II}}\text{-DPA}$ with NaBH_4 . Thermal ellipsoid plots of Ni_DPA (50% probability). Solvent molecules are omitted for clarity. Color code: nickel (green), nitrogen (purple), oxygen (red), fluor (yellow), carbon (grey), hydrogen (white) and sulfur (orange). Sequence proposed for the $1 e^-$ reduction of Ni^{II} complex by NaBH_4 (right).

We suggest that the $\text{Ni}^{\text{II}}\text{-DPA-NH}_2\text{Et}$ can be formed due to the chemical reduction of the acetonitrile used as solvent. Two BH_4 moieties were found as contra-ions instead the triflate present prior to the reduction (**Figure V.49**).

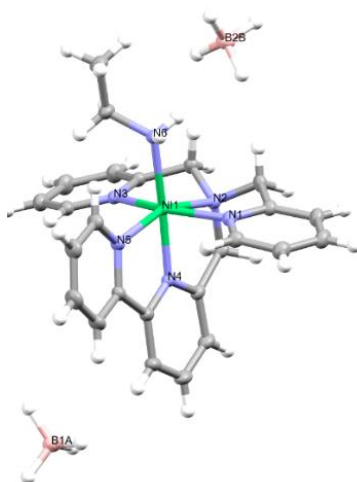


Figure V.49 X-Ray structure of $\text{Ni}^{\text{II}}\text{-DPA_NH}_2\text{Et}$ obtained during the chemical reduction of $\text{Ni}^{\text{II}}\text{-DPA}$ with NaBH_4 .

Exploring Stoichiometric Reactivity Between Ni-DPA and Alkyl Chlorides

Having demonstrated the reactivity between Ni^I intermediate with the substrate, our next objective was to determine how this reaction takes place. Based upon previous studies on nickel-catalyzed activation of *Carbon-Halogen* bonds, the activation of the Csp^3-Cl bond can proceed by two different pathways: i) a *Concerted Halogen Atom Abstraction* in which a $Ni^{II}-Cl$ is formed or ii) a S_N2 -type *Oxidative Addition*, with the formation of an organometallic Ni^{III} -Alkyl intermediate (Figure V.50).

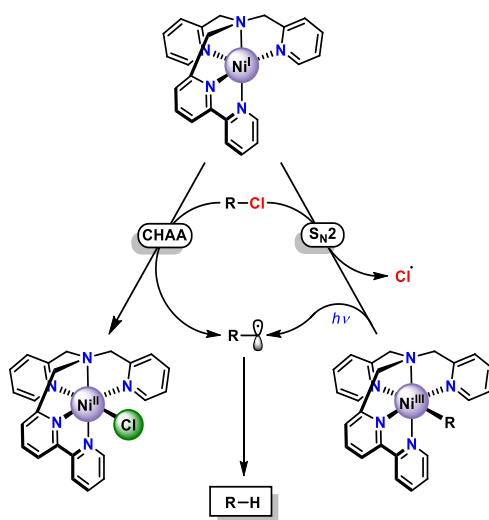


Figure V.50 Proposed reactivity of Ni^I and Alkyl-chlorides.

With that objective in mind, stoichiometric reactions between *Ni-DPA* and (3-chloropropyl)benzene were carried out. The addition of one equivalent of substrate onto a solution of chemical and photochemical generated Ni^I intermediate, produced the disappearance of the characteristic deep purple color solution observed with the formation of Ni^I species. After 30 minutes of reaction, no more color changes were observed, and the solvent of the reaction was removed. The brown solid obtained after fast precipitation of a fresh solution of the crude compound with dry diethyl ether showed a paramagnetic NMR spectra that was compared with the chemically synthesized Ni^{II} -DPA-Cl (Figure V.51).

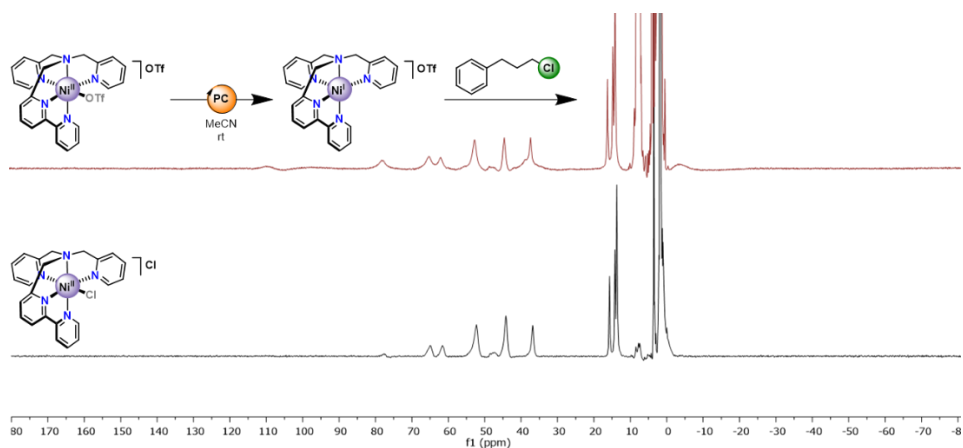


Figure V.51 Paramagnetic $^1\text{H-NMR}$ spectrum of the product obtained by reaction of the Ni^{I} intermediate formed photochemically and the substrate (top) and the $\text{Ni}^{\text{II}}\text{-DPA_Cl}$ chemically synthesized (bottom).

The analogies observed in both spectra suggest the $\text{Ni}^{\text{II}}\text{-DPA_Cl}$ as product of the reaction between $\text{Ni}^{\text{I}}\text{-DPA}$ and the alkyl chloride, and it was confirmed after X-ray measurement of the single crystal obtained from a slow diffusion of Et_2O into a solution of the complex in acetonitrile (**Figure V.52**).

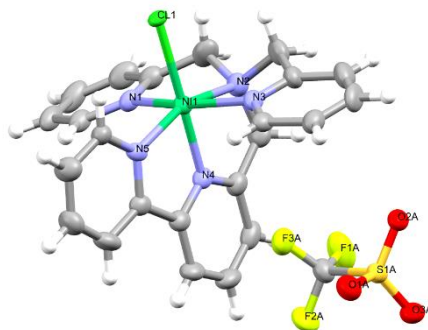


Figure V.52 X-Ray structure of $\text{Ni}^{\text{II}}\text{-DPA_Cl}$ obtained after reaction of $\text{Ni}^{\text{I}}\text{-DPA}$ with (3-chloropropyl)benzene. Thermal ellipsoid plots (50% probability). Solvent molecules are omitted for clarity. Color code: nickel (green), nitrogen (purple), oxygen (red), fluor (yellow), carbon (grey), hydrogen (white) and sulfur (orange).

In contrast with the electrochemical experiments performed for $\text{I}^{\text{H}}\text{Ni}$, no changes in cyclic-voltammetry were observed upon addition of 2 to 20 equivalents

of (3-chloropropyl)benzene suggesting that the formation of the intermediate by the reaction of the Ni^I intermediate with (3-chloropropyl)benzene is much slower (Figure V.53).

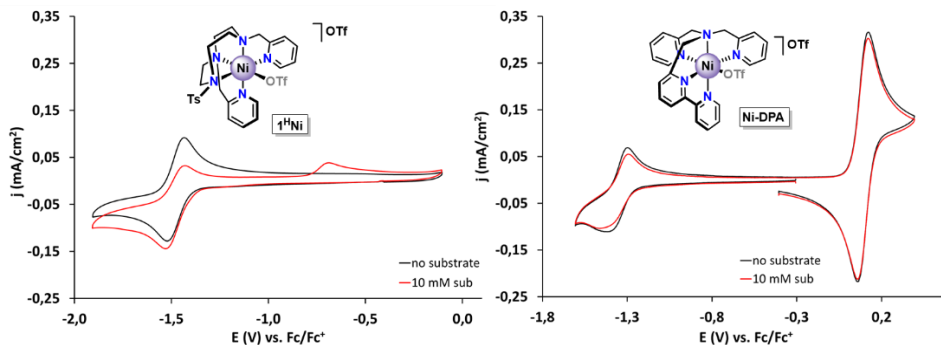


Figure V.53 CVs of $I^H Ni$ (0.5 mM) in 0.1 M TBAH/ CH_3CN electrolyte at $0.1 V s^{-1}$ in the absence (black) and presence (red) of 20 eq. of substrate (3-chloropropyl)benzene (left) and CVs of Ni-DPA (0.5 mM) in 0.1 M TBAH/ CH_3CN electrolyte at $0.1 V s^{-1}$ in the absence (black) and presence (red) of 20 eq. of substrate IV.3.a (right).

V.3.5 Mechanistic Proposal

Based on these results, we have proposed a plausible catalytic cycle for the visible-light reductive cyclization of alkyl chlorides with the $PC_{Cu}/I^H Ni$ catalytic system (Figure V.54). Under catalytic conditions, the photoreduced copper complex ($E_{1/2}(PC_{Cu}^{I^0}) = -1.69 V$ vs SCE) reduces $I^H Ni$ by one electron forming new Ni^I species ($Ni^{(III)}$ $-1.08 V$ and $-1.51 V$ vs SCE, for OTf^- and Cl^- complexes, respectively). Thermodynamics discard a potential outer-sphere SET from formally PC_{Cu}^0 or its excited state ($-1.02 V$)⁵⁰ to a Csp^3-Cl bond ($< -3 V$ vs SCE).⁵¹ EPR, UV-Vis and CV experiments suggest that the photo-generated Ni^I species can react with chloroalkanes, in agreement with the low energy barriers (12.9 and 19.3 kcal·mol⁻¹) calculated by DFT for the reaction of $I^H Ni^I$ (I_2) with (3-chloropropyl)benzene as a challenging non-activated model substrate. Based on DFT studies (Figure V.39), we hypothesize two different scenarios for the Csp^3-Cl bond cleavage. First, the activation of the Csp^3-Cl bond via an oxidative addition by a S_N2 mechanism (OA- S_N2) that generates the organometallic intermediate I_3 (Figure V.54, $\Delta G^\ddagger = 12.9 kcal\cdot mol^{-1}$ and $\Delta G = -3.0 kcal\cdot mol^{-1}$, see Figure V.41). Then,

homolytic cleavage of the relatively weak $M-C$ bond (~ 5 kcal·mol⁻¹ for (3-chloropropyl)benzene) could regenerate the divalent metal catalyst while forming C -centered radical intermediates (I_5).^{43,52} One electron reduction of complex alkyl- M^{III} to form I_4 is favorable ($\Delta G = -30.7$ kcal·mol⁻¹), for which homolytic cleavage of the $M-C$ bond at room temperature is also accessible ($\Delta G = 22.1$ kcal·mol for (3-chloropropyl)benzene).⁵³ Finally, the radical generated can be trapped by the tethered alkene to form the kinetically favored 5-*exo-trig* carbocyclic compound (I_6). Alternatively, the activation of the Csp^3-Cl bond can occur via *concerted halogen atom abstraction* (**CHAA**) to generate directly $M^{II}-Cl$ (I_1) complex and the corresponding organic radical I_5 (**Figure V.54**, $\Delta G^\ddagger = 19.3$ and $\Delta G = -1.4$ kcal·mol⁻¹ for (3-chloropropyl)benzene, see **Figure V.41**).

Although more detailed studies need to be done, the experiments carried out suggest that the more nucleophilic $I^H Ni^I$ undergoes an oxidative addition by a S_N2 mechanism, whereas the more delocalized Ni^I-DPA due to the presence of the bipyridine moiety goes preferentially through a **CHAA** mechanism.

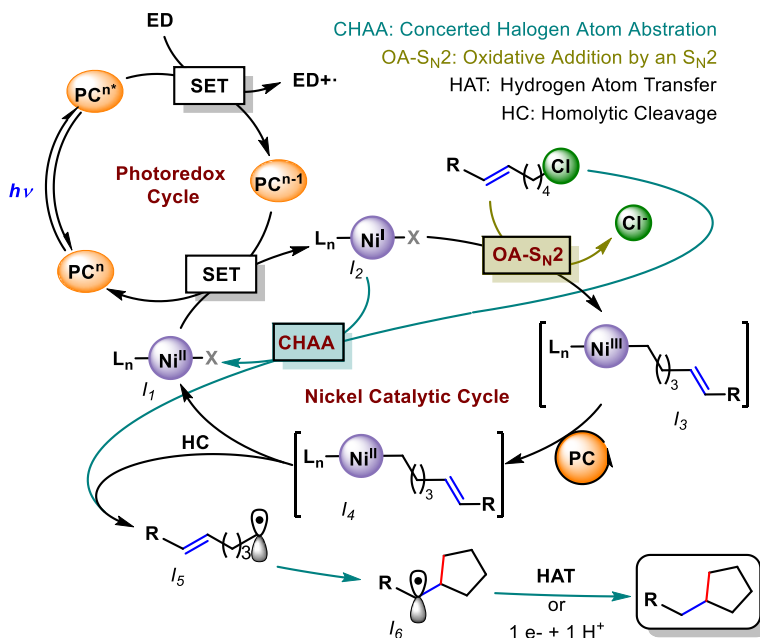


Figure V.54 Proposed catalytic cycle for the visible-light reductive cyclization of non-activated alkyl chlorides with tethered alkenes.

V.4. Conclusions

Significant increase of Ni catalyzed cross coupling reactions has been subject of interest in recent years. Although its use in combination with photocatalyst has also gained a great relevance, only bi and tridentate ligands have been used so far. In this regard, mechanisms based on $Ni^0-Ni^{II}-Ni^{III}-Ni^I$ ground on oxidative addition and reductive elimination pathways as key steps have been proposed. In spite of the fact that Diao and co-workers studied in more detail four different pathways using as basis of kinetic and theoretical studies, non-exhaustive studies have been performed in the field of the metallaphotoredox catalysis.

In this chapter, an oxidative-addition S_N2 pathway has been proposed based on on UV-Vis spectroscopy, cyclic voltamperometry, electronic paramagnetic resonance and theoretical calculations. Spring from these studies, the *in situ* photogenerated low-valent nickel complex undergo the nucleophilic substitution to the Csp^3-Cl bond to generate carbon-centered radical intermediates which can be reduced in the reaction conditions or attack to a radical acceptor performing an intramolecular cyclization reaction. The final radical is then reduced and subsequently protonated for the more easily reduced substrates or engage into a *HAT* from the solvent for the more difficult substrates to reduce.

Based on both theoretical and experimental studies, the more favored pathway for the more nucleophilic $I^H Ni$ is the prior formation of an organometallic $Ni^{III}-alkyl$ compound releasing the carbon-centered radical compound. Otherwise, less nucleophilic Ni^I-DPA may undergo a concerted halogen atom abstraction forming directly $Ni^{II}-Cl$ complex and the corresponding free organic radical. Nevertheless, both mechanisms could be operative for both catalysts, and more studies need to be performed to further clarify the relevance and consequences of the proposed mechanisms.

V.5. Experimental Section

V.5.1 Material and Reagents

Reagents and solvents were used as received from the commercial supplier unless otherwise stated. Triethylamine and di-*isopropylethylamine* were distilled over potassium hydroxide and were stored under argon. For the synthesis of reagents, the solvents (hexane, Et₂O, CH₂Cl₂, MeCN, DMF and toluene) were used from a SPS-400, Innovative Technology solvent purification system and stored under argon with activated 4 Å molecular sieves.

Anhydrous acetonitrile was purchased from Sigma-Aldrich® Gradient AIS system. Ethanol was degassed by freeze-pump-thaw method (repeated 3 cycles) and was stored under argon.

V.5.2 Instrumentation

NMR spectra were recorded on a Bruker 300 MHz, 400 MHz or 500 MHz spectrometers at room temperature. ¹H and ¹³C NMR chemical shifts are reported in parts per million (ppm), relative to the residual solvent peak as internal reference. Multiplicities are reported as follows: singlet (s), doublet (d), doublet of doublet (dd), triplet of doublets (td), triplet (t), broad signal (br) and multiplet (m). Deuterated solvents (CDCl₃, CD₃CN, EtOD) were stored with activated 4 Å molecular sieves and they were degassed by freeze-pump-thaw method when it was required for photocatalytic reactions.

Electron Paramagnetic Resonance (EPR) was collected on solutions of 1mM *I^HNi* complex with or without substrate **IV.3.i** (10 mM) in a reaction mixture containing *PCu* (0.4mM), DIPEA (114.5 mM) as sacrificial electron donor and a 3:2 ratio ethanol:butyronitrile solvent mixture. Samples were prepared anaerobically under dark conditions and investigated before and after irradiation with a 476 nm lamp (40 W) at room temperature. An EMX Micro X-band EPR spectrometer from

Bruker was used to collect the data using a finger Dewar for measurements at 77 K. Data was acquired in perpendicular mode with a modulation frequency of 100 KHz, a modulation amplitude of 10 G, a 5.1 ms time constant and 21.4 ms conversion time and a microwave power of 0.18 mW. Spectra was simulated using the EasySpin software package.⁵⁴

Cyclic Voltammetry (CV) measurements were carried out with a VSP potentiostat from Bio-Logic, equipped with the EC-Lab software. The experiments were performed under inert (Ar) atmosphere in a custom double-wall jacketed single-compartment cell. 0.1 M TBAH electrolyte solutions were employed using CH₃CN or CH₃CN:EtOH (2:3) as a solvent mixture. A 3 mm diameter glassy carbon (GC) disk and a Pt wire were used as working and counter electrodes, respectively. An Ag wire was employed as a pseudo-reference, immersed in a bridge tube containing the same electrolyte solution as the main compartment (0.1 M TBAH/CH₃CN) and separated from it by a porous tip. Ferrocene (Fc) was used as an internal standard and all the potentials are referenced vs. the Fc⁺⁰ redox couple.⁵⁵

UV-Vis spectra were recorded on an Agilent 8453 diode array spectrophotometer (190-1100 nm range) in a 1 cm quartz cells.

UV-Vis measurements with on-line irradiation were performed in a house-built apparatus using 1 cm quartz fluorescence cuvette in a fluorescence cuvette holder. LED (Royal blue, 447 nm.) was placed perpendicular to the optical pathway of the Agilent 8453 diode array spectrophotometer (190-1100 nm range).

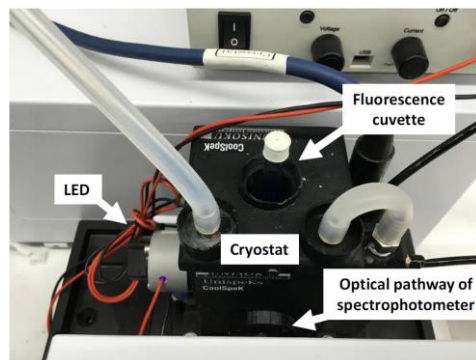


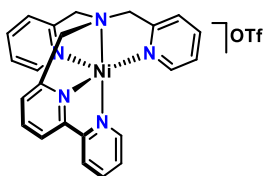
Figure V.55 Setup for UV-Vis measurement with on-line irradiation.

The solutions of PC_{Cu} were prepared in ethanol acetonitrile mixture (3:2). The concentration of PC_{Cu} was fixed to 20 μ M. As a blank the same ethanol-acetonitrile mixture was used. The absorption kinetics were studied on an Agilent 8453 diode array spectrophotometer (190–1100 nm range) in 1cm quartz cell.

UV-Vis Spectroelectrochemistry (UV-Vis, SEC) experiments were performed by using a SP-50 potentiostat from Bio-Logic under an Ar atmosphere. A 4 mM solution of complex in 0.2 M TBAH/CH₃CN or solvent mixture is introduced in an optically transparent thin-layer electrode (OTTLE) cell, equipped with Pt minigrad working and auxiliary electrodes, an Ag microwire pseudo-reference electrode and a CaF₂ window.⁵⁶ Blank 0.2 M TBAH/CH₃CN solutions were used for solvent subtractions. UV/Vis spectra were measured with an Agilent 8453 diode array spectrophotometer (λ =190–1100 nm range), with a cycle time equal to 2 s.

V.5.3 Synthesis of Metal Complexes

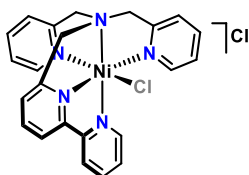
Synthesis of Ni^I-DPA



A solution of Ni^{II}-DPA_OTf was added dropwise to a vigorously stirred suspension of NaBH₄ in acetonitrile at -35 °C. After the addition was completed, the reaction was slowly warmed-up until 0 °C, moment where the solution changed to deep purple. At that moment, the reaction is cooled-down to -20 °C and filtered through a cooled path of dry Celite® under argon atmosphere. The obtained purple solution was dried under vacuum, redissolved in dry DCM and the slow diffusion of diethyl ether into the solution produced a deep purple solid (28 mg, 0.048 mmol, 70 %).

¹H NMR (400 MHz, CD₃CN) δ = 130.26, 80.46, 64.58, 54.25, 44.32, 39.96, 16.02, 14.64, 14.30, 11.39 ppm.

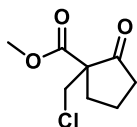
Synthesis of Ni^{II}-DPA-Cl



In a glovebox, a suspension of Ni(OTf)₂(MeCN)₂ (323 mg, 0.735 mmol) in anhydrous THF (2 mL) was added dropwise to a vigorously stirred solution of DPA-Bpy ligand (300 mg, 0.816 mmol) in THF (2 mL). After few minutes, a brown solution appeared. After stirring for an additional 5 hours, Et₂O (3 mL) was added, and the resulting solid was filtered off and dried under vacuum. The solid was dissolved in CH₂Cl₂, filtered through Celite®, and the slow diffusion of diethyl ether into the solution produced a pale brown solid (174 mg, 0.240 mmol, 80 %).

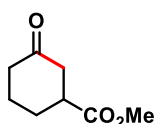
¹H NMR (400 MHz, CD₃CN) δ = 135.65, 112.00, 77.71, 64.99, 61.67, 52.25, 44.18, 36.82, 15.73, 14.25, 13.70 ppm.

V.5.4 Characterization of Products



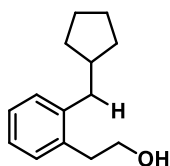
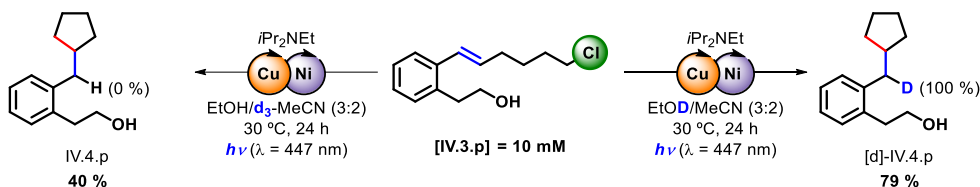
Substrate (V.1.a): A solution of the corresponding alcohol⁵⁷ (1 g, 5.81 mmol) in dry acetonitrile was added triphenylphosphine (1.83 g, 6.97 mmol) and tetrachlorocarbon (1.54 mL, 11.62 mmol, 2 eq.). The resulting mixture was stirred for 48h at room temperature. Then, the solvent was removed under vacuum and the residue was extracted with pentane (3 x 40 mL) and filtered through Celite®. The organic solvent was removed under reduced pressure and the crude material was purified by flash chromatography (SiO₂, 15 % EtOAc in hexane) to yield 1.1 g (31 %) of title compound as a light yellow liquid.

¹H NMR (400 MHz, CDCl₃): δ = 3.87 (q, *J* = 8 Hz, 2H), 3.74 (s, 3H), 2.60 – 2.43 (m, 2H), 2.40 – 2.24 (m, 2H), 2.18 – 1.99 (m, 2H) ppm. ¹³C NMR (101 MHz, CDCl₃): δ = 212.0, 169.6, 61.5, 53.1, 45.5, 38.6, 31.3, 19.7 ppm. **IR** (film): 2957, 1754, 1724, 1434, 1225, 1152, 1098, 1010, 516 cm⁻¹. **MS:** *m/z* calcd for C₈H₁₁ClNaO₃ [M + Na]⁺: 213.0284, found 213.0289.



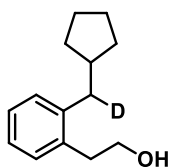
Product (**V.2.a**): The ring-expansion reaction of substrate **V.1.a** was carried out following the general procedure described in chapter IV for the reductive cyclization reaction obtaining the ring expansion product. Scale: 0.3 mmol, flash chromatography (SiO₂, (5 % - 10% of Et₂O in hexane) yielded 15 mg (33 %).

¹H NMR (400 MHz, CDCl₃): δ = 3.73 (s, 3H), 2.89 - 2.76 (m, 1H), 2.57 (d, J = 8.0 Hz, 2H), 2.46 - 2.28 (m, 2H), 2.22 - 2.04 (m, 2H), 1.95 - 1.82 (m, 1H), 1.82 - 1.71 (m, 1H) ppm. ¹³C NMR (101 MHz, CDCl₃): δ = 209.1, 174.2, 52.1, 43.1, 43.1, 40.9, 27.8, 24.5 ppm. IR (film): 2950, 2870, 1740, 1720 cm⁻¹. MS: m/z calcd for C₈H₁₃O₃ [M + H]⁺: 157.2, found 157.2. The spectroscopic characterization is in agreement with the literature reported.⁵⁸



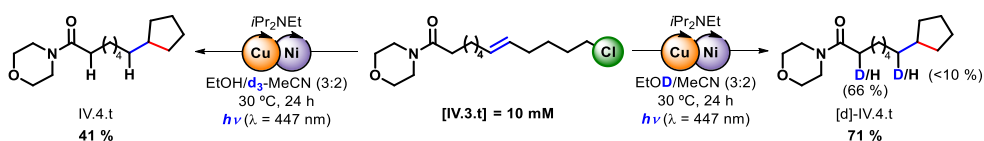
The reductive cyclization reaction of substrate **IV.3. p** was carried out following the general procedure using deuterated acetonitrile. Scale: 0.24 mmol, flash chromatography (SiO₂, (10 % of Et₂O in hexane) yielded 12 mg (40 %) of the pure product **IV.4. p** without deuterium insertion and 12 mg of the starting material (75 % of conversion).

¹H NMR (400 MHz, CDCl₃): δ = 7.20 - 7.13 (m, 4H), 3.85 (t, J = 7.0 Hz, 2H), 2.93 (t, J = 7.0 Hz, 2H), 2.66 (d, J = 7.4 Hz, 2H), 2.12 - 2.04 (m, 1H), 1.75 - 1.68 (m, 2H), 1.68 - 1.62 (m, 2H), 1.56 - 1.49 (m, 3H), 1.28 - 1.17 (m, 2H) ppm. ¹³C NMR (101 MHz, CDCl₃): δ = 140.8, 136.0, 130.2, 129.8, 126.5, 126.1, 63.5, 41.5, 38.7, 35.9, 32.8 (2C), 25.0 (2C) ppm. IR (film): 2948, 2867, 1450, 1043, 750 cm⁻¹. MS: m/z calcd for C₁₄H₁₉ [M - H₂O]: 187.1481, found 187.1481.



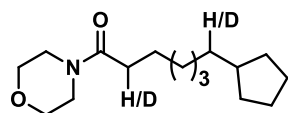
[d]-IV.4. p. In addition, the cyclization reaction of substrate using $\text{CH}_3\text{CH}_2\text{OD}$ as protic solvent yielded 38 mg (79 %) of the pure product with a deuterium insertion of 100 %. Scale: 0.24 mmol, flash chromatography (SiO_2 , (20 % of Et_2O in hexane).

$^1\text{H NMR}$ (300 MHz, CDCl_3): $\delta = 7.22 - 7.09$ (m, 4H), 4.28 - 3.75 (m, 2H), 2.93 (t, $J = 6.9$ Hz, 2H), 2.63 (dd, $J = 5.3, 3.4$ Hz, 1H), 2.07 (q, $J = 7.6$ Hz, 1H), 1.81 - 1.60 (m, 4H), 1.59 - 1.47 (m, 2H), 1.29 - 1.12 (m, 2H) ppm. $^2\text{H NMR}$ (500 MHz, CHCl_3): $\delta = 2.62$ ppm. $^{13}\text{C NMR}$ (126 MHz, CDCl_3) $\delta = 140.7, 135.9, 130.0, 129.7, 126.4, 125.9, 63.4, 41.3, 38.2$ (t), 35.8, 32.6, 32.6, 24.9 ppm.



The reductive cyclization reaction of substrate **IV.3. t** was carried out following the general procedure using deuterated acetonitrile in this case. Scale: 0.21 mmol, flash chromatography (SiO_2 , (10 % of Et_2O in hexane) yielded 23 mg (41 %) of the pure product **IV.4. t** without deuterium insertion and 28 mg of the starting material (55 % of conversion).

$^1\text{H NMR}$ (400 MHz, CDCl_3): $\delta = 3.70 - 3.64$ (m, 4H), 3.61 (d, $J = 4.9$ Hz, 2H), 3.46 (t, $J = 4.8$ Hz, 2H), 2.30 (t, $J = 7.6$ Hz, 2H), 1.76 - 1.69 (m, 2H), 1.67 - 1.55 (m, 6H), 1.54 - 1.46 (m, 2H), 1.37 - 1.25 (m, 7H), 1.10 - 1.00 (m, 2H) ppm. $^{13}\text{C NMR}$ (101 MHz, CDCl_3): $\delta = 172.1, 67.1, 66.8, 46.2, 42.0, 40.3, 36.3, 33.3, 32.8$ (2C), 29.8, 29.6, 28.8, 25.4, 25.3 (2C) ppm. **IR** (film): 2922, 2853, 1649, 1430, 1116 cm^{-1} . **MS**: m/z calcd for $\text{C}_{16}\text{H}_{29}\text{NNaO}_2$ [$\text{M} + \text{Na}$] $^+$: 290.2091, found 290.2093.



[d]-IV.4. t. Additionally the reaction of substrate **IV.3. t** using EtOD as protic solvent gave 46 mg (71 %) of the pure product with a deuterium insertion of 10 % and 15

mg of the starting material (80 % of conversion). Scale: 0.024 mmol, flash chromatography (SiO₂, (10 % of Et₂O in hexane)

¹H NMR (400 MHz, CDCl₃): δ = 3.66 (dd, *J* = 5.8, 3.9 Hz, 4H), 3.62 (d, *J* = 5.1 Hz, 2H), 3.52 – 3.37 (m, 2H), 2.67 – 2.16 (m, 2H), 2.00 – 1.65 (m, 2H), 1.65 – 1.52 (m, 4H), 1.51 – 1.43 (m, 2H), 1.40 – 1.21 (m, 8H), 1.04 (td, *J* = 4.2, 2.3 Hz, 2H). **²H NMR** (500 MHz, CHCl₃): δ = 0.92 ppm. **¹³C NMR** (10 MHz, CDCl₃) δ = 171.9, 67.0, 66.7, 46.1, 41.9, 40.1, 36.2, 33.2 (singlet of the non-deuterated product and t of the deuterated product), 32.7 (singlet of the non-deuterated product and t of the deuterated product), 29.7, 29.5, 29.5, 28.6, 25.3, 25.2, 25.2 ppm.

V.6. References of the Chapter

- (1) Magano, J.; Dunetz, J. R. Large-Scale Applications of Transition Metal-Catalyzed Couplings for the Synthesis of Pharmaceuticals. *Chem. Rev.* **2011**, *111*, 2177, doi: 10.1021/cr100346g.
- (2) Johansson Seechurn, C. C. C.; Kitching, M. O.; Colacot, T. J.; Snieckus, V. Palladium-Catalyzed Cross-Coupling: A Historical Contextual Perspective to the 2010 Nobel Prize. *Angew. Chem. Int. Ed.* **2012**, *51*, 5062, doi: 10.1002/anie.201107017.
- (3) Tasker, S. Z.; Standley, E. A.; Jamison, T. F. Recent Advances in Homogeneous Nickel Catalysis. *Nature* **2014**, *509*, 299, doi: 10.1038/nature13274.
- (4) Lin, C.-Y.; Power, P. P. Complexes of Ni(I): A “Rare” Oxidation State of Growing Importance. *Chem. Soc. Rev.* **2017**, *46*, 5347, doi: 10.1039/C7CS00216E.
- (5) Zheng, B.; Tang, F.; Luo, J.; Schultz, J. W.; Rath, N. P.; Mirica, L. M. Organometallic Nickel(III) Complexes Relevant to Cross-Coupling and Carbon–Heteroatom Bond Formation Reactions. *J. Am. Chem. Soc.* **2014**, *136*, 6499, doi: 10.1021/ja5024749.
- (6) Camasso, N. M.; Sanford, M. S. Design, Synthesis, and Carbon-Heteroatom Coupling Reactions of Organometallic Nickel(IV) Complexes. *Science* **2015**, *347*, 1218, doi: 10.1126/science.aaa4526.
- (7) Poli, R.; Cacelli, I. Orbital Splitting and Pairing Energy in Open-Shell Organometallics: A Study of Two Families of 16-Electron Complexes [Cp₂M] (M = Cr, Mo, W) and [CpM(Ph₃)] (M = Co, Rh, Ir). *Eur. J. Inorg. Chem.* **2005**, *2005*, 2324, doi: 10.1002/ejic.200400839.
- (8) Lin; Liu, L.; Fu, Y.; Luo, S.-W.; Chen, Q.; Guo, Q.-X. Comparing Nickel- and Palladium-Catalyzed Heck Reactions. *Organometallics* **2004**, *23*, 2114, doi: 10.1021/om034067h.
- (9) Leatherman, M. D.; Svejda, S. A.; Johnson, L. K.; Brookhart, M. Mechanistic Studies of Nickel(II) Alkyl Agostic Cations and Alkyl Ethylene Complexes: Investigations of Chain Propagation and Isomerization in (α-Diimine)Ni(II)-Catalyzed Ethylene Polymerization. *J. Am. Chem. Soc.* **2003**, *125*, 3068, doi: 10.1021/ja021071w.
- (10) Xu, H.; White, P. B.; Hu, C.; Diao, T. Structure and Isotope Effects of the B-H Agostic (α-Diimine)Nickel Cation as a Polymerization Intermediate. *Angew. Chem. Int. Ed.* **2017**, *56*, 1535, doi: 10.1002/anie.201611282.
- (11) Xu, H.; Hu, C. T.; Wang, X.; Diao, T. Structural Characterization of B-Agostic Bonds in Pd-Catalyzed Polymerization. *Organometallics* **2017**, *36*, 4099, doi: 10.1021/acs.organomet.7b00666.
- (12) Jin, L.; Zhang, H.; Li, P.; Sowa, J. R.; Lei, A. What Is the Rate of the C_{sp2}–C_{sp2} Reductive Elimination Step? Revealing an Unusually Fast Ni-Catalyzed Negishi-Type Oxidative Coupling Reaction. *J. Am. Chem. Soc.* **2009**, *131*, 9892, doi: 10.1021/ja903833u.
- (13) Tamao, K.; Sumitani, K.; Kumada, M. Selective Carbon–Carbon Bond Formation by Cross-Coupling of Grignard Reagents with Organic Halides. Catalysis by Nickel-Phosphine Complexes. *J. Am. Chem. Soc.* **1972**, *94*, 4374, doi: 10.1021/ja00767a075.
- (14) Tobisu, M.; Takahira, T.; Morioka, T.; Chatani, N. Nickel-Catalyzed Alkylative Cross-Coupling of Anisoles with Grignard Reagents Via C–O Bond Activation. *J. Am. Chem. Soc.* **2016**, *138*, 6711, doi: 10.1021/jacs.6b03253.

- (15) Quasdorf, K. W.; Antoft-Finch, A.; Liu, P.; Silberstein, A. L.; Komaromi, A.; Blackburn, T.; Ramgren, S. D.; Houk, K. N.; Snieckus, V.; Garg, N. K. Suzuki–Miyaura Cross-Coupling of Aryl Carbamates and Sulfamates: Experimental and Computational Studies. *J. Am. Chem. Soc.* **2011**, *133*, 6352, doi: 10.1021/ja200398c.
- (16) Schaub, T.; Backes, M.; Radius, U. Catalytic C–C Bond Formation Accomplished by Selective C–F Activation of Perfluorinated Arenes. *J. Am. Chem. Soc.* **2006**, *128*, 15964, doi: 10.1021/ja064068b.
- (17) Nielsen, D. K.; Doyle, A. G. Nickel-Catalyzed Cross-Coupling of Styrenyl Epoxides with Boronic Acids. *Angew. Chem. Int. Ed.* **2011**, *50*, 6056, doi: 10.1002/anie.201101191.
- (18) Huang, C.-Y.; Doyle, A. G. Nickel-Catalyzed Negishi Alkylations of Styrenyl Aziridines. *J. Am. Chem. Soc.* **2012**, *134*, 9541, doi: 10.1021/ja3013825.
- (19) Hie, L.; Fine Nathel, N. F.; Shah, T. K.; Baker, E. L.; Hong, X.; Yang, Y.-F.; Liu, P.; Houk, K. N.; Garg, N. K. Conversion of Amides to Esters by the Nickel-Catalysed Activation of Amide C–N Bonds. *Nature* **2015**, *524*, 79, doi: 10.1038/nature14615.
- (20) Ueda, Y.; Tsujimoto, N.; Yurino, T.; Tsurugi, H.; Mashima, K. Nickel-Catalyzed Cyanation of Aryl Halides and Triflates Using Acetonitrile Via C–CN Bond Cleavage Assisted by 1,4-Bis(Trimethylsilyl)-2,3,5,6-Tetramethyl-1,4-Dihydropyrazine. *Chem. Sci.* **2019**, *10*, 994, doi: 10.1039/C8SC04437F.
- (21) Inatomi, T.; Fukahori, Y.; Yamada, Y.; Ishikawa, R.; Kanegawa, S.; Koga, Y.; Matsubara, K. Ni(I)–Ni(III) Cycle in Buchwald–Hartwig Amination of Aryl Bromide Mediated by NHC-Ligated Ni(I) Complexes. *Catal. Sci. Technol.* **2019**, *9*, 1784, doi: 10.1039/C8CY02427H.
- (22) Diccianni, J. B.; Hu, C.; Diao, T. Binuclear, High-Valent Nickel Complexes: Ni–Ni Bonds in Aryl–Halogen Bond Formation. *Angew. Chem. Int. Ed.* **2017**, *56*, 3635, doi: 10.1002/anie.201611572.
- (23) Shu, W.; García-Domínguez, A.; Quirós, M. T.; Mondal, R.; Cárdenas, D. J.; Nevado, C. Ni-Catalyzed Reductive Dicarbofunctionalization of Nonactivated Alkenes: Scope and Mechanistic Insights. *J. Am. Chem. Soc.* **2019**, *141*, 13812, doi: 10.1021/jacs.9b02973.
- (24) Ermler, U.; Grabarse, W.; Shima, S.; Goubeaud, M.; Thauer, R. K. Crystal Structure of Methyl-Coenzyme M Reductase: The Key Enzyme of Biological Methane Formation. *Science* **1997**, *278*, 1457, doi: 10.1126/science.278.5342.1457.
- (25) Pelmeshikov, V.; Blomberg, M. R. A.; Siegbahn, P. E. M.; Crabtree, R. H. A Mechanism from Quantum Chemical Studies for Methane Formation in Methanogenesis. *J. Am. Chem. Soc.* **2002**, *124*, 4039, doi: 10.1021/ja011664r.
- (26) Pelmeshikov, V.; Siegbahn, P. E. M. Catalysis by Methyl-Coenzyme M Reductase: A Theoretical Study for Heterodisulfide Product Formation. *JBIC Journal of Biological Inorganic Chemistry* **2003**, *8*, 653, doi: 10.1007/s00775-003-0461-8.
- (27) Wongnate, T.; Sliwa, D.; Ginovska, B.; Smith, D.; Wolf, M. W.; Lehnert, N.; Raugei, S.; Ragsdale, S. W. The Radical Mechanism of Biological Methane Synthesis by Methyl-Coenzyme M Reductase. *Science* **2016**, *352*, 953, doi: 10.1126/science.aaf0616.
- (28) Jones, G. D.; Martin, J. L.; McFarland, C.; Allen, O. R.; Hall, R. E.; Haley, A. D.; Brandon, R. J.; Konovalova, T.; Desrochers, P. J.; Pulay, P.; Vicic, D. A. Ligand Redox Effects in the Synthesis, Electronic Structure, and Reactivity of an Alkyl–Alkyl Cross-Coupling Catalyst. *J. Am. Chem. Soc.* **2006**, *128*, 13175, doi: 10.1021/ja063334i.

- (29) Breitenfeld, J.; Ruiz, J.; Wodrich, M. D.; Hu, X. Bimetallic Oxidative Addition Involving Radical Intermediates in Nickel-Catalyzed Alkyl–Alkyl Kumada Coupling Reactions. *J. Am. Chem. Soc.* **2013**, *135*, 12004, doi: 10.1021/ja4051923.
- (30) Fu, G. C. Transition-Metal Catalysis of Nucleophilic Substitution Reactions: A Radical Alternative to S_N1 and S_N2 Processes. *ACS Cent. Sci.* **2017**, *3*, 692, doi: 10.1021/acscentsci.7b00212.
- (31) Schwarzwalder, G. M.; Matier, C. D.; Fu, G. C. Enantioconvergent Cross-Couplings of Alkyl Electrophiles: The Catalytic Asymmetric Synthesis of Organosilanes. *Angew. Chem. Int. Ed.* **2019**, *58*, 3571, doi: 10.1002/anie.201814208.
- (32) Diccianni, J. B.; Katigbak, J.; Hu, C.; Diao, T. Mechanistic Characterization of (Xantphos)Ni(I)-Mediated Alkyl Bromide Activation: Oxidative Addition, Electron Transfer, or Halogen-Atom Abstraction. *J. Am. Chem. Soc.* **2019**, *141*, 1788, doi: 10.1021/jacs.8b13499.
- (33) Zhao, C.; Jia, X.; Wang, X.; Gong, H. Ni-Catalyzed Reductive Coupling of Alkyl Acids with Unactivated Tertiary Alkyl and Glycosyl Halides. *J. Am. Chem. Soc.* **2014**, *136*, 17645, doi: 10.1021/ja510653n.
- (34) Arias-Rotondo, D. M.; McCusker, J. K. The Photophysics of Photoredox Catalysis: A Roadmap for Catalyst Design. *Chem. Soc. Rev.* **2016**, *45*, 5803, doi: 10.1039/C6CS00526H.
- (35) Tellis, J. C.; Primer, D. N.; Molander, G. A. Single-Electron Transmetalation in Organoboron Cross-Coupling by Photoredox/Nickel Dual Catalysis. *Science* **2014**, *345*, 433, doi: 10.1126/science.1253647.
- (36) Zuo, Z.; MacMillan, D. W. C. Decarboxylative Arylation of α -Amino Acids Via Photoredox Catalysis: A One-Step Conversion of Biomass to Drug Pharmacophore. *J. Am. Chem. Soc.* **2014**, *136*, 5257, doi: 10.1021/ja501621q.
- (37) Shaw, M. H.; Shurtleff, V. W.; Terrett, J. A.; Cuthbertson, J. D.; MacMillan, D. W. C. Native Functionality in Triple Catalytic Cross-Coupling: sp^3 C–H Bonds as Latent Nucleophiles. *Science* **2016**, *352*, 1304, doi: 10.1126/science.aaf6635.
- (38) Shields, B. J.; Doyle, A. G. Direct C_{sp³}–H Cross Coupling Enabled by Catalytic Generation of Chlorine Radicals. *J. Am. Chem. Soc.* **2016**, *138*, 12719, doi: 10.1021/jacs.6b08397.
- (39) Heitz, D. R.; Tellis, J. C.; Molander, G. A. Photochemical Nickel-Catalyzed C–H Arylation: Synthetic Scope and Mechanistic Investigations. *J. Am. Chem. Soc.* **2016**, *138*, 12715, doi: 10.1021/jacs.6b04789.
- (40) Dowd, P.; Choi, S. C. A New Tributyltin Hydride-Based Rearrangement of Bromomethyl β -Keto Esters. A Synthetically Useful Ring Expansion To γ -Keto Esters. *J. Am. Chem. Soc.* **1987**, *109*, 3493, doi: 10.1021/ja00245a069.
- (41) Beckwith, A. L. J.; O'Shea, D. M.; Gerba, S.; Westwood, S. W. Cyano or Acyl Group Migration by Consecutive Homolytic Addition and B-Fission. *J. Chem. Soc., Chem. Commun.* **1987**, 666, doi: 10.1039/C39870000666.
- (42) Schrauzer, G. N.; Deutsch, E. Reactions of Cobalt(I) Supernucleophiles. The Alkylation of Vitamin B₁₂S, Cobaloximes(I), and Related Compounds. *J. Am. Chem. Soc.* **1969**, *91*, 3341, doi: 10.1021/ja01040a041.
- (43) Halpern, J. Mechanisms of Coenzyme B₁₂-Dependent Rearrangements. *Science* **1985**, *227*, 869, doi: 10.1126/science.2857503.

- (44) Helvenston, M. C.; Castro, C. E. Nickel(I) Octaethylisobacteriochlorin Anion. An Exceptional Nucleophile. Reduction and Coupling of Alkyl Halides by Anionic and Radical Processes. A Model for Factor F-430. *J. Am. Chem. Soc.* **1992**, *114*, 8490, doi: 10.1021/ja00048a021.
- (45) Gosden, C.; Healy, K. P.; Pletcher, D. Reaction of Electrogenerated Square-Planar Nickel(I) Complexes with Alkyl Halides. *J. Chem. Soc., Dalton Trans.* **1978**, 972, doi: 10.1039/DT9780000972.
- (46) Bakac, A.; Espenson, J. H. Kinetics and Mechanism of the Alkylnickel Formation in One-Electron Reductions of Alkyl Halides and Hydroperoxides by a Macrocyclic Nickel(I) Complex. *J. Am. Chem. Soc.* **1986**, *108*, 713, doi: 10.1021/ja00264a023.
- (47) Call, A.; Casadevall, C.; Acuña-Parés, F.; Casitas, A.; Lloret-Fillol, J. Dual Cobalt–Copper Light-Driven Catalytic Reduction of Aldehydes and Aromatic Ketones in Aqueous Media. *Chem. Sci.* **2017**, *8*, 4739, doi: 10.1039/C7SC01276D.
- (48) Mishra, V.; Mishra, H.; Mukherjee, R. Generation and Properties of CoI/NII Species Stabilized by a Tetradentate Pyridylpyrazole Ligand: Crystal Structures of Dialkyl-Co^{III} Complexes. *Eur. J. Inorg. Chem.* **2009**, *2009*, 2973, doi: 10.1002/ejic.200900203.
- (49) Holah, D. G.; Hughes, A. N.; Hui, B. C.; Kan, C.-T. Production of Ni(I) Complexes from Reactions between Ni^{II} and NaBH₄ in the Presence of Triphenylphosphine and Some Bidentate Phosphines. *Can. J. Chem.* **1978**, *56*, 2552, doi: 10.1139/v78-419.
- (50) Michelet, B.; Deldaele, C.; Kajouj, S.; Moucheron, C.; Evano, G. A General Copper Catalyst for Photoredox Transformations of Organic Halides. *Org. Lett.* **2017**, *19*, 3576, doi: 10.1021/acs.orglett.7b01518.
- (51) Lambert, F. L.; Ingall, G. B. Voltammetry of Organic Halogen Compounds. IV. The Reduction of Organic Chlorides at the Vitreous (Glassy) Carbon Electrode. *Tetrahedron Lett.* **1974**, *15*, 3231, doi: 10.1016/S0040-4039(01)91870-2.
- (52) Schrauzer, G. N.; Lee, L.-P.; Sibert, J. W. Alkylcobalamins and Alkylcobaloximes. Electronic Structure, Spectra, and Mechanism of Photodealkylation. *J. Am. Chem. Soc.* **1970**, *92*, 2997, doi: 10.1021/ja00713a012.
- (53) Scheffold, R.; Dike, M.; Dike, S.; Herold, T.; Walder, L. Synthesis and Reactions of Porphine-Type Metal Complexes. 8. Carbon–Carbon Bond Formation Catalyzed by Vitamin B₁₂ and a Vitamin B₁₂ Model Compound. Electrosynthesis of Bicyclic Ketones by 1,4 Addition. *J. Am. Chem. Soc.* **1980**, *102*, 3642, doi: 10.1021/ja00530a064.
- (54) Stoll, S.; Schweiger, A. Easyspin, a Comprehensive Software Package for Spectral Simulation and Analysis in Epr. *Journal of Magnetic Resonance* **2006**, *178*, 42, doi: 10.1016/j.jmr.2005.08.013.
- (55) Pavlishchuk, V. V.; Addison, A. W. Conversion Constants for Redox Potentials Measured Versus Different Reference Electrodes in Acetonitrile Solutions at 25°C. *Inorg. Chim. Acta* **2000**, *298*, 97, doi: 10.1016/S0020-1693(99)00407-7.
- (56) Krejčík, M.; Daněk, M.; Hartl, F. Simple Construction of an Infrared Optically Transparent Thin-Layer Electrochemical Cell: Applications to the Redox Reactions of Ferrocene, Mn₂(Co)₁₀ and Mn(Co)₃(3,5-Di-*t*-Butyl-Catecholate)⁻. *J. Electroanal. Chem. Interf. Electrochem.* **1991**, *317*, 179, doi: 10.1016/0022-0728(91)85012-E.
- (57) Lecomte, V.; Bolm, C. Iron(III)-Catalyzed Tandem Sequential Methanol Oxidation/Aldol Coupling. *Adv. Synth. Catal.* **2005**, *347*, 1666, doi: 10.1002/adsc.200505163.

- (58) Moteki, S. A.; Usui, A.; Zhang, T.; Solorio Alvarado, C. R.; Maruoka, K. Site-Selective Oxidation of Unactivated C–H Bonds with Hypervalent Iodine(III) Reagents. *Angew. Chem. Int. Ed.* **2013**, *52*, 8657, doi: 10.1002/anie.201304359.

UNIVERSITAT ROVIRA I VIRGILI
DEVELOPMENT OF VISIBLE LIGHT PHOTOREDOX METHODOLOGIES TOWARDS THE ACTIVATION
OF CARBON-HALOGEN BONDS
Miguel Claros Casielles

Chapter IV

CASIELLES



General Conclusions

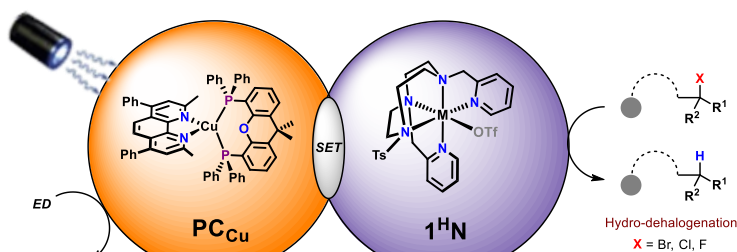
GENERAL CONCLUSIONS

UNIVERSITAT ROVIRA I VIRGILI
DEVELOPMENT OF VISIBLE LIGHT PHOTOREDOX METHODOLOGIES TOWARDS THE ACTIVATION
OF CARBON-HALOGEN BONDS
Miguel Claros Casielles

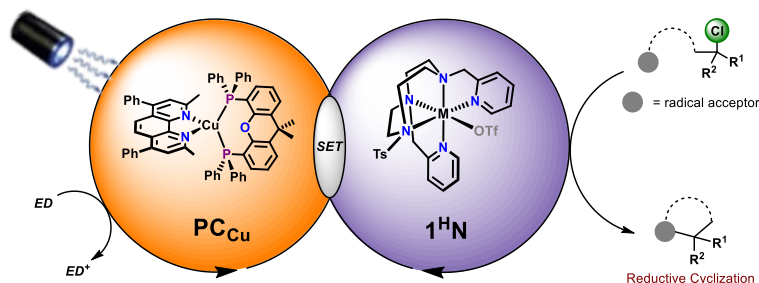
At the beginning of this doctoral dissertation, the use of photoredox catalysis as tool for organic synthesis was in full growth since its youth in 2008. At that point the use of alkyl halides as carbon-centered radical precursors was limited to alkyl and aryl iodides or bromides. Few examples described the use of activated alkyl and aryl chlorides that employ harsh reaction conditions.

In **Chapter III** a new dual catalyst system based on first-row transition metals has been developed for the activation of inert *Carbon-Halogen* bonds. The pair formed by $[\text{Cu}(\text{bathocuproine})(\text{Xantphos})](\text{PF}_6)$ (PC_{Cu}) and $[\text{M}(\text{OTf})(\text{Py}_2\text{Tstacn})](\text{OTf})$ ($\text{I}^{\text{H}}\text{M}$, $\text{M} = \text{Co}, \text{Ni}$) in the presence of tri-alkyl amines as electron donor is a powerful system for the activation of $\text{Csp}^3\text{-Halogen}$ bonds. The presence of ethanol as protic solvent proved to be of great importance for the dehalogenation of non-activated alkyl chlorides. Polyhalogenated biologically active molecules such as drugs or pesticides have been used as substrates with the objective to selectively activate the specific *Carbon-Halogen* bond. In most of the studied cases, the reaction gave a complete destruction of the substrate, which can be employed to transform this waste into non-pollutant mixture.

The stronger $\text{Csp}^3\text{-F}$ bond has been also activated with this dual-catalyst system. In this case, the ethanol was not crucial for the reaction to occur, suggesting a different reaction pathway in comparison with alkyl chlorides. Control experiments have been performed, revealing that all the components in the reaction (photocatalyst, catalyst, ED, and light) are needed to be present.

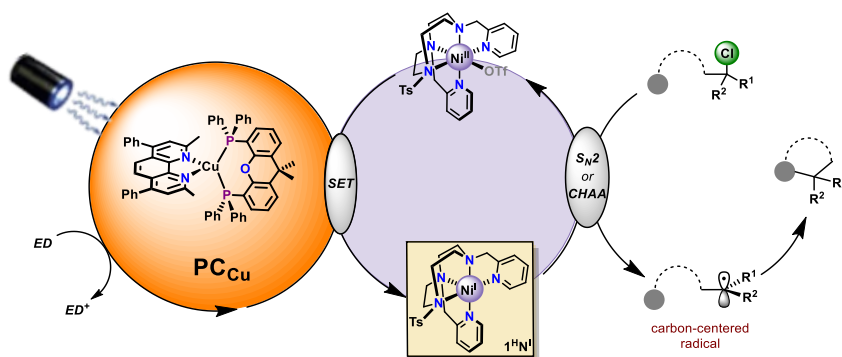


As described in **Chapter IV** the dual-catalyst system developed in **Chapter III** has been tested in the formation of new C–C bonds using as precursors non-activated alkyl halides (bromides and chlorides) for the radical cyclization reaction. The presence of protic solvents turned out to be of great impact, obtaining higher yields with less acidic protic solvents. A broad family of cobalt and nickel complexes were tested, identifying that 4 and 5 coordinative cobalt and nickel complexes bearing basic N-based ligands are remarkably active for this reaction. As it was previously described by our group, cobalt poly-aminopyridine complexes are highly active catalyst over the generation of H₂ in protic solvents. As a result, nickel catalysts showed up faster kinetics than the analogous cobalt catalyst in the conditions described for the fact of being inactive in abovementioned reaction. This side reaction was detected to be critical for the cyclization of the linear substrates, getting good to excellent yields for a broad scope when **I^HNi** is used. Selectivity experiments between bromides and chlorides were also performed accomplishing the complete consumption of the alkyl bromide before the beginning of the activation of the alkyl chloride.



In **Chapter V** mechanistic studies for the photoredox promoted activation of inert *Csp*³–Cl bonds have been described. Radical-clock experiments alongside isotope labeling experiments confirmed the presence of *carbon-centered radicals*. This photogenerated radical intermediate is trapped by the radical acceptor (olefin or triple bond) to form the cyclic product. The final radical formed is quenched by reaction with the protic solvent by *HAT* or by one-electron reduction followed by protonation for the more easily reduced substrates.

Low-valent $I^H Ni^I$ intermediates have been detected as the metal-reacting species by the combination of EPR, UV-Vis and electrochemistry techniques. Stoichiometric reactions have been also performed to elucidate the interaction between the Ni-active compound and the alkyl chloride substrate. Cyclic voltammetry experiments in combination with DFTs calculations showed the formation of a transient $I^H Ni^{III}$ organometallic intermediate as result of an *oxidative addition* S_N2 type reaction. The less nucleophilic *Ni-DPA* undergoes a *concerted halogen atom abstraction* forming directly $Ni^{II}-Cl$ complex and the free-radical intermediate.



To conclude, during this *Doctoral Thesis* a dual photoredox methodology for the hydro-dehalogenation (*Chapter III*) and reductive cyclization (*Chapter IV*) of non-activated alkyl halides has been developed. The bimetallic catalyst is based on earth-abundant metals $PC_{Cu}/L^H M$ ($M = Co, Ni$). The discussed mechanistic studies support the *in-situ* formation of a low-valent cobalt or nickel complex upon reaction with the photoredox PC_{Cu} catalyst under visible-light irradiation (*Chapter V*). The results summarized over this thesis represent an initial step for the use of non-activated alkyl halides as radical precursors in photoredox catalysis with first-row transition metals. Further work should aim at the development of sustainable photoredox methods to enable intermolecular bond-forming reactions using alkyl chlorides as coupling partners and at mild reaction conditions.

UNIVERSITAT ROVIRA I VIRGILI
DEVELOPMENT OF VISIBLE LIGHT PHOTOREDOX METHODOLOGIES TOWARDS THE ACTIVATION
OF CARBON-HALOGEN BONDS
Miguel Claros Casielles

UNIVERSITAT ROVIRA I VIRGILI
DEVELOPMENT OF VISIBLE LIGHT PHOTOREDOX METHODOLOGIES TOWARDS THE ACTIVATION
OF CARBON-HALOGEN BONDS
Miguel Claros Casielles

UNIVERSITAT ROVIRA I VIRGILI
DEVELOPMENT OF VISIBLE LIGHT PHOTOREDOX METHODOLOGIES TOWARDS THE ACTIVATION
OF CARBON-HALOGEN BONDS
Miguel Claros Casielles



UNIVERSITAT
ROVIRA i VIRGILI



**Institut
Català
d'Investigació
Química**